π-Electron Systems Containing 3,3′-Bithiophene as a Key Skeleton

（3,3′-ビチオフェンを鍵骨格に含む π 電子系の創製）

Kengo Asai

浅井健吾

主論文

π-Electron Systems Containing 3,3′-Bithiophene as a Key Skeleton

（3,3′-ビチオフェンを鍵骨格に含むπ電子系の創製）

Kengo Asai

浅井健吾

Department of Chemistry, Graduate School of Science
Nagoya University

2016

Preface

This thesis summarizes the author's study that has been carried out under the direction of Professor Shigehiro Yamaguchi at Nagoya University during the period of April 2012 to March 2016. This study is concerned with the π electron systems containing 3,3′-bithiophene units.

First, the author is most grateful to Professor Shigehiro Yamaguchi and Associate Professor Aiko Fukazawa for their constant and precise guidance, valuable discussion, reliable support and hearty encouragement.

Also, the author expresses his great appreciation to Associate Professor Masayasu Taki and Assistant Professor Shohei Saito for their valuable suggestions, kind guidance, crucial advises, and technical assistants.

The author would like to express his appreciation to Professor Kunio Awaga, Associate Professor Michio M. Matsushita, Assistant Professor Hirofumi Yoshikawa, and Dr. Yoshiaki Shuku for help of measurement of electron paramagnetic resonance spectroscopy. He also appreciates Professor Hiroshi Nakajima and Assistant Professor Hiroyuki Matsui for valuable suggestion on the electron paramagnetic resonance spectroscopy. The author appreciates to Dr. Kengo Suzuki, Hamamatsu Photonics, for his efforts in measuring absolute fluorescence quantum yields.

The author greatly thanks to Ms. Hideko Natsume and Mr. Hisakazu Okamoto for their excellent works of scientific glassware. The author also thanks Research Center for Materials Science, Nagoya University for the use of chemical instruments. The author is thankful to Ms. Komina Nakazawa, Ms. Aya Yamamoto, Ms. Mamiko Shinzawa, and Ms. Yuki Kobayashi for their kind assistance.

The author is deeply grateful to former and present Yamaguchi research group members for stimulating discussion, brilliant advice, and kind help; Dr. Christoph Glotzbach, Dr. Andreas Feldmann, Mr. Masahiko Yoshimura, Mr. Atsushi Hayakawa, Ms. Anna Sekioka, Ms. Ayumi Shuto, Ms. Yuka Kureishi, Mr. Kosuke Usui, Dr.

Kengo Asai

Department of Chemistry
Graduate School of Science
Nagoya University
2016

Contents

General Introduction

Oligothiophenes are one of the representative scaffolds of functional π-conjugated materials because of their intriguing electronic, photophysical, and redox properties.[1] Oligothiophenes have long been considered as the structurally defined model compounds for polythiophenes with discrete chain lengths. Therefore, the oxidized species of oligothiophenes have been intensively investigated, as their radical cations and dications are crucial for understanding the mechanism of the charge carrier transport of polythiophene. Recently, oligothiophene derivatives have also attracted increasing attentions as a key building block of small molecule-based π-electron materials for a variety of applications, such as field effect transistor (OFETs),[2] photovoltaic cells,[3] light-emitting diodes (OLEDs),[4] and fluorescent probes[5].
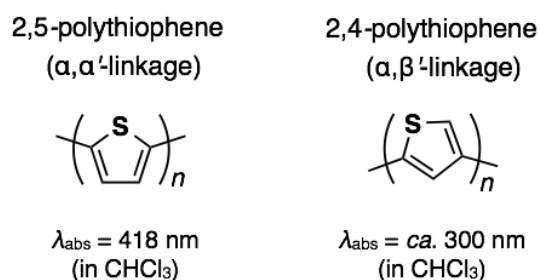
Chart 0-1. Polythiophene with α,α′- or α,β′-linkages.

In the chemistry of oligo- and polythiophenes, major interests have been focused on α,α′-linked systems, in which thiophene rings are linked at the 2,5-positions to one another, because π-conjugation through the α-positions is more effectively extended compared to that through the 3,4-positions. In 1983, Yamamoto and co-workers reported the positional effect on the π-conjugation in polythiophene (Chart 0-1).[6] They demonstrated that the longest-wavelength absorption band of a 2,5-linked polythiophene was significantly red-shifted by more than 100 nm compared to that of a 2,4-linked congener. Thereafter, the physical properties of α-oligothiophenes have been extensively studied.

So far, the chain-length dependent properties of α-oligothiophenes have been investigated in detail (Chart 0-2). Oligothiophene **1**,[7] their functionalized derivatives **2**,[8] and **3**[9] show red-shifted absorption and fluorescence, higher quantum yields, and longer fluorescence lifetimes as the chain length increases. The oxidized species, such as radical cations and dications, of oligothiophenes were also experimentally investigated,

using end-capped derivatives **4**[10] and **5**[11] with varied chain lengths. Furthermore, the device characteristics in organic electronic applications also correlate with the chain lengths of oligothiophenes. Bäuerle and co-workers reported the effect of conjugation length on the photovoltaic cell properties using oligothiophenes **3** with dicyanovinyl substituents.[9] Open-circuit voltage (V_{OC}) gradually decreased with increasing π-conjugation length due to the increasing HOMO levels. Takimiya and co-workers reported that a series of long oligomers **6** with 20–41 thiophene units formed lamellar packing structures in the solid states and their hole mobilities gradually increased as the chain length increased.[12] The accumulated knowledge on the structure-properties relationships for α-oligothiophenes are now available for further molecular design of functional π-conjugated materials.
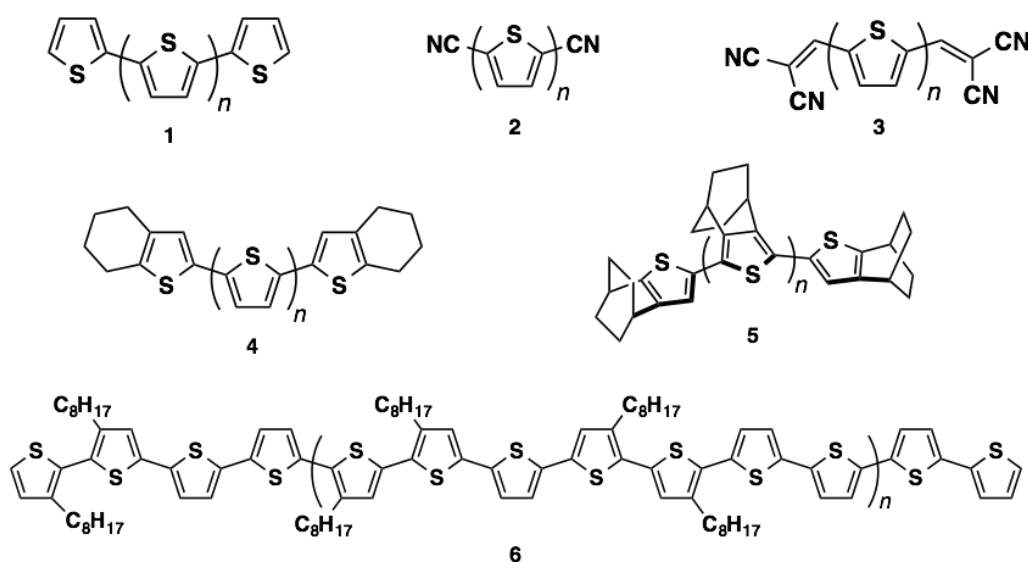
Chart 0-2. Representative examples of α-oligothiophenes.

For practical applications of π-electron materials, their solid-state properties largely affect the device performances, and thus the control of molecular alignment in the solid state is a crucial issue. However, α-linked oligothiophenes tend to have linear-shaped structures, resulting in the limited patterns of packing structures. Therefore, the development of more versatile π-conjugated scaffolds in terms of dimensionality of the molecular structure have been required for the control of packing structures (Chart 0-3). From this point of view, the oligothiophenes linked at the β-positions have been studied.

3

	α,α'-linkage	α,β'-linkage β,β'-linkage
π-conjugation	effective	less effective
structure	linear planar	branched twisted

Chart 0-3. Impacts of the linkage patterns of oligothiophenes.

Structural features of β-linked oligothiophenes

While the linkages at the β-positions were regarded as 'mislinkages' in polymer chains, in other words, defects in π-conjugation,[13] these linkage patterns impart oligothiophene diverse structural features, such as twisted, dendritic, and tubular shapes, which are totally different from the linear-shaped structures for the α-linked oligothiophene. For instance, Scherf and co-workers reported α-oligothiophene dimers with a β,β'-linkage (**7** in Chart 0-4), which formed swivel-cruciformed structures.[14] In this report, they successfully demonstrated that β,β'-linked quinquethiophene dimer **7** exhibited high so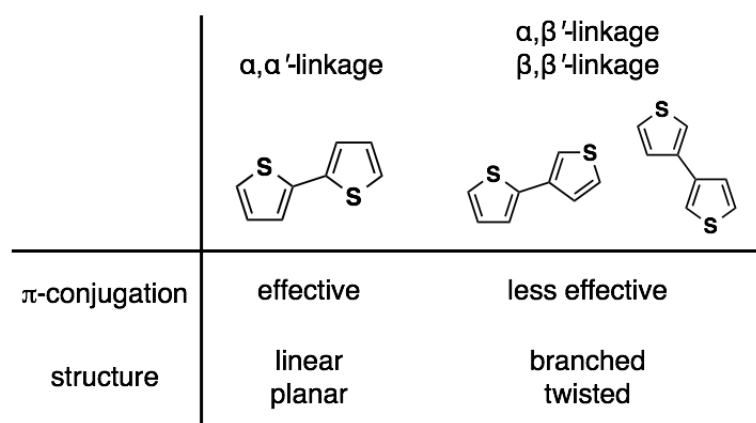lubility in organic solvents due to the nonplanar structure, enabling the facile fabrication of a OFET device by solution process, which showed high hole mobility up to 0.012 cm^2/V·s.

A β-linked substructure is also useful for the construction of dendritic π-electron systems based on oligothiophene frameworks. Bäuerle and co-workers reported the synthesis of dendritic oligothiophenes **8** as a highly soluble 3D π-conjugated systems, and its application to a p-type semiconducting material in bulk heterojunction (BHJ) photovoltaic cells.[15] They clearly demonstrated that branched nonathiophene **9**, which was one of the shortest dendrons they studied, exhibited characteristic packing structure consisting of both face-to-face and herringbone-like arrangement due to the branched and partially twisted structure. These studies clearly demonstrated that the β-linked substructure impart oligothiophene twisted and/or branched structures with high dimensionality. These structural features give rise to the enhanced solubility as well as the diversity in molecular packing.
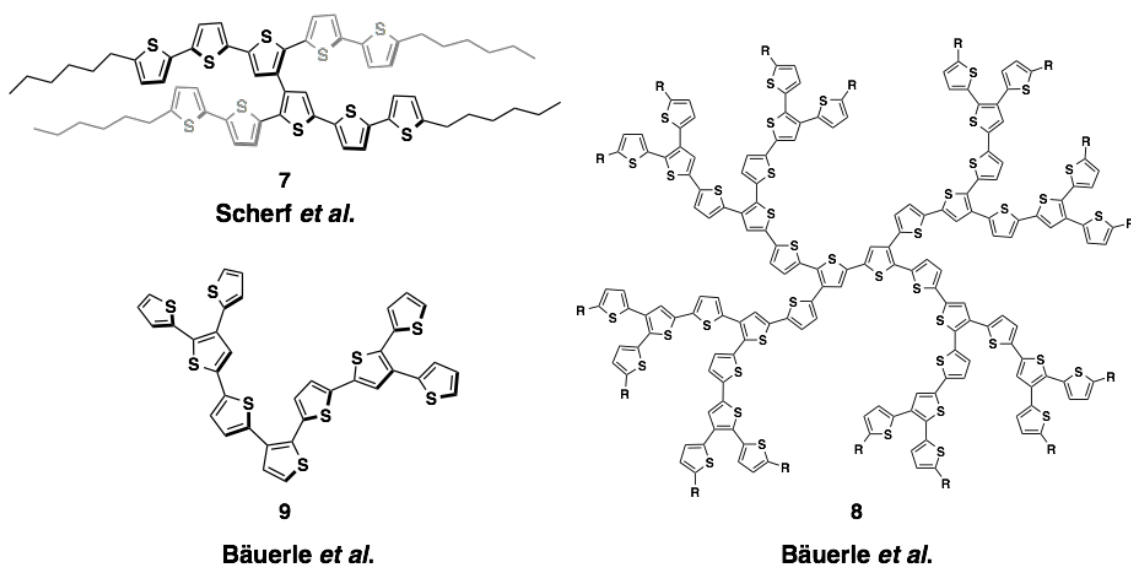
Chart 0-4. Representative examples of oligothiophenes linked at β-positions.

Cyclic oligothiophenes partially containing the linkages at **β**-positions are of another interest in terms of structural diversity (Chart 0-5). Cyclic sexithiophenes **10** containing 3,3′-bithiophene substructures, which were reported by Marsella[16] and Wang,[17] adopted tubular-shaped structures that cannot be realized by α-linked oligothiophenes. The twisted structural feature of β-linked bithiophene unit has also been attracted emerging interest as a building block for the chiral macrocyclic π systems. For instance, Marsella and co-workers reported that macrocyclic dithienylacethylene oligomer **11** with the β,β′-linkages has a helical cyclic structure due to the axial chirality of the β-linked bithiophene unit.[18] Very recently, Sannicoló and co-workers reported the synthesis of cyclic α-sexithiophene oligomer **12** connected *via* β-linked bis(benzothiophene) units, which exhibited a circularly polarized fluorescence (CPL) due to the axial chirality.[19]
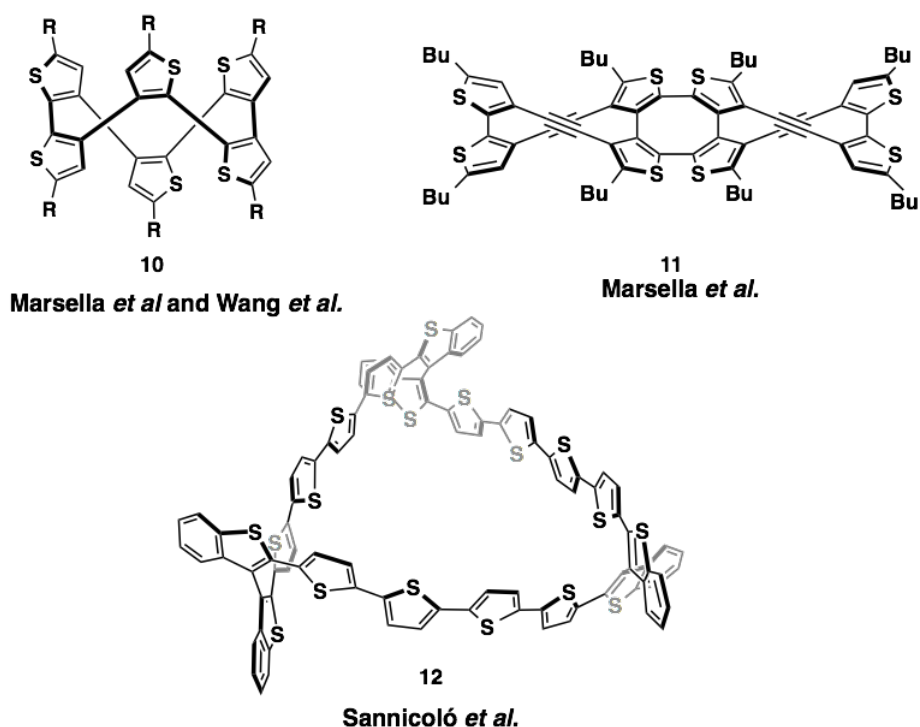
Chart 0-5. Representative examples of cyclic oligothiophenes linked at β-positions.

π-Conjugation through the linkage at β-positions

Although the Yamamoto's study on polythiophenes clearly demonstrated that the connections at the β-positions is much less effective for the extension of π-conjugation compared to that at the α-positions, the detailed studies using short-chain oligothiophenes had long been untouched. The first report that disclosed the π-conjugation through a β,β′-linkage was reported by Mori and co-workers in 2010 (Chart 0-6).[20] In this report, they studied the photophysical properties of α-quaterthiophene dimer **14** connected at the β-positions, which showed slightly more red-shifted absorption (λ_{abs} = 408 nm) and fluorescence (λ_{em} = 507 nm) than those of the parent α-quaterthiophene monomer **13** (λ_{abs} = 400 nm and λ_{em} = 494 nm). Although the reported absorption and fluorescence maximum of **14** are much shorter than those of α-octithiophene **15**.[21] These results imply that there are some extent of electronic interaction between the two quaterthiophene moieties through the β,β′-linkage. Nevertheless, the nature of the π-conjugation through the β,β′-linkage remains unclear. For further development of the materials science based on oligothiophenes, precise understanding of the π-conjugation and electronic interaction through the β,β′-linkage should be a crucial issue.

13
λ_{abs} = 400 nm
λ_{em} = 494 nm
(in CHCl₃)

14
λ_{abs} = 408 nm
λ_{em} = 507 nm
(in CHCl₃)

15
λ_{abs} = 463 nm
λ_{em} = 598 nm
(in C₂H₂Cl₄)

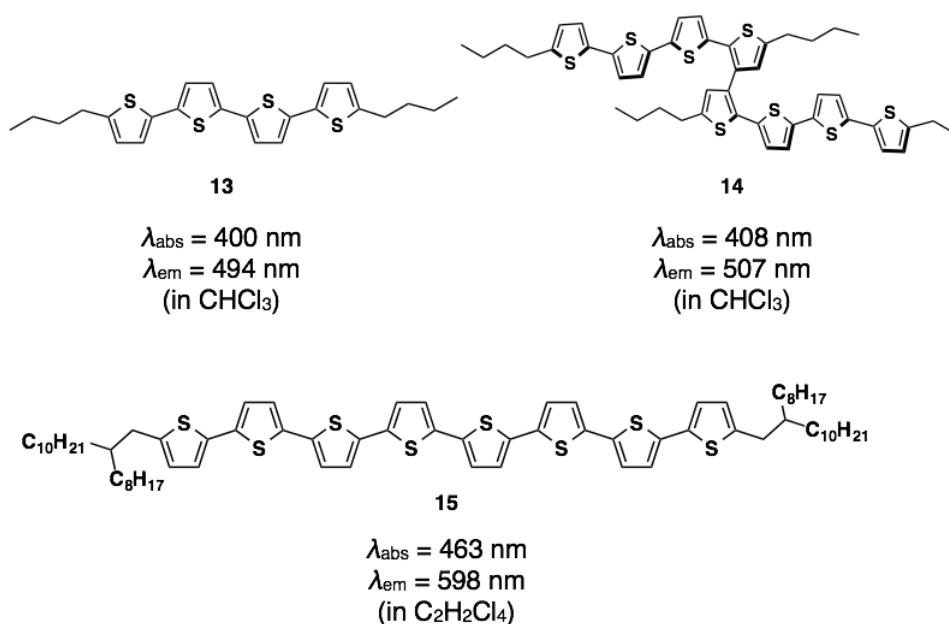**Chart 0-6.** Comparison in photophysical properties among oligothiophenes connected at the α-positions and those connected at the β-positions.

Effect of the β,β′-linkage on the properties of fused-bithiophene derivatives

Fused bithiophene derivatives containing β,β′-linkage show characteristic properties, which are totally different from those containing a α,α′-linkage. For instance, Shi, Kan, Wang, and co-workers reported bithiophene-fused cyclopentanones **16** and cyclopentylidenemalononitriles **17**, and demonstrated that their photophysical properties are highly dependent on the fused fashion of bithiophene moieties.[22] Whereas **16α** and **17α** composed of a 2,2′-bithiophene substructure have weak electronic interaction between electron-donating π framework with electron-accepting carbonyl/dicyanomethylene moieties, the corresponding β-linked isomers **16β** and **17β** have significant charge-transfer characters, resulting in the characteristic absorption band in the long-wavelength region.

The fused fashion of bithiophene moiety also plays an important role on the aromaticity of the resulting π-electron systems. Wakamiya, Yamaguchi and co-workers reported the synthesis and properties of bithiophene-fused diborin dianions **18α** and **18β,** and investigated the effect of the fused bithiophene moieties on the aromaticity of the resulting diborin diaions.[23] They demonstrated that **18β** exhibits pronounced 6π aromaticity in the central diborin ring, whereas peripheral 14π aromaticity is predominant in **18α**. These results strongly indicate that the fused fashion of the

bithiophene moieties influences the preferential π-conjugation mode in the resulting π system.

Quinoidal bithiophene moieties also give similar influences in terms of the positional effect on the π-conjugation mode. Otsubo, Ogura and co-workers reported that the quinoidal bithiophene **19β** with the β,β′-linkage exhibits significantly red-shifted absorption, reaching the NIR region, relative to that of the α-linked isomer **19α**.[24] All of these reports indicate that less effective orbital interaction through the β,β′-linkage likely makes π-conjugation lengths longer through α-positions, leading to the characteristic properties.
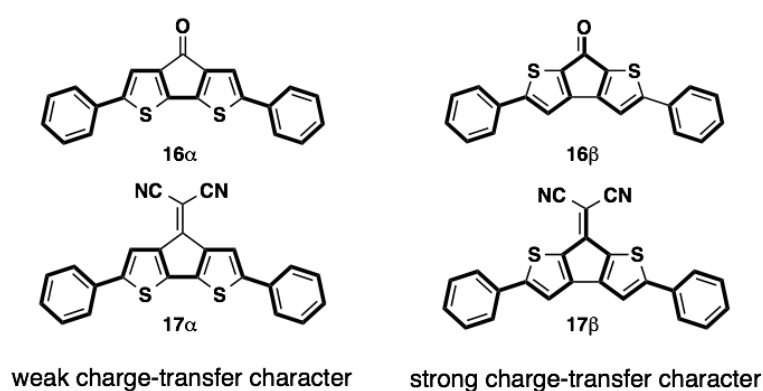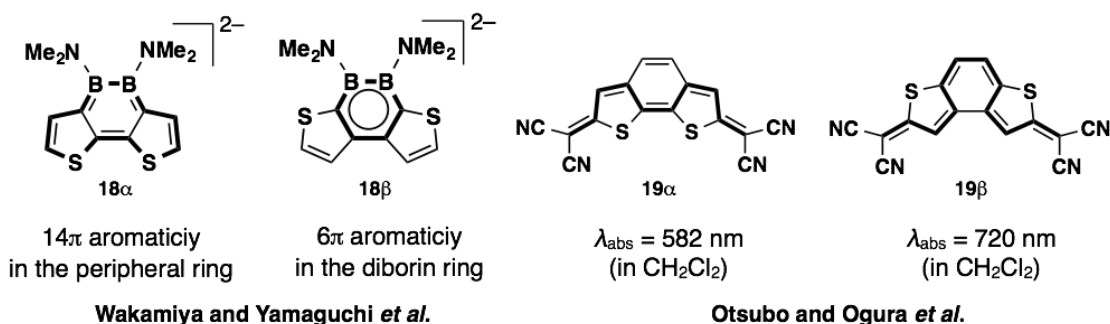
Chart 0-7. Comparison of fused bithiophene derivatives.

Survey of this thesis

As described in the previous sections, oligothiophene-based molecules with the linkage at β-positions are attractive π-conjugated systems in terms of the structural diversity as well as their characteristic properties. For further progress in the chemistry of oligothiophenes, understanding of π-conjugation and electronic interaction through the β,β′-linkage is crucial. In this thesis, aiming at the elucidation of the impacts of the β,β′-linkage and development of new oligothiophene-based materials, the author has designed and synthesized a cyclic oligothiophene containing the β,β′-linkages and the polymethine dyes based on 3,3′-bithiophene-fused cycloheptatriene. This thesis consists of three chapters, which are outlined as follows.

Chapter 1 describes the synthesis of a cyclic octithiophene containing the β,β′-linkages. Its structure and properties are investigated for the elucidation of the π-conjugation through the β,β′-linkages.[25] The formation of a cyclic Pt-complex precursor followed by the reductive elimination gave the cyclic octithiophene in high yield. X-ray crystal structure analysis revealed its ellipsoidal structure with twisted conformation of the bithiophene moieties. This compound showed a red-shifted emission compared to that of the parent quaterthiophene due to the large structural change in the excited state. Spin delocalization over the entire molecular skeleton was also indicated in the one-electron oxidized species.
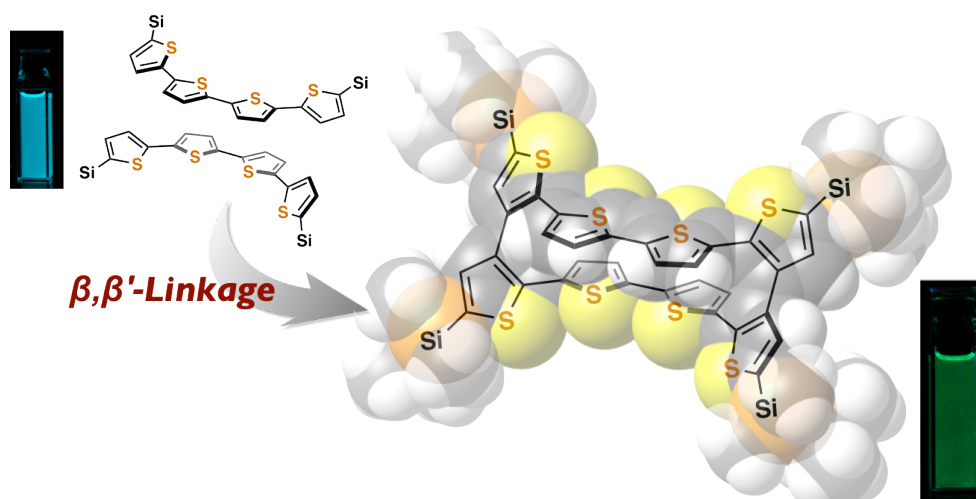
Chapter 2 describes the design and synthesis of amino-substituted dithienotropylium ions containing a 3,3′-bithiophene unit as a new entity of stable cationic dyes. As the electron-donating ability of the terminal amino group increases,

the tropylium ion becomes more stable with the increased pK_R^+ value. X-ray crystallographic analyses revealed that the contribution of the quinoidal structure becomes more pronounced as the electron-donating ability of amino groups increases. Reflecting the quinoidal resonance structures, the amino-substituted dithienotropylium ions show strong absorption bands and red fluorescences.

Charge Delocalization

R=Me R=Ph
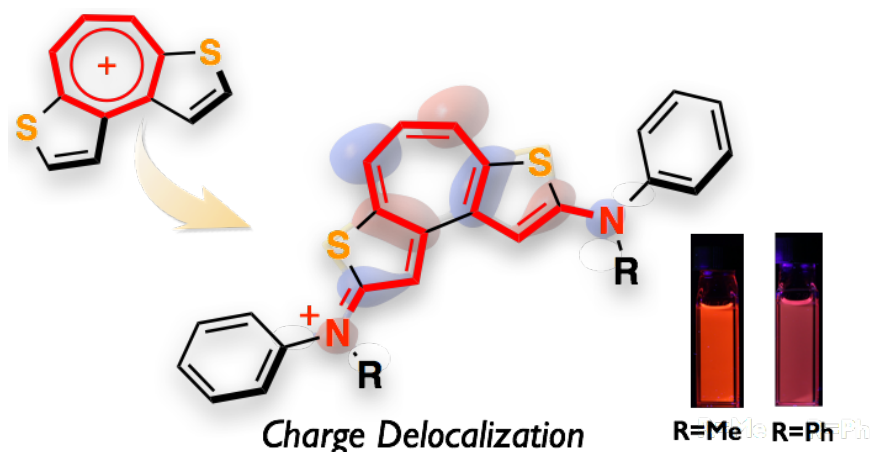
Chapter 3 describes the design of a polymethine π-conjugated system, which consists of a 3,3′-bithiophene-fused cycloheptatriene and two terminal phenol moieties, as a new entity of the NIR-absorbing dye. The charge neutral compound shows the pH-responsive photophysical properties due to the acid-base equilibria among three species. Whereas strong absorption bands in the visible region and a red fluorescence were observed under the acidic conditions, the NIR absorption bands were observed under the neutral and basic conditions. Furthermore, a persistent radical was obtained by the chemical oxidation of the compound. This neutral radical shows the electrochemically reversible redox properties, producing the corresponding one-electron oxidized and reduced species. In consonant with the interconversion among the various species, this 3,3′-bithiophene-fused π skeleton shows dramatic multifaceted change in the photophysical properties.
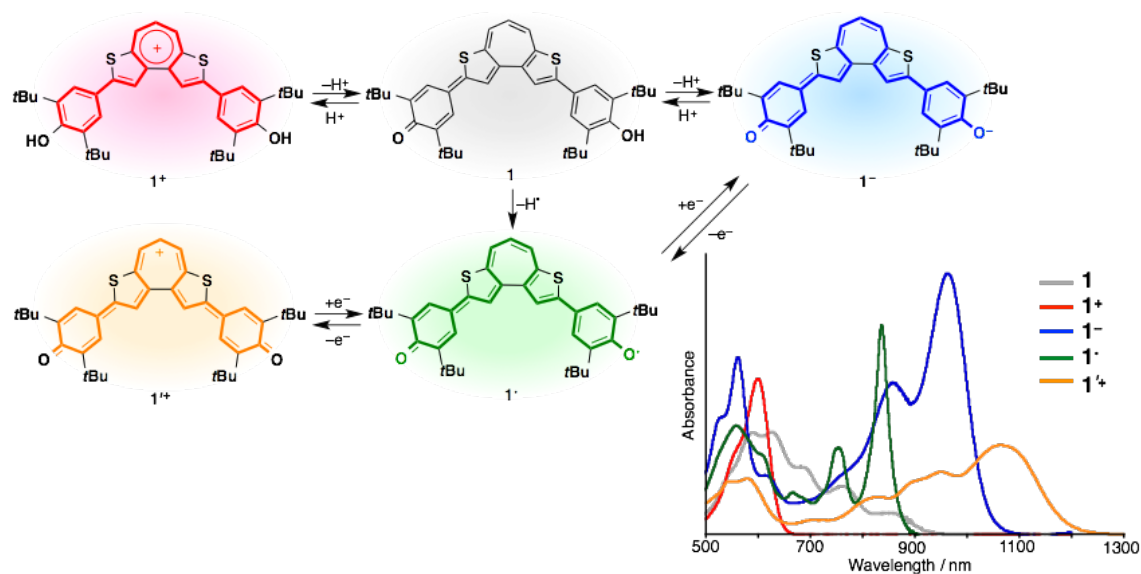
References

(1)   (a) *Handbook of Thiophene-Based Materials: Applications in Organic Electronics and Photonics*, Perepichka, I. F.; Perepichka, D. F.; Ed., Wiley, Chichester, UK, **2009**. (b) Mishra, A.; Ma, C.-Q.; Bäuerle, P.; *Chem. Rev.*, **2009**, *109*, 1141. (c) Segura, J. L.; Herrera, H.; Bäuerle, P. *J. Mater. Chem.* **2012**, *22*, 8717.

(2)   (a) Mei, J.; Diao, Y.; Appleton, A. L.; Fang, L.; Bao, Z. *J. Am. Chem. Soc.* **2013**, *135*, 6724. (b) Zhang, L.; Colella, N. S.; Cherniawski, B. P.; Mannsfeld, S. C. B.; Briseno, A. L. *ACS Appl. Mater. Interfaces* **2014**, *6*, 5327.

(3)   (a) Ni, W.; Wan, X.; Li, M.; Wang, Y.; Chen, Y. *Chem. Commun.* **2015**, *51*, 4936. (b) Dou, L.; Liu, Y.; Hong, Z.; Li, G.; Yang, Y. *Chem. Rev.* **2015**, *115*, 12633.

(4)   (a) Rasmussen, S. C.; Evenson, S. J.; McCausland, C. B. *Chem. Commun.* **2015**, *51*, 4528. (b) *Organic Light Emitting Diodes*, Mazzo, M.; Ed., InTech **2010**, p.1–24.

(5)   Capobianco, M. L.; Barbarella, G.; Manetto, A. *Molecules.* **2012**, *17*, 910.

(6)   Yamamoto, T.; Sanechika, K.; Yamamoto, A. *Bull. Chem. Soc. Jpn.* **1983**, *56*, 1497.

(7)   (a) Becker, R. S.; Sexias de Melo, J.; Maçanita, A. L.; Elisei, F. *Pure. Appl. Chem.* **1995**, *67*, 9. (b) Becker, R. S.; Sexias de Melo, J.; Maçanita, A. L.; Elisei, F. *J. Phys. Chem.* **1996**, *100*, 18683.

(8)   Pina, J.; Burrows, H. D.; Becker, R. S.; Dias, F. B.; Maçanita, A. L.; Sexias de

Melo, J. *J. Phys. Chem. B* **2006**, *110*, 6499.

(9)   Fitzner, R.; Reinold, E.; Mishra, A.; Mena-Osteritz, E.; Ziehlke, H.; Körner, C.; Leo, K.; Riede, M.; Weil, M.; Tsaryova, O.; Weiβ, A.; Uhrich, C.; Pfeiffer, M.; Bäuerle, P. *Adv. Funct. Mater.* **2011**, *21*, 897.

(10)   (a) Hill, M. G.; Mann, K. R.; Miller, L. L.; Penneau, J.-F. *J. Am. Chem. Soc.* **1992**, *114*, 2728. (b) Bäuerle, P.; Segelbacher, U.; Maier, A.; Mehring, M. *J. Am. Chem. Soc.* **1993**, *115*, 10217. (c) Graf, D. D.; Campbell, J. P.; Miller, L. L.; Mann, K. R. *J. Am. Chem. Soc.* **1996**, *118*, 5480. (d) Graf, D. D.; Duan, R. G.; Campbell, J. P.; Miller, L. L.; Mann, K. R. *J. Am. Chem. Soc.* **1997**. *119*, 5888.

(11)   (a) Nishinaga, T.; Wakamiya, A.; Yamazaki, D.; Komatsu, K. *J. Am. Chem. Soc.* **2004**, *126*, 3163. (b) Tateno, M.; Takase, M.; Iyoda, M.; Komatsu, K.; Nishinaga, T. *Chem. Eur. J.* **2013**, *19*, 5457. (c) Nishinaga, T; Yamazaki, D.; Tateno, M.; Iyoda, M.; Komatsu, K. *Materials* **2010**, *3*, 2037.

(11)   Fitzner, R.; Mena-Osteritz, E.; Mishra, A.; Schulz, G.; Reinold, E.; Weil, M.; Körner, C.; Ziehlke, H.; Elschner, C.; Leo, K.; Riede, M.; Pfeiffer, M.; Uhrich, C.; Bäuerle, P. *J. Am. Chem. Soc.* **2012**, *134*, 11064.

(12)   Takimiya, K.; Sakamoto, K.; Otubo, T.; Kunugi, Y. *Chem. Lett.* **2006**, *35*, 942.

(13)   *Electronic Materials: The Oligomer Approach*, Müllen, K.; Wegner, G.; Ed., Wiley, Weinheim, Germany, **1998**.

(14)   (a) Zen, A.; Bilge, A.; Galbrecht, F.; Alle, R.; Meerholz, K.; Grenzer, J.; Neher, D.; Scherf, U.; Farrell, T. *J. Am. Chem. Soc.* **2006**, *128*, 3914. (b) Bilge, A.; Zen, A.; Forster, M. ; Li, H.; Galbrecht, F.; Nehls, B. S.; Farrell, T.; Neher, D.; Scherf, U. *J. Mater. Chem.* **2006**, *16*, 3177.

(15)   (a) Ma, C.-Q.; Mena-Osteritz, E.; Debaerdemaeker, T.; Wienk, M. M.; Janssen, R. A. J.; Bäuerle, P. *Angew. Chem. Int. Ed.* **2007**, *46*, 1679. (b) Ma, C.-Q.; Fonrodona, M.; Schikora, M. C.; Wienk, M. M.; Janssen, R. A. J.; Bäuerle, P. *Adv. Funct. Mater.* **2008**, *18*, 3323. (c) Ma, C.-Q.; Mena-Osteritz, E.; Wunderlin, M.; Shulz, G.; Bäuerle, P. *Chem. Eur. J.* **2012**, *18*, 12880.

(16)   Marsella, M. J.; Yoon, K.; Tham, F. S. *Org. Lett.* **2001**, *3*, 2129.

(17)   Wang, Y.; Wang, Z.; Zhao, D.; Wang, Z.; Cheng, Y.; Wang, H. *Synlett* **2007**, *15*, 2390.

(18)   (a) Marsella, M. J.; Kim, I, T.; Tham, F. *J. Am. Chem. Soc.* **2000**, *122*, 974. (b) Marsella, M. J. *Acc. Chem. Res.* **2002**, *35*, 944.

(19) Sannicolò, F.; Mussini, P. R.; Benincori, T.; Cirilli, R.; Abbate, S.; Arnaboldi, S.; Casolo, S.; Castiglioni, E.; Longhi, G.; Martinazzo, R.; Panigati, M.; Pappini, M.; Procopio E. Q.; Rizzo, S. *Chem. Eur. J.* **2014**, *20*, 15298.

(20) Ashizawa, M.; Yu, Y.; Niimura, T.; Tsuboi, K.; Matsumoto, H.; Tanioka, A.; Mori, T. *Physica B* **2010**, *405*, S373.

(21) Ellinger, S.; Kreyes, A.; Ziener, U.; Hoffmann-Richer, C.; Landfester, K.; Möller, M. *Eur. J. Org. Chem.* **2007***, 5686.

(22) Shi, J.; Zhao, W.; Xu, L.; Kan, Y.; Li, C.; Song, J.; Wang, H. *J. Phys. Chem. C* **2014**, *118*, 7844.

(23) Araki, T.; Wakamiya, A.; Mori, K.; Yamaguchi, S. *Chem. Asian. J.* **2012**, *7*, 1594.

(24) Yoshida, S.; Fujii, M.; Aso, Y.; Otsubo, T.; Ogura, F. *J. Org. Chem.* **1994**, *59*, 3077.

(25) Asai, K.; Fukazawa, A.; Yamaguchi, S. *Chem. Commun.* **2015**, *51,* 6096.

Chapter 1

A Cyclic Octithiophene Containing β,β ′-Linkages

ABSTRACT. A cyclic octithiophene containing two β,β′-linkages was synthesized. Due to the large structural change in the excited state, this compound exhibited a bathochromically shifted fluorescence relative to the parent quaterthiophene. It also showed a small difference between the first and second oxidation potentials, indicative of spin delocalization through the β,β′-linkage in the one electron-oxidized state.

1.1 Introduction

Oligothiophenes represent a well-established scaffold for π-electron materials, as they demonstrate great potential for a wide variety of applications in organic electronics, including light-emitting diodes, field-effect transistors, and photovoltaics.[1] Most of the oligothiophenes reported to date contain thiophene units catenated in the α-positions, *i.e.* *via* α,α′-linkages, mostly because the π-conjugation is effectively extended through these α,α′-linkages. Apart from a number of linear α-oligothiophenes, cyclic α-oligothiophenes[2] and related macrocycles[3] have recently attracted substantial attention due to their intriguing π-conjugation in the circular topology. On the other hand, linkage in the β-positions affords oligothiophenes with swivel-cruciform,[4] twisted,[5] branched,[6] or tubular structures.[7] These characteristic structures are advantageous as they improve the solubility in common organic solvents[4] and afford control over the packing structure in the condensed phase.[6a]

For this study, the author designed a new type of cyclic oligothiophene, namely cyclic octithiophene **1**, containing two β,β′-linkages (Figure 1-1). This compound can be regarded as the cyclic dimer of α-quaterthiophenes. In contrast to the cyclic α-oligothiophenes, which serve as model compounds for polythiophene with infinite π-conjugation, compound **1** should furnish the opportunity to investigate the intrinsic nature of the π-conjugation *via* β,β′-linkages. During the course of this study, Sannicolò and co-workers reported similar cyclic oligothiophenes, cyclic oligo(sexithiophene)s connected *via* 3,3′-bi(benzothiophene) units, which represent a new type of chiral macrocycles.[8] A notable difference to the compounds in their study is that compound **1** consists of merely eight thiophene rings. In such a small ring skeleton, the π-conjugation *via* the β,β′-linkages should affect the electronic properties of **1** to a greater extent. In this chapter, the synthesis of cyclic octithiophene **1**, its crystal structure, and a comparison of its photophysical and electrochemical properties with those of the α-quaterthiophene **2** are reported. The combination of detailed experimental and theoretical studies allows a in-depth description of the π-conjugation through the β,β′-linkages in the excited state as well as in the one electron-oxidized state.
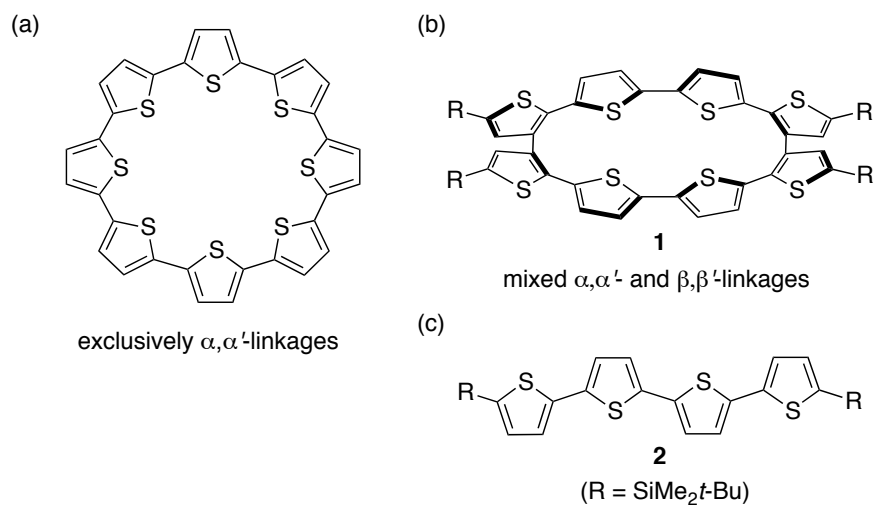
Figure 1-1. (a), (b) Connection modes of cyclic oligothiophene, and (c) a substructure of the cyclic oligothiophene **1**.

1.2 Results and Discussion

The targeted cyclic oligothiophene **1** was obtained from the dimerization of quaterthiophene **3** *via* the formation of a cyclic diarylplatinum complex **5**, followed by a reductive elimination (Scheme 1-1).[2f,9–11] This method is well known as an efficient synthetic route to macrocyclic π-conjugated skeletons, such as cyclic α-oligothiophenes,[2f] cyclic oligo(*p*-phenylene)s,[9] and related compounds.[10,11] Quaterthiophene **3** was chosen as the starting material for the synthesis of **1**, as it already contains a pre-established β,β′-linkage between two thiophene moieties. Compound **3** was dilithiated with *n*-BuLi, followed by treatment with Me$_3$SnCl. Distannylated quaterthiophene **4** was subsequently treated with Pt(cod)Cl$_2$ in THF under high dilution conditions (4 mM, reflux, 3 days) to produce a precipitate, which contained diarylplatinum complex **5**. This mixture was treated with 1,1′-bis(diphenylphosphino)ferrocene (dppf) in order to substitute the 1,5-cyclooctadiene (cod) ligand. An ensuing treatment with PPh$_3$[12] successfully promoted a reductive elimination to yield cyclic octithiophene **1** in 68%.

Scheme 1-1. One-pot synthesis of cyclic octithiophene **1**.

Single crystals of **1** suitable for X-ray crystallographic analyses were obtained by recrystallization from 1-methylnaphthalene. In the crystal structure, **1** adopts an elliptical shape with two α-quaterthiophene substructures along the major axis (Figure 1-2 and 1-19). The molecular framework of **1** has a symmetry center and therefore no axial chirality exists in this system in contrast to the similar macrocyclic oligothiophenes.[8] Notably, both of the α-quaterthiophene substructures assume an all-*s*-cis conformation, in which the central 2,2′-bithiophene moieties exhibit high degrees of planarity, reflected in dihedral angles of 8.7(2)° between the two mean thiophene planes. Conversely, the outer 2,2′-bithiophene moieties are highly twisted, as evident from dihedral angles of 50.5(1)° and 57.9(1)° between the two mean thiophene planes. These α-quaterthiophene substructures are connected to each other *via* β,β′-linkages, whereby the 3,3′-bithiophene moieties adopt a highly twisted conformation with dihedral angles of 55.1(1)°. As a consequence of this connecting motive, the central planar 2,2′-bithiophene moieties within the α-quaterthiophene substructures are fixed in a close face-to-face fashion. The interatomic distance between the C1 and C5 atoms is only 3.30 Å, which is shorter than the sum of the van der Waals radii of two carbon atoms (3.40 Å). The variable-temperature ^{1}H NMR spectra of **1** showed a pair of doublet peaks for the central 2,2′-bithiophene moiety at 130 °C, whereas one of the doublet peak broadened at 40 °C (Figure 1-3). This result suggests

that the free rotation of the thiophene rings within this ellipsoid cyclic skeleton is partly hindered at ambient temperature.
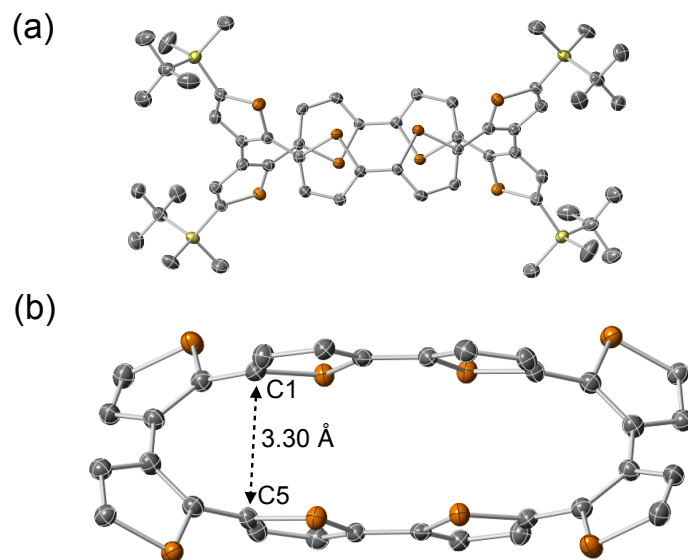

Figure 1-2. X-ray crystal structure of **1** (thermal ellipsoids at 50% probability): (a) a top view and (b) a side view. All hydrogen atoms as well as the silyl groups in (b) are omitted for clarity (color code : grey = C, orange = S, yellow = Si).
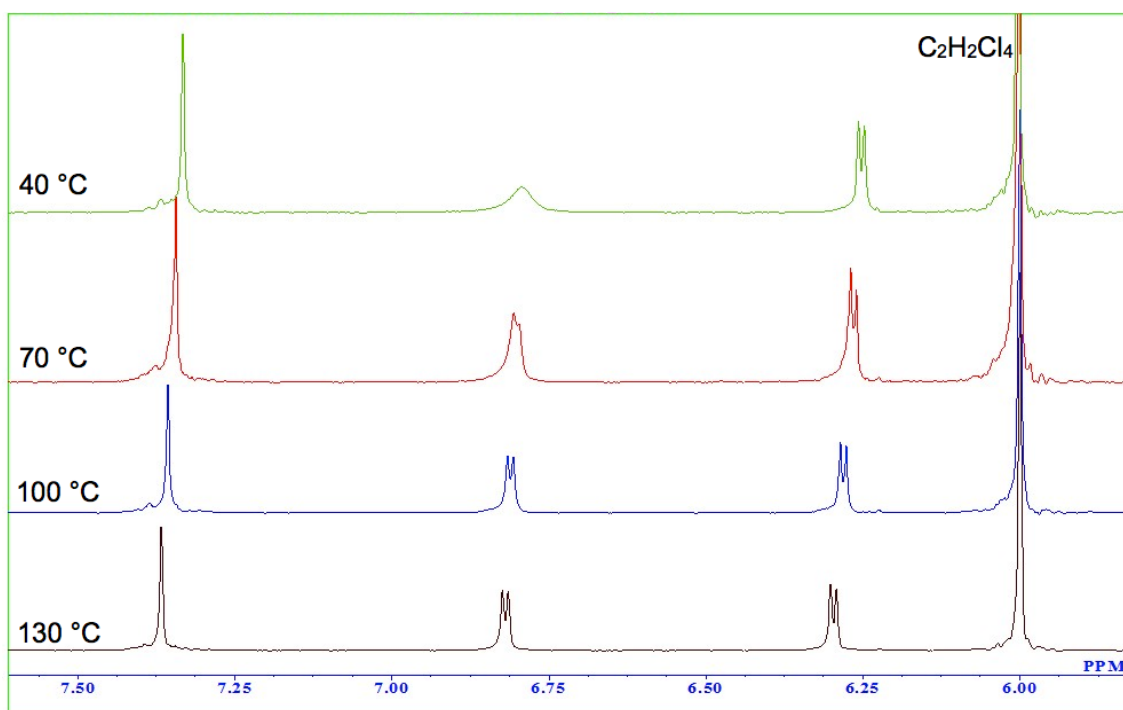

Figure 1-3. ^{1}H NMR spectrum of **1** (400 MHz, $C_2D_2Cl_4$,) at various temperatures ranged from 6.0 ppm to 7.5 ppm.

UV-vis absorption spectrum of **1** in CH_2Cl_2 showed an intense absorption band (λ_{abs} = 367 nm), which is by ca. 35 nm hypsochromically shifted relative to planar quaterthiophene **2**, reflecting the twisted conformation of the α-quaterthiophene substructure in **1** (Table 1-1 and Figure 1-4). In contrast to that, the fluorescence spectra of **1** showed a significantly bathochromically shifted fluorescence band (λ_{em} = 516 nm; green) relative to that of quaterthiophene **2** (λ_{em} = 465 nm; blue). Correspondingly, the Stokes shift is significantly larger for cyclic oligothiophene **1** (7870 cm^{-1}) than for **2** (3370 cm^{-1}). The fluorescence quantum yield of **1** in CH_2Cl_2 is 0.02, and the fluorescence spectra of **1** did not show any significant solvent dependence ($\lambda_{em/toluene}$ = 518 nm; $\lambda_{em/THF}$ = 515 nm, Figure 1-5).
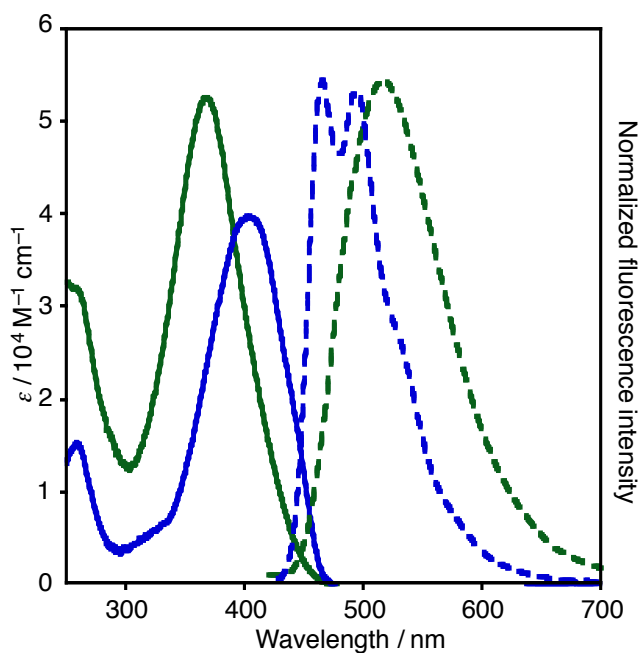

Figure 1-4. Absorption (solid line) and fluorescence spectra (dashed line) of **1** (green) and **2** (blue) in CH_2Cl_2.

Table 1-1. Photophysical and Electrochemical Properties of **1** and **2** in CH_2Cl_2

Cmpd	λ_{abs} [nm][a]	$\varepsilon / 10^4$ [$M^{-1}cm^{-1}$][b]	λ_{em} [nm][c]	Φ_F[d]	$E_{1/2}^{ox}$ [V][e]
					+0.50
1	367	5.27	516	0.02	+0.77
					+1.01
2	402	3.98	465	0.18	+0.48
					+0.82

[a] Maximum absorption wavelengths; [b] molar absorption coefficients; [c] maximum emission wavelengths of the highest energy fluorescence band when exciting **1** (370 nm) and **2** (400 nm); [d] absolute fluorescence quantum yields determined by a calibrated integrating sphere system; [e] oxidation potential vs. Fc/Fc$^+$; CV measurements were conducted in CH_2Cl_2 with $Bu_4NPF_6^-$ (0.1 M) as a supporting electrolyte at a scan rate of 0.1 Vs^{-1}.
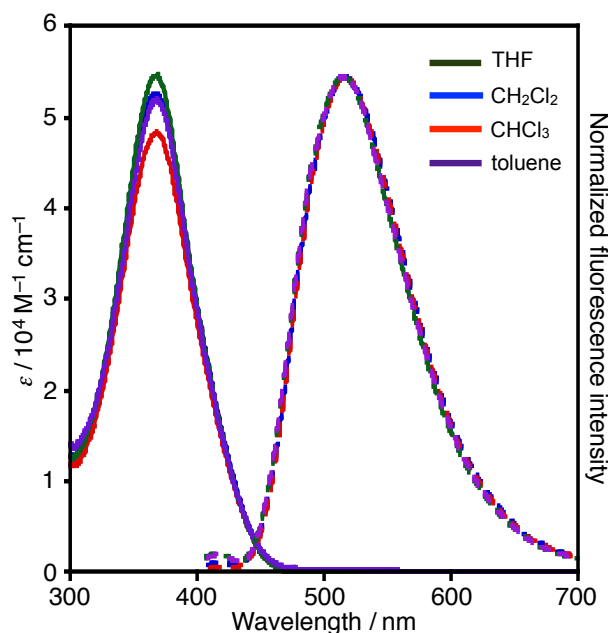
Figure 1-5. Absorption (solid line) and fluorescence spectra (dashed line) of **1** in various solvents.

To gain an insight into the origin of the large Stokes shift observed for **1**, the author carried out DFT calculations on model compound **1′** and **2′**, where the SiMe$_2$t-Bu groups were substituted with SiMe$_3$ groups (Figures 1-6, 1-7, 1-21, and 1-24). Geometry optimizations at the PBE0/6-31G(d) level of theory revealed that the

energetically most favourable conformation is not the one observed in the crystal structure, but one adopting a 1.5 kcal mol^{-1} more stable *s*-cis,*s*-trans,*s*-cis conformation within the α-quaterthiophene substructure (Figure 1-7). On the basis of the geometry of this conformer, TD-DFT calculation was carried out at the same level of theory (Tables 1-2 and 1-3, and Figure 1-8). The absorption band observed for **1** at 367 nm should be assigned to the HOMO–1→LUMO+1 transition (S$_4$), which is associated with a high oscillator strength (f = 1.67). On the other hand, the lowest excited singlet state (S$_1$) resulting from of the HOMO→LUMO+1 transition is forbidden, which is reflected in a very low f value (0.0531). Geometry optimization in S$_1$ was conducted at the PBE0/6-31G(d) level of theory (Figures 1-9, 1-22–1-23, and 1-25–28). Most notably, both of the α-quaterthiophene moieties and the 3,3′-bithiophene moieties become flattened upon changing from S$_0$ to S$_1$, which is reflected in the decrease in the dihedral angles of the two mean thiophene planes in the 3,3′-bithiophene moieties (S$_0$ = 55.1°, S$_1$ = 45.3°) (Figure 1-9). In S$_1$, the α-quaterthiophene moieties exhibit a more pronounced quinoidal character relative to S$_0$. Moreover, the bond length of the β,β′-linkages in the 3,3′-bithiophene moieties is slightly contracted in S$_1$ (1.457 Å) compared to S$_0$ (1.475 Å). Consequently, the bond alternation in the entire π-conjugated skeleton in the cyclic octithiophene framework decreases in S$_1$, despite including the β,β′-linkages. This substantial structural change is most likely responsible for the bathochromically shifted fluorescence of **1** relative to **2**. Similar observations have been reported for other highly strained cyclic oligoarenes.[3e,13]

Figure 1-6. Energy diagram of the various conformers of **2′** optimized at the PBE0/6-31G(d) level. Hydrogen atoms are omitted for clarity.
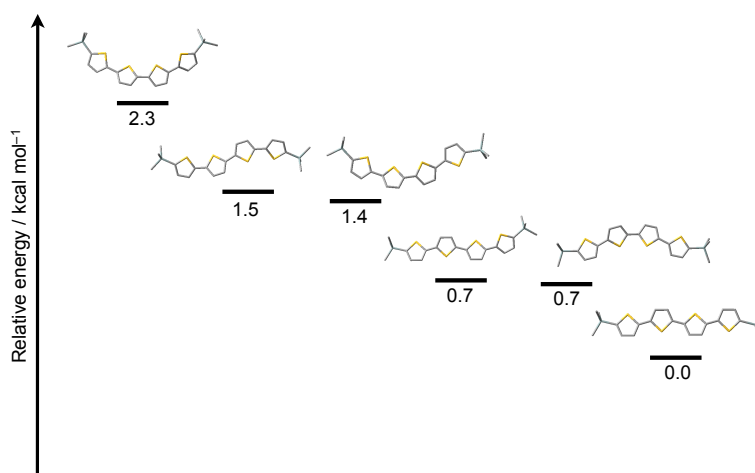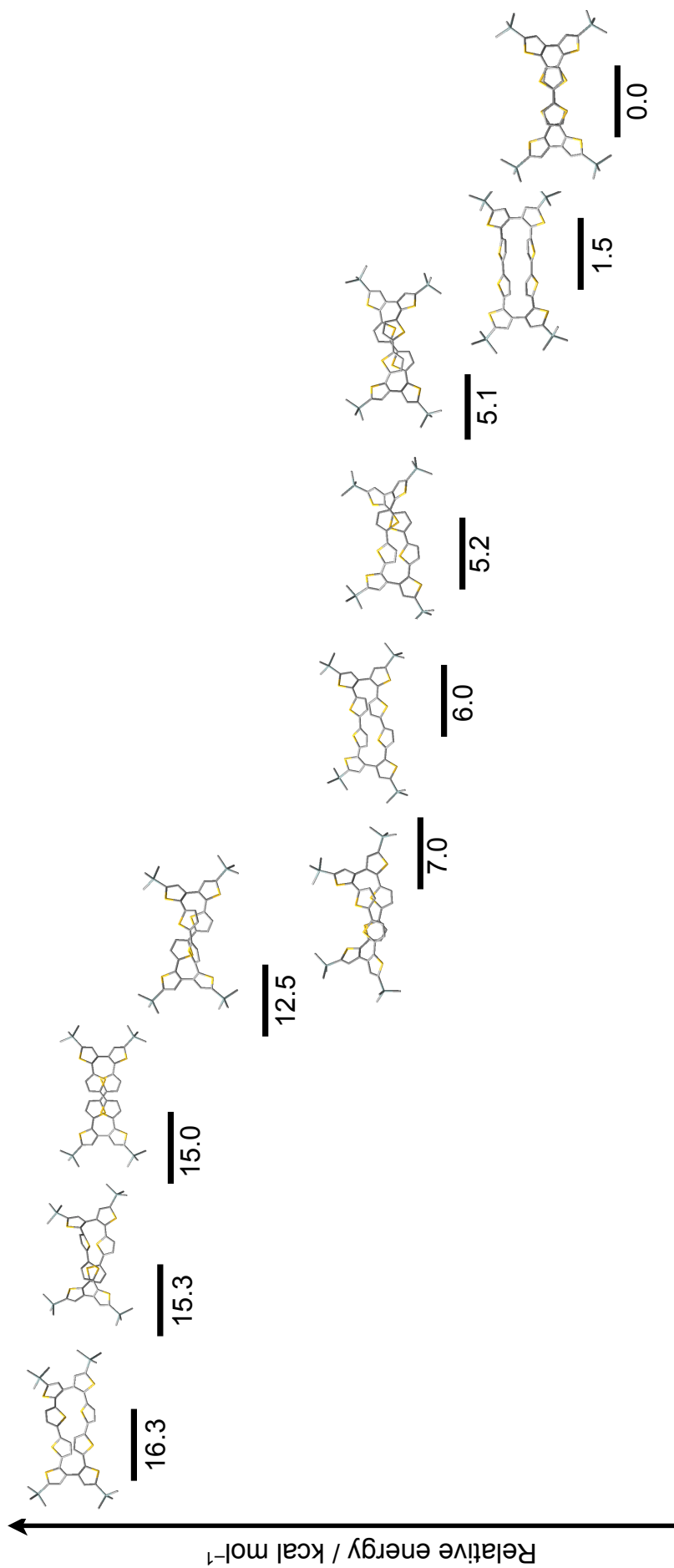
Figure 1-7. Energy diagram of the various conformers of **1′** optimized at the PBE0/6-31G(d) level. Hydrogen atoms are omitted for clarity.
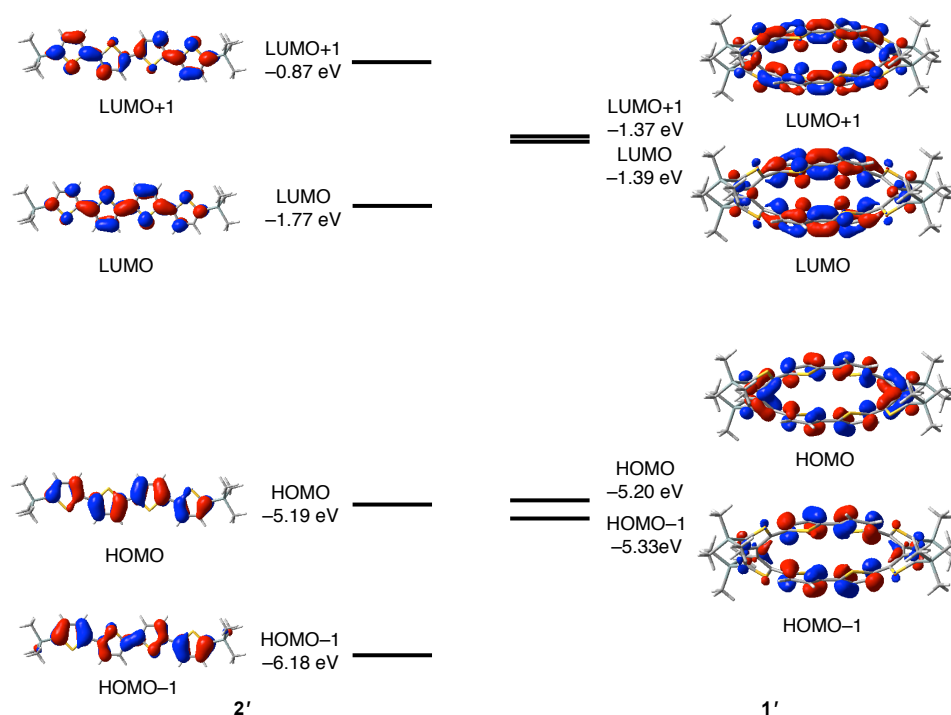
Figure 1-8. Kohn-Sham molecular orbitals of **1′** and **2′** in the neutral state calculated at the PBE0/6-31G(d) level. Hydrogen atoms are omitted for clarity.

Table 1-2. Excitation Energies of **1′** Calculated at the PBE0/6-31G(d) Level

excited state	transition energy [eV] (wavelength [nm])	main CI coefficient	oscillator strength f
1	3.05 (406)	−0.20871 (HOMO‑1→LUMO) 0.66683 (HOMO→LUMO+1)	0.0531
2	3.17 (391)	0.33167 (HOMO‑1→LUMO+1) 0.62021 (HOMO→LUMO)	0.1698
3	324 (382)	0.67134 (HOMO‑1→LUMO) 0.21215 (HOMO→LUMO+1)	0.0272
4	3.40 (365)	0.61841 (HOMO‑1→LUMO+1) −0.32946 (HOMO→LUMO)	1.6735
5	3.71 (335)	0.22751 (HOMO‑2→LUMO+1) 0.66002 (HOMO→LUMO+2)	0.0431

Table 1-3. Excitation Energies of **2′** Calculated at the PBE0/6-31G(d) Level

excited state	transition energy [eV] (wavelength [nm])	main CI coefficient	oscillator strength f
1	2.95 (421)	0.70485 (HOMO→LUMO)	1.5779
2	3.72 (333)	−0.39778 (HOMO‑1→LUMO)	0.0004
		0.57309 (HOMO→LUMO+1)	
3	4.01 (309)	0.57723 (HOMO‑1→LUMO)	0.0042
		0.39497 (HOMO→LUMO+1)	
4	4.51 (275)	−0.22431 (HOMO‑6→LUMO)	0.0068
		0.19080 (HOMO‑3→LUMO)	
		0.60446 (HOMO→LUMO+2)	
		−0.15662 (HOMO→LUMO+4)	
5	4.63 (268)	0.14271 (HOMO‑4→LUMO)	0.0026
		0.66738 (HOMO‑2→LUMO)	
		0.10705 (HOMO→LUMO+3)	
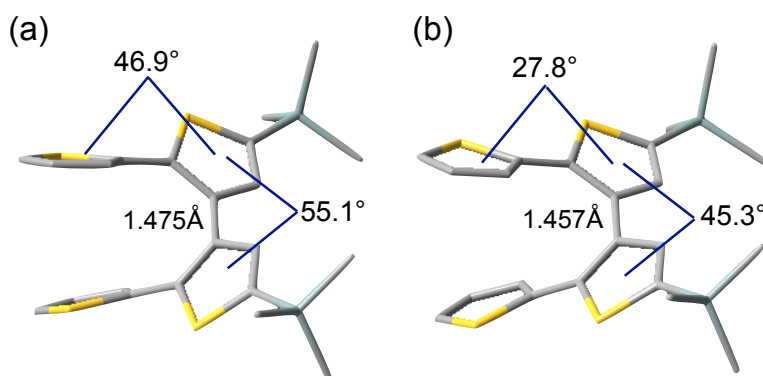
Figure 1-9. Structural changes in the quaterthiophene substructures of **1'** (R = SiMe$_3$) between (a) S$_0$ and (b) S$_1$. The geometries were optimized at the PBE0/6-31G(d) level of theory.

Cyclic voltammetry (CV) measurements between −1.0 V and 1.5 V showed three-step redox waves with $E_{1/2}$ at +0.50 V, +0.77 V, and +1.01 V for **1**. For α-quaterthiophene **2**, two-step redox waves were observed at $E_{1/2}$ = +0.48 V and +0.82 V (Figure 1-10). Differential pulse voltammogram of **1** also showed three

distinct peaks corresponding to the redox waves in CV (Figure 1-11), demonstrating that each wave is attributable to a one-electron process. The difference between the first and second oxidation potentials in **1** (+0.27 V) is smaller than that in **2** (+0.34 V), indicating that the π-conjugation in the radical cation **1**$^{•+}$ is not confined within one α-quaterthiophene moiety, but extends, at least in part, over the two α-quaterthiophene moieties.
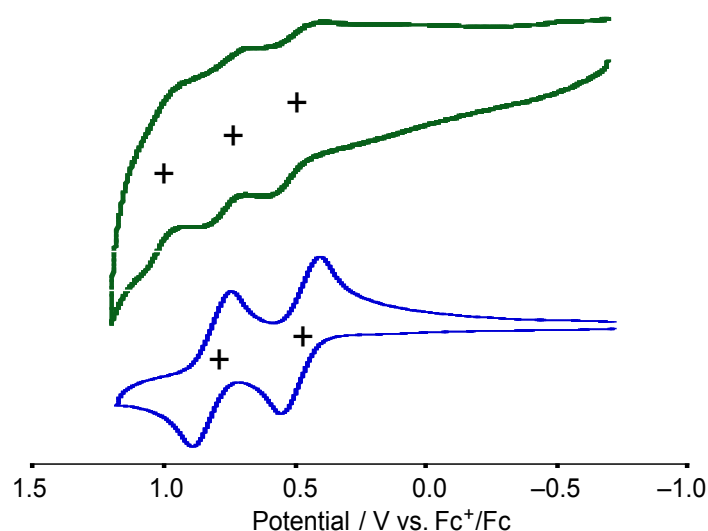
Figure 1-10. Cyclic voltammograms of **1** (green) and **2** (blue) at a scan rate of 0.1 V s^{-1} in CH$_2$Cl$_2$ with Bu$_4$NPF$_6$ as the supporting electrolyte. All oxidation potentials are referenced vs. Fc / Fc$^+$.
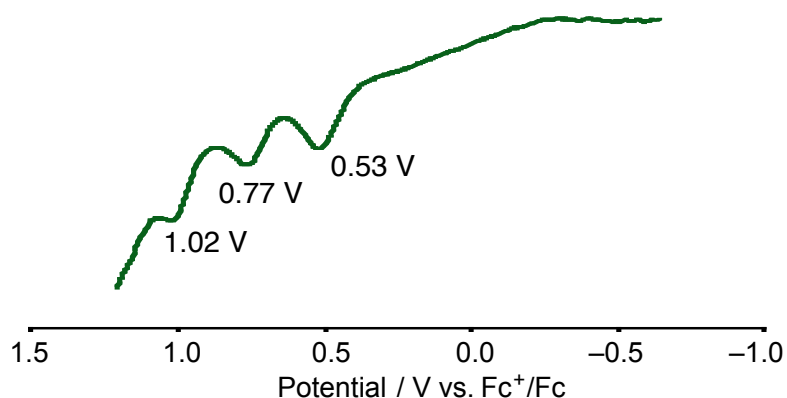

Figure 1-11. Differential pulse voltammogram of **1** at a scan rate of 0.1 V s^{-1} in CH$_2$Cl$_2$ with Bu$_4$NPF$_4$ as a supporting electrolyte. All oxidation potentials are referenced by Fc/Fc$^+$.

To experimentally examine the π-conjugation in radical cation **1**[·+], cyclic octithiophene **1** and quaterthiophene **2** were chemically oxidized using tris(*p*-bromophenyl)aminium hexachloroantimonate[14] and their EPR spectra were compared (Figure 1-12). Upon addition of 1.1 equivalents of the oxidant to **2** in CH₂Cl₂ at ambient temperature, **2** exhibited strong absorption bands at 673 nm and 1115 nm, which seems feasible for a hitherto known quaterthiophene radical cation.[15] Compound **1** also featured emerging broad absorption bands at 659 nm and 1248 nm upon addition of 1.1 equivalents of the oxidant. These characteristic absorption bands are almost identical to those of the corresponding radical cations generated by the electrochemical oxidation (Figure 1-13 and Table 1-4).
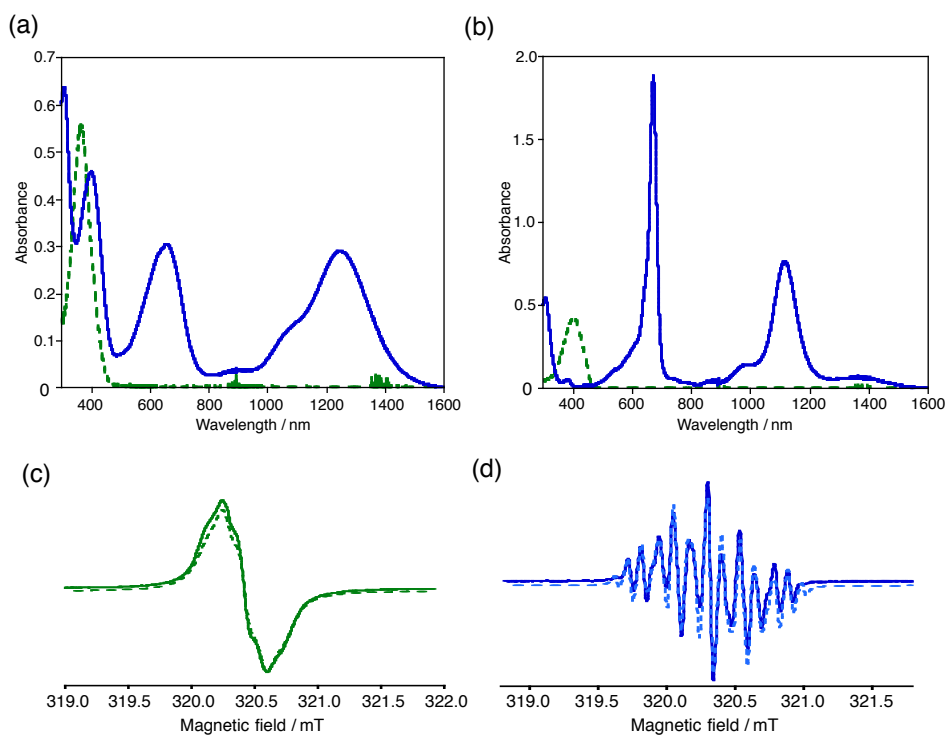

Figure 1-12. UV-vis-NIR absorption spectra of (a) **1** and (b) **2** before (dashed line) and after (solid line) the addition of 1.1 equivalents of (*p*-BrC₆H₄)₃N[·+]SbCl₆^{−} in CH₂Cl₂. EPR spectra of (c) **1** and (d) **2** in CH₂Cl₂ after addition of 1.1 equivalents of (*p*-BrC₆H₄)₃N[·+]SbCl₆^{−} (solid line) and simulated spectra (dashed line).
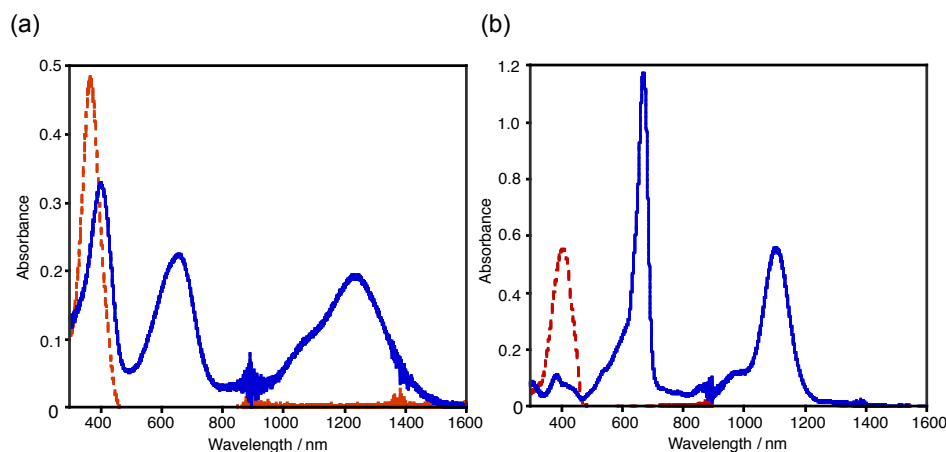
Figure 1-13. UV-vis-NIR absorption spectra of (a) **1** before oxidation (broken line) and upon oxidation at + 0.64 V (solid line) and (b) **2** before oxidation (broken line) and upon oxidation at +0.67 V (solid line) in CH_2Cl_2 with Bu_4NPF_4 as a supporting electrolyte. All oxidation potentials are referenced by Fc/Fc^+.

Table 1-4. Electrochemical Absorption in CH_2Cl_2

cmpd	potential [V]	λ_{abs} [nm]
1	+ 0.64	401, 654, 1229
2	+0.67	671, 1103

As the products of the chemical oxidation of **1** and **2** are both EPR active, we concluded that the corresponding radical cations **1**$^{•+}$ and **2**$^{•+}$ were generated *in situ* under these conditions. While the EPR spectrum of **2**$^{•+}$ displayed a distinct hyperfine structure (g = 2.0023), that of **1**$^{•+}$ exhibited a broad signal (g = 2.0023). The simulation of the latter EPR signal, taking account of the spin densities derived from DFT calculations, gave the hyperfine coupling constants $|a_H|$ of 0.126 mT (4H) as a major contribution together with two minor coupling constants, which are much smaller than the line width of the simulated signal (0.12 mT) (Table 1-5). Since these values are relatively smaller than those of **2**$^{•+}$ (0.26 mT, 0.23 mT, 0.11 mT, and 0.08 mT), the unpaired electron spin of **1**$^{•+}$ is likely delocalized over the entire cyclic π-conjugated skeleton.

Table 1-5. Hyperfine Coupling Constants of $1^{\bullet+}$ and $2^{\bullet+}$

cmpd	coupling constant (spin density)[a]
$1^{\bullet+}$	0.126 mT (0.048)
	0.015 mT (0.006)
	0.013 mT (0.005)
$2^{\bullet+}$	0.259 mT (0.098)
	0.228 mT (0.086)
	0.105 mT (0.040)
	0.089 mT (0.034)

[a] Estimated with McConnell's equation: $a_H = Q\rho$, $(Q = -2.64 \text{ mT})$.[16]

The spin concentration upon the addition of the oxidant into a 1.0 mM solution of **1** in CH_2Cl_2 was determined to be 0.53 mM by EPR measurements using the standard curve of TEMPO solution in CH_2Cl_2 (Figures 1-14 and 1-15, and Table 1-6). Since the addition of 2.0 equivalents of the oxidant resulted the increase of spin concentration to 0.9 mM, the addition of 1.1 equivalents of oxidant does not produce the over-oxidized dicationic species but likely produces the mixture of $1^{\bullet+}$ and unreacted **1**.
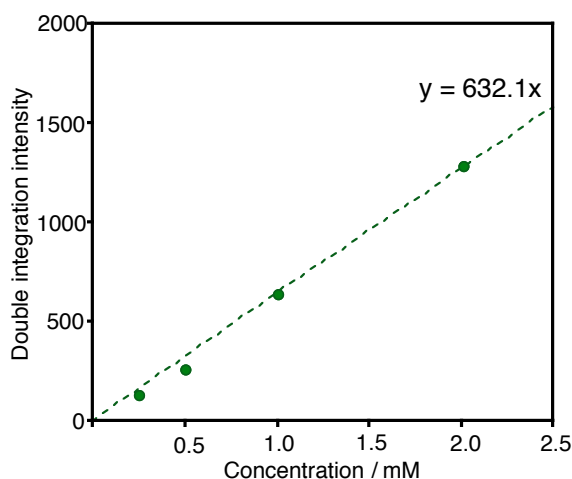

Figure 1-14. A plot of the EPR signal integration of TEMPO as a function of concentration in CH_2Cl_2. The obtained standard curve was used for the determination of spin concentration of $1^{\bullet+}$.
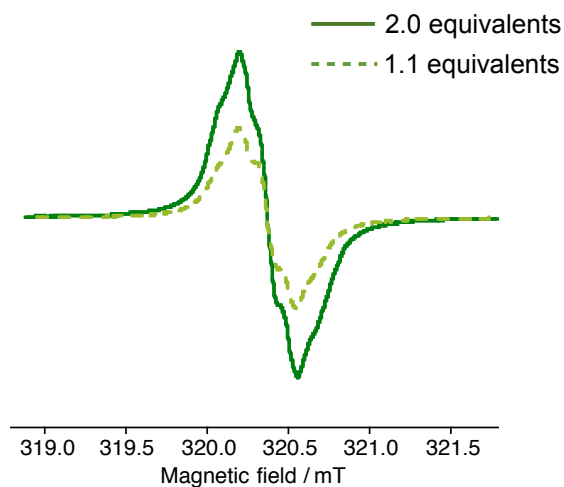
Figure 1-15. EPR spectra of **1** in CH_2Cl_2 after addition of 1.1 equivalents (broken line)and 2.0 equivalents (solid line) of $(p\text{-}BrC_6H_4)_3N^{\bullet+}SbCl_6^-$.

Table 1-6. Estimated Concentration of $\mathbf{1}^{\bullet+}$ after Addition of $(p\text{-}BrC_6H_4)_3N^{\bullet+}SbCl_6^-$

cmpd	Amount of $(p\text{-}BrC_6H_4)_3N^{\bullet+}SbCl_6^-$ [equivalent]	Ideal concentration of radical cation [mM]	Estimated concentration of radical cation [mM]
$\mathbf{1}^{\bullet+}$	1.1	1.0	0.53
	2.0	1.0	0.90

To gain an insight into the structural features of $\mathbf{1}^{\bullet+}$, the DFT calculation was performed on model compound $\mathbf{1'}^{\bullet+}$, whose geometry was optimized at the UB3LYP/6-31G(d) level of theory (Figures 1-30–1-34). The bond length of the β,β′-linkages in the 3,3′-bithiophene moiety (1.475 Å) was observed to be shorter than that of neutral **1′** (1.483 Å). Concomitant with this change, the degree of bond alternation in the entire cyclic π-conjugated skeleton also decreased relative to uncharged **1**. This result indicates a significant contribution of a quinoidal resonance structure to the radical cation. Indeed, the calculations demonstrated that the spin densities on the peripheral carbon atoms in $\mathbf{1'}^{\bullet+}$ are smaller than those in $\mathbf{2'}^{\bullet+}$ (Figures 1-16–1-18). Specifically, the unpaired electron in $\mathbf{1'}^{\bullet+}$ is delocalized over the entire cyclic skeleton. This result is in good agreement with the observation of a broad signal in the EPR spectrum.

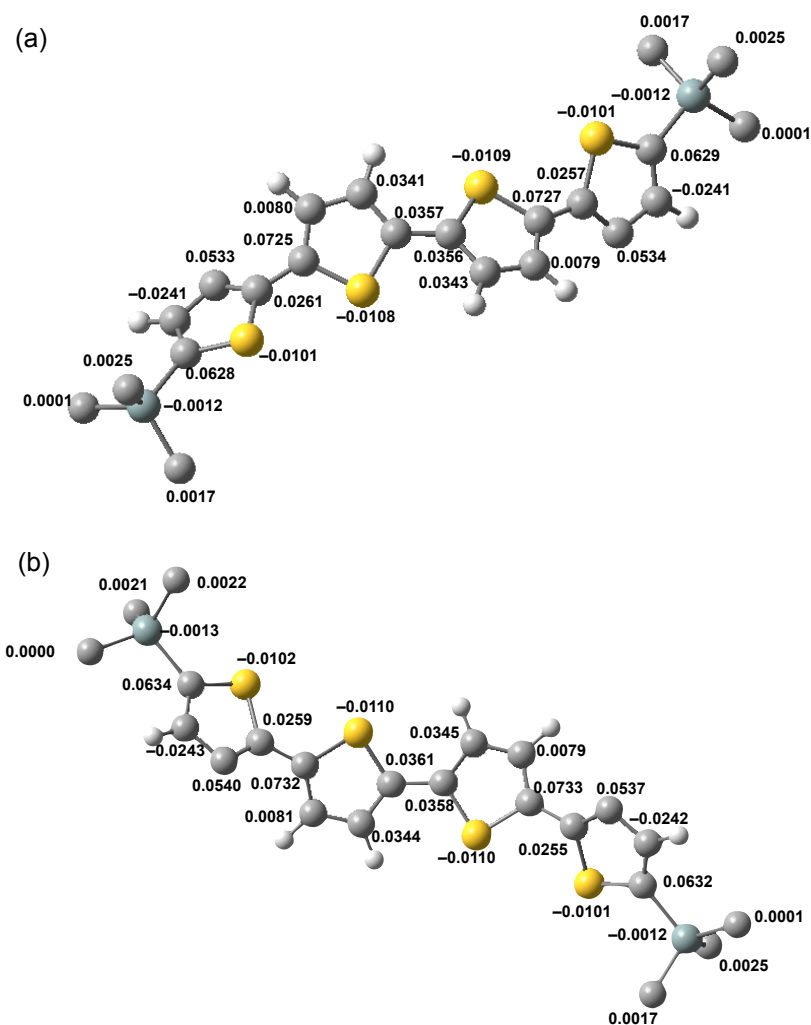**Figure 1-16.** Spin densities of **1**$^{\bullet+}$ calculated at the UB3LYP/6-31G(d) level: (a) one of the quaterthiophene substructures and (b) the other quaterthiophene. Hydrogen atoms on Me$_3$Si groups are omitted for clarity.
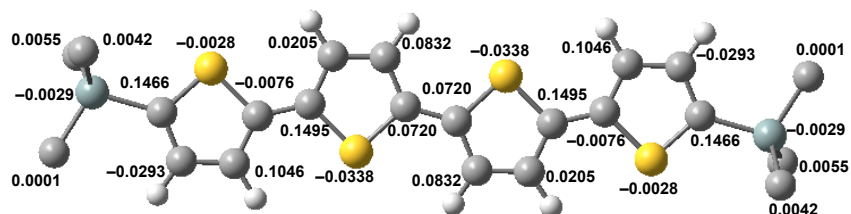

Figure 1-17. Spin densities of **2**$^{\bullet+}$ calculated at the UB3LYP/6-31G(d) level. Hydrogen atoms on Me$_3$Si groups are omitted for clarity.
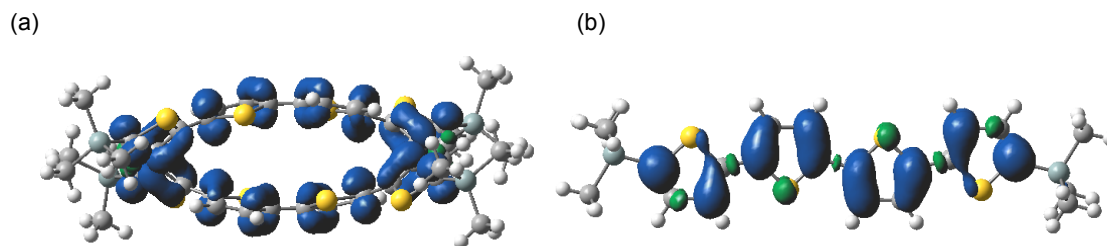
(a)   (b)

Figure 1-18. Spin density distribution of compounds (a) **1**$^{•+}$ and (b) **2**$^{•+}$, calculated at the UB3LYP/6-31G(d) level (isovalue = 0.001).

1.3 Conclusion

A cyclic octithiophene containing β,β′-linkages has been successfully synthesized. Macrocycle **1** can be regarded as the dimer of α-quaterthiophenes connected *via* highly twisted 3,3′-bithiophene moieties. The change from the ground state into the excited state is accompanied by a large structural change of the nonplanar cyclic structure. As a consequence, **1** exhibited a bathochromically shifted fluorescence relative to the corresponding linear α-quaterthiophene. In the radical cation state, the π-conjugation is extended through the β,β′-linkages, resulting in extensive spin delocalization. Compound **1** moreover features an intriguing elliptical structure, which is different from previously reported cyclic α-oligothiophenes. This structural particularity may ultimately lead to various interesting solid-state properties. Further studies pursuing this research avenue are currently in progress in our laboratory and their results will be disseminated in due course.

1.4 Experimental Section

General. Melting points (mp) were determined with a Yanaco MP-S3 instrument (MP-S3). Thermal gravimetric analyses (TGA) for the determination of the 5% weight loss temperature (T_{d5}) were conducted using a SII TGA6200 instrument. ^{1}H and ^{13}C{^{1}H} NMR spectra were recorded with a JEOL AL-400 spectrometer in CDCl$_3$, CD$_2$Cl$_2$ or C$_2$D$_2$Cl$_4$ (400 MHz for ^{1}H and 100 MHz for ^{13}C). The chemical shifts in ^{1}H NMR spectra are reported in δ ppm using the residual proton of the solvents, CHCl$_3$ (7.26 ppm), CH$_2$Cl$_2$, (5.32 ppm), and C$_2$H$_2$Cl$_4$ (6.00 ppm) as an internal standard. The chemical shifts in ^{13}C NMR spectra are reported in δ ppm using the solvent signals of CDCl$_3$ (77.16 ppm) as an internal standard. Electron paramagnetic resonance (EPR)

spectrum was measured with a JEOL JES-FA 200 ESR spectrometer in a sealed tube in CH_2Cl_2. Mass spectra were measured with a Bruker micrOTOF Focus spectrometer with the ionization method of APCI. Thin layer chromatography (TLC) was performed on plates coated with 0.25 mm thickness of silica gel $60F_{254}$ (Merck). Column chromatography was performed using PSQ100B (Fuji Silysia Chemicals). Anhydrous THF, CH_2Cl_2, toluene, and *i*-Pr$_2$NH were purchased from Kanto Chemicals and further purified by Glass Contour solvent systems. 5-(*t*-Butyldimethylsilyl)-2-bromothiophene,[17] 2-(4,4,5,5-tetramethyl-1,3,2-dioxaborolan-2-yl)thiophene,[18] 5,5′-dibromo-2,2′-bithiophene,[19] and Pd complex **10**[20] were prepared according to the literature methods. All reactions were preformed under a nitrogen or argon atmosphere, unless stated otherwise.
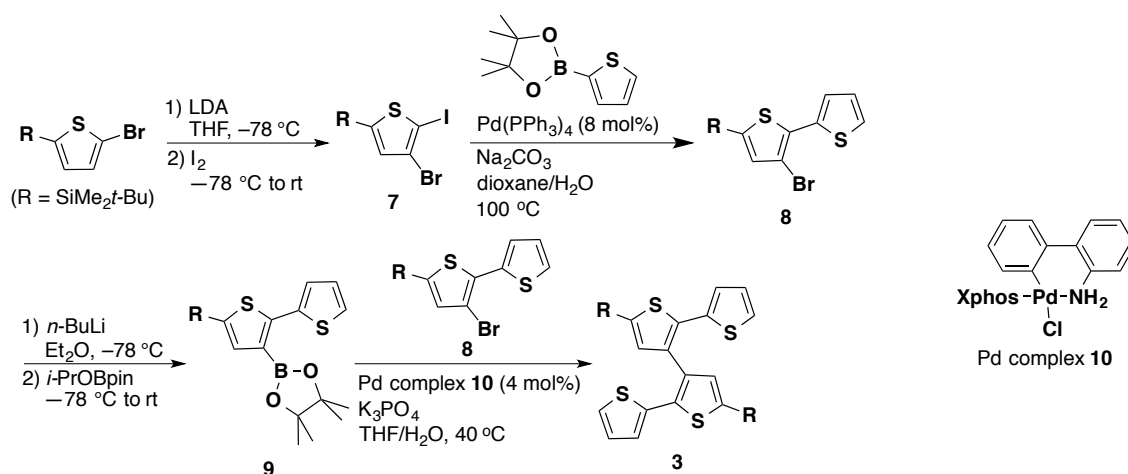
5-(*t*-Butyldimethylsilyl)-3-bromo-2-iodothiophene (7). To a solution of *i*-Pr$_2$NH (6.28 mL, 4.84 g, 47.5 mmol) in THF (14.4 mL) was added a hexane solution of *n*-BuLi (1.60 M, 29.7 mL, 47.5 mmol) at −78 °C, and the mixture was stirred for 1 h at −78 °C. The LDA solution thus prepared was added dropwise to a solution of 5-(*t*-butyldimethylsilyl)-2-bromothiophene (12.0 g, 43.3 mmol) in THF (54 mL) at −78 °C. The reaction mixture was stirred at the same temperature for 2 h and transferred into a solution of I$_2$ (16.4 g, 64.8 mmol) in THF (65 mL). The reaction mixture was allowed to warm to ambient temperature and stirred for 26 h. After addition of water (100 mL), the aqueous layer was extracted with Et$_2$O. The combined organic layer was washed with a 10wt% Na$_2$SO$_3$ solution, dried over MgSO$_4$, filtered, and concentrated under reduced pressure. The crude product was purified by column chromatography

(hexane, R_f = 0.75) to afford **7** as light yellow oil (15.1 g, 37.5 mmol, 87%). ^{1}H NMR (400 MHz, CDCl$_3$): δ 0.27 (s, 6H), 0.92 (s, 9H), 6.98 (s, 1H). ^{13}C{^{1}H} NMR (CDCl$_3$, 100 MHz): δ −5.1, 17.0, 26.3, 81.9, 121.8, 137.5, 146.1. HRMS (APCI): *m/z* Calcd. for C$_{10}$H$_{16}$^{79}BrISSi: 401.8965 ([*M*]$^+$). Obsd. 401.8978.

5-(*t*-Butyldimethylsilyl)-3-bromo-2,2′-bithiophene (8). To a solution of **7** (16.3 g, 40.4 mmol), 2-(4,4,5,5-tetramethyl-1,3,2-dioxaborolan-2-yl)thiophene (9.34 g, 44.5 mmol), and Pd(PPh$_3$)$_4$ (3.74 g, 3.24 mmol) in degassed dioxane (420 mL) was added a degassed 2M Na$_2$CO$_3$ aqueous solution (70 mL). The reaction mixture was stirred at 100 °C for 22 h. After addition of water (100 mL), the aqueous layer was extracted with CHCl$_3$ and washed with brine. The combined organic layer was dried over Na$_2$SO$_4$, filtered, and concentrated under reduced pressure. The crude product was purified by column chromatography (hexane, R_f = 0.50) to afford **8** as white solids (9.24 g, 25.7 mmol, 64%). Mp: 76.2–77.2 °C. ^{1}H NMR (400 MHz, CDCl$_3$): δ 0.30 (s, 6H), 0.95 (s, 9H), 7.08 (dd, *J* = 4.8, 4.0 Hz 1H), 7.10 (s, 1H), 7.35 (d, *J* = 4.8 Hz, 1H), 7.45 (d, *J* = 4.0 Hz, 1H). ^{13}C{^{1}H} NMR (100 MHz, CDCl$_3$): δ −5.1, 17.1, 26.4, 109.0, 126.2, 126.7, 127.4, 134.7, 137.1, 137.3, 139.3. HRMS (APCI): *m/z* Calcd. for C$_{14}$H$_{19}$^{79}BrS$_2$Si: 357.9875 ([*M*]$^+$). Obsd. 357.9892.

5-(*t*-Butyldimethylsilyl)-3-(4,4,5,5-tetramethyl-1,3,2-dioxaborolan-2-yl)-2,2′-bithiophene (9). To a solution of **8** (4.49 g, 12.5 mmol) in Et$_2$O (90 mL) was added a hexane solution of *n*-BuLi (1.65 M, 7.60 mL, 12.5 mmol) dropwise at −78 °C. The reaction mixture was stirred at the same temperature for 1.5 h, and then 2-isopropoxy-4,4,5,5-tetramethyl-1,3,2-dioxaborolane (2.80 mL, 2.55 g, 13.7 mmol) was added to the solution. The reaction mixture was warmed gradually to ambient temperature and stirred for 18 h. After addition of water (20 mL), the aqueous layer was extracted with Et$_2$O. The combined organic layer was washed with brine, dried over Na$_2$SO$_4$, filtered, and concentrated under reduced pressure. The crude product was recrystallized from MeOH to afford **9** as white solids (4.03 g, 9.91 mmol, 79%). Mp: 111.0–112.0 °C. ^{1}H NMR (400 MHz, CD$_2$Cl$_2$): δ 0.31 (s, 6H), 0.95 (s, 9H), 1.33 (s, 12H), 7.05 (dd, *J* = 5.2, 3.6 Hz 1H), 7.31 (dd, *J* = 5.2, 1.2 Hz, 1H), 7.43 (s, 1H), 7.45 (dd, *J* = 3.6, 1.2 Hz, 1H). ^{13}C{^{1}H} NMR (100 MHz, CDCl$_3$): δ −4.6, 17.0, 25.0, 26.6, 83.8, 125.8, 127.2, 127.4, 136.8, 137.2, 143.1, 151.6. HRMS (APCI): *m/z* Calcd. for

$C_{20}H_{31}BO_2S_2Si$: 406.1622 ($[M]^+$). Obsd. 406.1637.

5′,5″-Bis(*t*-butyldimethylsilyl)-2,2′:3′,3″:2″,2‴-quaterthiophene (3). To a solution of **8** (1.62 g, 4.51 mmol), **9** (2.01 g, 4.94 mmol), and Pd complex **10** (71.1 mg, 0.090 mmol) in THF (45 mL) was added a 0.5 M K_3PO_4 aqueous solution (18 mL). The reaction mixture was stirred at 40 °C for 2 h. After addition of water (15 mL), the aqueous layer was extracted with $CHCl_3$. The combined organic layer was washed with brine, dried over Na_2SO_4, filtered, and concentrated under reduced pressure. The crude product was purified by column chromatography (hexane, R_f = 0.18) to afford **3** as white solids (2.41 g, 4.31 mmol, 96%). Mp: 110.0–111.0 °C. ^{1}H NMR (400 MHz, $CDCl_3$): δ 0.29 (s, 12H), 0.94 (s, 18H), 6.85 (dd, *J* = 5.2, 4.0 Hz, 2H), 7.00 (d, *J* = 4.0, 0.8 Hz, 2H), 7.03 (s, 2H), 7.07 (d, *J* = 5.2, 0.8 Hz, 2H). ^{13}C{^{1}H} NMR ($CDCl_3$, 100Hz): δ −4.9, 17.1, 26.5, 125.1, 125.6, 127.0, 133.6, 135.7, 136.3, 138.7, 140.2. HRMS (APCI): *m/z* Calcd. for $C_{28}H_{38}S_4Si_2$: 558.1389 ($[M]^+$). Obsd. 558.1390.

Cyclic octithiophene (1). To a solution of **3** (534 mg, 0.955 mmol) in THF (7 mL) was added a hexane solution of *n*-BuLi (1.65 M, 1.25 mL, 2.06 mmol) at −78 °C. After the reaction mixture was stirred at the same temperature for 1.5 h, Me_3SnCl (398 mg, 2.00 mmol) in THF (1.8 mL) was added to the solution. The reaction mixture was warmed gradually to ambient temperature and stirred for 1.5 h. After addition of water (10 mL), the aqueous layer was extracted with EtOAc. The combined organic layer was dried over Na_2SO_4, filtered, and concentrated under reduced pressure. The resulting mixture was dissolved in THF (240 mL) and $Pt(cod)Cl_2$ (358 mg, 0.957 mmol) was added to the solution. The reaction mixture was stirred at reflux temperature for 3 days. The reaction mixture was cooled to ambient temperature and the precipitates were collected by filtration and washed with hexane. The obtained solid was dissolved in CH_2Cl_2 (160 mL) and 1,1′-bis(diphenylphosphino)ferrocene (530 mg, 0.956 mmol) was added to the solution. The reaction mixture was stirred at room temperature for 15 h. The solvent was removed under reduced pressure and the resulting mixture was dissolved in toluene (160 mL) and then PPh_3 (2.51 g, 9.57 mmol) was added to the solution. The reaction mixture was stirred at 95 °C for 20 h and cooled to ambient temperature. The precipitates were collected by filtration and washed with hexane and CH_2Cl_2. The crude product was recrystallized from chlorobenzene to afford **1** as yellow solids (361 mg,

0.324 mmol, 68%). TGA: T_{d5} = 434.6 °C. ^{1}H NMR (400 MHz, $C_2D_2Cl_4$, 130 °C): δ 0.45 (s, 24H), 1.11 (s, 36H), 6.30 (d, J = 3.6 Hz, 4H), 6.82 (d, J = 3.6 Hz, 4H), 7.37 (s, 4H). ^{13}C NMR spectrum was not obtained due to the poor solubility. HRMS (APCI): m/z Calcd. for $C_{56}H_{73}S_8Si_4$: 1113.2550 ([M+H]$^+$). Obsd. 1113.2501.
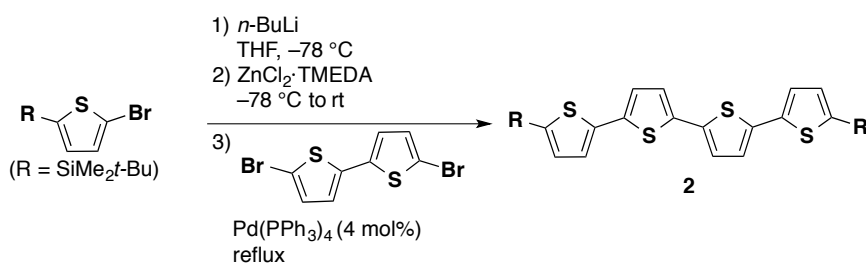
5′,5‴-Bis(*t*-butyldimethylsilyl)-2,2′:5′,2″:5″,2‴-quaterthiophene (2). To a solution of 5-(*t*-butyldimethylsilyl)-2-bromothiophene (157 mg, 0.566 mmol) in THF (2.7 mL) was added a hexane solution of *n*-BuLi (1.65 M, 0.370 mL, 0.610 mmol) at −78 °C. After stirring at the same temperature for 1.5 h, $ZnCl_2$(tmeda) (152 mg, 0.602 mmol) was added. The reaction mixture was allowed to warm to ambient temperature and stirred for 1.5 h. The mixture was transferred into a solution of 5,5′-dibromo-2,2′-bithiophene (80.7 mg, 0.249 mmol) and Pd(PPh$_3$)$_4$ (28.9 mg, 0.025 mmol) in THF (1.3 mL). The reaction mixture was stirred at reflux temperature for 13.5 h. After addition of a saturated aqueous NH_4Cl solution (5 mL), the aqueous layer was extracted with Et_2O. The combined organic layer was washed with brine, dried over Na_2SO_4, filtered, and concentrated under reduced pressure. The crude product was purified by column chromatography (hexane, R_f = 0.15) and recrystallized from hexane to afford to **2** as yellow solids (39.7 mg, 0.071 mmol, 29 %). Mp: 197.8–198.5 °C. ^{1}H NMR (400 MHz, CDCl$_3$): δ 0.31 (s, 12H), 0.95 (s, 18H), 7.07 (d, J = 3.6 Hz, 2H), 7.10 (d, J = 3.6 Hz, 2H), 7.14 (d, J = 3.6 Hz, 2H), 7.24 (d, J = 3.6 Hz, 2H). ^{13}C{^{1}H} NMR (CDCl$_3$, 100Hz): δ −4.8, 17.1, 26.5, 124.4, 124.6, 125.0, 136.1, 136.1, 136.5, 137.4, 142.3. HRMS (APCI): m/z Calcd. for $C_{28}H_{38}S_4Si_2$: 558.1389 ([M]$^+$). Obsd. 558.1386.

Chemical oxidation of 1. To a solution of **1** (5.6 mg, 5.0 μmol) in degassed and dehydrated CH_2Cl_2 (5 mL) was added tris(*p*-bromophenyl)aminium hexachloroantimonate (4.6 mg, 5.6 μmol) under an argon atmosphere. The mixture was stirred at ambient temperature for 1 h. The resulting solution of **1$^{•+}$** (ca. 1.0×10^{-3} M) was directly used for the EPR measurement. UV-vis-NIR measurement was carried out using a diluted solution of **1$^{•+}$** (ca. 1.0×10^{-4} M).

Chemical oxidation of 2. To a solution of **2** (2.8 mg, 5.0 μmol) in degassed and dehydrated CH_2Cl_2 (5 mL) was added tris(*p*-bromophenyl)aminium hexachloroantimonate (4.6 mg, 5.6 μmol) under argon atmosphere. The mixture was stirred at ambient temperature for 1 h. The solution of **2$^{•+}$** (ca. 1.0×10^{-3} M) was directly used for the for EPR measurement. UV-vis-NIR measurement was carried out using the diluted solution of **2$^{•+}$** (ca. 1.0×10^{-4} M).

X-ray Crystallographic Analysis

X-ray Data Collection of 1. Single crystals of **1** suitable for X-ray crystallographic analysis were obtained by recrystallization from 1-methylnaphthalene. Intensity data were collected at 123 K on a Rigaku X-ray diffractometer equipped with a molybdenum FR-X microfocus generator, VariMax-Mo optics, and a PILATUS 200K detector. Total of 29857 reflections were measured with the maximum 2θ angle of 55.0°, of which 6967 were independent reflections (R_{int} = 0.0566). The structure was solved by direct methods (SHELXS-2013) and refined by the full-matrix least-squares on F^2 (SHELXL-2013). All non-hydrogen atoms were refined anisotropically and all hydrogen atoms were placed using AFIX instructions. The crystal data are as follows: $C_{56}H_{72}S_8Si_4$; FW = 1113.98, crystal size 0.14 × 0.02 × 0.01 mm^3, monoclinic, *C2/c*, a = 43.196(17) Å, b = 6.377(2) Å, c = 24.5113(10) Å, β = 115.408(5)°, V = 6099(3) Å^3, Z = 4, D_c =1.213 g cm^{-3}, μ = 0.406 mm^{-1}, R_1 = 0.0617 ($I > 2\sigma(I)$), wR_2 = 0.2189 (all data), GOF = 1.115. CCDC 1043632.
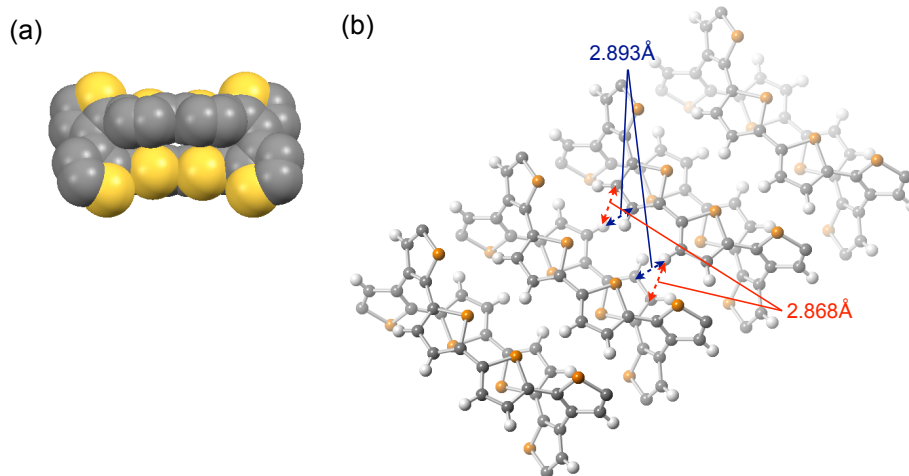
Figure 1-19. X-ray crystal structure of **1**: (a) Space filling model and (b) packing structure, where silyl groups are omitted for clarity.

Photophysical Measurements. UV-vis absorption spectra were measured with a Shimadzu UV-3150 spectrometer with a resolution of 0.5 nm using dilute sample solutions in spectral grade solvents in a 1 cm or 1 mm-thickness quartz cuvette. Emission spectra were measured with a Hitachi F-4500 spectrometer with a resolution of 1 nm. For the fluorescence measurement, the sample solutions were excited at 370 nm for **1** and 400 nm for **2**. Absolute fluorescence quantum yields were determined with a Hamamatsu Photonics C-9920-02 calibrated integrating sphere system.

Electrochemical Properties

Cyclic Voltammetry and Differential Pulse Voltammetry. Cyclic voltammetry (CV) and differential pulse voltammetry (DPV) measurements were performed on an ALS/chi-617A electrochemical analyzer. The CV cell consisted of a glassy carbon electrode, a Pt wire counter electrode, and an $Ag/AgNO_3$ reference electrode. The measurements were carried out under an argon atmosphere using CH_2Cl_2 solution of sample with a concentration of 0.1 mM (**1**) and 1 mM (**2**), and 0.1 M tetrabutylammonium hexafluorophosphate as a supporting electrolyte. The oxidation potentials were calibrated with ferrocene/ferrocenium ion couple.

Electrochemical Absorption Spectroscopy. Electrochemical absorption spectra of **1** and **2** were measured with a Shimadzu UV-3150 spectrometer with a resolution of 0.5 nm by cooperating with ALS/chi-617A electrochemical analyzer. The electrochemical cell consisted of 1 mm of thin layer quartz cell, a Pt mesh working electrode, a Pt wire counter electrode, and a $Ag/AgNO_3$ reference electrode. The measurements were carried out under flow of nitrogen gas using CH_2Cl_2 solution of sample with a concentration of ca. 0.1 mM (**1**) and 1 mM (**2**), and 0.1 M tetrabutylammonium hexafluorophosphate as a supporting electrolyte. The oxidation potentials were calibrated with ferrocene/ferrocenium ion couple. Electrochemical absorption spectra of **1** and **2** were recorded during oxidation at each oxidation potential.

EPR Measurements

Sample Preparation. The ca. 1.0×10^{-3} M solutions of **1** and **2** in CH_2Cl_2 with tris(*p*-bromophenyl)aminium hexachloroantimonate were prepared. The solutions were charged into a quartz EPR tube under an argon atmosphere and degassed by freeze-pump-thaw cycles. The tubes were sealed off under vacuum.

Analyses of the EPR Spectra. The obtained spectra were simulated with Lorentz functions. The spin densities of the carbon atoms adjacent to protons are estimated from McConnell's equation ($a_H = Q\rho$).[16] The splitting pattern of $\mathbf{2}^{\bullet+}$ can be explained by the presence of four kinds of hydrogen nuclei. The best-fit simulated spectrum was obtained by the hyperfine coupling constants $|a_H|$ of 0.259 mT (2H), 0.228 mT (2H), 0.105 mT (2H), and 0.089 mT (2H) (Figure 1-12(d) and Table 1-5). On the other hand, the chemically generated $\mathbf{1}^{\bullet+}$ showed a broad EPR signal without hyperfine structures, which is totally different from that of $\mathbf{2}^{\bullet+}$. In light of the spin densities derived from

DFT calculations (Figure 1-16), we assumed that the delocalization of spin density over the entire cyclic π framework might be responsible for the line broadening. Therefore, taking the results of DFT calculations into account, the author assumed that $1^{\bullet+}$ has three kinds of nonequivalent protons on the thiophene rings, i.e., H^a, H^b, and H^c,(Figure 1-20) and their coupling constants were simulated with Lorenz functions.
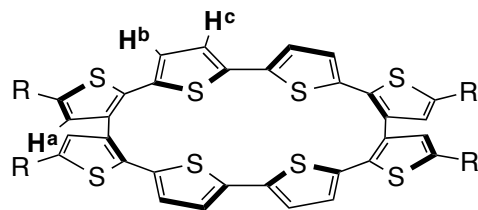

Figure 1-20. The positions of H^a, H^b, and H^c protons.

As a result, the best-fit simulated spectrum was obtained with a major contribution of the hyperfine coupling constant $|a_H|$ of 0.126 mT (4H) together with two minor coupling constants (0.015 mT and 0.013 mT), although the latter two values have less accuracy because they are too small compared to the line width of the major signal (0.12 mT). Since these values are much smaller than those of $2^{\bullet+}$, the corresponding spin densities in $1^{\bullet+}$ are likely smaller than those of $2^{\bullet+}$, supporting the effective delocalization of spin densities over the cyclic octithiophene framework.

Determination of the Spin Concentration. The concentration of radical cation of $1^{\bullet+}$ was determined using a standard curve obtained by the plot of the concentration of 2,2,6,6-tetramethylpiperidine-1-oxyl (TEMPO) versus the corresponding peak area (R^2 = 0.995). The peak area was determined using double integration.

Theoretical Calculations

Computational Method. The geometry optimizations of **1′** and **2′** in the ground state (S_0) were performed using PBE0 (Gaussian keyword: PBE1PBE) hybrid exchange-correlation functional[21] with the 6-31G(d) basis set[22] implemented in the Gaussian 09 program.[23] For the geometry optimizations, a stationary point was optimized without any symmetry assumptions and characterized by frequency analysis at the same level of theory (the number of imaginary frequencies, NIMAG, was 0). The energy calculations and geometry optimizations of **1′** and **2′** in the first excited singlet state (S_1) were performed using the time-dependent PBE0 method implemented in the

Gaussian 09 program. The Cartesian coordinates for **1′** and **2′** in S_0 and S_1 are given in Tables 1-7–1-10. TD-DFT vertical excitation calculations of **1′** and **2′** were performed using the optimized geometry at the PBE0/6-31G(d) level, implemented in the Gaussian 09 program. The geometry optimizations of **1**$^{•+}$ and **2**$^{•+}$ were performed using UB3LYP functional[24] with 6-31G(d) basis set implemented in the Gaussian 09 program and the obtained structures were compared with those of the neutral state optimized with the B3LYP functional. The Kohn-Sham molecular orbitals of **1**$^{•+}$ and **2**$^{•+}$ are illustrated in Figures 1-35 and 1-36. TD-DFT vertical excitation calculations of **1**$^{•+}$ and **2**$^{•+}$ were performed using the optimized geometry at the UB3LYP/6-31G(d) level, implemented in the Gaussian 09 program. The Cartesian coordinates for **1′** and **2′** in the neutral state and in the radical cation state are given in Tables 1-11–1-14.

Figure 1-21. Selected bond lengths, interatomic distances, and dihedral angles for the optimized structure of **1′** in S_0 calculated at the PBE0/6-31G(d) level. The distances are shown in Å. Hydrogen atoms are omitted for clarity.

Figure 1-22. Selected bond lengths, interatomic distances, and dihedral angles for the optimized structure of **1′** (S_1) calculated at the PBE0/6-31G(d) level. The distances are shown in Å. Hydrogen atoms are omitted for clarity.

Figure 1-23. Differences of bond lengths between **1′** (S_0) and **1′** (S_1) calculated at the PBE0/6-31G(d) level. The elongated bond length and shortened bond length from S_0 to S_1 are displayed in blue and red colors, respectively. The distances are shown in Å. Hydrogen atoms are omitted for clarity.

Figure 1-24. Selected bond lengths and dihedral angles for the optimized structure of **2′** in S_0 calculated at the PBE0/6-31G(d) level. The distances are shown in Å. Hydrogen atoms are omitted for clarity.

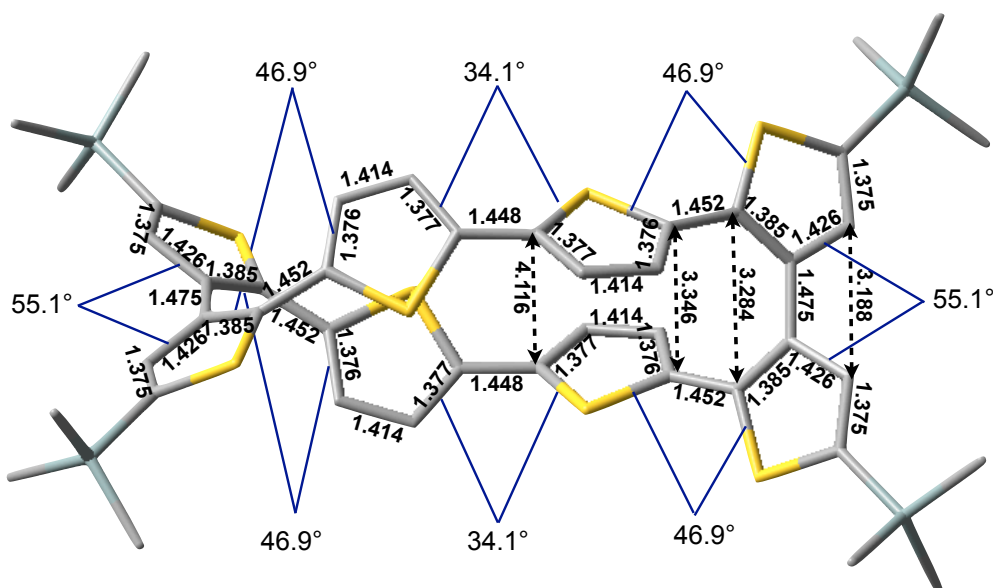**Figure 1-25.** Selected bond lengths and dihedral angles for the optimized structure of **2′** in S_1 calculated at the PBE0/6-31G(d) level. The distances are shown in Å. Hydrogen atoms are omitted for clarity.

Figure 1-26. Differences of bond lengths between **2′** (S_0) and **2′** (S_1) calculated at the PBE0/6-31G(d) level. The elongated and shortened bond lengths from S_0 to S_1 are displayed in blue and red colors, respectively. The distances are shown in Å. Hydrogen atoms are omitted for clarity.

Figure 1-27. Optimized structures of **1′** in S_0 and S_1 calculated at the PBE0/6-31G(d) level. TD-DFT vertical excitation in S_0 and vertical transition in S_1 with relative energies of the S_0 and S_1 states are shown. Hydrogen atoms are omitted for clarity.
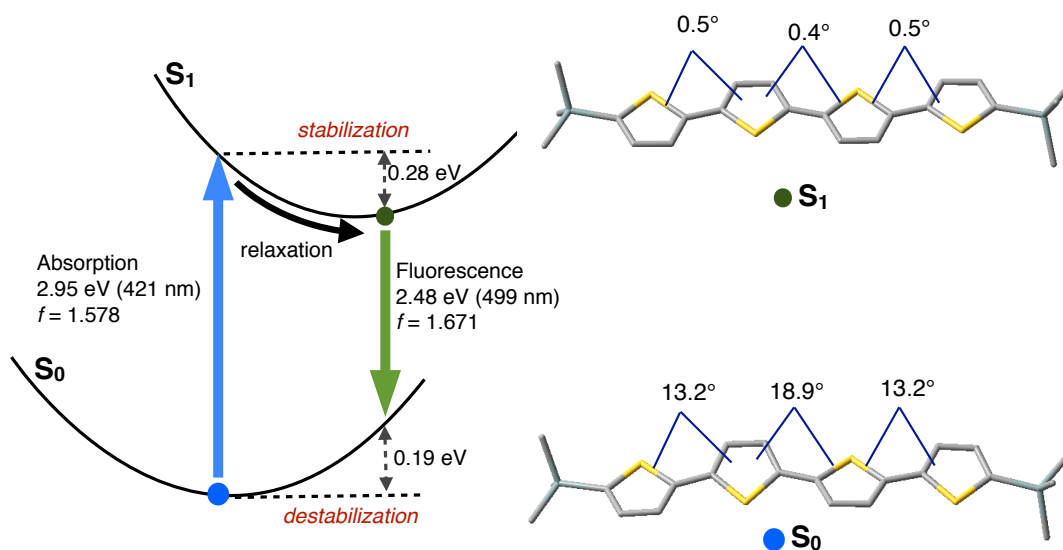
Figure 1-28. Optimized structures of **2′** in S_0 and S_1 at PBE0/6-31G(d) level. Hydrogen atoms are omitted for clarity. TD-DFT vertical excitation in S_0 and vertical transition in S_1 with relative energies of the S_0 and S_1 states are shown.

Figure 1-29. Selected bond lengths, interatomic distances, and dihedral angles for the optimized structure of neutral **1′** calculated at the B3LYP/6-31G(d) level. The distances are shown in Å. Hydrogen atoms are omitted for clarity.
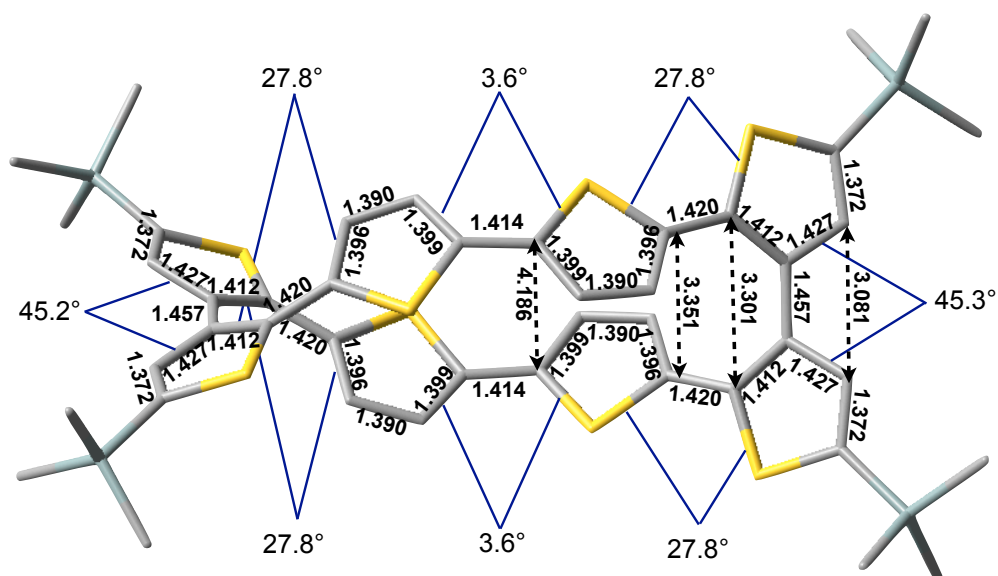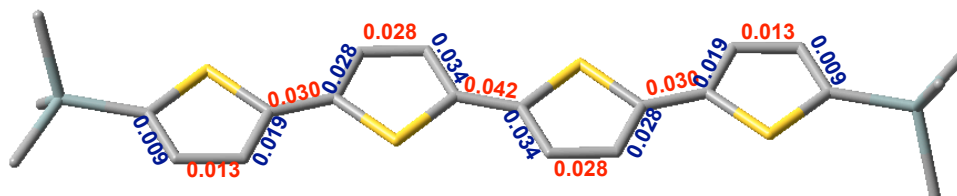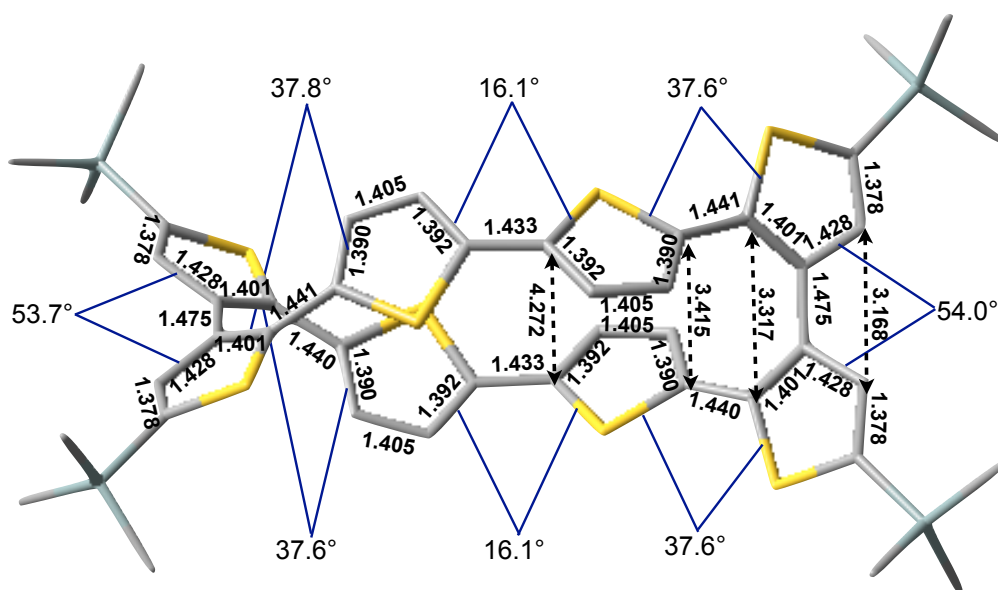
Figure 1-30. Selected bond lengths, interatomic distances, and dihedral angles for the optimized structure of radical cation of $\mathbf{1}^{\bullet+}$ calculated at UB3LYP/6-31G(d) level. The distances are shown in Å. Hydrogen atoms are omitted for clarity.
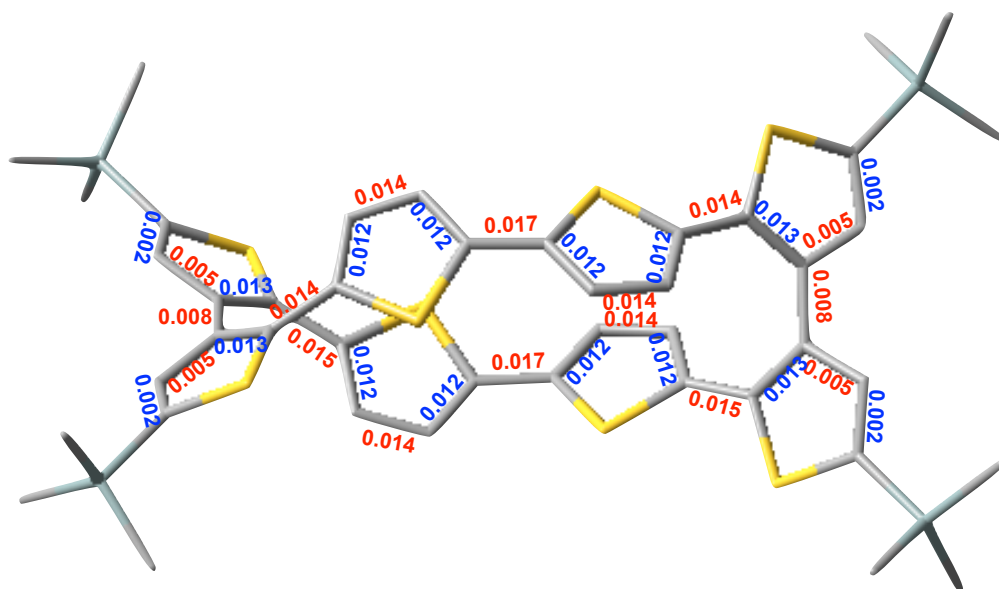
Figure 1-31. Differences of bond lengths between $\mathbf{1}^{\bullet+}$ and $\mathbf{1}'$ calculated at the UB3LYP/6-31G(d) and B3LYP/6-31G(d) level, respectively. The elongated and shortened bond lengths by the one-electron oxidation are displayed in blue and red colors, respectively. The distances are shown in Å. Hydrogen atoms are omitted for clarity.
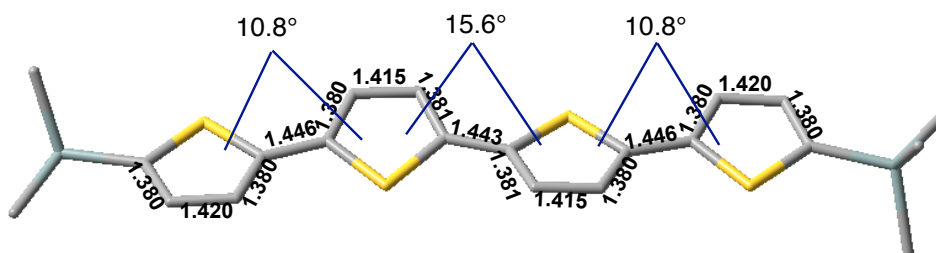
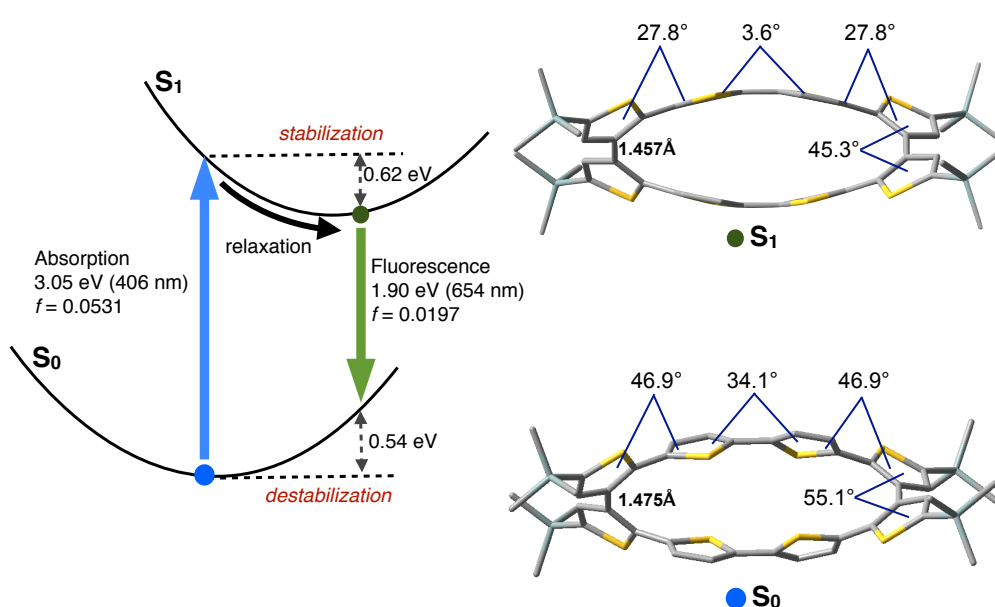**Figure 1-32.** Selected bond lengths and dihedral angles for the the optimized structure of neutral **2′** calculated at the B3LYP/6-31G(d) level. The distances are shown in Å. Hydrogen atoms are omitted for clarity.
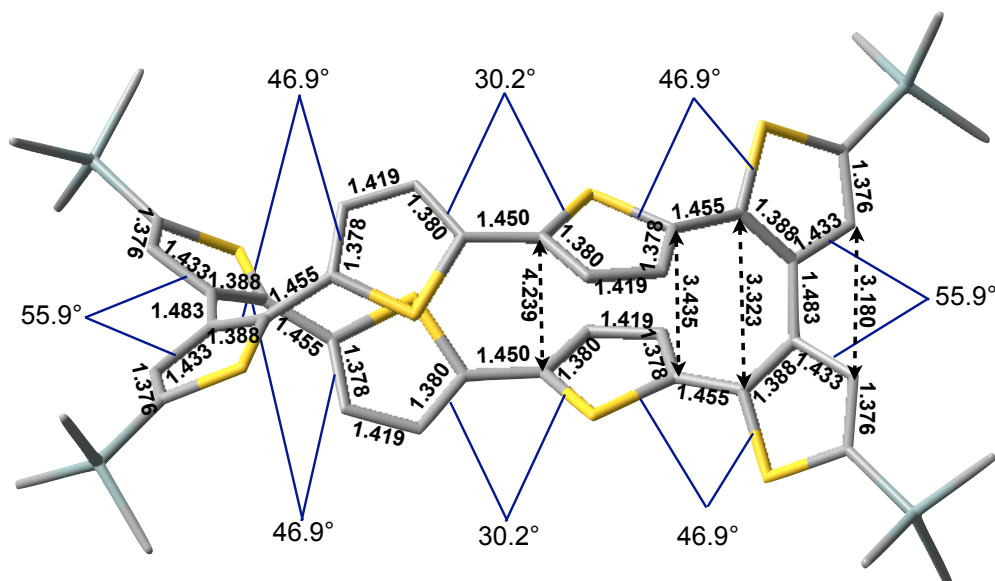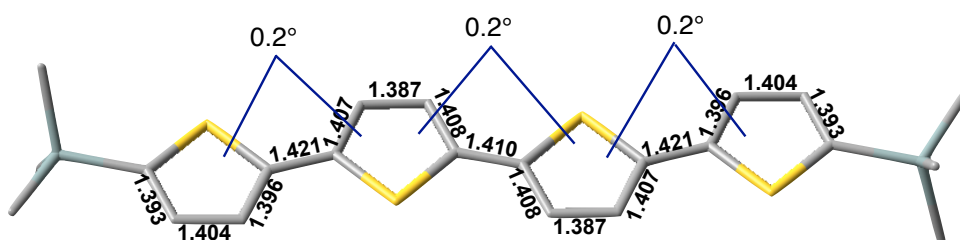
Figure 1-33. Selected bond lengths and dihedral angles for the optimized structure of radical cation of **2′⁺** calculated at the UB3LYP/6-31G(d) level. The distances are shown in Å. Hydrogen atoms are omitted for clarity.
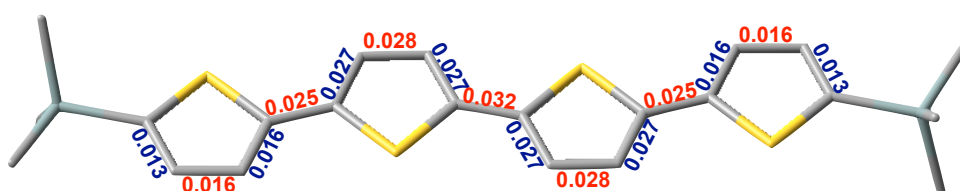
Figure 1-34. Differences of bond lengths between **2′⁺** and **2′** calculated at the UB3LYP/6-31G(d) and B3LYP/6-31G(d) level, respectively. The elongated and shortened bond lengths upon the oxidation are displayed in blue and red colors, respectively. The distances are shown in Å. Hydrogen atoms are omitted for clarity.
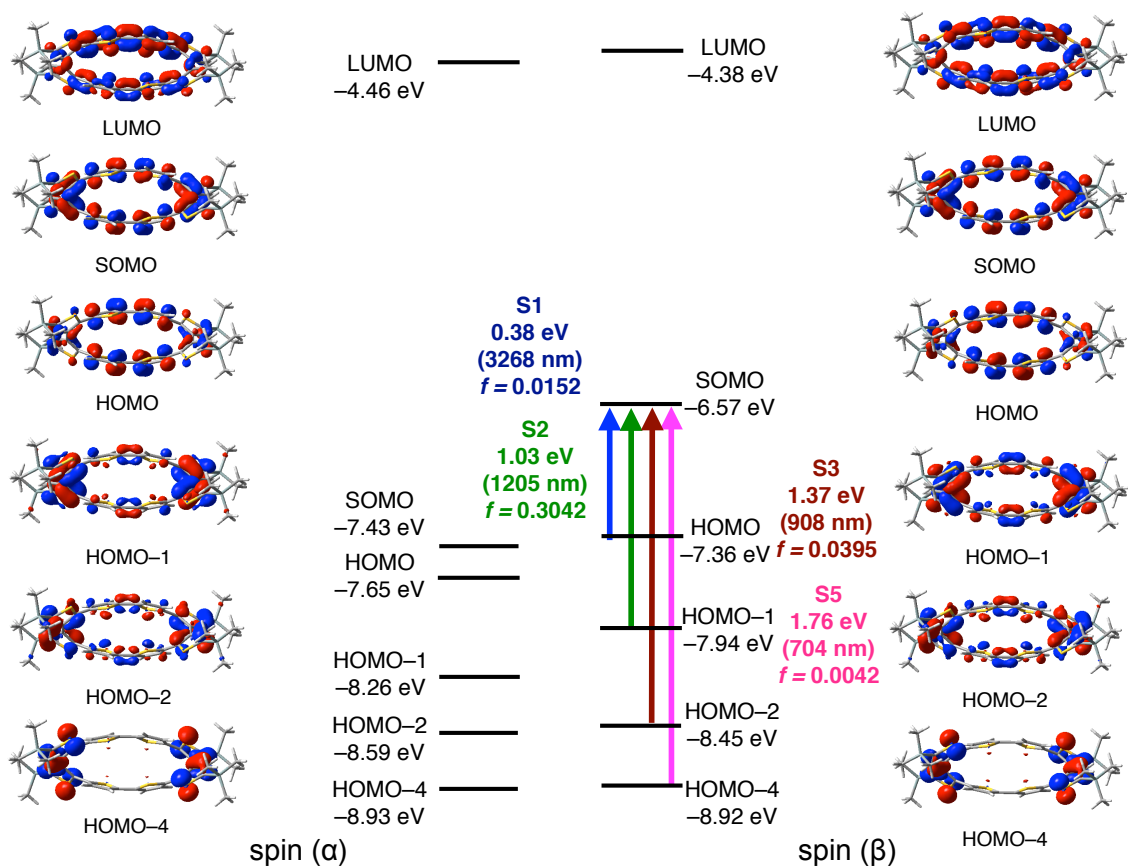
Figure 1-35. Kohn-Sham molecular orbitals of **1**$^{\cdot+}$ calculated at the UB3LYP/6-31G(d) level. TD-DFT vertical excitation in **1**$^{\cdot+}$ calculated at the UB3LYP/6-31G(d) level. Hydrogen atoms are omitted for clarity.

Figure 1-36. Kohn-Sham molecular orbitals of **2**$^{•+}$ calculated at the UB3LYP/6-31G(d) level. TD-DFT vertical excitation in **2**$^{•+}$ calculated at the UB3LYP/6-31G(d) level. Hydrogen atoms are omitted for clarity.

Table 1-7. Cartesian Coordinates (Å) of the Optimized Structure of **1′** (S₀) at the PBE0/6-31G(d) Level

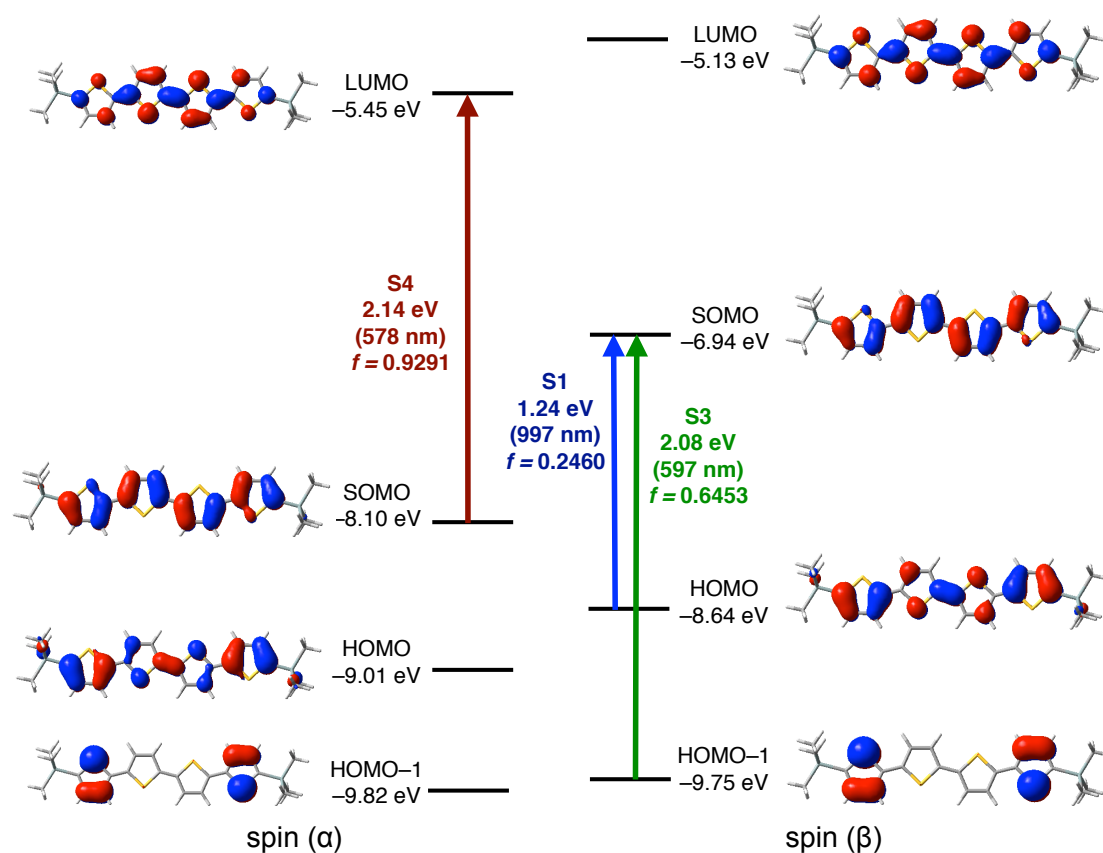| atom	x	y	z	atom	x	y	z
C	-1.57334958	1.07667263	2.28997149	Si	-7.43442297	4.24872298	-0.86575401
H	-1.22286358	2.04319684	2.63701729	H	-6.15393447	5.62853803	0.77728045
C	-0.72382761	0.01782771	2.05779728	C	-6.51647798	5.77349688	-0.24631251
C	-2.9298056	0.77542848	2.02865982	H	-5.64859465	5.99929454	-0.87655009
H	-3.74613364	1.47780561	2.15436827	H	-7.16886145	6.65474343	-0.25170915
C	-3.1266893	-0.5142341	1.59213978	C	-8.87513999	3.8348268	0.27456917
S	-1.614999	-1.36378161	1.50570115	H	-9.42022791	2.9490054	-0.070175
C	-5.35000183	-0.65604577	0.33686742	H	-9.58697865	4.66778561	0.30863869
C	-4.36161564	-1.1508226	1.17140857	H	-8.53635993	3.64687872	1.29943067
C	-6.422974	-1.58343547	0.18432359	C	-8.05159001	4.54992637	-2.62056472
C	-6.26753888	-2.77493009	0.85197822	Si	7.43447261	4.24861644	0.86577929
S	-4.77065609	-2.74519818	1.71853079	Si	7.43469216	-4.24849011	-0.86594586
C	-6.4229386	1.58345665	-0.18429013	Si	-7.43453278	-4.24866955	0.86580058
C	-6.26748104	2.77494211	-0.85195609	C	6.51665065	5.77342057	0.24623075
C	-5.34998828	0.65604191	-0.33683473	H	5.64880478	5.99935153	0.87647208
C	-4.36159379	1.15079259	-1.17138159	H	6.15406692	5.62840574	-0.77734001
S	-4.77063143	2.74514824	-1.71856394	H	7.16911483	6.65460796	0.25153337
C	-2.92980195	-0.77550225	-2.02856567	H	8.53649709	3.64666994	-1.29933385
H	-3.74613486	-1.47788088	-2.15423451	C	8.87522699	3.83459557	-0.2744516
C	-3.12667455	0.51417988	-1.59209885	H	9.58713655	4.66749552	-0.30848029
C	-1.57334837	-1.07676885	-2.28986588	H	9.42021987	2.94873105	0.07033185
H	-1.22287022	-2.0433121	-2.6368667	C	8.0515625	4.54984875	2.62061242
C	-0.72381882	-0.01791738	-2.05774857	H	7.16954351	-6.65454292	-0.25185806
S	-1.61498108	1.36372887	-1.50573043	C	6.51704521	-5.77338215	-0.24635734
C	1.5732859	1.0765213	-2.29027974	H	6.15464669	-5.62847035	0.77729367
H	1.22278204	2.04302709	-2.63735945	H	5.64909033	-5.99929242	-0.87645596
C	0.72376291	0.01772545	-2.05787459	C	8.05165764	-4.54963058	-2.62083928
C	2.92975795	0.77528503	-2.02903487	H	9.58746914	-4.6672404	0.30815569
H	3.74608126	1.47765212	-2.15482897	C	8.87551116	-3.83438002	0.27417185
C	3.12664152	-0.51430927	-1.59230645	H	9.42042937	-2.94848945	-0.07066249
S	1.61498869	-1.36392736	-1.50599289	H	8.53684814	-3.64646165	1.29907752
C	5.34986282	-0.65606368	-0.33681418	C	-8.8752625	-3.8347182	-0.27448674
C	4.36154191	-1.15085499	-1.17143288	H	-9.58711184	-4.66766722	-0.30857358
C	6.42288764	-1.58339554	-0.18428934	H	-8.53649624	-3.64673966	-1.29934722
C	6.26754703	-2.77487157	-0.85199745	H	-9.42033412	-2.94890181	0.070296
S	4.77053266	-2.7453225	-1.71832358	H	-8.73465222	-5.40703603	2.65473976
C	6.42282758	1.58341881	0.18428726	C	-8.05166976	-4.5498539	2.62062531
C	6.26744357	2.77490481	0.85196777	H	-7.22169441	-4.75865135	3.30532143
C	5.3498507	0.65604005	0.33686239	H	-8.5877524	-3.6759792	3.0068421
C	4.36152404	1.15080739	1.17148791	C	-6.5166579	-5.7734755	0.24633455
S	4.77054425	2.74522978	1.71848857	H	-7.22162154	4.75867921	-3.30528278
C	2.9297475	-0.7753812	2.02899057	H	-8.58772452	3.67607521	-3.00676288
C	3.12662784	0.51424018	1.59234149	H	-8.73453183	5.40714128	-2.65466777
C	1.57327783	-1.07663147	2.29023416	H	-6.15416731	-5.62854264	-0.7772809
H	1.22277664	-2.04315861	2.63725713	H	-5.64874472	-5.99928194	0.87652797
C	0.72375382	-0.01781945	2.05790687	H	-7.16906111	-6.65470707	0.25178231
S	1.61497382	1.36386202	1.50608835	H	7.22162381	-4.75851273	-3.30543883
H	3.74607115	-1.47775819	2.15472813	H	8.73471794	-5.40674784	-2.65502655
H	7.28211068	1.36852681	-0.44444931	H	8.58761228	-3.67570755	-3.00712424
H	-7.28223276	1.36860732	0.44444607	H	8.58765371	3.67599292	3.00686008
H	7.28219736	-1.36846023	0.4443959	H	8.73452686	5.40704534	2.65472585
H	-7.28227107	-1.36855913	-0.44439921	H	7.22156698	4.75864385	3.30528493

Table 1-8. Cartesian Coordinates (Å) of the Optimized Structure of **1′** (S₁) at the PBE0/6-31G(d) Level

atom	x	y	z	atom	x	y	z
C	-1.51534021	1.16389531	1.94268421	Si	-7.55040148	4.09918177	-1.2028983
H	-1.11623476	2.1721012	1.98307724	H	-6.38901882	5.5997283	0.42351501
C	-0.70629768	0.03248027	2.09268038	C	-6.70386912	5.67972932	-0.62272931
C	-2.84469189	0.87326865	1.65927724	H	-5.81222572	5.89753359	-1.22181663
H	-3.60665963	1.62315308	1.4838276	H	-7.37856916	6.5398383	-0.70738233
C	-3.12325403	-0.49346768	1.60130591	C	-9.02561647	3.69340687	-0.10488289
S	-1.68422285	-1.41576048	1.98147198	H	-9.52771201	2.77397202	-0.42631878
C	-5.37219029	-0.61071468	0.39710372	H	-9.7639978	4.50267612	-0.14509174
C	-4.33846125	-1.11758196	1.21466338	H	-8.72692041	3.5691307	0.94187165
C	-6.49617906	-1.49062108	0.38880456	C	-8.10099247	4.295472	-2.99461051
C	-6.33737641	-2.66926235	1.07240433	Si	7.55039402	4.09917695	1.20292499
S	-4.76967489	-2.69733106	1.82482748	Si	7.550372	-4.0991831	-1.20303636
C	-6.49618689	1.4906134	-0.38872009	Si	-7.55037835	-4.09918876	1.20300806
C	-6.33739456	2.66925772	-1.0723164	C	6.7038542	5.67972318	0.62276279
C	-5.37219648	0.61070961	-0.39703528	H	5.81221212	5.89752285	1.22185368
C	-4.33847791	1.11758214	-1.21460489	H	6.38900056	5.5997237	-0.42348065
S	-4.76970058	2.69733426	-1.82475448	H	7.37855149	6.53983433	0.70741566
C	-2.84471243	-0.87326284	-1.65925896	H	8.7269139	3.56914406	-0.94184918
H	-3.60667816	-1.62315011	-1.48381258	C	9.02560959	3.69341298	0.10490633
C	-3.12327427	0.49347271	-1.60126588	H	9.76398923	4.50268346	0.14512124
C	-1.51536325	-1.16388532	-1.94268306	H	9.52770704	2.77397676	0.42633535
H	-1.1162577	-2.17209059	-1.98309306	C	8.10098644	4.29546336	2.99463715
C	-0.70632273	-0.03246787	-2.092673	H	7.37852751	-6.53984497	-0.70755024
S	-1.68424772	1.41577077	-1.98143651	C	6.70383319	-5.67973297	-0.6228825
C	1.51534588	1.16391809	-1.94268313	H	6.38898929	-5.59974328	0.42336465
H	1.11624008	2.17212432	-1.98306312	H	5.81218503	-5.89752433	-1.22196744
C	0.70630226	0.03250471	-2.09268511	C	8.10094923	-4.2954534	-2.99475505
C	2.84469828	0.87328865	-1.65928398	H	9.76397462	-4.50270662	-0.14525554
H	3.60666639	1.6231711	-1.4838284	C	9.025598	-3.69343412	-0.10502616
C	3.12325899	-0.49344856	-1.60132151	H	9.52769577	-2.77399629	-0.42645026
S	1.68422892	-1.41573698	-1.98150246	H	8.72691168	-3.56917472	0.94173314
C	5.3721914	-0.61070933	-0.39711138	C	-9.02560324	-3.69342923	0.10500022
C	4.33846369	-1.1175672	-1.21468012	H	-9.76398209	-4.50269996	0.14522433
C	6.49617996	-1.49061616	-0.38882118	H	-8.72691623	-3.56916397	-0.94175818
C	6.33737551	-2.66925264	-1.07242845	H	-9.52769857	-2.77399208	0.42642999
S	4.76967901	-2.69730882	-1.82486271	H	-8.80671494	-5.12830488	3.09845751
C	6.49618785	1.49060802	0.38873768	C	-8.10095537	-4.29546417	2.99472625
C	6.3373934	2.66924799	1.07234068	H	-7.24902567	-4.49631434	3.65422361
C	5.37219769	0.61070379	0.39704409	H	-8.59476231	-3.38775985	3.35857944
C	4.33848046	1.11756707	1.21462271	C	-6.70384552	-5.67973911	0.62284727
S	4.76970554	2.69731095	1.82479221	H	-7.24906827	4.49633071	-3.65411233
C	2.84471862	-0.87328305	1.65926572	H	-8.5947994	3.38776961	-3.35846832
C	3.12327922	0.49345338	1.60128215	H	-8.80675521	5.1283116	-3.09832896
C	1.5153688	-1.16390824	1.94268223	H	-6.38900294	-5.59974666	-0.42340007
H	1.11626277	-2.17211382	1.98307899	H	-5.81219725	-5.89753566	1.22193011
C	0.70632728	-0.03249239	2.09267819	H	-7.3785426	-6.5398492	0.70751288
S	1.68425389	1.41574713	1.98146776	H	7.24901895	-4.49629669	-3.65425382
H	3.60668463	-1.62316836	1.48381303	H	8.80670489	-5.12829701	-3.09848943
H	7.38758925	1.26990168	-0.19146041	H	8.59476067	-3.38774985	-3.35860402
H	-7.38758978	1.26989967	0.19147302	H	8.59479972	3.38776263	3.35849054
H	7.38758888	-1.26991379	0.19136684	H	8.8067441	5.12830701	3.09835784
H	-7.3875893	-1.2699114	-0.19137877	H	7.24906202	4.496314	3.65414111

Table 1-9. Cartesian Coordinates (Å) of the Optimized Structure of **2′** (S_0) at the PBE0/6-31G(d) Level

atom	x	y	z	atom	x	y	z
C	1.27978704	1.41437863	-0.49044774	S	-1.92133842	1.03476705	-0.06821344
H	0.70199835	2.31407371	-0.67508446	Si	8.92611278	0.09700941	0.25580674
C	0.69857435	0.17676989	-0.31934738	Si	-8.92611363	-0.09702388	0.25578058
C	2.68953821	1.38480065	-0.44172748	C	-9.17565266	-1.17241189	1.78302091
H	3.31496802	2.26047596	-0.58083788	H	-8.85475265	-0.64992691	2.69086268
C	3.20713326	0.12550559	-0.23217585	H	-8.60086235	-2.10333696	1.71596002
S	1.92133623	-1.03474628	-0.06817141	H	-10.2312829	-1.44301147	1.90434634
C	5.11719974	-1.55525552	-0.15827603	C	-9.86749053	1.52482472	0.43138871
H	4.50926479	-2.44673834	-0.27670383	H	-9.73823063	2.16609314	-0.44768914
C	4.58786036	-0.28357407	-0.1344638	H	-9.53865984	2.08634294	1.31278957
C	6.52676011	-1.57184056	-0.03247287	H	-10.94068168	1.33103486	0.54258066
H	7.10993667	-2.48762858	-0.03397757	C	-9.50358481	-1.02922321	-1.27712758
C	7.10298757	-0.3262814	0.08630456	H	-9.37273542	-0.4231943	-2.18031366
S	5.86124854	0.88287465	0.05398387	H	-10.5645101	-1.29533103	-1.19950473
C	-6.52676037	1.57183977	-0.03241113	H	-8.93668066	-1.9569374	-1.4154686
H	-7.1099391	2.48762648	-0.03389697	C	9.17570473	1.17212418	1.78323036
C	-7.10298804	0.32627458	0.0863048	H	8.60089389	2.10305025	1.71636147
C	-5.11720038	1.55526055	-0.15821545	H	10.23133572	1.44271987	1.90455739
H	-4.5092665	2.44674696	-0.2766211	H	8.85485451	0.64946981	2.69099217
C	-4.58785952	0.28357867	-0.1344406	C	9.86751382	-1.52486217	0.43107447
S	-5.86124092	-0.88287377	0.05402308	H	10.94070851	-1.33108338	0.54225019
C	-2.68953385	-1.38479067	-0.44171592	H	9.73821301	-2.16596136	-0.44812055
H	-3.31496037	-2.2604716	-0.58080572	H	9.5387335	-2.08655189	1.31238481
C	-3.2071323	-0.12549594	-0.23217137	C	9.50349511	1.02949653	-1.27696022
C	-1.27978257	-1.41436577	-0.49043499	H	8.93656816	1.95722703	-1.4151
H	-0.70199176	-2.31406367	-0.67505101	H	9.37260466	0.42363131	-2.18025007
C	-0.69857267	-0.17675385	-0.31935025	H	10.56441983	1.29560854	-1.19934726

Table 1-10. Cartesian Coordinates (Å) of the Optimized Structure of **2′** (S_1) at the PBE0/6-31G(d) Level

atom	x	y	z	atom	x	y	z
C	-1.27915161	1.44192141	0.02018044	S	1.91822338	1.08581143	0.01140886
H	-0.69284777	2.35482507	0.02448025	Si	-8.92245331	0.0966102	-0.00942295
C	-0.68022517	0.16377153	0.0174381	Si	8.92245384	-0.09661294	-0.00924688
C	-2.66191136	1.40690983	0.01714955	C	9.30168512	-1.25706702	-1.44620041
H	-3.28988196	2.29175009	0.01769221	H	9.06567174	-0.78696482	-2.40707574
C	-3.20165847	0.10883647	0.01118435	H	8.71840373	-2.18257122	-1.37755424
S	-1.91822274	-1.08580657	0.01153095	H	10.36287701	-1.53351393	-1.45626797
C	-5.10080966	-1.56869889	-0.01596952	C	9.87153392	1.51967254	-0.19873596
H	-4.48688284	-2.46374528	-0.02629741	H	9.67528801	2.20530349	0.63318558
C	-4.55961132	-0.28142735	0.00290586	H	9.6107078	2.03264302	-1.1310164
C	-6.50309139	-1.57596726	-0.02466709	H	10.9504087	1.32596856	-0.2178618
H	-7.09007718	-2.48936259	-0.04198681	C	9.38006394	-0.94006305	1.61430486
C	-7.09259902	-0.32001171	-0.01191906	H	9.18352788	-0.28467059	2.46976042
S	-5.85526371	0.89660513	0.0104204	H	10.44347092	-1.20790075	1.63022803
C	6.50309398	1.57596511	-0.02491225	H	8.80226689	-1.85966529	1.76119678
H	7.0900821	2.48935982	-0.04218774	C	-9.30145963	1.25710492	-1.44640433
C	7.09259987	0.32001011	-0.01202395	H	-8.71818899	2.18260736	-1.37764169
C	5.10081173	1.56869858	-0.01628954	H	-10.36264967	1.5335531	-1.45663104
H	4.48688661	2.46374591	-0.02663743	H	-9.06529576	0.7870289	-2.40725554
C	4.55961125	0.28142878	0.00264398	C	-9.87150191	-1.51967133	-0.19910721
S	5.85526048	-0.89660785	0.01001234	H	-10.95037388	-1.32596829	-0.21840252
C	2.66191015	-1.4069058	0.01692902	H	-9.67538998	-2.20532444	0.6328277
H	3.28988	-2.29174662	0.0174084	H	-9.61052492	-2.03261698	-1.13135908
C	3.20165812	-0.10883284	0.01097809	C	-9.38032001	0.94001334	1.61407949
C	1.27915066	-1.44191627	0.02004735	H	-8.80254984	1.85961399	1.76108669
H	0.69284632	-2.35481952	0.02436225	H	-9.18391577	0.28459856	2.46954824
C	0.68022512	-0.16376586	0.01738377	H	-10.44373069	1.20784543	1.62984229

Table 1-11. Cartesian Coordinates (Å) of the Optimized Structure of Neutral **1′** at the B3LYP/6-31G(d) Level

atom	x	y	z	atom	x	y	z
C	-1.56856447	-1.09836908	-2.3120683	Si	-7.51696018	-4.21173139	0.9741024
H	-1.2126144	-2.07313249	-2.6289195	H	-6.25462256	-5.65303783	-0.6433411
C	-0.72484657	-0.02338651	-2.11932835	C	-6.6189167	-5.76908227	0.3838848
C	-2.93160239	-0.80831432	-2.04706911	H	-5.75378466	-5.99755677	1.01756915
H	-3.73345395	-1.53113114	-2.14502069	H	-7.2854365	-6.64017063	0.4072367
C	-3.15199435	0.49125786	-1.64563904	C	-8.9620254	-3.81012355	-0.17781142
S	-1.63989952	1.37922954	-1.60517124	H	-9.50014939	-2.91143531	0.14516526
C	-5.37088978	0.64775202	-0.36054796	H	-9.68171254	-4.63768483	-0.19048354
C	-4.39415851	1.12234844	-1.22537944	H	-8.62653088	-3.64969936	-1.20888219
C	-6.45544982	1.57401107	-0.22538841	C	-8.14384646	-4.47290461	2.74009922
C	-6.32881961	2.74873534	-0.93127807	Si	7.51725789	-4.21154013	-0.97419665
S	-4.82925402	2.70939871	-1.82657133	Si	7.51695467	4.21173119	0.97414279
C	-6.45541934	-1.57403421	0.22541088	Si	-7.51721275	4.21156986	-0.9741999
C	-6.32887618	-2.74863985	0.93151498	C	6.61940306	-5.76929045	-0.38477535
C	-5.37088708	-0.64774454	0.36055567	H	5.754938	-5.99818739	-1.01921814
C	-4.39422011	-1.12222956	1.22552328	H	6.25414413	-5.65337105	0.6421225
S	-4.82936483	-2.70920386	1.82688667	H	7.28633357	-6.64007966	-0.40749891
C	-2.93155476	0.80842734	2.0471248	H	8.62625476	-3.65021847	1.20928034
H	-3.73335678	1.53129951	2.14508208	C	8.96197327	-3.80998088	0.17818028
C	-3.15203975	-0.49114478	1.645765	H	9.68201909	-4.63723407	0.19052889
C	-1.56848847	1.09841726	2.31204781	H	9.49976002	-2.91089892	-0.14426322
H	-1.21247808	2.07317258	2.62885635	C	8.14465319	-4.47191481	-2.74013462
C	-0.72483794	0.02337775	2.11932237	H	7.28552456	6.6401938	0.40732916
S	-1.63997898	-1.37919099	1.60519444	C	6.61903285	5.76909	0.38375903
C	1.56848948	-1.09844188	2.31199953	H	6.25501569	5.65308445	-0.64356988
H	1.21248547	-2.07320822	2.6287825	H	5.75372507	5.99751169	1.01722219
C	0.72483417	-0.02339912	2.11931404	C	8.14363198	4.47295957	2.74020617
C	2.93155012	-0.80844716	2.04705855	H	9.68185865	4.63756958	-0.19020941
H	3.73334987	-1.53132707	2.14497973	C	8.9621433	3.81003211	-0.17758408
C	3.1520318	0.49113579	1.64573054	H	9.50019845	2.91134028	0.14549687
S	1.6399669	1.37918479	1.60520874	H	8.62676727	3.64957372	-1.20868828
C	5.37086263	0.64777296	0.36049048	C	-8.96217187	3.80980232	0.17779779
C	4.3941893	1.1222405	1.22546058	H	-9.68198882	4.63725006	0.19049253
C	6.4553896	1.57406924	0.22536474	H	-8.62663767	3.64940024	1.20885752
C	6.32883538	2.74867047	0.93147808	H	-9.50016347	2.91104309	-0.14520278
S	4.82927863	2.70925076	1.82676711	H	-8.83879314	5.32007622	-2.78881744
C	6.45548591	-1.57395688	-0.22544583	C	-8.14422159	4.47216403	-2.74025777
C	6.32888565	-2.74868708	-0.93133026	H	-7.32015921	4.67927586	-3.43322011
C	5.3708974	-0.64773075	-0.36059851	H	-8.67158032	3.5852765	-3.10999219
C	4.39416658	-1.12236223	-1.22541415	C	-6.61952493	5.76928119	-0.38445459
S	4.82927163	-2.70942879	-1.82654829	H	-7.31973619	-4.67997165	3.43301801
C	2.93158073	0.80828013	-2.04709295	H	-8.67141845	-3.58623147	3.11004912
C	3.15199107	-0.49128936	-1.64566528	H	-8.83821898	-5.32099006	2.7884994
C	1.56853599	1.09832157	-2.31207553	H	-6.25527683	5.65366607	0.64283701
H	1.21257219	2.07307823	-2.62893091	H	-5.75437728	5.99769007	-1.01814538
C	0.72483371	0.02332671	-2.11933027	H	-7.28617391	6.64025995	-0.40815549
S	1.63990186	-1.37927196	-1.60516161	H	7.31944059	4.68008511	3.43301157
H	3.73342367	1.53110517	-2.14505349	H	8.83802398	5.32102631	2.78865386
H	7.30252618	-1.36619915	0.42123762	H	8.67112878	3.58628727	3.11026476
H	-7.30241897	-1.36637843	-0.4213607	H	8.67218406	-3.58501593	-3.10959744
H	7.30241256	1.36641085	-0.42137505	H	8.83916907	-5.31987529	-2.7886769
H	-7.30247495	1.3662925	0.42132688	H	7.32075342	-4.67883773	-3.43334619

Table 1-12. Cartesian Coordinates (Å) of the Optimized Structure of **1**$^{\bullet+}$ at the UB3LYP/6-31G(d) Level

atom	x	y	z	atom	x	y	z
C	1.55698828	-1.12993558	2.1815769	Si	7.48557965	-4.241324	-0.92557046
H	1.19754171	-2.12937701	2.402522	H	6.19717804	-5.64721905	0.70370567
C	0.71576346	-0.02153074	2.13568558	C	6.56288535	-5.77446527	-0.32154147
C	2.90108372	-0.83465712	1.89779127	H	5.70099917	-6.00687146	-0.95810687
H	3.69415365	-1.57243752	1.88810018	H	7.22383572	-6.6495677	-0.33252639
C	3.13095502	0.50957424	1.62936894	C	8.92028686	-3.81271112	0.22237271
S	1.64234215	1.42663639	1.77773787	H	9.45871841	-2.91837488	-0.11174523
C	5.34669421	0.64920046	0.35021948	H	9.6423734	-4.6376375	0.2446445
C	4.34778136	1.14791895	1.19686994	H	8.58547731	-3.64410501	1.25227288
C	6.43225763	1.56823711	0.21894255	C	8.08355444	-4.48484634	-2.6994506
C	6.28446281	2.76425563	0.88731818	Si	-7.4859968	-4.24094571	0.9260077
S	4.76703394	2.75644878	1.74983054	Si	-7.48701245	4.23874735	-0.92502102
C	6.43209003	-1.56945524	-0.21687078	Si	7.48582683	4.24022811	0.92611983
C	6.28460685	-2.7650094	-0.88622164	C	-6.56381659	-5.77482856	0.32309259
C	5.34695303	-0.65002061	-0.34870697	H	-5.70185327	-6.00684516	0.95969895
C	4.34888159	-1.14794871	-1.196782	H	-6.19829953	-5.64859533	-0.70234299
S	4.76801712	-2.75633824	-1.75014782	H	-7.22496763	-6.64976556	0.33503129
C	2.90382081	0.83586511	-1.89743121	H	-8.58587456	-3.64490524	-1.25219491
H	3.69731579	1.57316522	-1.88697959	C	-8.92064416	-3.81267981	-0.22214614
C	3.13283995	-0.50877121	-1.62986153	H	-9.64296904	-4.63741787	-0.24377063
C	1.56001376	1.13208502	-2.18108321	H	-9.45880334	-2.91796139	0.11138549
H	1.20107766	2.131894	-2.40119191	C	-8.08410134	-4.48295133	2.70006025
C	0.7181603	0.02403509	-2.13595066	H	-7.35280992	6.55305223	-0.0065547
S	1.64394592	-1.4249782	-1.77922535	C	-6.68680564	5.68161044	-0.00548583
C	-1.55537012	-1.1266183	-2.1814096	H	-6.47592332	5.42622521	1.03921018
H	-1.19602006	-2.12590409	-2.40319156	H	-5.74349502	5.98758972	-0.47273605
C	-0.71410025	-0.01811422	-2.13545354	C	-7.81722614	4.70208615	-2.72471449
C	-2.89907228	-0.83158176	-1.89649128	H	-9.80033752	4.5000237	-0.05503916
H	-3.69216783	-1.56931548	-1.88672244	C	-9.06992024	3.68216285	-0.06191402
C	-3.12878805	0.5126282	-1.6271739	H	-9.53617424	2.83178298	-0.57233279
S	-1.64046795	1.42989589	-1.77621242	H	-8.89201122	3.39735658	0.98159717
C	-5.34666839	0.64850337	-0.35192281	C	8.92016044	3.81076671	-0.22200957
C	-4.34580032	1.15020083	-1.19475241	H	9.6427788	4.63522368	-0.2443845
C	-6.43591535	1.56390317	-0.22629591	H	8.58515451	3.64230795	-1.25187106
C	-6.28829675	2.76071812	-0.89326919	H	9.45808853	2.91610637	0.11206831
S	-4.76756261	2.75732556	-1.74988516	H	8.7866677	5.32491497	2.75493163
C	-6.43174723	-1.56987516	0.21577862	C	8.08446086	4.48416784	2.69972141
C	-6.28454081	-2.76508481	0.88563962	H	7.25543866	4.70233676	3.38298078
C	-5.34635839	-0.65050972	0.34710246	H	8.60104692	3.5939089	3.07576536
C	-4.34825778	-1.14830605	1.19536492	C	6.56348157	5.77346418	0.32185147
S	-4.7679087	-2.75627565	1.74955451	H	7.25428707	-4.7030112	-3.38241948
C	-2.90215344	0.83414474	1.89860377	H	8.59988638	-3.59447235	-3.07556639
C	-3.13179495	-0.50981188	1.62877945	H	8.78583001	-5.32550754	-2.75507927
C	-1.55809289	1.12934132	2.18276674	H	6.19642714	5.64563284	-0.70283968
H	-1.19879666	2.12861365	2.40471781	H	5.70253887	6.00700915	0.95928399
C	-0.71670268	0.02111228	2.13572922	H	7.22503875	6.64812591	0.33130357
S	-1.64306513	-1.42681619	1.77632486	H	-6.89875928	4.99437509	-3.24733383
H	-3.69530533	1.57185089	1.88962778	H	-8.50971834	5.55072368	-2.78051716
H	-7.29215817	-1.35190469	-0.40842729	H	-8.26572349	3.86983097	-3.27879322
H	7.29251187	-1.35134355	0.4072712	H	-8.60041371	-3.59218977	3.0753015
H	-7.30055891	1.34134964	0.39047055	H	-8.78645682	-5.32349418	2.75641175
H	7.29318292	1.3494754	-0.40427803	H	-7.25492039	-4.7005196	3.38332133

Table 1-13. Cartesian Coordinates (Å) of the Optimized Structure of Neutral **2′** at the B3LYP/6-31G(d) Level

atom	x	y	z	atom	x	y	z
C	1.28740027	1.41752414	-0.40086076	S	-1.93587999	1.05635024	-0.05250883
H	0.71304681	2.3252278	-0.55294262	Si	8.98604581	0.09375394	0.2071857
C	0.69989507	0.17548052	-0.2612461	Si	-8.98602088	-0.09371482	0.2074029
C	2.70144036	1.38834189	-0.36089834	C	-9.27082053	-1.18828653	1.72428922
H	3.31983676	2.27224697	-0.47565698	H	-8.96751482	-0.67752314	2.64537046
C	3.23000056	0.12470002	-0.18940541	H	-8.69958423	-2.12211481	1.66100562
S	1.93585722	-1.05644843	-0.05273995	H	-10.33039436	-1.45548489	1.82183954
C	5.15040121	-1.55395058	-0.12934181	C	-9.93716862	1.53108553	0.38596539
H	4.54454659	-2.44914846	-0.22650777	H	-9.79424293	2.18544701	-0.48178348
C	4.61512064	-0.28180476	-0.11027726	H	-9.62808349	2.08403603	1.28034048
C	6.5663804	-1.57123616	-0.02580235	H	-11.01242176	1.33380652	0.47447912
H	7.14267009	-2.49117553	-0.02792114	C	-9.54691813	-1.01143448	-1.3497204
C	7.15404857	-0.32684998	0.07240675	H	-9.4013049	-0.39809075	-2.24632126
S	5.90295904	0.89938508	0.04617058	H	-10.61081798	-1.2729349	-1.29063078
C	-6.56640866	1.57121978	-0.02649539	H	-8.98399959	-1.94167036	-1.4906889
H	-7.14271417	2.49114827	-0.02888828	C	9.27116339	1.18901383	1.72351461
C	-7.15405354	0.32685349	0.07211641	H	8.69981712	2.12276124	1.66003404
C	-5.1504367	1.55392202	-0.13015432	H	10.33073896	1.45634874	1.82066259
H	-4.54459974	2.44908925	-0.22770697	H	8.96816872	0.67857399	2.64487906
C	-4.61514152	0.281789	-0.11072325	C	9.93720662	-1.53096791	0.3864073
S	-5.90294507	-0.89936892	0.04620204	H	11.01246462	-1.33364109	0.47476517
C	-2.70146012	-1.38830778	-0.36172382	H	9.79422912	-2.18573873	-0.48102226
H	-3.31986373	-2.27214928	-0.47693147	H	9.62817922	-2.08349446	1.28106478
C	-3.23001904	-0.12472115	-0.1898341	C	9.54663301	1.01069324	-1.35050717
C	-1.28741428	-1.41748959	-0.40155276	H	8.98374452	1.9409027	-1.49176415
H	-0.71305527	-2.32513901	-0.55393872	H	9.40074122	0.3969397	-2.24678211
C	-0.69990925	-0.17550792	-0.26138353	H	10.61056747	1.27214238	-1.29181322

Table 1-14. Cartesian Coordinates (Å) of the Optimized Structure of **2′⁺** at the UB3LYP/6-31G(d) Level

atom	x	y	z	atom	x	y	z
C	1.29102137	1.42870584	0.01205978	S	-1.92333027	1.0991482	0.00857698
H	0.71615052	2.34843253	0.01392771	Si	8.97888498	0.1075982	-0.00643615
C	0.6872922	0.15692844	0.01143329	Si	-8.97889864	-0.10749621	-0.00662475
C	2.67759015	1.39256714	0.01002485	C	-9.30457416	-1.28370102	-1.44511425
H	3.30203372	2.27878376	0.01004433	H	-8.73157849	-2.21377529	-1.35237112
C	3.21312762	0.09136548	0.00738963	H	-9.04850804	-0.82605844	-2.40717509
S	1.92332089	-1.09928296	0.00847456	H	-10.3664388	-1.55573534	-1.47891881
C	5.12461887	-1.57853202	-0.00311924	C	-9.38267257	-0.92918897	1.64339247
H	4.51894804	-2.47917593	-0.00368123	H	-9.16361859	-0.26741588	2.48872853
C	4.58078155	-0.2926995	0.00295199	H	-8.81523395	-1.85599082	1.78641986
C	6.52892857	-1.58518192	-0.01040593	H	-10.44824939	-1.18488596	1.68853008
H	7.11573074	-2.49704691	-0.01787456	C	-9.90910873	1.51822848	-0.21585976
C	7.11461126	-0.32146294	-0.0091506	H	-9.71982256	2.21196086	0.61130436
S	5.87795038	0.89738847	-0.00111618	H	-10.98873568	1.32764058	-0.2378641
C	-6.52883925	1.58531418	-0.01049977	H	-9.64831156	2.02316596	-1.15287041
H	-7.11555944	2.49723166	-0.01813025	C	9.38300765	0.9299653	1.64312932
C	-7.11463878	0.32165989	-0.00921227	H	8.81594718	1.85704341	1.78582252
C	-5.12453365	1.57853992	-0.00303456	H	10.44869511	1.18528152	1.68786677
H	-4.51879379	2.47913835	-0.00350478	H	9.16392747	0.26869273	2.48885081
C	-4.58079742	0.29266401	0.00314375	C	9.9089413	-1.51828906	-0.21522916
S	-5.87807559	-0.89732075	-0.00102345	H	10.98850057	-1.3275948	-0.23931544
C	-2.67766066	-1.39268213	0.0102963	H	9.646593	-2.02423564	-1.15126799
H	-3.3021309	-2.27888035	0.01039676	C	9.72111825	-2.21114928	0.61298938
C	-3.21316782	-0.09146692	0.00760244	C	9.3046701	1.28312026	-1.44549057
C	-1.29109226	-1.4288538	0.01223606	H	8.73130597	2.21304618	-1.35355086
H	-0.71623706	-2.34859059	0.01410936	H	9.04912776	0.82476918	-2.40735239
C	-0.68733281	-0.1570896	0.01149391	H	10.36645001	1.55552706	-1.47907745

1.5 References and Notes

(1)   (a) *Handbook of Thiophene-Based Materials: Applications in Organic Electronics and Photonics* Perepichka, I. F.; Perepichka D. F.; Ed., Wiley, Chichester, UK, **2009**. (*b*) Mishra, A.; Ma, C.-Q.; P. Bäuerle.; *Chem. Rev.* **2009**, *109*, 1141. (c) Zhang, L.; Colella, N. S.; Cherniawski, B. P.; Mannsfeld S. C. B.; Briseno, A. L. *ACS Appl. Mater. Interfaces* **2014**, *6*, 5327.

(2)   (a) Krömer, J.; Rios-Carreras, I.; Fuhrmann, G.; Musch, C.; Wunderlin, M.; Debaerdemaeker, T.; Mena-Osteritz E.; Bäuerle, P. *Angew. Chem. Int. Ed.* **2000**, *39*, 3481. (b) Fuhrmann, G.; Krömer J.; Bäuerle, P. *Synth. Met.* **2001**, *119*, 125. (c) Mena-Osteritz, E. *Adv. Mater.* **2002**, *14*, 609. (d) Fuhrmann, G.; Debaerdemaeker T.; Bäuerle, P. *Chem. Commun.* **2003**, 948. (e) Mena-Osteritz E.; Bäuerle, P. *Adv. Mater.* **2006**, *18*, 447. (f) Zhang, F.; Götz, G.; Winkler, H. D. F.; Schalley, C. A.; Bäuerle, P. *Angew. Chem. Int. Ed.* **2009**, *48*, 6632. (g) Zhang, F.; Götz, G.; Mena-Osteritz, E.; Weil, M.; Sarkar, B.; Kaim, W.; Bäuerle, P. *Chem. Sci.* **2011**, *2*, 781. (h) Mena-Osteritz, E.; Zhang, F.; Götz, G.; Reineker, P. Bäuerle, P. *Beilstein. J. Nanotechnol.* **2011**, *2*, 720.

(3)   (a) Nakao, K.; Nishimura, M.; Tamachi, T.; Kuwatani, Y.; Miyasaka, H.; Nishinaga, T.; Iyoda, M. *J. Am. Chem. Soc.* **2006**, *128*, 16740. (b) Williams-Harry, M.; Bhaskar, A.; Ramakrishna, G.; Goodson, III. T.; Imamura, M.; Mawatari, A.; Nakao, K.; Enozawa, H.; Nishinaga T.; Iyoda, M. *J. Am. Chem. Soc.* **2008**, *130*, 3252. (c) Iyoda, M.; Tanaka, K.; Shimizu, H.; Hasegawa, M.; Nishinaga, T.; Nishiuchi, T.; Kunugi, Y.; Ishida, T.; Otani, H.; Sato, H.; Inukai, K.; Tahara K.; Tobe, Y. *J. Am. Chem. Soc.* **2014**, *136*, 2389. (d) Bhaskar, A.; Ramakrishna, G.; Hagedorn, K.; Varnavski, O.; Mena-Osteritz, E.; Bäuerle P.; Goodson, III. T. *J. Phys. Chem. B* **2007**, *111*, 946. (e) Ito, H.; Mitamura, Y.; Segawa Y.; Itami, K. *Angew. Chem. Int. Ed.* **2015**, *54*, 159.

(4)   (a) Zen, A.; Bilge, A.; Galbrecht, F.; Alle, R.; Meerholz, K.; Grenzer, J.; Neher, D.; Scherf U.; Farrell, T. *J. Am. Chem. Soc.* **2006**, *128*, 3914. (b) Bilge, A.; Zen, A.; Forster, M.; Li, H.; Galbrecht, F.; Nehls, B. S.; Farrell, T.; Neher, D.; Scherf, U. *J. Mater. Chem.* **2006**, *16*, 3177.

(5)   (a) Karpe. S.; Cravino, A.; Frère, P.; Allain, M.; Mabon, G.; Roncali, J. *Adv. Funct. Mater.* **2007**, *17*, 1163. (b) Ashizawa, M.; Yu, Y.; Niimura, T.; Tsuboi, K.; Matsumoto, H.; Tanioka A.; Mori, T. *Physica B* **2010**, *405*, S373. (c)

Sannicolò, F.; Arnaboldi, S.; Benincori, T.; Bonometti, V.; Cirilli, R.; Dunsch, L.; Kutner, W.; Longhi, G.; Mussini, P. R.; Panigati, M.; Pierini, M.; Rizzo, S. *Angew. Chem. Int. Ed.* **2014**, *53*, 2623.

(6)   (a) Ma, C.-Q.; Mena-Osteritz, E.; Debaerdemaeker, T.; Wienk, M. M.; Janssen, R. A. J.; Bäuerle, P. *Angew. Chem. Int. Ed.* **2007**, *46*, 1679. (b) Ma, C.-Q.; Fonrodona, M.; Schikora, M. C.; Wienk, M. M.; Janssen, R. A. J.; Bäuerle, P. *Adv. Funct. Mater.* **2008**, *18*, 3323. (c) Ma, C.-Q.; Mena-Osteritz, E. Wunderlin, M.; Shulz, G.; Bäuerle, P. *Chem. Eur. J.* **2012**, *18*, 12880.

(7)   (a) Marsella, M. J.; Yoon, K.; Tham, F. S. *Org. Lett.* **2001**, *3*, 2129. (b) Wang, Y.; Wang, Z.; Zhao, D.; Wang, Z.; Cheng Y.; Wang, H. *Synlett* **2007**, *15*, 2390.

(8)   Sannicolò, F.; Mussini, P. R.; Benincori, T.; Cirilli, R.; Abbate, S.; Arnaboldi, S.; Casolo, S.; Castiglioni, E.; Longhi, G.; Martinazzo, R.; Panigati, M.; Pappini, M.; Procopio, E. Q.; Rizzo, S. *Chem. Eur. J.* **2014**, *20*, 15298.

(9)   (a) Yamago, S.; Watanabe, Y.; Iwamoto, T.; *Angew. Chem. Int. Ed.* **2010**, *49*, 757. (b) Iwamoto, T.; Watanabe, Y.; Sakamoto, Y.; Suzuki, T.; Yamago, S. *J. Am. Chem. Soc.* **2011**, *133*, 8354.

(10)   (a) Hitosugi, S.; Nakanishi, W.; Yamasaki, T.; Isobe, H. *Nat. Commun.* **2011**, *2*, 492. (b) Hitosugi, S.; Yamasaki, T.; Isobe, H. *J. Am. Chem. Soc.* **2012**, *134*, 12442. (c) Matsuno, T.; Kamata, S.; Hitosugi, S.; Isobe, H. *Chem. Sci.* **2013**, *4*, 3179.

(11)   Iwamoto, T.; Kayahara, E.; Yasuda, N.; Suzuki, T.; Yamago, S. *Angew. Chem. Int. Ed.* **2014**, *53*, 6430.

(12)   Shekhar, S. Hartwig, J. F. *J. Am. Chem. Soc.* **2004**, *126*, 13016.

(13)   (a) Fujitsuka, M.; Cho, D. W.; Iwamoto, T.; Yamago, S.; Majima, T. *Phys. Chem. Chem. Phys.* **2012**, *14*, 14585. (b) Segawa, Y.; Fukazawa, A.; Matsuura, S.; Omachi, H.; Yamaguchi, S.; Irle, S.; Itami, K. *Org. Biomol. Chem.* **2012**, *10*, 5979.

(14)   Tris(*p*-bromophenyl)aminium hexachloroantimonate was chosen as an oxidant because its first reduction potential (E^{o}_{1} = 0.70 V vs. Fc/Fc^{+}) is suitable for the controlled oxidation of compounds **1** and **2** into the corresponding radical cations; see: Connelly, N. G.; Geiger, W. E. *Chem. Rev.* **1996**, *96*, 877.

(15)   (a) Bäuerle, P.; Segalbacher, U.; Maier, A.; Mehring, M; *J. Am. Chem. Soc.* **1993**, *115*, 10217. (b) Takita, R.; Song, C.; Swager, T. M. *Org. Lett.* **2008**,

10, 5003. (c) Sato, M.; Kamine, H.; Kato, T. *Bull. Chem. Soc. Jpn.* **2010**, *83*, 1539. (d) Shomura, R.; Sugiyasu, K.; Yasuda, T.; Sato A.; Takeuchi, M. *Macromolecules* **2012**, *45*, 3759. (e) Tateno, M.; Takase, M.; Iyoda, M.; Komatsu, K.; Nishinaga, T. *Chem. Eur. J.* **2013**, *19*, 5457.

(16) Smith, J. R.; Cox, P. A.; Campbell, S. A.; Ratcliffe, N. M. *J. Chem. Soc. Fraday Trans.* **1995**, *91*, 2331.

(17) Ishikawa, M.; Teramura, H.; Lee, K. K.; Schneider, W.; Naka, A.; Kobayashi, H.; Yamaguchi, Y.; Kikugawa, M.; Ohshita, J.; Kunai, A.; Tang, H.; Harima, Y.; Yamabe, T.; Takeuchi, T. *Organometallics* **2001**, *20*, 5331.

(18) Dienes, Y.; Durben, S.; Kárpáti, T.; Neumann, T.; Englert, U.; Nyulászi, L.; Baumgartner, T. *Chem. Eur. J.* **2007**, *13*, 7487.

(19) Getmanenko, Y. A.; Twieg, R. J. *J. Org. Chem.* **2008**, *73*, 830.

(20) Kinzel, T.; Zhang, Y.; Buchwald, S. L. *J. Am. Chem. Soc.* **2010**, *132*, 14073.

(21) Adamo, C.; Barone, V. *J. Chem. Phys,* **1999**, *110*, 6158.

(22) (a) Ditchfield, R.; Hehre, W. J.; Pople, J. A. *J. Chem. Phys.* **1971**, *54*, 724; (b) Hehre, W. J.; Ditchfield, R.; Pople, J. A. *J. Chem. Phys.* **1972**, *56*, 2257; (c) Hariharan, P. C.; Pople, J. A. *Theor. Chim. Acta.* **1973**, *28*, 213. (d) Francl, M. M.; Pietro, W. J.; Hehre, W. J.; Binkley, J. S.; Gordon, M. S.; DeFrees, D. J.; Pople, J. A. *J. Chem. Phys*. **1982**, *77*, 3654.

(23) Gaussian 09, (Revision C.01), Frisch, M. J.; Trucks, G. W.; Schlegel, H. B.; Scuseria, G. E.; Robb, M. A.; Cheeseman, J. R.; Scalmani, G.; Barone, V.; Mennucci, B.; Petersson, G. A.; Nakatsuji, H.; Caricato, M.; Li, X.; Hratchian, H. P.; Izmaylov, A. F.; Bloino, J.; Zheng, G.; Sonnenberg, J. L.; Hada, M.; Ehara, M.; Toyota, K.; Fukuda, R.; Hasegawa, J.; Ishida, M.; Nakajima, T.; Honda, Y.; Kitao, O.; Nakai, H.; Vreven, T.; Montgomery, J. A., Jr.; Peralta, J. E.; Ogliaro, F.; Bearpark, M.; Heyd, J. J.; Brothers, E.; Kudin, K. N.; Staroverov, V. N.; Kobayashi, R.; Normand, J.; Raghavachari, K.; Rendell, A.; Burant, J. C.; Iyengar, S. S.; Tomasi, J.; Cossi, M.; Rega, N.; Millam, J. M.; Klene, M.; Knox, J. E.; Cross, J. B.; Bakken, V.; Adamo, C.; Jaramillo, J.; Gomperts, R.; Stratmann, R. E.; Yazyev, O.; Austin, A. J.; Cammi, R.; Pomelli, C.; Ochterski, J. W.; Martin, R. L.; Morokuma, K.; Zakrzewski, V. G.; Voth, G. A.; Salvador, P.; Dannenberg, J. J.; Dapprich, S.; Daniels, A. D.; Farkas, O.; Foresman, J. B.; Ortiz, J. V.; Cioslowski, J.; Fox, D. J. Gaussian, Inc., Wallingford CT, 2010.

(24)   (a) Becke, A. D. *Phys. Rev. A* **1988**, *38*, 3098. (b) Lee, C.; Yang, W.; Parr, R. G. *Phys. Rev. B* **1988**, *37*, 785. (c) Becke, A. D. *J. Chem. Phys*. **1993**, *98*, 5648.

1.6 Acknowledgement

Chapter 2

Stable and Red-Emissive Cationic Dyes Based on Dithienotropylium Ion

ABSTRACT: Thiophene-fused tropylium ions comprising electron-donating amino groups were synthesized as a new entity of cationic dyes with long-wavelength absorption and fluorescence. Fused thiophene rings as well as terminal amino groups impart excellent stability with high pK_R^+ values to the cationic tropylium ion. X-ray crystallographic analyses revealed that the pronounced quinoidal characters of amino-substituted dithienotropylium ions. These compounds exhibit attractive photophysical properties, such as strong absorptions that cover the visible region, and red fluorescence. Theoretical calculations demonstrated that 3,3′-bithiophene substructure is crucial for attaining these electronic properties.

2.1 Introduction

Carbocations are of interest not only as key intermediates in many chemical reactions, but also as fundamental skeleton of functional dyes. Especially, stabilized carbocations, such as trityl cations, rhodamines, and cyanines, are representative classes of fluorescent dyes with strong absorptions and fluorescence that are widely employed as fluorescent probes for bio-imaging.[1] Their common molecular design for attaining high stability toward nucleophiles as well as attractive photophysical properties is to introduce electron-donating amino groups to a highly extended π-conjugated cationic scaffold, which allows the delocalization of a positive charge over the entire skeleton.

In this context, tropylium ion should be a useful building block as a stable carbocation due to the pronounced Hückel aromaticity.[2,3] Since the first report by Knox *et al* in 1954,[2] the structure–stability relationship of tropylium ions have been extensively studied. For examples, Komatsu and co-workers achieved thermodynamic stabilization of tropylium ions by the introduction of electron-donating alkyl groups,[4] the intramolecularly fixed π-electron donors,[5] and the bicyclo[2.2.2]oct-2-ene-fused structure.[6] Gronowitz and co-workers studied the effect of annulation of heterocyclic rings onto the tropylium ion.[7] Taking advantage of high stability as well as the electron-deficient nature of tropylium ions, several fascinating π-electron materials, such as stimuli responsive materials[8,9] and near-infrared (NIR) absorbing dyes,[10] have been developed. In addition, the moderately reactive tropylium ions have been also recently employed as a mediator for the α-substitution of amines[11] or the nucleophilic substitution reactions,[12] and as a ligand for metal-sandwich complexes.[13]

To enhance the potential utility of the tropylium ion as a building block and establish a molecular design for new cationic dyes, we herein disclose amino-substituted dithienotropylium ions **2** that contain 3,3′-bithiophene as a substructure (Figure 2-1). The parent dithienotropylium ion, 4*H*-dithieno[1,2-*b*;4,3-*b′*]tropylium tetrafluoroborate **1a** has been already reported by Gronowitz and co-workers.[7a] By the introduction of the electron-donating amino-groups to the 5,5′-positions of the 3,3′-bithiophene skeleton, contribution from two resonance forms can be considered, namely a tropylium resonance form **2**$_t$ and a quinoidal resonance form **2**$_q$ (Figure 2-1(c)). The latter resonance form would delocalize the positive charge over the entire π-conjugated skeleton, and thereby impart high stability as well as intense absorption and fluorescence properties. In this work, we achieved the

rapid construction of the dithienotropylium scaffold, and the synthesis of a highly stable tropylium-based cationic dye with pK_R^+ value of 15.6. Comparative study on a series of dithienotropylium ions **2** with various amino groups enabled us to elucidate the impact of the amino groups on the resonance mode and properties.
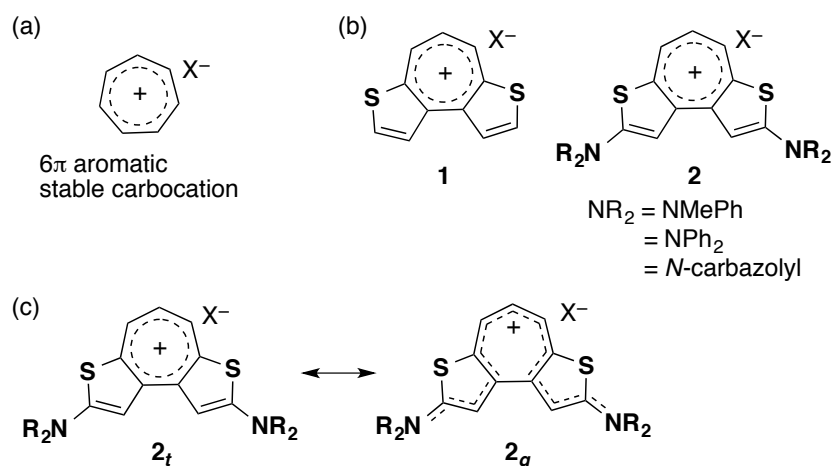

Figure 2-1. Chemical structures of (a) a tropylium ion, (b) dithienotropylium ions **1** and **2**, and (c) resonance structures in the diamino-substituted **2**.

2.2 Results and Discussion

A series of amino-substituted dithienotropylium ions were synthesized via 4*H*-cyclohepta[1,2-*b*;4,3-*b'*]dithiophene **6** as a key precursor (Scheme 2-1). Starting from 2,2′-dibromo-3,3′-bithiophene, which was prepared in 2 steps from 3-bromothiophene, selective mono-metalation was conducted with 1 equivalent of *i*-PrMgCl·LiCl. Further transmetallation with CuCN·2LiCl followed by a treatment with allyl bromide gave monoallylated bithiophene **3**. A vinyl group was next introduced *via* formylation followed by Wittig reaction. Thus prepared 2-allyl-2′-vinyl-3,3′-bithiophene **5** was subjected to a ring-closing metathesis (RCM) reaction using the 2nd generation Grubbs catalyst to afford **6** in 94% yield. It is noteworthy that this synthetic route enables us to access **6** in only 6 steps from commercially available 3-bromothiophene, which is much shorter than the previously reported synthetic method (11 steps).[7a] Dibromination of **6** followed by the Pd-catalyzed amination with several arylamines produced the corresponding diamino-substituted 4*H*-cyclohepta[1,2-*b*;4,3-*b'*]dithiophenes **8a–c**. Finally, hydride abstraction with Ph$_3$C$^+$BF$_4^-$ successfully gave a series of amino-substituted dithienotropylium

tetrafluoroborates **2a–c**. Non-substituted dithienotropylium ions **1a** and **1b** bearing tetrafluoroborate and tetrakis(pentafluorophenyl)borate as counter anions, respectively, were also synthesized in similar manners from **6** as the reference compounds. Notably, all of the dithienotropylium ions thus obtained were stable toward moisture and air under ambient conditions.
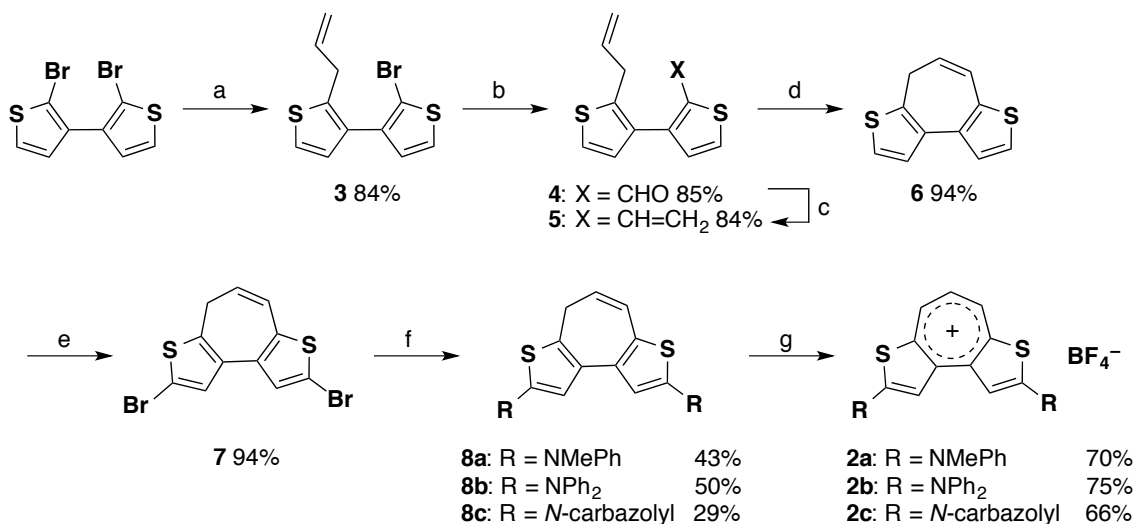
Scheme 2-1. Synthesis of amino-substituted dithienotropylium ions. *Reagents and conditions:* (a) i, *i*PrMgCl·LiCl, THF, 0 °C; ii, CuCN·2LiCl, iii, allyl bromide; (b) i, *n*BuLi, Et₂O, −78 °C; ii, DMF, −78 °C to rt; (c) Ph₃P=CH₂, THF, −78 °C to 0 °C; (d) (H₂IMes)(PCy₃)Cl₂Ru=CHPh (5 mol%), CH₂Cl₂, reflux; (e) i, *n*BuLi, THF, −78 °C; ii, BrCl₂CCCl₂Br; (f) PhMeNH or Ph₂NH, Pd(dba)₂, QPhos, NaO*t*Bu, toluene, reflux for **8a** and **8b**; carbazole, 3.0 M MeMgCl in THF, [PdCl(allyl)]₂ (2 mol%), cBRIDP (8 mol%), toluene/THF, reflux for **8c**; (g) Ph₃C⁺BF₄⁻, MeCN/EtOAc, rt for **2a** and **2b**; Ph₃C⁺BF₄⁻, MeCN/THF, rt for **2c**.

The molecular structures of dithienotropylium ions **2a–c** and **1b** were verified by X-ray crystallographic analyses (Figures 2-2–2-5 and Table 2-1). As a representative example, the structure of **2a,** together with atom-labels, are shown in Figure 2-2. In all compounds, the dithienotropylium skeletons adopt almost coplanar geometries. The sum of the internal angles of the seven-membered ring in **2a**, **2b**, **2c**, and **1b** are 900.0°, 899.2°, 899.0°, and 899.0°, and the dihedral angles between the two thiophene mean planes are 1.4(1)°, 6.5(1)°, 9.5(2)°, and 10.2(1)°, respectively. In addition, irrespective of the substituents on the thiophene rings, the four non-fused C–C bonds in the

64

seven-membered rings are much shorter (1.37–1.40 Å) than the other three C–C bonds that are part of the bithiophene substructure (1.42–1.45 Å): for instance, C5–C11 1.395(2) Å, C5–C6 1.386(2) Å, C6–C7 1.398(2) Å, C7–C8 1.388(2) Å, C8–C9 1.431(2) Å, C9–C10 1.445(2) Å, and C10–C11 1.421(2) Å for **2a**. The short bond lengths as well as the small bond alternation of the C11–C5–C6–C7–C8 moiety indicate significant contribution of a pentadienyl cation character.
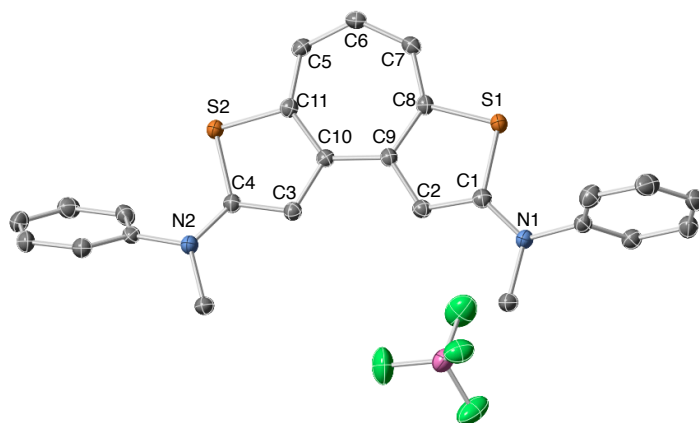

Figure 2-2. Crystal structure of **2a** drawn with thermal ellipsoids at 50% probability level. Hydrogen atoms are omitted for clarity.

Figure 2-3. X-ray crystal structure of **2b** drawn with thermal ellipsoid at 50% probability level. Hydrogen atoms are omitted for clarity. Selected bond length (Å) for **2b**: C5–C6 = 1.384(3), C6–C7 = 1.398(3), C7–C8 = 1.386(3), C8–C9 = 1.431(3), C9–C10 = 1.440(3), C10–C11 = 1.420(2), C11–C5 = 1.402(3). The sum of the internal angles in the seven-membered ring is 899.2°. The dihedral angle between the mean planes of S1–C1–C2–C9–C8 and S2–C4–C3–C10–C11 is 6.5(1)°.

Figure 2-4. X-ray crystal structure of **2c**·1,2-dichloroethane drawn with thermal ellipsoid at 50% probability level, where hydrogen atoms are omitted for clarity. Selected bond distances (Å): C5–C6 = 1.393(6), C6–C7 = 1.397(5), C7–C8 = 1.392(5), C8–C9 = 1.431(5), C9–C10 = 1.439(5), C10–C11 = 1.426(5), C11–C5 = 1.391(6). The sum of the internal angles in the seven–membered ring is 899.0°. The dihedral angle between the mean planes of S1–C1–C2–C9–C8 and S2–C4–C3–C10–C11 is 9.5(2)°.
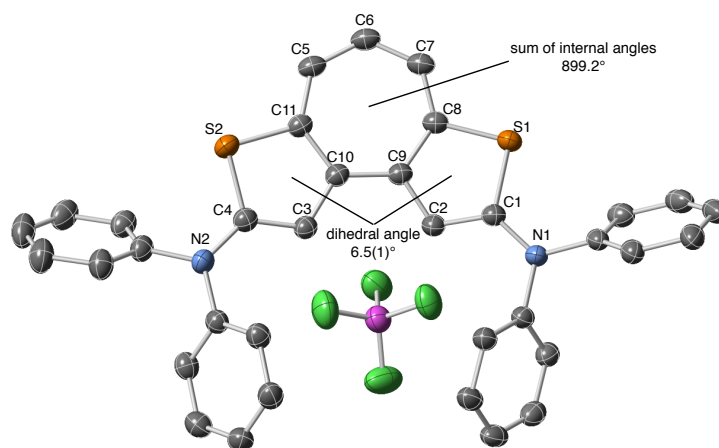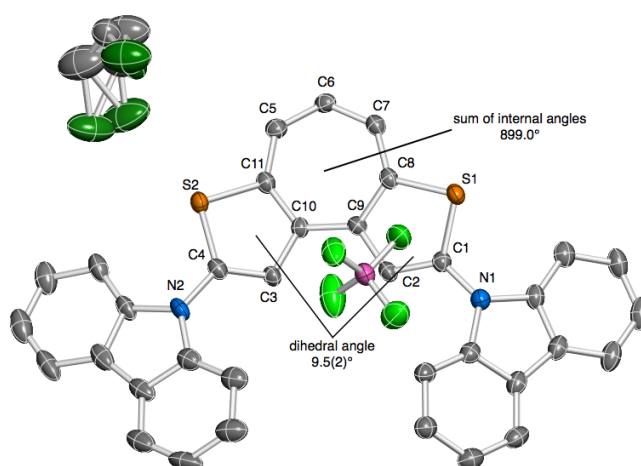

Figure 2-5. X-ray crystal structure of **1b**·toluene drawn with thermal ellipsoid at 50% probability level. Hydrogen atoms are omitted for clarity. Selected bond distance (Å) for **1b**: C5–C6 = 1.381(3), C6–C7 = 1.377(4), C7–C8 = 1.391(4), C8–C9 = 1.423(3), C9–C10 = 1.423(3), C10–C11 = 1.426(3), C11–C5 = 1.390(3). The sum of the internal angles in the seven-membered ring is 899.0°. The dihedral angle between the mean planes of S1–C1–C2–C9–C8 and S2–C4–C3–C10–C11 is 10.2(1)°.
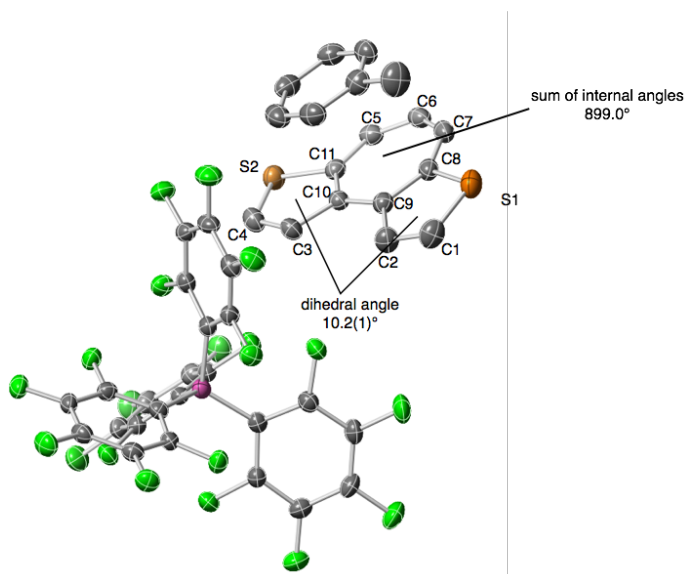
66

In contrast, the geometries of the bithiophene skeletons are highly dependent on the electron-donating ability of the terminal substituents (Table 2-1). As electron-donating ability of the substituents becomes larger in the order of **1b** (R = H), **2c** (R = *N*-carbazolyl), **2b** (R = NPh$_2$), and **2a** (R = NMePh), the C1–C2 and C3–C4 bonds in the end of fused thiophene rings become longer from 1.359(4) and 1.354(3) Å in **1b** to 1.394(2) Å in **2a**. Similarly, the β,β′-linkage in the bithiophene substructure, the C9–C10 bond, also becomes longer from 1.423(3) Å for **1b** and 1.445(2) Å for **2a**. Conversely, the terminal C–N bonds, C1–N1 and C4–N2, become considerably shorter from **2c** (1.375(5) Å and 1.394(5) Å) to **2a** (1.342(2) Å and 1.345(2) Å), as the electron-donating ability of the amino groups increase. Notably, the latter values for **2a** are within the range of C=N double bonds. These results demonstrate that the contribution of the quinoidal resonance form **2$_q$** becomes more pronounced rather than the tropylium resonance form **2$_t$** (Figure 2-1(c)) as the electron-donating ability of the terminal amino groups increases. The quinoidal resonance structure in the amino-substituted dithienotropylium ions is reminiscent of nitrogen-containing cationic dyes, such as rhodamine and cyanine dyes which displays attractive optical properties.

Table 2-1. Bond Lengths and NICS(0) Values of Dithinenotropylium Ion Derivatives
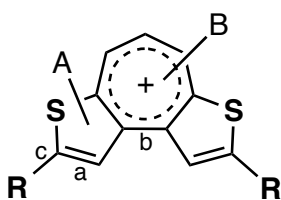
Cmpd	R	Bond length [Å][a]			NICS(0)[b] (HF/6-31+G(d,p))	
		a	b	c	A	B
2a	NMePh	1.394(2) 1.394(2)	1.445(2)	1.342(2) 1.345(2)	−8.9 −9.1	−5.5
2b	NPh$_2$	1.383(3) 1.392(3)	1.440(3)	1.352(2) 1.366(2)	−8.9 −9.3	−5.1
2c	Cz	1.383(5) 1.384(5)	1.439(5)	1.375(5) 1.394(5)	−9.9 −10.0	−5.4
1b	H	1.354(3) 1.359(4)	1.423(3)	–	−11.4 −11.4	−7.1

[a] Determined by X-ray crystallographic analyses [b] NICS (0) values calculated at the HF/6-31+G(d,p) level of theory using X-ray crystal structures, without including the respective counter anions.

In order to gain insight into the impacts of the terminal amino groups on the resonance structures in the dithienotropylium ions **2**, we evaluated the aromaticity of the central seven-membered ring as well as two outer thiophene rings in terms of their magnetic character. The nucleus-independent chemical shift (NICS)[14] values for **1b** and **2a–c** were calculated at the HF/6-31+G(d,p) level of theory using their crystal structures. As the electron-donating ability of substituents increases in the order of **1b**, **2c**, **2b**, and **2a**, the NICS (0) values for all the three rings become higher. For instance, NICS(0) values of the two thiophene rings and the seven-membered ring in PhMeN-substituted **2a** were $-8.9/-9.1$ ppm and -5.5 ppm, respectively, which were higher than those of the parent dithienotropylium ion **1b** (-11.4 ppm/-11.4 ppm and -7.1 ppm). In accordance with these computational results, the resonance signals for the protons H_a and H_b on the central seven-membered ring in the ^{1}H NMR spectra in CD_3CN were gradually upfield-shifted in the order of **1b** (9.55 ppm/8.38 ppm), **2c** (8.97 ppm/8.07 ppm), **2b** (8.09 ppm/7.28 ppm), and **2a** (7.99 ppm and 7.17 ppm, Figure 2-6). These results clearly demonstrate that the introduction of the electron-donating amino groups to the dithienotropylium ion diminishes the aromaticity of both thiophene rings and tropylium ion moiety, giving rise to the pronounced quinoidal character.
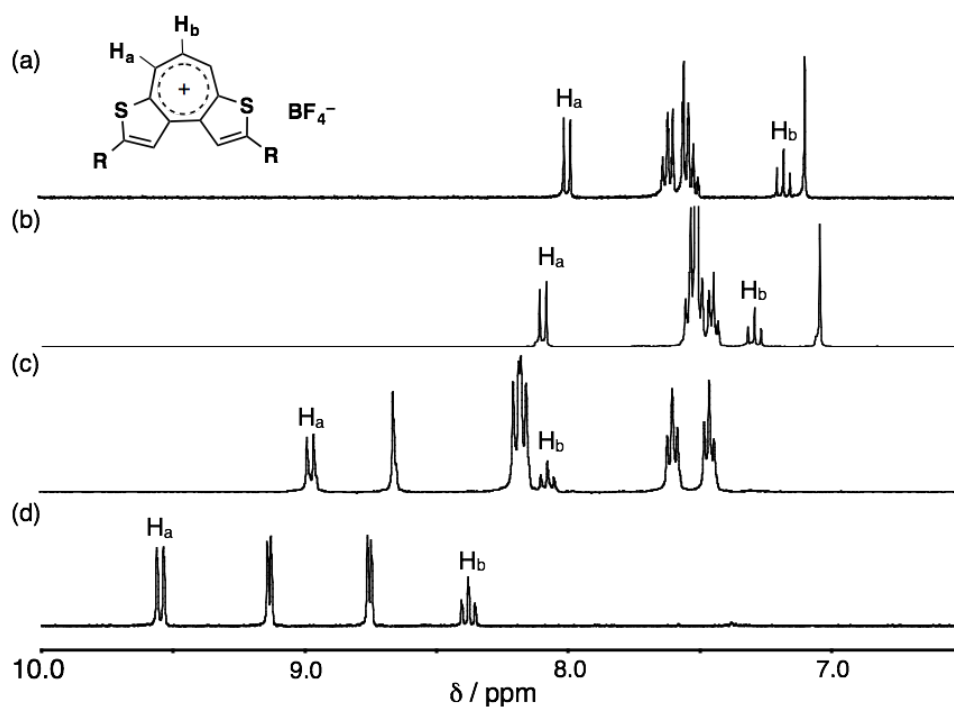

Figure 2-6. ^{1}H NMR (400 MHz) spectra of a series of dithienotropylium ions (a) **2a**, (b) **2b**, (c) **2c** and (d) **1b** in CD_3CN.

The electron-donating amino groups also significantly perturb the reactivities of tropylium ion moiety. Whereas significant discoloration was observed for carbazolyl-substituted **2c** in Lewis basic solvents, such as acetone and DMSO, the more electron-donating PhMeN- or Ph$_2$N-substituted **2a** and **2b** did not show any decomposition under the same conditions. In light of the fact that even representative trityl cation-based dyes, such as Malachite Green and Crystal Violet, show similar discoloration,[15] the pronounced stability of **2a** and **2b** should be worth noting as a new entity of stable carbocations. To quantitatively assess the stability of the carbocations, the affinities toward hydroxide ions, namely pK_R^+ values,[16] were investigated. Based on the UV/Vis absorption spectra in aqueous buffer solutions containing 50% CH$_3$CN with varied pH values, the pK_R^+ values of Ph$_2$N- and carbazolyl-substituted **2b** and **2c** were determined to be 13.8 and 5.2, respectively, while that of the parent dithienotropylium ion **1a** was 5.1 (Figures 2-7–2-9).

Figure 2-7. (a) pH-dependent change of absorption spectra of **1a** (1.0 x 10^{-5} M) in 50% CH$_3$CN aqueous solutions and (b) a plot of absorbance of **1a** at 442 nm in the 50% CH$_3$CN aqueous solutions as a function of pH values. The pK_R^+ value was determined to be 5.1.

69
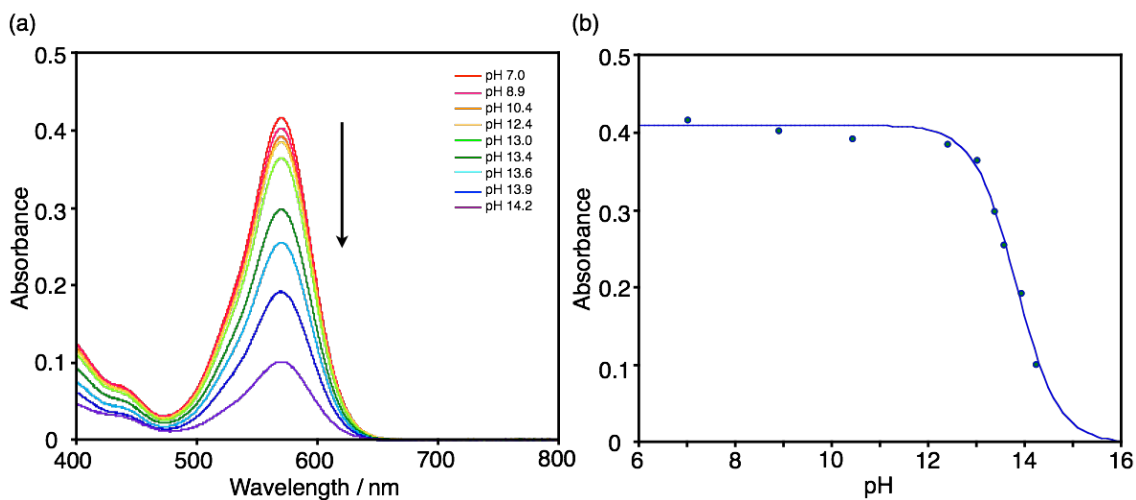
Figure 2-8. (a) pH-dependent change of absorption spectra of **2b** (1.0×10^{-5} M) in 50% CH$_3$CN aqueous solutions and (b) a plot of absorbance of **2b** at 570 nm in the 50% CH$_3$CN aqueous solutions as a function of pH values. The pK_R^+ value was determined to be 13.8.
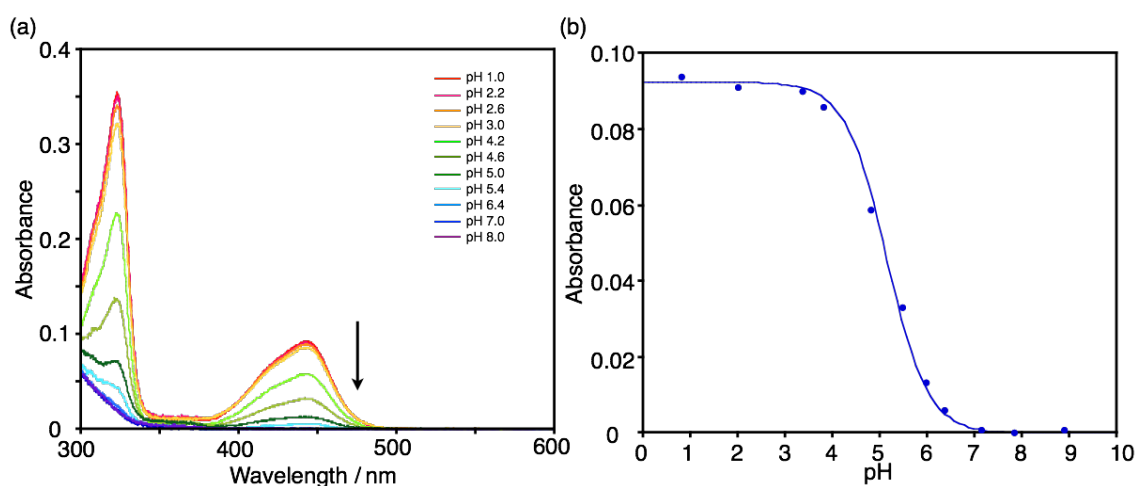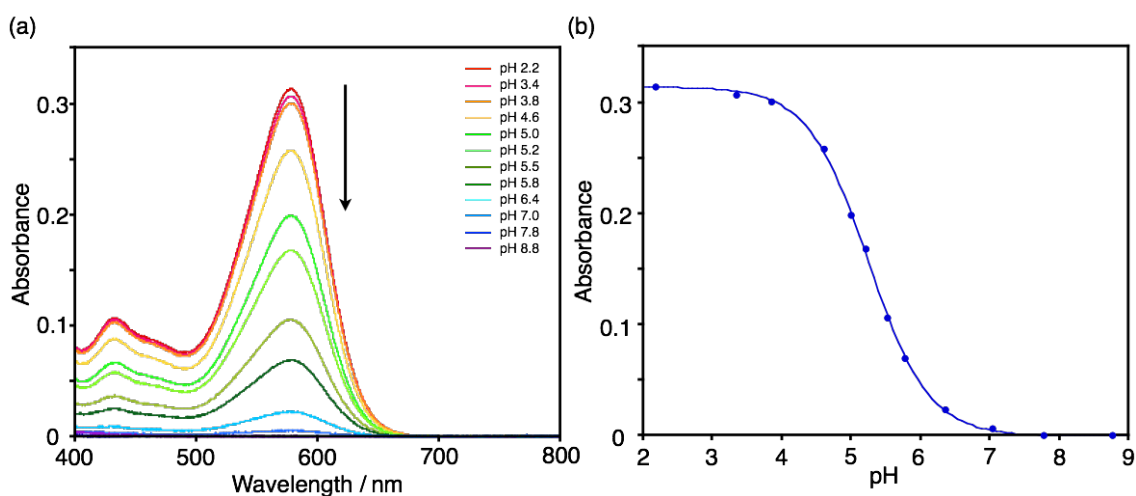

Figure 2-9. (a) pH-dependent change of absorption spectra of **2c** (1.0×10^{-5} M) in 50% CH$_3$CN aqueous solutions and (b) a plot of absorbance of **2c** at 578 nm in the 50% CH$_3$CN aqueous solutions as a function of pH values. The pK_R^+ value was determined to be 5.2.

Since the absorption spectra of more electron-donating PhMeN-substituted **2a** did not show any change even upon increasing the pH values of the buffer solution to 14, its pK_R^+ value was determined on the basis of Laursen's acidity function C_-, which is a typical method for the evaluation of a stable carbocation with the pK_R^+ value higher than

70

14 (Table 2-2).[17] Using basic DMSO/H$_2$O solutions of tetraammonium hydroxide with varied DMSO/H$_2$O ratios, the pK_R^+ value of **2a** was determined to be 15.6 (Figures 2-10 and 2-11). Comparison of these values demonstrates that the dithienotropylium ion moiety is highly stabilized by the electron-donating PhMeN- or Ph$_2$N- groups in **2a** and **2b**, whereas the carbazolyl group in **2c** does not have substantial stabilization effect. Notably, the pK_R^+ values of **2a** and **2b** are much higher than that of Crystal Violet (pK_R^+ = 9.4)[18] and even higher than that of a bicyclooctene-fused tropylium ion (pK_R^+ = 13.0) reported by Komatsu *et al*,[6a] which has been recognized as the most stable tropylium ion to date. The significantly high stabilities of **2a** and **2b** suggest promising utility of the amino-substituted dithienotropylium scaffold as a building block for the cationic organic dyes.

Table 2-2. Absorption Spectral Data for **2a** in Various DMSO/water Solutions with 0.011 M of Me$_4$NOH

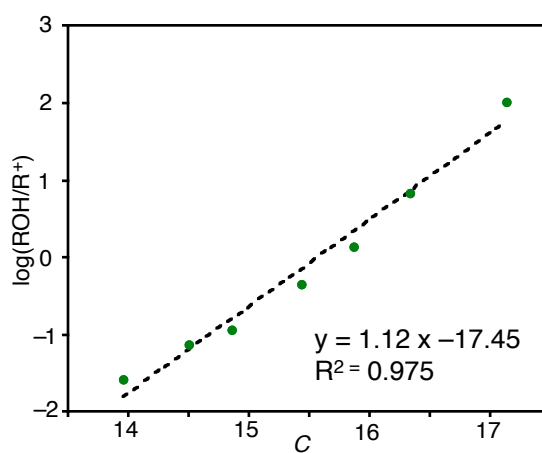| DMSO mol%	C_- [a]	Absorbance at 560 nm	log[ROH/[R$^+$]
14.5	13.96	0.4076	−1.568
17.8	14.50	0.3889	−1.116
20.2	14.86	0.3744	−0.927
24.4	15.44	0.2886	−0.346
27.6	15.87	0.1760	0.139
31.1	16.34	0.0541	0.829
37.2	17.14	0.0039	2.025

[a] Laursen's acidity function.

$$y = 1.12\,x - 17.45$$
$$R^2 = 0.975$$

Figure 2-10. A plot of log([ROH/R$^+$]) values as a function of C_- values for **2a**.
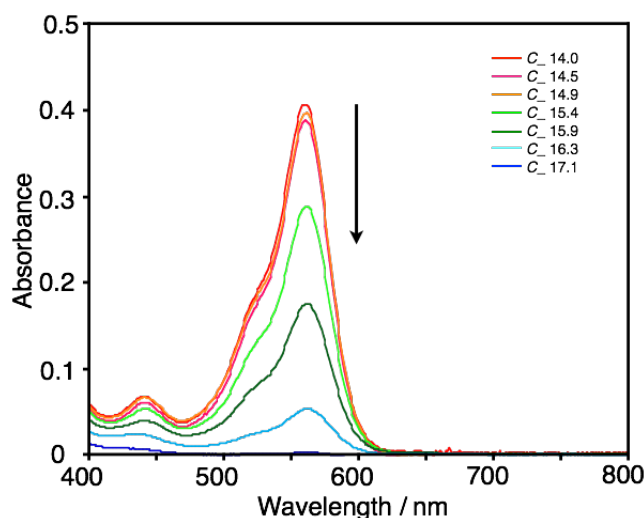
Figure 2-11. Change in absorption spectra of **2a** $(1.0 \times 10^{-5}$ M) in DMSO/water/NMe$_4$OH solutions with varied $C\_$values.

The substantial quinoidal characters of **2a** and **2b** lead to attractive photophysical properties, which are different from those of the parent **1a** and the carbazolyl-substituted **2c** (Figures 2-12–2-15 and Table 2-3). Thus, while **1a** showed a weak absorption band with the maximum wavelength (λ_{abs}) of 442 nm ($\varepsilon = 4800$), amino-substituted derivatives **2a–c** showed significantly red-shifted absorption bands with significant increase in the molar absorption coefficients (**2a**: $\lambda_{abs} = 558$ nm, $\varepsilon = 44100$; **2b**: $\lambda_{abs} = 571$ nm, $\varepsilon = 37800$; **2c**: $\lambda_{abs} = 580$ nm, $\varepsilon = 35300$), indicating the distinct character of the electronic transitions between them (*vide infra*). In addition, whereas **2c** exhibited negative solvatochromism in the absorption spectra (Figure 2-15), compounds **2a** and **2b** did not show significant solvent dependency (Figures 2-13 and 2-14). Importantly, while **1a** and **2c** were virtually non-fluorescent, **2a** and **2b** showed orange and deep-red fluorescences with the maximum wavelengths (λ_{em}) of 604 nm ($\Phi_F = 0.17$) and 666 nm ($\Phi_F = 0.10$), respectively, in CHCl$_3$. Compound **2b** has a larger Stokes shift (2320 cm^{-1}) relative to that of **2a** (960 cm^{-1}). Similar to the absorption spectra, these compounds did not show noticeable solvatochromism in the fluorescent spectra. This behavior is similar to other cationic fluorescent dyes such as rhodamines derivatives.[19]

72

Table 2-3. Photophysical Properties of **1a** and **2a–c** in Various Solvents

Cmpd	solvent	λ_{abs} [nm]	ε [x 10^4 $M^{-1}cm^{-1}$]	λ_{em} [nm]	Φ_F[a]
1a	CH$_3$CN	441	0.48	_[b]	_[b]
2a	CHCl$_3$	571	4.75	604	0.17
	CH$_2$Cl$_2$	560	4.86	601	0.11
	acetone	558	4.60	602	0.07
	CH$_3$CN	558	4.10	601	0.04
	DMSO	563	4.14	610	0.06
2b	CHCl$_3$	577	3.97	666	0.10
	CH$_2$Cl$_2$	580	3.91	666	0.06
	acetone	572	3.79	666	n.d.
	CH$_3$CN	571	3.78	663	n.d.
	DMSO	572	3.49	664	0.06
2c	CH$_2$Cl$_2$	616	3.66	_[b]	_[b]
	CH$_3$CN	580	3.53	_[b]	_[b]

[*a*] Absolute fluorescence quantum yields determined by a calibrated integrating sphere system. [*b*] Not observed.
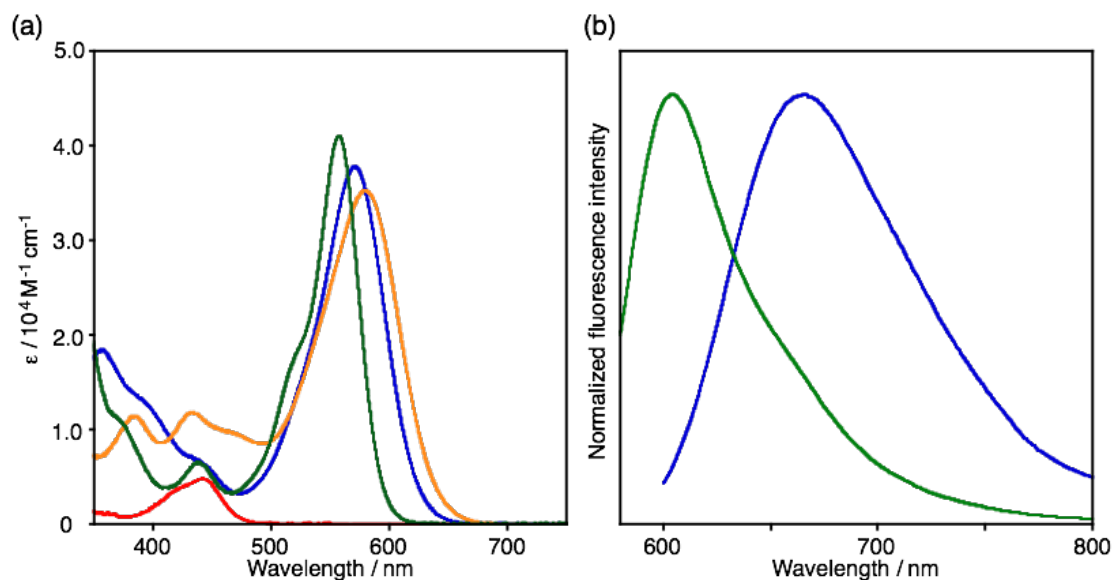
Figure 2-12. (a) UV/Vis absorption spectra of a series of dithienotropylium ions **1b** (red), **2a** (green), **2b** (blue), and **2c** (orange) in CH$_3$CN and (b) fluorescence spectra of **2a** (green) and **2b** (blue) in CHCl$_3$.
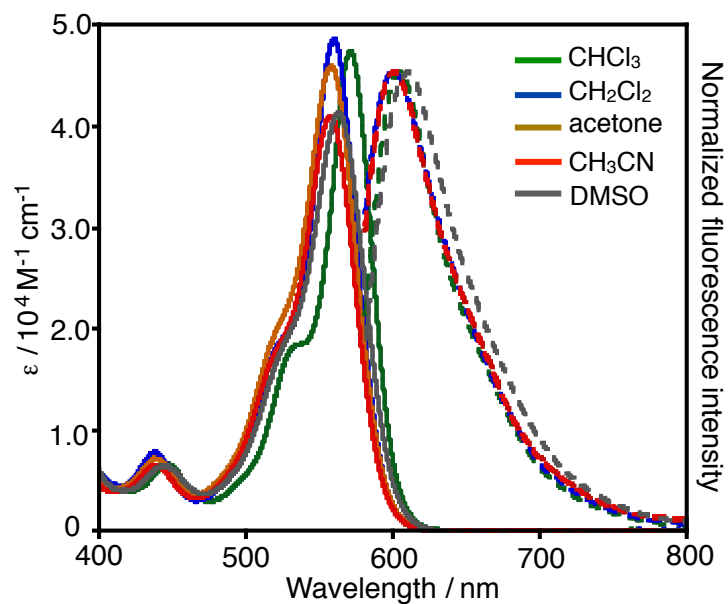
Figure 2-13. Absorption (solid line) and fluorescence spectra (broken line) of **2a** in various solvents.
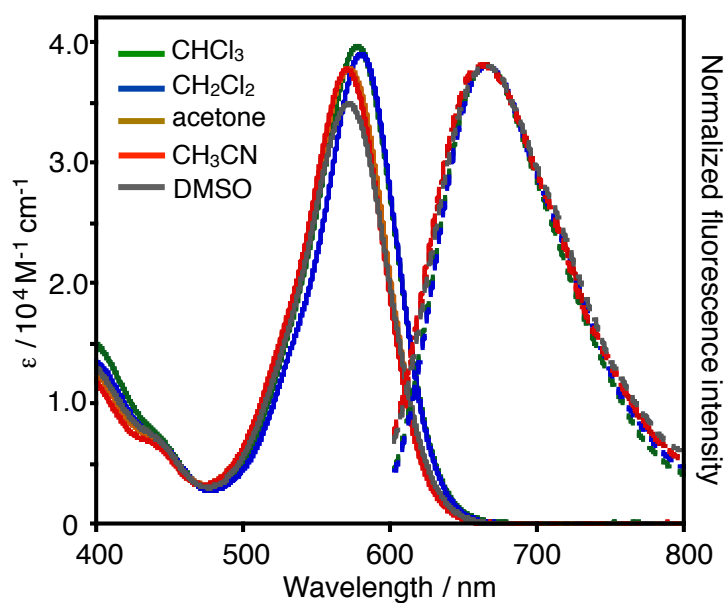
Figure 2-14. Absorption (solid line) and fluorescence spectra (broken line) of **2b** in various solvents.
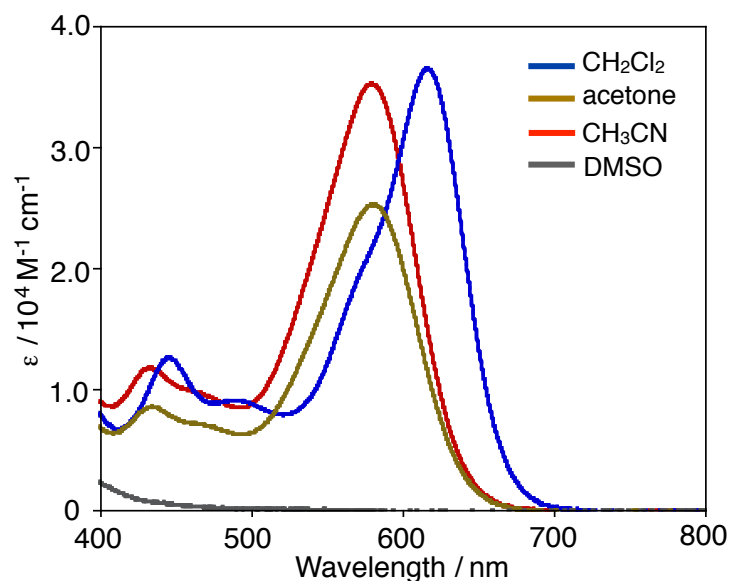
Figure 2-15. Absorption spectra of **2c** in various solvents. **2c** was not dissolved in CHCl₃. Discoloration occurred in acetone and in DMSO. **2c** did not show any fluorescence.

Theoretical calculations allowed us to elucidate the differences in the photophysical properties among these compounds. The structural optimizations and TD-DFT calculations were conducted at the CAM-B3LYP/6-31G(d) level of theory for the corresponding model compounds **2a′–2c′** and **1a′**, where counter anions were not included (Figure 2-16). Parent dithienotropylium ion **1a′** has doubly degenerated HOMO and HOMO−1, which are delocalized over the π skeleton. Its lowest-energy transition can be assigned to a transition from HOMO−1 to LUMO with a symmetry-forbidden character ($f = 0.0036$). In contrast, the introduction of amino groups to the terminal thiophene rings results in the delocalization of HOMO and LUMO over the entire π skeleton including the amino groups, and thereby decreases the HOMO–LUMO energy gap. In addition, the amino groups broke the degeneracy of HOMO and HOMO−1. As a consequence, compounds **2a′**, **2b′**, and **2c′**, can have symmetry-allowed HOMO→LUMO transitions with high oscillator strengths ($f = 0.5347$, 0.5802, and 0.6012, for **2a′**, **2b′**, and **2c′**, respectively). In contrast to the fact that HOMOs and LUMOs of **2a′** and **2b′** are delocalized over the amino-substituted dithienotropylium moieties, those in carbazolyl-substituted **2c′** are rather localized on the carbazolyl moieties and dithienotropylium moiety, respectively. As a result, **2c′** has the intramolecular charge transfer (ICT) character from carbazole to dithienotropylium

75

ion moiety in the HOMO→LUMO transition, which should be responsible for the solvatochromic behavior in the absorption spectra.
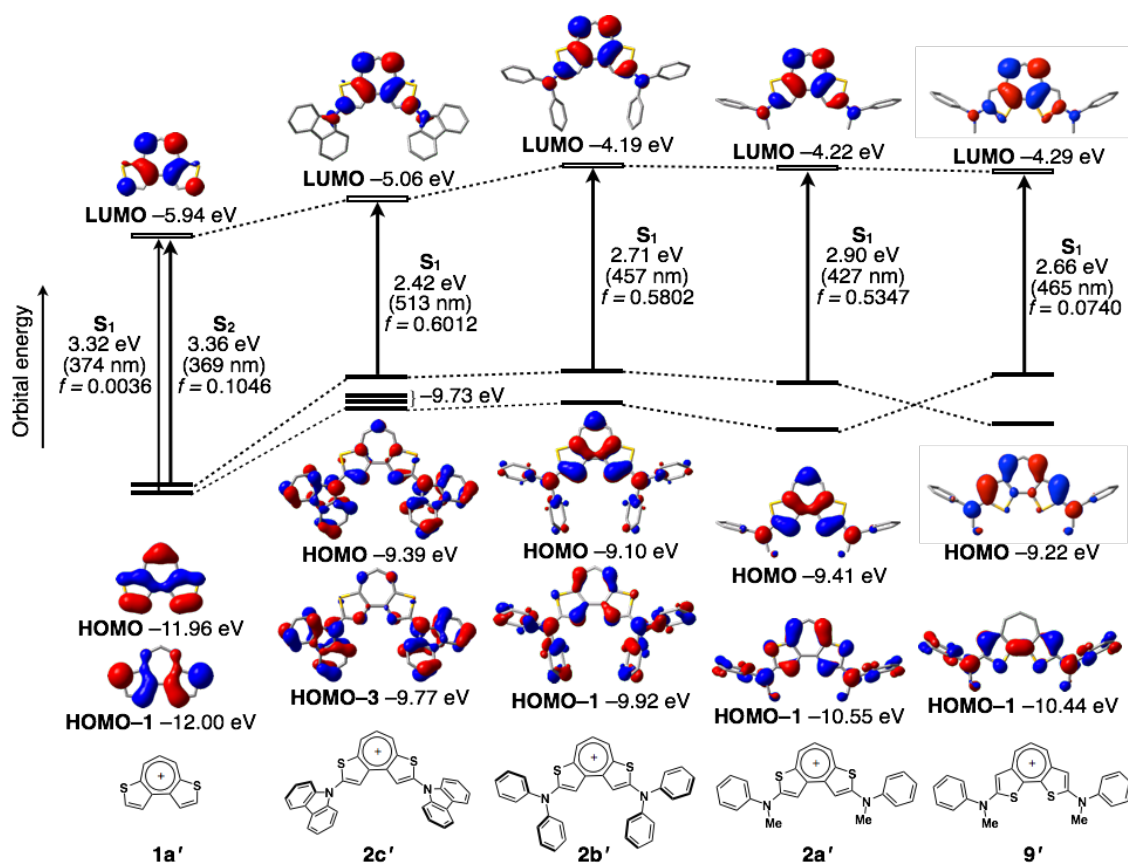
Figure 2-16. Kohn-Sham molecular orbitals and relevant vertical excitations of model compounds **1a′**, **2a′**, **2b′**, **2c′**, and **9′** estimated by the TD-DFT calculations at the CAM-B3LYP/6-31G(d) level.

Importantly, the fusing mode of the thiophene rings to the tropylium moiety plays a crucial role for making the quinoidal resonance being a major contribution. For comparison, an analogous compound, amino-substituted 4*H*-dithieno[2,1-*b*;3,4-*b′*]tropylium ion **9′** with a 2,2′-bithiophene substructure was calculated at the same level of theory used for **2**. The NICS(0) value of the central seven-membered ring in **9′** was –6.7 ppm indicative of the significant aromaticity of this ring and thereby a larger contribution of the tropylium resonance structure. With regard to the delocalization modes of molecular orbitals, while both **2a′** and **9′** have similar LUMOs mainly localized on the tropylium ring, the orbital symmetries of HOMO and

HOMO–1 are switched from **2a′** to **9′** (Figure 2-16). This is due to more effective π-conjugation in the 2,2′-bithiophene moiety in **9′** compared to the 3,3′-bithiophene moiety in **2a′**. As a consequence, the oscillator strengths *f* of **9′** for the S_0–S_1 transition becomes a much smaller value of 0.074 compared to that of **2a′** (*f* = 0.5347). These comparisons clearly demonstrate that the 3,3′-bithiophene substructure in **2** is crucial for producing the strong absorption in visible region.

2.3 Conclusion

The author synthesized the amino-substituted dithienotropylium ions as a new entity for the cationic dyes. These compounds exhibited outstanding stability even under highly basic condition due to both the strong electron-donating effect by amino groups as well as the effective delocalization of a positive charge over the π-conjugated skeleton. X-ray crystallographic analyses clearly demonstrated that the aromaticity of tropylium ions and thiophene rings significantly diminishes by the increase of the electron-donating ability of amino groups, giving rise to the pronounced contribution of a quinoidal resonance form. Reflecting the strong contribution of quinoidal resonance structure, amino-substituted dithienotropylium ions **2a** and **2b** showed a set of attractive photophysical properties such as intense absorption in the visible region and the orange to red fluorescences. For these characteristic structural features and photophysical properties, 3,3′-bithiophene-fused fashion is found to be crucial. Further studies on these tropylium-based cationic dyes and the application for the bio-imaging fluorophores are investigated underway.

2.4 Experimental Section

General. Melting points (mp) were determined with a Yanaco MP-S3 instrument (MP-S3). ^{1}H and ^{13}C{^{1}H} NMR spectra were recorded with a JEOL AL-400 spectrometer in CDCl$_3$, CD$_2$Cl$_2$, C$_6$D$_6$, THF-d_8, or CD$_3$CN (400 MHz for ^{1}H and 100 MHz for ^{13}C). ^{13}C{^{1}H} NMR spectrum of **2c** was recorded with a JEOL ECA 600 II spectrometer equipped with an UltraCOOL probe in CD$_2$Cl$_2$ (150 MHz for ^{13}C). The chemical shifts in ^{1}H NMR spectra are reported in *δ* ppm using the residual proton of the solvents, *i.e.,* CHCl$_3$ (7.26 ppm), CH$_2$Cl$_2$ (5.32 ppm), C$_6$H$_6$ (7.16 ppm), THF (1.72 ppm) and CH$_3$CN (1.94 ppm), as an internal standard. The chemical shifts in ^{13}C NMR spectra are reported in *δ* ppm using the solvent signals of CDCl$_3$ (77.16 ppm), CD$_2$Cl$_2$

(53.84 ppm), C_6D_6 (128.06 ppm), THF-d_8 (67.21 ppm) and CD_3CN (118.26 ppm) as an internal standard. Mass spectra were measured with a Bruker micrOTOF Focus spectrometer with the ionization method of APCI or ESI. Thin layer chromatography (TLC) was performed on plates coated with 0.25 mm thickness of silica gel 60F$_{254}$ (Merck). Column chromatography was performed using PSQ100B (Fuji Silysia Chemicals) or Wakosil 50NH$_2$(HC) (Wako Pure Chemicals Industries, Ltd). Recycling preparative gel permeation chromatography (GPC) was performed using YMC LC-forte/R equipped with a polystyrene gel column (YMC-GPC T2000 and T400) and toluene as an eluent. Anhydrous THF, Et$_2$O, and CH_2Cl_2 were purchased from Kanto Chemicals and further purified by Glass Contour solvent purifier systems. CH_3CN and EtOAc were stored over 3 Å molecular sieves prior to use. 2,2′-Dibromo-3,3′-bithiophene[20] and iPrMgCl·LiCl[21] were prepared according to the literature methods. All reactions were preformed under a nitrogen or argon atmosphere unless stated otherwise.

2-Allyl-2′-bromo-3,3′-bithiophene (3). To a solution of 2,2′-dibromo-3,3′-bithiophene (14.6 g, 45.1 mmol) in THF (450 mL) was added of a THF solution of iPrMgCl·LiCl (1.64 M, 27.4 mL, 44.9 mmol) dropwise over 12 min at 0 °C. The reaction mixture was stirred for 3 h at the same temperature. A THF solution of CuCN·2LiCl (0.999 g/mL, 0.160 mL, 0.917 mmol) and then allyl bromide (4.70 mL, 6.57 g, 54.3 mmol) were subsequently added to the mixture, which was further stirred for 3 h at the same temperature. After the addition of a saturated aqueous solution of NH_4Cl, the aqueous layer was extracted with Et$_2$O. The combined organic layer was dried over Na_2SO_4, filtered, and concentrated under reduced pressure. The mixture was purified by column chromatography (PSQ100B, hexane, R_f = 0.27) to afford **3** as colorless liquid (10.8 g, 37.9 mmol, 84%). ^{1}H NMR (400 MHz, CDCl$_3$): δ 3.50 (dt, J = 6.4, 1.6 Hz, 2H), 5.07 (dd, J = 10.4, 1.6 Hz, 1H), 5.08 (dd, J = 16.4, 1.6 Hz ,1H), 5.93 (ddt, J = 16.4, 10.4, 6.4 Hz, 1H), 6.90 (d, J = 5.6 Hz, 1H), 7.03 (d, J = 5.2 Hz, 1H), 7.20 (d, J = 5.2 Hz, 1H), 7.28 (d, J = 5.6 Hz, 1H). ^{13}C{^{1}H} NMR (CDCl$_3$, 100 MHz): δ 33.2, 110.7, 116.5, 122.7, 125.7, 129.2, 129.5, 132.0, 136.5, 137.1, 140.1. HRMS (APCI): m/z Calcd. for $C_{11}H_{10}^{79}BrS_2$: 284.9402 ([M+H]$^+$). Obsd. 284.9409.

2-Allyl-2′-formyl-3,3′-bithiophene (4). To a solution of **3** (1.54 g, 5.40 mmol) in Et$_2$O (27 mL) was added a hexane solution of *n*BuLi (1.61 M, 3.68 mL, 5.92 mmol) over 4 min at −78 °C. The reaction mixture was stirred for 1.5 h at the same temperature, and then DMF (0.625 mL, 0.590 g, 8.07 mmol) was added dropwise over 1 min to the resulting solution. The reaction mixture was allowed to warm to an ambient temperature and further stirred for 9.5 h. After the addition of water, the aqueous layer was extracted with Et$_2$O. The combined organic layer was washed with brine, dried over Na$_2$SO$_4$, filtered, and concentrated under reduced pressure. The mixture was purified by column chromatography (PSQ100B, hexane/EtOAc = 15/1, R_f = 0.38) to afford **4** as orange liquid (1.07 g, 4.57 mmol, 85%). ^{1}H NMR (400 MHz, C$_6$D$_6$): δ 3.15 (dt, J = 6.4, 1.6 Hz, 2H), 4.84 (dd, J = 16.8, 1.6 Hz, 1H), 4.86 (dd, J = 10.0, 1.6 Hz 1H), 5.64 (ddt, J = 16.8. 10.0, 6.4 Hz, 1H), 6.54 (d, J = 5.2 Hz, 1H), 6.59 (d, J = 5.2 Hz, 1H), 6.69 (d, J = 5.2 Hz, 1H), 6.82 (dd, J = 5.2, 1.2Hz, 1H), 9.74 (d, J = 1.2 Hz, 1H). ^{13}C{^{1}H} NMR (CDCl$_3$, 100 MHz): δ 32.9, 117.0, 123.6, 129.9, 130.8, 130.9, 134.1, 136.0, 139.4, 140.9, 145.9, 184.1. HRMS (APCI): m/z Calcd. for C$_{12}$H$_{10}$OS$_2$: 234.0168 ([*M*]$^+$). Obsd. 234.0176.

2-Allyl-2′-vinyl-3,3′-bithiophene (5). To a solution of methyltriphenylphosphonium bromide (1.61 g, 4.51 mmol) in THF (10 mL) was added a hexane solution of *n*BuLi (1.61 M, 2.81 mL, 4.52 mmol) dropwise over 4 min at −78 °C. The reaction mixture was stirred at 0 °C for 1 h, and then a solution of **4** (0.883 g, 3.77 mmol) in THF (20 mL) was added to the reaction mixture over 8 min at −78 °C. After stirred at the same temperature for 1 h, the reaction mixture was warmed to 0 °C and stirred for another 12 h. After the addition of water, the aqueous layer was extracted with Et$_2$O. The combined organic layer was washed with brine, dried over Na$_2$SO$_4$, filtered, and concentrated under reduced pressure. The mixture was purified by column chromatography (PSQ100B, hexane, R_f = 0.40) to afford **5** as colorless liquid (0.737 g, 3.17 mmol, 84%). ^{1}H NMR (400 MHz, CDCl$_3$): δ 3.45 (dt, J = 6.4, 1.6 Hz, 2H), 5.05 (dd, J = 10.0, 1.6 Hz, 1H), 5.07 (dd, J = 16.8, 1.6 Hz 1H), 5.10 (d, J = 10.8 Hz, 1H), 5.56 (d, J = 16.8 Hz, 1H), 5.90 (ddt, J = 16.8. 10.0, 6.4 Hz, 1H), 6.92 (d, J = 5.2 Hz, 1H), 6.93 (d, J = 5.2, 1H), 7.17 (d, J = 5.2, 1H), 7.19 (d, J = 5.2, 1H). ^{13}C{^{1}H} NMR (CDCl$_3$, 100 MHz): δ 33.0, 113.6, 116.4, 122.7, 123.1, 129.4, 129.8, 130.0, 132.9, 135.0, 136.6, 138.9, 139.5. HRMS (APCI): m/z Calcd. for C$_{13}$H$_{13}$S$_2$: 233.0453 ([*M*+H]$^+$). Obsd. 233.0458.

4H-Cyclohepta[1,2-b;4,3-b']dithiophene (6). To a solution of **5** (0.518 g, 2.23 mmol) in degassed CH_2Cl_2 (230 mL) was added $(H_2IMes)(PCy_3)Cl_2Ru=CHPh$ (2nd generation Grubbs catalyst) (94.7 mg, 0.112 mmol) in one portion. The reaction mixture was stirred at reflux temperature for 19 h. The reaction was quenched by the addition of ethyl vinyl ether (1 mL), and the resulting mixture was concentrated under reduced pressure. The mixture was purified by column chromatography (PSQ100B, hexane, $R_f =$ 0.33) to afford **6** as colorless solids (0.430 g, 2.10 mmol, 94%). Mp: 44.1–45.0 °C. ^{1}H NMR (400 MHz, C_6D_6): δ 2.97 (d, $J = 6.8$ Hz, 2H), 5.26 (dt, $J = 10.0$, 6.8 Hz, 1H), 6.41 (d, $J = 10.0$ Hz, 1H), 6.72 (d, $J = 5.2$ Hz, 1H), 6.81 (d, $J = 5.2$ Hz, 1H), 6.97 (d, $J = 5.2$ Hz, 1H), 7.02 (d, $J = 5.2$ Hz, 1H). ^{13}C{^{1}H} NMR (CDCl$_3$, 100 MHz): δ 27.1, 122.0, 123.4, 124.1, 124.4, 126.9, 127.5, 132.2, 134.3, 136.0, 136.8. HRMS (APCI): m/z Calcd. for $C_{11}H_8S_2$: 204.0062 ($[M]^+$). Obsd. 204.0067.

2,8-Dibromo-4H-cyclohepta[1,2-b;4,3-b']dithiophene (7). To a solution of **6** (0.429 g, 2.10 mmol) in THF (21 mL) was added a pentane solution of tBuLi (1.61 M, 3.90 mL, 6.28 mmol) dropwise over 5 min at –78 °C. The reaction mixture was stirred for 1.5 h at the same temperature, and then 1,2-dibromotetrachloroethane (2.05 g 6.30 mmol) was added in one portion to the solution. The reaction mixture was stirred for 2 h at the same temperature. After the addition of water, the aqueous layer was extracted with Et_2O. The combined organic layer was washed with brine, dried over Na_2SO_4, filtered, and concentrated under reduced pressure. The mixture was purified by column chromatography (PSQ100B, hexane, $R_f = 0.50$) to afford **7** as white solids (0.712 g, 1.97 mmol, 94%). Mp: 115.0–116.0 °C. ^{1}H NMR (400 MHz, CDCl$_3$): δ 3.22 (d $J = 6.8$ Hz, 2H), 5.67 (dt, $J = 10.0$, 6.8 Hz, 1H), 6.51 (d, $J = 10.0$ Hz, 1H), 7.11 (s, 1H), 7.17 (s, 1H). ^{13}C{^{1}H} NMR (CDCl$_3$, 100 MHz): δ 27.1, 108.3, 112.5, 123.2, 123.7, 129.3, 129.9, 132.9, 133.7, 135.6, 138.8. HRMS (APCI): m/z Calcd. for $C_{11}H_6{}^{79}Br_2S_2$: 359.8272 ($[M]^+$). Obsd. 359.8276.

2,8-Bis(N-methyl-N-phenylamino)-4H-cyclohepta[1,2-b;4,3-b']dithiophene (8a). To a solution of **7** (0.145 g, 0.400 mmol) in toluene (4 mL) was added N-methylaniline (0.130 mL, 0.128 g, 1.19 mmol), NaOtBu (0.115 g, 1.20 mmol), Pd(dba)$_2$ (9.17 mg, 0.0159 mmol) and 1,2,3,4,5-pentaphenyl-1$'$-(di-$tert$-butylphosphino)ferrocene (QPhos) (22.7 mg, 0.0319 mmol). The reaction mixture was stirred at reflux temperature for 17 h

and then was filtered through a plug of Celite®. The filtrate was concentrated under reduced pressure. The mixture was purified by column chromatography (Wakosil 50NH₂(HC), hexane/toluene = 10/1, R_f = 0.25) and further purified by GPC (toluene) to afford **8a** as white solids (71.3 g, 0.118 mmol, 43%). Mp: 124.1 °C (decomp.). ¹H NMR (400 MHz, THF-d_8): δ 3.22 (d, J = 6.4 Hz, 2H), 3.27 (s, 3H), 3.35 (s, 3H), 5.54 (dt, J = 10.0, 6.4 Hz, 1H), 6.43 (d, J = 10.0 Hz), 6.72 (s, 1H), 6.76 (t, J = 7.2 Hz, 1H), 6.87 (s, 1H), 6.90 (d, J = 8.4 Hz, 2H), 6.91 (t, J = 7.2 Hz, 1H), 7.13 (d, J = 8.4 Hz, 2H), 7.15 (dd, J = 8.4, 7.2 Hz, 2H), 7.23 (dd, J = 8.4, 7.2 Hz, 2H). ¹³C{¹H} NMR (C₆D₆, 100 MHz): δ 27.6, 41.7, 41.8, 115.5, 116.0, 119.1, 119.9, 121.0, 121.4, 122.0, 124.1, 126.6, 129.3, 129.4, 129.5, 133.0, 136.1, 149.1, 149.3, 149.7, 153.4. HRMS (APCI): m/z Calcd. for C₂₅H₂₃N₂S₂: 415.1297 ([M+H]⁺). Obsd. 415.1313.

2,8-Bis(*N,N*-diphenylamino)-4*H*-cyclohepta[1,2-*b*;4,3-*b'*]dithiophene (8b). To a solution of **7** (0.109 g, 0.301 mmol) in toluene (3 mL) was added diphenylamine (112 mg, 6.62 mmol), NaO*t*Bu (72.3 mg, 0.752 mmol), Pd(dba)₂ (3.46 mg, 6.02 μmol) and QPhos (5.69 mg, 8.01 μmol). The reaction mixture was stirred at reflux temperature for 8 h, and then was filtered through a plug of Celite®. The filtrate was concentrated under reduced pressure. The mixture was purified by column chromatography (Wakosil 50NH₂(HC), hexane/toluene = 10/1, R_f = 0.25) to afford **8b** as colorless solids (80.9 mg, 0.150 mmol, 50%). Mp: 77.0 °C (decomp.). ¹H NMR (400 MHz, THF-d_8): δ 3.24 (d, J = 6.4 Hz, 2H), 5.61 (dt, J = 10.0, 6.4 Hz, 1H), 6.45 (d, J = 10.0 Hz, 1H), 6.86 (s, 1H), 6.90 (s, 1H), 6.94 (t, J = 7.2 Hz, 2H), 6.99 (t, J = 7.2 Hz, 2H), 7.07 (d, J = 8.4 Hz, 4H), 7.13 (d, J = 8.4 Hz, 4H), 7.17–7.25 (m, 8H). ¹³C{¹H} NMR (THF-d_8 100 MHz): δ 27.8, 121.1, 122.5, 122.7, 123.2, 123.4, 123.6, 123.9, 124.5, 127.9, 129.6, 129.8, 132.0, 133.5, 136.1, 147.4, 148.5, 148.7, 151.2. HRMS (APCI): m/z Calcd. for C₃₅H₂₇N₂S₂: 539.1610 ([M+H]⁺). Obsd. 539.1619.

2,8-Bis(*N*-carbazolyl)-4*H*-cyclohepta[1,2-*b*;4,3-*b'*]dithiophene (8c). To a solution of carbazole (101 mg, 0.604 mmol) in toluene (2 mL) was added a THF solution of CH₃MgCl (3.0 M, 0.200 mL, 0.600 mmol) dropwise at 0 °C. The mixture was stirred at the same temperature for 1 h, and then **7** (72.0 mg, 0.199 mmol) and a solution of di-tert-butyl(1-methyl-2,2-diphenylcyclopropyl)phosphine (cBRIDP) (5.70 mg, 0.0162 mmol) and [PdCl(allyl)]₂ (1.70 mg, 4.65 μmol) in THF (0.5 mL) were subsequently

added. The reaction mixture was stirred at reflux temperature for 14 h, and then was filtered through a plug of Celite®. The filtrate was concentrated under reduced pressure. The mixture was purified by column chromatography (Wakosil 50NH₂(HC), hexane/toluene = 5/1, R_f = 0.20) and recrystallized with toluene/hexane to afford **8c** as white solid (31.3 mg, 0.0585 mmol, 29%). Mp: 210.0 °C (decomp.). ^{1}H NMR (400 MHz, CD₂Cl₂): δ 3.53 (d, J = 6.8 Hz, 2H), 5.92 (dt, J = 10.0, 6.8 Hz, 1H), 6.78 (d, J = 10.0 Hz, 1H), 7.30 (dd, J = 8.4, 8.0 Hz, 2H), 7.32 (dd, J = 8.0, 7.2 Hz, 2H), 7.40 (s, 1H), 7.45 (t, J = 8.4Hz, 2H), 7.47 (s 1H), 7.47 (dd, J = 8.4, 7.2 Hz, 2H), 7.54 (d, J = 8.4 Hz, 2H), 7.63 (d, J = 8.4 Hz, 2H), 8.11 (d, J = 8.0 Hz, 2H), 8.12 (d, J = 8.0 Hz, 2H). ^{13}C{^{1}H} NMR (100 MHz, CD₂Cl₂): δ 27.9, 110.7, 110.7, 120.6, 120.7, 121.1, 121.3, 124.0, 124.2, 124.2, 124.8, 125.0, 125.3, 126.8, 126.9, 131.3, 133.2, 135.3, 135.3, 136.0, 138.1, 142.2, 142.5. HRMS (APCI): m/z Calcd. for C₃₅H₂₃N₂S₂: 535.1297 ([M+H]$^+$). Obsd. 535.1318.
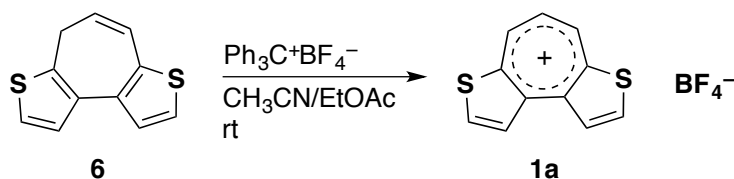
Dithieno[1,2-b;4,3-b′]tropylium tetrafluoroborate (1a). To a solution of **6** (30.9 mg, 0.151 mmol) in EtOAc (3 mL) was added a solution of triphenylmethylium tetrafluoroborate (59.1 mg, 0.179 mmol) in CH₃CN (1.5 mL) at room temperature. The reaction mixture was stirred for 30 min and then cooled to 0 °C. The precipitates was collected by filtration and washed with toluene to afford **1a** as yellow solids (37.3 mg, 0.129 mmol, 85%). Mp: 206.0 °C (decomp.). ^{1}H NMR (400 MHz, CD₃CN): δ 8.38 (t, J = 10.0 Hz, 1H), 8.76 (d, J = 5.6 Hz, 2H), 9.14 (d, J = 5.6 Hz, 2H), 9.55 (d, J = 10.0 Hz, 2H). ^{13}C{^{1}H} NMR (CD₃CN, 100 MHz): δ 129.2, 130.8, 148.4, 149.8, 150.0, 154.0. HRMS (ESI): m/z Calcd. for C₁₁H₇S₂: 202.9984 ([M]$^+$). Obsd. 202.9993.
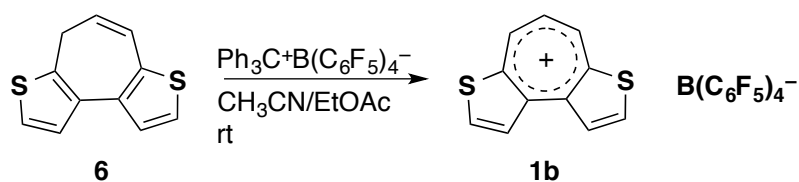
Dithieno[1,2-b;4,3-b′]tropylium tetrakis(pentafluorophenyl)borate (1b). To a

solution of **6** (21.0 mg, 0.103 mmol) in EtOAc (2 mL) was added a solution of triphenylmethylium tetrakis(pentafluorophenyl)borate (111 mg, 0.120 mmol) in CH_3CN (1.5 mL) at room temperature. The reaction mixture was stirred for 3 h followed by concentration under reduced pressure. The mixture was washed with hexane and recrystallized from $CHCl_3$/hexane to afford **1b** as yellow solids (63.5 mg, 0.0720 mmol, 70%). Mp: 195.1 °C (decomp.). ^{1}H NMR (400 MHz, CD_3CN): δ 8.38 (t, J = 10.0 Hz, 1H), 8.76 (d, J = 5.6 Hz, 2H), 9.13 (d, J = 5.6 Hz, 2H), 9.55 (d, J = 10.0 Hz, 2H). $^{13}C\{^1H\}$ NMR (CD_2Cl_2, 100 MHz): δ 128.4, 130.1, 135.4, 137.4, 137.9, 139.8, 147.1, 147.3, 149.0, 149.1, 149.7, 153.6. HRMS (ESI): m/z Calcd. for $C_{11}H_7S_2$: 202.9984 ($[M]^+$). Obsd. 202.9993.

2,8-Bis(*N*-methyl-*N*-phenylamino)-dithieno[1,2-*b*;4,3-*b′*]tropylium tetrafluoroborate (2a). To a solution of **8a** (33.3 mg, 0.0803 mmol) in EtOAc (2 mL) was added a solution of triphenylmethylium tetrafluoroborate (32.0 mg, 0.0969 mmol) in CH_3CN (1 mL) at room temperature. The reaction mixture was stirred for 15 h and then concentrated under reduced pressure. The crude product was washed with toluene and recrystallized from CH_2Cl_2/hexane to afford **2a** as brown solids (28.2 mg, 0.0564 mmol, 70%). Mp: >300 °C. ^{1}H NMR (400 MHz, CD_3CN): δ 3.67 (s, 6H), 7.09 (s, 2H), 7.17 (t, J = 10.0 Hz, 1H), 7.49–7.63 (m, 10H), 7.99 (d, J = 10.0 Hz, 2H). $^{13}C\{^1H\}$ NMR (CD_3CN, 100 MHz): δ 43.9, 107.3, 124.0, 126.2, 129.9, 131.6, 135.7, 141.2, 146.5, 147.0, 170.1. HRMS (ESI): m/z Calcd. for $C_{25}H_{21}N_2S_2$: 413.1141 ($[M]^+$). Obsd. 413.1151.

2,8-Bis(*N,N*-diphenylamino)-dithieno[1,2-*b*;4,3-*b′*]tropylium tetrafluoroborate (2b). To a solution of **8b** (53.8 mg, 0.100 mmol) in EtOAc (2 mL) was added a solution of triphenylmethylium tetrafluoroborate (39.7 mg, 0.120 mmol) in CH_3CN (1 mL) at room temperature. The reaction mixture was stirred for 5 h and then concentrated under reduced pressure. The crude product was washed with toluene and recrystallized from $CHCl_3$/hexane to afford **2b** as brown solids (46.6 mg, 0.0746 mmol, 75%). Mp: >300 °C. ^{1}H NMR (400 MHz, CD_3CN): δ 7.04 (s, 2H), 7.28 (t, J = 10.0 Hz, 1H), 7.42–7.55 (m, 20H), 8.09 (d, J = 10.0 Hz, 2H). $^{13}C\{^1H\}$ NMR ($CDCl_3$, 100 MHz): δ 109.3, 125.5, 126.1, 128.9, 130.8, 136.3, 142.3, 144.3, 146.2, 168.1. HRMS (ESI): m/z Calcd. for $C_{35}H_{25}N_2S_2$: 537.1454 ($[M]^+$). Obsd. 537.1442.

2,8-Bis(*N*-carbazolyl)-dithieno[1,2-*b*;4,3-*b′*]tropylium tetrafluoroborate (2c). To a solution of **8c** (33.0 mg, 0.0617 mmol) in THF (1.2 mL) was added a solution of triphenylmethylium tetrafluoroborate (24.7 mg, 0.0748 mmol) in CH_3CN (0.6 mL) at room temperature. The reaction mixture was stirred for 2.5 h. To complete the reaction, a solution of triphenylmethylium tetrafluoroborate (24.8 mg, 0.0751 mmol) in CH_3CN (0.9 mL) was again added and the resulting solution and the reaction mixture was stirred for another 10.5 h at the same temperature. The reaction mixture was concentrated under reduced pressure and then washed with toluene. Further recrystallization from CH_2Cl_2/hexane afforded **8c** as brown solids (25.2 mg, 0.0406 mmol, 66%). Mp: 193.8 °C (decomp.). ^{1}H NMR (400 MHz, CD_3CN): δ 7.46 (t, J = 8.0 Hz, 4H), 7.60 (t, J = 8.0 Hz, 4H), 8.07 (t, J = 10.0 Hz, 1H), 8.16 (d, J = 8.0 Hz, 4H), 8.19 (d, J = 8.0 Hz, 4H), 8.66 (s, 2H), 8.97 (d, J = 10.0 Hz, 2H). ^{13}C{^{1}H} NMR (CD_2Cl_2, 150 MHz): δ 111.5, 120.2, 121.6, 125.1, 126.5, 128.3, 129.7, 139.7, 142.6, 147.4, 148.1, 157.8. HRMS (ESI): *m/z* Calcd. for $C_{35}H_{21}N_2S_2$: 533.1141 ([*M*]$^+$). Obsd. 533.1164.

X-ray Crystallographic Analysis

Structural analysis of 2a. Single crystals of **2a** suitable for X-ray crystallographic analysis were obtained by slow diffusion of *i*PrOH into a solution of **2a** in CH_3CN. Intensity data were collected at 123 K on a Rigaku X-ray diffractometer equipped with a molybdenum FR-X microfocus generator, VariMax-Mo optics, and a PILATUS 200K detector. Total of 56438 reflections were measured with the maximum 2θ angle of 55.0°, of which 5128 were independent reflections (R_{int} = 0.0234). The structure was solved by direct methods (SHELXS-2013) and refined by the full-matrix least-squares on F^2 (SHELXL-2013). All non-hydrogen atoms were refined anisotropically and all hydrogen atoms were placed using AFIX instructions. The crystal data are as follows: $C_{25}H_{21}BF_4N_2S_2$; FW = 500.37, crystal size 0.25 × 0.06 × 0.04 mm^3, monoclinic, $P2_1/n$, a = 7.4626(7) Å, b = 19.2881(19) Å, c = 15.5950(15) Å, β = 95.773 (3)°, V = 2233.3(3) Å^3, Z = 4, D_c = 1.488 g cm^{-3}, μ = 0.290 mm^{-1}, R_1 = 0.0407 ($I > 2\sigma(I)$), wR_2 = 0.1286 (all data), GOF = 1.115.

Structural analysis of 2b. Single crystals of **2b** suitable for X-ray crystallographic analysis were obtained by slow diffusion of hexane into a solution of **2b** in

1,2-dichloroethane. Intensity data were collected at 123 K on a Rigaku X-ray diffractometer equipped with a molybdenum FR-X microfocus generator, VariMax-Mo optics, and a PILATUS 200K detector. Total of 36943 reflections were measured with the maximum 2θ angle of 55.0°, of which 6860 were independent reflections (R_{int} = 0.0246). The structure was solved by direct methods (SHELXS-2013) and refined by the full-matrix least-squares on F^2 (SHELXL-2013). All non-hydrogen atoms were refined anisotropically and all hydrogen atoms were placed using AFIX instructions. The crystal data are as follows: $C_{35}H_{25}BF_4N_2S_2$; FW = 624.50, crystal size 0.27 × 0.06 × 0.04 mm^3, monoclinic, $P2_1/c$, a = 13.7855(7) Å, b = 11.3394(10) Å, c = 19.1120(15) Å, β = 90.993(2)°, V = 2987.1(4) Å^3, Z = 4, D_c = 1.389 g cm^{-3}, μ = 0.232 mm^{-1}, R_1 = 0.0536 ($I > 2\sigma(I)$), wR_2 = 0.1685 (all data), GOF = 1.155.

Structural analysis of 2c. Single crystals of **2c** suitable for X-ray crystallographic analysis were obtained by slow diffusion of octane into a solution of **2c** in 1,2-dichloroethane. Intensity data were collected at 123 K on a Rigaku X-ray diffractometer equipped with a molybdenum FR-X microfocus generator, VariMax-Mo optics, and a PILATUS 200K detector. Total of 33499 reflections were measured with the maximum 2θ angle of 50.0°, of which 5629 were independent reflections (R_{int} = 0.0722). The structure was solved by direct methods (SHELXS-2013) and refined by the full-matrix least-squares on F^2 (SHELXL-2013). All non-hydrogen atoms were refined anisotropically and all hydrogen atoms were placed using AFIX instructions. The crystal data are as follows: $C_{37}H_{25}BCl_2F_4N_2S_2$; FW = 719.42, crystal size 0.15 × 0.03 × 0.02 mm^3, monoclinic, $P2_1/c$, a = 7.1931(8) Å, b = 34.535(4) Å, c = 13.2220(18) Å, β = 102.841(5)°, V = 3202.4(7) Å^3, Z = 4, D_c = 1.492 g cm^{-3}, μ = 0.389 mm^{-1}, R_1 = 0.0647 ($I > 2\sigma(I)$), wR_2 = 0.2330 (all data), GOF = 1.075.

Structural analysis of 1b. Single crystals of **1b** suitable for X-ray crystallographic analysis were obtained by slow diffusion of hexane into a solution of **1b** in toluene. Intensity data were collected at 123 K on a Rigaku X-ray diffractometer equipped with a molybdenum FR-X microfocus generator, VariMax-Mo optics, and a PILATUS 200K detector. Total of 61819 reflections were measured with the maximum 2θ angle of 55.0°, of which 8575 were independent reflections (R_{int} = 0.0298). The structure was solved by direct methods (SHELXS-2013) and refined by the full-matrix least-squares on F^2

(SHELXL-2013). All non-hydrogen atoms were refined anisotropically and all hydrogen atoms were placed using AFIX instructions. The crystal data are as follows: $C_{42}H_{15}BF_{20}S_2$; FW = 974.47, crystal size $0.15 \times 0.04 \times 0.03$ mm^3, monoclinic, $P2_1/a$, a = 14.211(3) Å, b = 17.997(4) Å, c = 15.980(15) Å, β = 114.073(3)°, V = 3731.5(15) Å^3, Z = 4, D_c = 1.389 g cm^{-3}, μ = 0.278 mm^{-1}, R_1 = 0.0472 ($I > 2\sigma(I)$), wR_2 = 0.1521 (all data), GOF = 1.137.

Photophysical Properties.

UV-vis-NIR absorption spectra of **1a** and **2a–c** were measured with a Shimadzu UV-3150 spectrometer with a resolution of 0.5 nm using dilute sample solutions in spectral grade solvents in a 1 cm quartz cuvette. Emission spectra were measured with a Hitachi F-4500 spectrometer with a resolution of 1 nm. For the fluorescence measurements, the sample solutions were excited at 560 nm and 570 nm for **2a** and **2b**, respectively. Absolute fluorescence quantum yields were determined with a Hamamatsu Photonics C-9920-02 calibrated integrating sphere system. The PMMA films were prepared on the surface of a quartz cell by casting a CHCl$_3$ solution (1 mL) of the sample (1.0 mg) and PMMA (100 mg, WAKO Pure Chemicals Industries, Ltd).

Determination of pK_R^+ value of 2a. The UV-vis-NIR spectra of **2a** were measured with Agilent 8453 UV-vis spectrophotometer in DMSO/water/Me$_4$NOH solution in a 1 cm quartz cuvette. DMSO was purified by distillation from CaH$_2$. Dissolved oxygen was removed from all stock solution by N$_2$ bubbling. A 5.0×10^{-5} M DMSO solution of **2a** was prepared and diluted to be 1.0×10^{-5} M solution in the cuvette with a known volume of DMSO/water solution with a 0.011 M of Me$_4$NOH. The equilibrium distribution between cations and carbinols were obtained from the relative concentrations, which were determined by UV-vis-NIR spectrophotometry. The pK_R^+ values were derived from the linear fits to plots of log([ROH]/[R$^+$]) versus $C_\_$ for each solution.[17b] After each measurement, 20 μL HCl was added to check the reversibility.

Determination of pK_R^+ values for compounds 1a, 2b, and 2c. The UV-vis-NIR spectra of **1a**, **2b** and **2c** were measured with a Shimadzu UV-3150 spectrometer with a resolution of 0.5 nm using dilute sample solutions in various pH values of 50% aqueous acetonitrile solutions in a 1 cm quartz cuvette. The pH value of each solution was

determined using a pH meter calibrated with standard buffer solutions. The observed absorbance at the longest absorption maxima at 442 nm for **1a,** 570 nm for **2b,** and at 578 nm for **2c** were plotted against pH values to give a classical titration curve, of which midpoints were taken as the pK_R^+ values.

Theoretical Calculations

Computational Method. The geometry optimizations of **1a′**, **2a′–2c′***,* and **9′** without including counter anions in the ground state (S_0) were performed using CAM-B3LYP range-separated exchange-correlation functional [22] with the 6-31G(d) basis set [23] implemented in the Gaussian 09 program. [24] For the geometry optimizations, a stationary point was optimized without any symmetry assumptions and characterized by frequency analysis at the same level of theory (the number of imaginary frequencies, NIMAG, was 0). The energy calculations and geometry optimizations of **2a′** and **2b′** in the first excited singlet state (S_1) were performed using the time-dependent CAM-B3LYP method implemented in the Gaussian 09 program. The Cartesian coordinates for **1a′**, **2a′–2c′***,* and **9′** in S_0, are given in Tables 2-4–2-8. TD-DFT vertical excitation calculations of **1a′**, **2a′–c′***,* and **9′** were performed using the optimized geometries at the CAM-B3LYP/6-31G(d) level, implemented in the Gaussian 09 program.

Table 2-4. Cartesian Coordinates (Å) of the Optimized Structure of **1a′** (S_0) at the CAM-B3LYP/6-31G(d) Level

atom	x	y	z	atom	x	y	z
S	-3.23467093	0.10641375	0.0003859	H	3.60933443	-2.30367891	-0.00030557
C	-1.55290774	0.56459607	-0.00001667	C	1.48629712	-1.78344722	-0.00007699
C	-2.8262353	-1.55623528	-0.00014008	H	1.06774417	-2.77975455	-0.00009941
H	-3.60933412	-2.30367943	-0.00024591	C	0.71204581	-0.58621801	0.00003026
C	-1.48629687	-1.78344746	-0.00001704	C	1.24588709	1.92336991	-0.00017549
H	-1.06774377	-2.77975472	-0.00009524	H	2.09737239	2.59970345	-0.00020198
C	-0.71204571	-0.58621811	0.00007332	C	-0.00000016	2.53322114	-0.00017254
S	3.2346709	0.10641421	0.00002805	H	-0.00000024	3.61810048	-0.0001893
C	1.55290766	0.56459628	-0.00009742	C	-1.24588734	1.92336973	-0.00010732
C	2.8262355	-1.55623487	-0.00020715	H	-2.09737273	2.59970315	-0.00004296

Table 2-5. Cartesian Coordinates (Å) of the Optimized Structure of **2a′** (S_0) at the CAM-B3LYP/6-31G(d) Level

atom	x	y	z	atom	x	y	z
S	-3.24184914	1.27287541	0.0120328	C	7.284856	-0.67034903	-1.15904368
C	-1.54257569	1.71872232	0.00681792	H	5.44840282	-1.27156921	-2.11809295
C	-2.84693887	-0.42358864	0.00797881	H	5.22148641	-0.64454125	2.11781572
C	-1.47330149	-0.62909	-0.00060201	H	7.62892678	-0.03495547	2.15857738
H	-1.04255017	-1.61797077	-0.00901095	H	7.86073441	-0.68241929	-2.07830275
C	-0.71958681	0.55807665	0.00148373	H	8.94567853	-0.0603124	0.06038797
S	3.24186136	1.27284849	-0.01197758	C	-5.20299569	-0.98658887	0.003096
C	1.54259109	1.71871008	-0.0067366	C	-7.89246144	-0.320088	-0.04254482
C	2.8469356	-0.42361103	-0.00798351	C	-5.80603086	-0.64148346	-1.20338445
C	1.47329586	-0.6291025	0.00058216	C	-5.93611432	-1.00267154	1.18644085
H	1.04253789	-1.61798069	0.00896813	C	-7.28495432	-0.67062326	1.1589304
C	0.7195919	0.55806973	-0.00145834	C	-7.15403063	-0.30345924	-1.22097056
C	1.24359684	3.07376057	-0.00481592	H	-5.22135316	-0.64406919	-2.11777662
H	2.09875316	3.74538813	-0.00783069	H	-5.44856072	-1.27202122	2.11798094
C	0.00001537	3.68834569	0.00008738	H	-7.86089856	-0.68290646	2.07814541
H	0.0000207	4.77305351	0.00011334	H	-7.62879126	-0.03449456	-2.15857299
C	-1.24357031	3.07377177	0.00496075	H	-8.94569636	-0.06033454	-0.0604855
H	-2.09872155	3.74540562	0.00800589	C	3.44739791	-2.76795964	-0.05993644
N	3.8126021	-1.35474009	-0.02661675	H	2.82463945	-2.98790275	-0.933126
N	-3.81260924	-1.35471546	0.0266138	H	2.90527288	-3.05368013	0.84804998
C	5.20298826	-0.98660379	-0.0031267	H	4.36106087	-3.35629902	-0.12183008
C	7.89244578	-0.3200762	0.04246651	C	-3.44739872	-2.76793547	0.05986634
C	5.93601938	-1.0024134	-1.18652974	H	-2.90521769	-3.05359136	-0.84810701
C	5.80610388	-0.6417548	1.20338583	H	-4.36106174	-3.35628452	0.12166366
C	7.15410159	-0.3037205	1.22095043	H	-2.8246903	-2.98793262	0.93307812

Table 2-6. Cartesian Coordinates (Å) of the Optimized Structure of **2b′** (S$_0$) at the CAM-B3LYP/6-31G(d) Level

atom	x	y	z	atom	x	y	z
S	-3.23978271	-2.29207987	-0.23591204	C	2.98203558	4.44347265	-0.19138327
C	-1.54254491	-2.73664705	-0.29357747	C	2.8834736	2.23461626	-1.15152764
C	-2.84441836	-0.60747445	-0.02581503	C	3.87857069	2.56667049	1.0270918
C	-1.47182978	-0.40708137	-0.00415729	C	3.61578917	3.92744318	0.93417116
H	-1.04718334	0.57617466	0.12469924	C	2.6161132	3.59586897	-1.23157891
C	-0.71997683	-1.58417833	-0.1546555	H	2.61825976	1.56903809	-1.96667051
S	3.23978261	-2.29208026	-0.23591107	H	4.37616745	2.15590451	1.89911725
C	1.54254479	-2.73664722	-0.29357704	H	3.90668364	4.58580853	1.74592764
C	2.84441841	-0.60747481	-0.0258139	H	2.13500593	3.99631961	-2.11794711
C	1.47182987	-0.40708158	-0.00415662	H	2.78047343	5.5072287	-0.26091508
H	1.04718352	0.57617452	0.12469972	C	-3.50856599	1.72423915	-0.01660402
C	0.71997681	-1.58417844	-0.15465519	C	-2.98203575	4.4434733	-0.19137917
C	1.24389902	-4.08317221	-0.44716983	C	-2.88347474	2.23461831	-1.15152682
H	2.09908794	-4.75089602	-0.51919113	C	-3.87856983	2.56666941	1.02709401
C	-0.00000014	-4.69321149	-0.52093298	C	-3.61578834	3.92744225	0.93417507
H	-0.0000002	-5.77082766	-0.64484983	C	-2.61611438	3.59587112	-1.23157641
C	-1.24389926	-4.08317206	-0.44717008	H	-2.61826176	1.56904127	-1.96667089
H	-2.09908822	-4.75089578	-0.51919156	H	-4.37616588	2.15590225	1.89911931
N	3.81923782	0.32276172	0.06805172	H	-3.90668207	4.58580644	1.74593275
N	-3.81923784	0.32276197	0.06805049	H	-2.13500796	3.99632305	-2.11794448
C	5.19976624	-0.05283378	0.22358981	H	-2.78047365	5.50722944	-0.26090965
C	7.86961506	-0.7405907	0.5215379	C	-5.19976611	-0.05283378	0.22358899
C	6.11460819	0.29258655	-0.76722362	C	-7.86961474	-0.74059125	0.52153761
C	5.61388083	-0.72912897	1.36842542	C	-5.61388009	-0.72913017	1.36842411
C	6.9516924	-1.07890604	1.50938576	C	-6.1146085	0.29258727	-0.76722378
C	7.45074116	-0.05172071	-0.61273759	C	-7.45074137	-0.05172022	-0.61273747
H	5.77690542	0.83089459	-1.64650847	C	-6.95169156	-1.07890748	1.50938471
H	4.89407764	-0.9715705	2.14368066	H	-4.89407651	-0.97157254	2.14367874
H	7.27741132	-1.60565241	2.4001083	H	-5.7769061	0.83089607	-1.64650831
H	8.16620679	0.21578542	-1.38307293	H	-8.16620737	0.2157865	-1.38307226
H	8.91433679	-1.00902014	0.63755199	H	-7.27741005	-1.60565477	2.40010688
C	3.50856594	1.72423873	-0.01660473	H	-8.91433637	-1.0090209	0.6375519

89

Table 2-7. Cartesian Coordinates (Å) of the Optimized Structure of **2c′** (S_0) at the CAM-B3LYP/6-31G(d) Level

atom	x	y	z	atom	x	y	z
C	-1.54509779	2.92455296	-0.0815935	C	3.9206515	-3.8987325	2.08647953
C	-0.71603213	1.76912689	-0.04106001	C	2.60303732	-1.90288038	1.65821598
C	-1.4738358	0.57989331	-0.05721515	C	4.84658767	-2.14988802	0.74046366
H	-1.05192067	-0.40898188	0.03060736	C	4.97710908	-3.39834672	1.33927851
C	-2.83650185	0.77670099	-0.12443067	C	2.75305938	-3.1514925	2.25076456
S	-3.23047106	2.47585431	-0.18013779	H	1.70296189	-1.32659351	1.82903618
C	2.83650138	0.77670046	0.12443143	H	5.89565893	-3.96600334	1.23199423
C	1.47383528	0.579893	0.05721674	H	1.94547895	-3.54594349	2.85832835
C	0.71603183	1.76912677	0.04106194	H	4.00655746	-4.87105655	2.55912232
C	1.54509783	2.92455259	0.08159366	C	-3.65475391	-1.42585636	-0.88586519
S	3.23047089	2.47585365	0.18014007	C	-3.92065023	-3.89873159	-2.08648047
H	1.05191995	-0.40898211	-0.03060585	C	-2.60303723	-1.90287868	-1.65821704
C	1.24457654	4.28145153	0.04503311	C	-4.84658713	-2.1498879	-0.74046409
H	2.09759456	4.95521691	0.06386482	C	-4.97710791	-3.3983466	-1.33927908
C	0.00000033	4.89254741	-0.00000122	C	-2.75305866	-3.15149081	-2.25076576
H	0.00000046	5.97733966	-0.00000175	H	-1.70296227	-1.32659116	-1.82903752
C	-1.24457609	4.2814518	-0.04503477	H	-5.8956574	-3.9660038	-1.23199466
N	3.79739376	-0.18411693	0.2074526	H	-1.94547818	-3.54594115	-2.8583299
N	-3.79739431	-0.18411618	-0.20745309	H	-4.00655573	-4.87105561	-2.55912341
C	5.10157909	-0.14029881	-0.35599389	C	-5.10157967	-0.14029886	0.35599359
C	7.67061351	-0.58099665	-1.26900957	C	-7.67061372	-0.58099849	1.26900956
C	5.75936996	-1.33942273	-0.04558267	C	-5.75936975	-1.33942323	0.04558244
C	5.69948594	0.8344089	-1.14526438	C	-5.69948716	0.83440845	1.14526408
C	6.99539874	0.59766764	-1.58956305	C	-6.99539975	0.59766627	1.58956292
C	7.05412334	-1.55928079	-0.50232648	C	-7.05412297	-1.55928219	0.50232639
H	5.19173867	1.74597638	-1.43324339	H	-5.19174063	1.74597636	1.43324295
H	7.48499205	1.34629469	-2.2031292	H	-7.48499353	1.34629302	2.20312907
H	7.57057414	-2.48403836	-0.26661424	H	-7.57057313	-2.48404011	0.26661418
H	8.68133703	-0.73566205	-1.63048355	H	-8.68133714	-0.73566459	1.63048363
C	3.65475394	-1.42585724	0.88586458	H	-2.09759391	4.95521743	-0.06386687

90

Table 2-8. Cartesian Coordinates (Å) of the Optimized Structure of **9′** at the CAM-B3LYP/6-31G(d) Level

atom	x	y	z	atom	x	y	z
C	-3.12224609	-0.43919841	0.04518589	z	7.22020281	0.65836248	1.25485227
C	-2.95967047	0.92810778	0.04021943	H	5.37884035	-0.09047792	2.09452329
H	-3.79191339	1.61766967	0.05444843	H	5.90779582	-0.73720395	-2.11003379
C	-1.61146029	1.34943949	0.02072291	H	8.12270249	0.38205999	-2.00623378
C	-0.68749886	0.24106107	0.00823563	H	7.58523997	1.04644442	2.19993401
S	-1.57099156	-1.2764564	0.0186535	H	8.95605935	1.27622254	0.14874836
C	0.68750312	0.24105568	-0.00839547	C	-5.52464514	-0.47532416	0.0131838
C	1.61147563	1.34942592	-0.02072941	C	-7.98970242	0.78525362	-0.102221
C	2.95968151	0.92808139	-0.04028658	C	-5.98473116	0.02480424	-1.2011524
H	3.79193355	1.61763492	-0.05439265	C	-6.28585603	-0.34764464	1.17043981
C	3.12224365	-0.43922522	-0.0454945	C	-7.52373523	0.28150077	1.10761181
S	1.5709804	-1.27646983	-0.01904473	C	-7.22018831	0.6591614	-1.25425911
C	-1.25750284	2.7034946	0.01708026	H	-5.37878579	-0.08911745	-2.09434628
H	-2.09709537	3.39249244	0.02899371	H	-5.90790605	-0.73858395	2.10977058
C	0.00001779	3.2874236	0.00015001	H	-8.12283828	0.38065687	2.00659562
H	0.00002365	4.37363394	0.00023685	H	-7.58519144	1.0478559	-2.19910222
C	1.25753257	2.70348356	-0.01687743	H	-8.95611422	1.27624214	-0.14782485
H	2.0971324	3.39247426	-0.02868734	C	-4.23865911	-2.61695026	0.0905606
N	4.257859	-1.15608245	-0.07130356	H	-3.8348736	-3.02234889	-0.84424624
N	-4.25785398	-1.15607458	0.07079996	H	-5.26170993	-2.96985969	0.20736776
C	5.52463043	-0.47531926	-0.01326646	H	-3.64469902	-2.99000097	0.93134677
C	7.98965738	0.78524095	0.10286069	C	4.23875572	-2.61696047	-0.09075658
C	5.98475264	0.02402126	1.20137976	H	5.2616456	-2.96980929	-0.20917342
C	6.28578306	-0.34685626	-1.17047232	H	3.64352246	-2.99015	-0.93057212
C	7.52364458	0.28228858	-1.10728805	H	3.83646552	-3.0222823	0.84473088

3.5 References

(1)   Lavis, L. D.; Raines, R.T. *ACS Chem. Biol.* **2008**, *3*, 142.

(2)   Doering, W. v. E.; Knox, L. H. *J. Am. Chem. Soc.* **1954**, *76*, 3203.

(3)   Komatsu, K. *Chem. Rec.* **2015**, *15*, 160.

(4)   Komatsu, K.; Takeuchi, K.; Arima, M.; Waki, Y.; Shirai, S.; Okamoto, K. *Bull. Chem. Soc. Jpn.* **1982**, *55*, 3257.

(5)   (a) Komatsu, K.; Abe, N.; Takahashi, K.; Okamoto, K. *J. Org. Chem.* **1979**, *44*, 2712. (b) Komatsu, K.; Takahashi, K.; Okamoto, K. *Tetrahedron Lett.* **1979**, *20*, 4747. (c) Komatsu, K.; Tsuji, R.; Takeuchi, K. *Tetrahedron Lett.* **1989**, *30*, 4689. (d) Tsuji, R.; Komatsu, K.; Inoue, Y.; Takeuchi, K. *J. Org. Chem.* **1992**, *57*, 636. (e) Tsuji, R.; Komatsu, K.; Takeuchi, K.; Shiro, M.; Cohen, S.; Rabinovitz, M. *J. Phys. Org. Chem.* **1993**, *6*, 435. (f) Komatsu, K.; Tsuji, R.; Inoue, Y.; Takeuchi, K. *Tetrahedron Lett.* **1993**, *34*, 99.

(6)   (a) Komatsu, K.; Akamatsu, H.; Jinbu, Y.; Okamoto, K. *J. Am. Chem. Soc.* **1988**, *110*, 633. (b) Komatsu, K.; Aonuma, S.; Jinbu, Y.; Tsuji, R.; Hirosawa, C.; Takeuchi, K. *J. Org. Chem.* **1991**, *56*, 195. (c) Komatsu, K.; Akamatsu, H.; Aonuma, S.; Jinbu, Y.; Maekawa, N.; Takeuchi, K. *Tetrahedron* **1991**, *47*, 6951. (d) Kagayama, A.; Komatsu, K.; Nishinaga, T.; Takeuchi, K.; Kabuto, C. *J. Org. Chem.* **1994**, *59*, 4999. (e) Komatsu, K.; Nishinaga, T.; Maekawa, N.; Kagayama, A.; Takeuchi, K. *J. Org. Chem.* **1994**, *59*, 7316.

(7)   (a) Gronowitz, S.; Pedaja, P. *Tetrahedron* **1978**, *34*, 587. (b) Yom-Tov, B.; Gronowitz, S. *J. Heterocyclic Chem.* **1978**, *15*, 285.

(8)   (a) Wang, Z.; Xing, Y.; Shao, H.; Liu, P.; Weber, W. P. *Org. Lett.* **2005**, *7*, 87. (b) Weis, J. G.; Swager, T. M. *ACS Macro. Lett.* **2015**, *4*, 138.

(9)   (a) Wang, X.; Ng, J. K.-P.; Jia, P.; Lin, T.; Cho, C. M.; Xu, J.; Lu, X.; He, C.; *Macromolecules* **2009**, *42*, 5534. (b) Murai, M.; Amir, E.; Amir, R. J.; Hawker, C. J. *Chem. Sci.* **2012**, *3*, 2721. (c) Wang, F.; Lin, T. T.; He, C.; Chi, H.; Tang, T.; Lai, Y.-H. *J. Mater. Chem.* **2012**, *22*, 10448. (d) Amir, E.; Murai, M.; Amir, R. J.; Cowart, Jr., J. S.; Chabinyc, M. L.; Hawker, C. J. *Chem. Sci.* **2014**, *5*, 4483.

(10)   Ruggiero, A.; Fuchter, M. J.; Kokas, O. J.; Negru, M.; White, A. J. P.; Haycock, P. R.; Hoffman, B. M.; Barrett, A. G. M. *Tetrahedron* **2009**, *7*, 9690.

(11)   Allen, J. M.; Lambert, T. H. *J. Am. Chem. Soc.* **2011**, *133*, 1260.

(12)   Nguyen, T. V.; Bekensir, A. *Org. Lett.* **2014**, *16*, 1720.

(13)   (a) Green, M. L. H.; Ng, D. K. P. *Chem. Rev.* **1995**, *95*, 439. (b) Murahashi, T.; Fujimoto, M.; Oka, M.; Hashimoto, Y.; Uemura, T.; Tatsumi, Y.; Nakao, Y.; Ikeda, A.; Sakaki, S.; Kurosawa, H. *Science* **2006**, *313*, 1104. (c) Murahashi, T.;

Hashimoto, Y.; Chiyoda, K.; Fujimoto, M.; Uemura, T.; Inoue, R.; Ogoshi, S.; Kurosawa, H. *J. Am. Chem. Soc.* **2008**, *130*, 8586. (d) Tamm, M. *Chem. Commun.* **2008**, 3089. (e) Mulligan, F. L.; Babbini, D. C.; Davis, I. R.; Hurst, S. K.; Nichol, G. S. *Inorg. Chem.* **2009**, *48*, 2708. (f) Babbini, D. C.; Mulligan, F. L.; Schulhauser, H. R.; Sweigart, T. C.; Nichol, G. S.; Hurst, S. K. *Inorg. Chem.* **2010**, *49*, 4307. (g) Murahashi, T.; Usui, K.; Inoue, R.; Ogoshi, S.; Kurosawa, H. *Chem. Sci.* **2011**, *2*, 117.

(14)   (a) Schleyer, P. v. R.; Maerker, C.; Dransfeld, A.; Jiao, H.; van Eikema Hommes, N. J. R. *J. Am. Chem. Soc.* **1996**, *118*, 6317. (b) Corminboeuf, C.; Heine, T.; Seifert, G.; Schleyer, P. v. R.; Weber, J. *Phys. Chem. Chem. Phys.* **2004**, *6*, 273. (c) Fallah-Bagher-Shaidaei, H.; Wannere, C. S.; Corminboeuf, C.; Puchta, R.; Schleyer, P. v. R. *Org. Lett.* **2006**, *8*, 863.

(15)   Kalinowski, M. K.; Stachurski, J.; Janowski, K. R. *Anal. Chim. Acta* **1980**, *117*, 353.

(16)   Freedman, H. H. *Carbonium Ions*; Olah, G. A.; Schleyer, P. v. R. Eds.; Wiley-Interscience, New York, **1973**.

(17)   (a) Laursen, B. W.; Krebs, F. C.; Nielsen, M. F.; Bechgaard, K.; Christensen, J. B.; Harrit, N. *J. Am. Chem. Soc.* **1998**, *120*, 12255. (b) Laursen, B. W.; Krebs, F. C. *Chem. Eur. J.* **2001**, *7*, 1773. (c) Laursen, B. W.; Sørensen, T. J. *J. Org. Chem.* **2009**, *74*, 3183.

(18)   Goldacre, R. J.; Phillips, J. N. *J. Chem. Soc.* **1949**, 1724.

(19)   Zakerhamidi, M. S.; Moghadam, M.; Ghanadzadeh, A.; Hosseini, S. *J. Lumin.* **2012**, *132*, 931.

(20)   Kellogg, R. M.; Schaap, A. P.; Wynberg, H. *J. Org. Chem.* **1969**, *34*, 343.

(21)   Krasovskiy, A.; Knochel, P. *Angew, Chem. Int. Ed.* **2004**, *43*, 3333.

(22)   Yanai, T.; Tew, D.; Handy, N. *Chem. Phys. Lett.* **2004**, *393,* 51.

(23)   (a) Ditchfield, R.; Hehre, W. J.; Pople, J. A. *J. Chem. Phys.* **1971**, *54*, 724. (b) Hehre, W. J.; Ditchfield, R.; Pople, J. A. *J. Chem. Phys.* **1972**, *56*, 2257. (c) Hariharan, P. C.; Pople, J. A. *Theor. Chim. Acta.* **1973**, *28*, 213. (d) Francl, M. M.; Pietro,W. J.; Hehre, W. J.; Binkley, J. S.; Gordon, M. S.; DeFrees, D. J.; Pople, J. A.; *J. Chem. Phys.* **1982**, *77*, 3654.

(24) Gaussian 09, (Revision C.01), Frisch, M. J.; Trucks, G. W.; Schlegel, H. B.; Scuseria, G. E.; Robb, M. A.; Cheeseman, J. R.; Scalmani, G.; Barone, V.; Mennucci, B.; Petersson, G. A.; Nakatsuji, H.; Caricato, M.; Li, X.; Hratchian, H. P.; Izmaylov, A. F.; Bloino, J.; Zheng, G.; Sonnenberg, J. L.; Hada, M.; Ehara, M.; Toyota, K.; Fukuda, R.; Hasegawa, J.; Ishida, M.; Nakajima, T.; Honda, Y.; Kitao, O.; Nakai, H.; Vreven, T.; Montgomery, J. A., Jr.; Peralta, J. E.; Ogliaro, F.; Bearpark, M.; Heyd, J. J.; Brothers, E.; Kudin, K. N.; Staroverov, V. N.; Kobayashi, R.; Normand, J.; Raghavachari, K.; Rendell, A.; Burant, J. C.; Iyengar, S. S.; Tomasi, J.; Cossi, M.; Rega, N.; Millam, J. M.; Klene, M.; Knox, J. E.; Cross, J. B.; Bakken, V.; Adamo, C.; Jaramillo, J.; Gomperts, R.; Stratmann, R. E.; Yazyev, O.; Austin, A. J.; Cammi, R.; Pomelli, C.; Ochterski, J. W.; Martin, R. L.; Morokuma, K.; Zakrzewski, V. G.; Voth, G. A.; Salvador, P.; Dannenberg, J. J.; Dapprich, S.; Daniels, A. D.; Farkas, O.; Foresman, J. B.; Ortiz, J. V.; Cioslowski, J.; Fox, D. J. Gaussian, Inc., Wallingford CT, 2010.

Chapter 3

A Cycloheptadithiophene-Containing Polymethine NIR Dye: Multifaceted Interconversion Based on the Acid-Base Equilibria and Reversible Redox Properties

ABSTRACT: As a new entity for NIR-absorbing dyes, polymethine dye **1** consisted of a 3,3′-bithiophene-fused cycloheptatriene and two phenol terminal moieties was synthesized. The charge neutral **1** exhibited pH-responsive photophysical properties due to the acid-base equilibria among three species including the corresponding cation and anion forms, **1**$^+$ and **1**$^-$. While **1** showed an absorption band in the visible region and a red fluorescence band under the acidic conditions, the moderate and strong absorption bands in the NIR region were observed under neutral and basic conditions, respectively. Chemical oxidation of **1** gave a stable neutral radical **1**$^•$, which showed a NIR absorption band. The neutral radical **1**$^•$ showed reversible redox process in cyclic voltammetry. Notably, the one-electron oxidized species **1**$^{r+}$ *in situ* generated is different from **1**$^+$. This species also showed a characteristic absorption band in the NIR region. Overall, compound **1** underwent the multifaceted conversion among five different states. A crucial point to attain this characteristic behavior is to extend the polymethine π-conjugation with the cycloheptadithiophene skeleton, which enables the effective delocalization of cationic or anionic charge, or electron spin over the entire π-conjugated skeleton.

3.1 Introduction

π-Conjugated chromophores that absorb and emit a light in the near-infrared (NIR) region[1] have attracted significant attention in the past decades from application points of view including photovoltaic cells,[2] fluorescent probes,[3] photothermal agents,[4] photoacoustic probes,[5] and light-emitting diodes.[6] One promising molecular design for the NIR dyes is to construct a positively charged polymethine skeleton, such as cyanines and hemicyanines. In these dyes, charge delocalization over the odd-number carbon chain comprising terminal electron-donating groups gives rise to a narrow HOMO-LUMO gap. The fact that extension of π-conjugated skeleton with one vinylene unit results in a bathochromic shifts by ca. 100 nm demonstrates the importance of the effective charge delocalization in a long range for attaining the NIR absorption and fluorescence properties.[7]

Phenol-terminated polymethines are a counter class of dyes for the cationic polymethine dyes. Their anionic forms can display absorption and fluorescence in the long-wavelength region due to the effective delocalization of the negative charge. Representative and important examples are fluorescein derivatives. Notably, their photophysical properties are pH-responsive due to the acid-base equilibrium between the neutral and anionic forms, and therefore make them attractive core skeletons not only for fluorescent probes for bioimaging,[8] but also for molecular logic gates.[9] However, their absorption and fluorescence maxima are generally located in the visible region. To attain the long-wavelength absorption and fluorescence, the fluorescein skeletons have been modified in various fashions. One promising approach is to extend the π-conjugation length by annulation of additional benzene rings to the fluorescein skeleton. Naphthofluorescein[10] and seminaphthofluorescein[11] derivatives, which have benzene-fused fluorescein skeletons, exhibit red-shifted fluorescence compared to the parent fluorescein. Recently, based on further structural modification of naphthofluorescein and seminaphthofluorescein, NIR absorption and fluorescence have been achieved.[12,13]

The phenol-terminated polymethine dye is also a good precursor for a stable radical with intriguing properties. A representative example is galvinoxyl, which is a persistent phenoxy radical with extended π-conjugated framework composed of two phenol moieties linked with one sp^2 carbon atom.[14] Delocalization of unpaired electron spin over the π-conjugated skeleton gives rise to not only high stability, but also the

absorption in the NIR region. Its absorption maximum wavelength (λ_{abs} = 870 nm) is 470 nm longer than that of its phenol counterpart.[14a] Several other persistent phenoxy radicals with long-wavelength absorption properties have also been reported using extended π-conjugated skeletons, such as corannulene, [15] phenalenyl, [16] and perylenebisimide,[17] as a core.
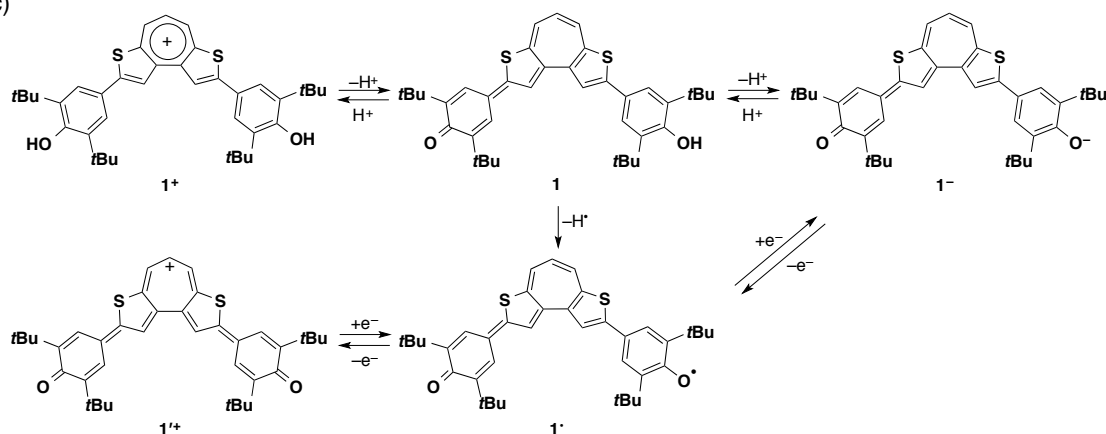
(a) *fluorescein*
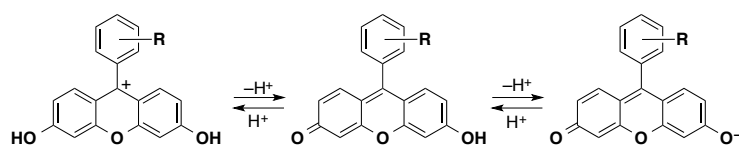
(b) *galvinoxyl*
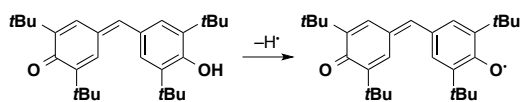
(c)

Scheme 3-1. Chemical structures of (a) fluorescein and (b) galvinoxyl and (c) interconversion between **1** and relevant species.

As a new entity of the NIR-absorbing dyes, the author now designed a bis(hydroxyphenyl)-substituted cyclohepta[1,2-*b*;4,3-*b′*]dithiophene **1**. In Chapter 2, the author described that the amino-substituted dithienotropylium ions exhibit high stability as well as the long-wavelength absorptions and fluorescences due to the significant contribution of the rhodamine-like quinoidal resonance structure. The author now envisioned that a fluorescein-like congener **1** can be produced by introducing two phenol moieties to the cycloheptadithiophene moiety (Scheme 3-1). This compound would be readily interconverted with its protonated and deprotonated counterparts based

on the acid-base equilibria. In addition, **1** would be also transformed to the corresponding radical **1**˙ by the abstraction of a hydrogen radical. These species can be regarded as the π-extended analogues of fluorescein and galvinoxyl, respectively, and thereby should show intriguing photophysical and redox properties. In this Chapter, the synthesis of charge neutral **1**, its pH-dependent photophysical properties, as well as the synthesis and properties **1**˙ are described. The author found that the extended fluorescein analogue **1** can be also converted to another cation form **1**$^{r+}$. The impacts of the cycloheptatriene skeleton on the properties of these species are discussed.

3.2 Results and Discussion

Synthesis. The synthesis of 2,8-dibromo-4*H*-cyclohepta[1,2-*b*;4,3-*b'*]dithiophene **2** was already described in Chapter 2. Starting form this compound, bis(hydroxyphenyl)-substituted cycloheptadithiophene **1** was obtained in two steps as shown in Scheme 3-2. Thus, the Suzuki-Miyaura cross-coupling between **2** and 3,5-di(*tert*-butyl)-4-hydroxyphenylboronic acid afforded hydoxyphenyl-substituted cycloheptadithiophene **3** in 69% yield. The compound was further oxidized with DDQ to produce quinoidal cycloheptatdithiophene **1** in 62% yield. Compound **3** was also converted to a cationic species, phenol-substituted dithienotropylium tetrafluoroborate **1**$^+$·**BF**$_4^-$, by hydride abstraction of **3** with Ph$_3$C$^+$BF$_4^+$. This compound was isolated by recrystallization from a CH$_2$Cl$_2$/hexane solution as an air- and moisture-stable compound.
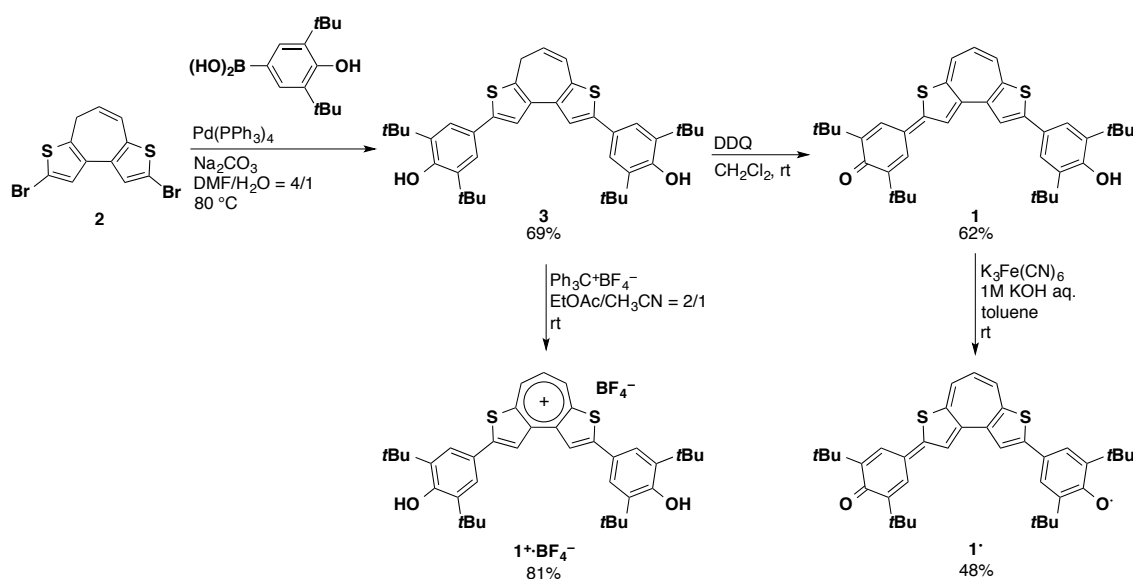
Scheme 3-2. Synthesis of **1**, **1**$^+$·**BF**$_4^-$, and **1**˙.

98

In the ^{1}H NMR spectra, compound **1** showed eight resonance signals in the range between 6.36 ppm and 7.45 ppm, indicative of the unsymmetrical structure composed of a quinone and a phenol moiety (Figure 3-1). In contrast, **1$^+$·BF$_4^-$** showed only three resonance peaks in the aromatic region, demonstrating its symmetrical structure at ambient temperature. Notably, the resonance signals for the protons on the seven-membered ring in **1$^+$·BF$_4^-$** were significantly downfield shifted to 7.95 ppm and 8.85 ppm in CD$_2$Cl$_2$, compared to those of **1** (6.36 ppm, 6.83 ppm, and 6.89 ppm in CDCl$_3$), due to the paratropic ring current effect in the tropylium ion.

Compound **1** is also a good precursor for neutral radical **1$^•$**. Chemical oxidation of **1** with K$_3$Fe(CN)$_6$ as an oxidant afforded **1$^•$** in 48% yield as deep purple solid. This neutral radical exhibited outstanding stability toward air and moisture. Thus, this neutral radical compound was purified by recrystallization from a toluene/hexane solution after aqueous work-up of the reaction. While **1$^•$** did not show any signals in the NMR spectrum, **1$^•$** showed a pronounced signal with a hyperfine coupling structure in the EPR spectrum, supporting the formation of a radical species (*vide infra*).
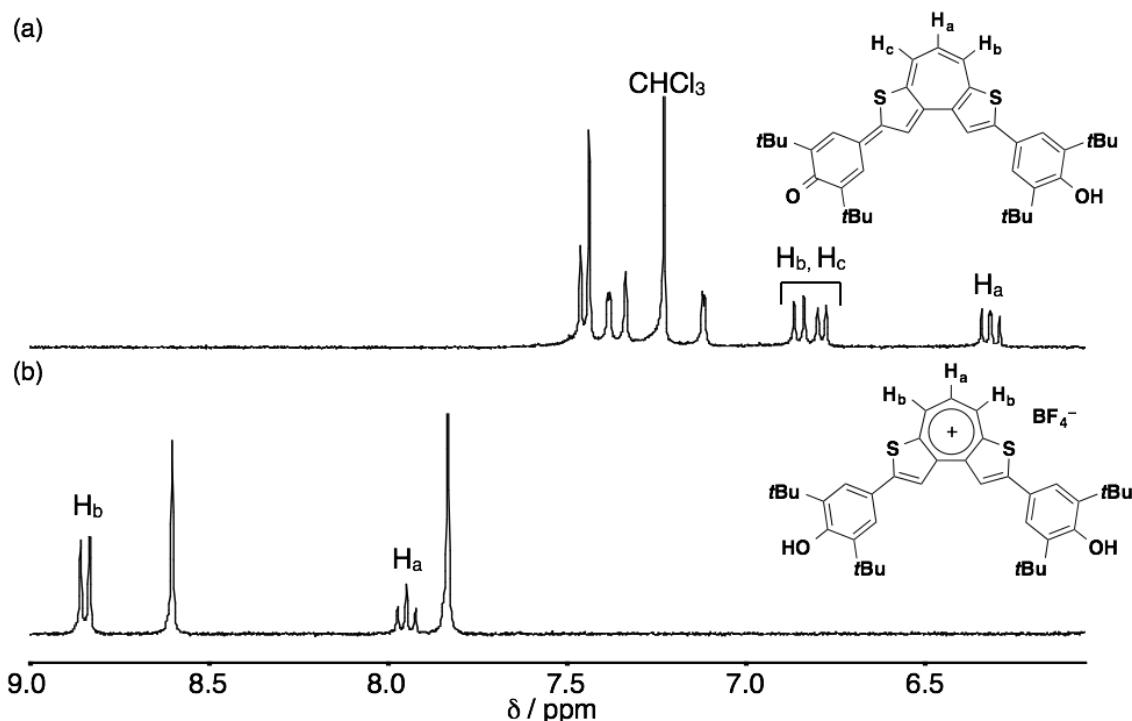

**Figure 3-1.** ^{1}H NMR spectra of (a) **1** in CDCl$_3$ and (b) **1$^+$·BF$_4^-$** in CD$_2$Cl$_2$ (400 MHz).

X-ray Crystallographic Analysis. Single crystals of **1**, **1$^+$·BF$_4^-$**, and **1$^•$** suitable for the

X-ray crystallographic analyses were successfully obtained by recrystallization from acetone/CH$_3$CN, chlorobenzene/cyclohexane, and 1,2-dicloroethane/CH$_3$CN solutions, respectively. In all the compounds, the entire bis(hydroxyphenyl)-substituted cyclohepta[1,2-*b*;4,3-*b′*]dithiophene skeletons adopt relatively planar structures. The dihedral angles between the two thiophene mean planes are 7.1(1)°, 1.4(1)°, and 2.9(2)° for **1**, **1$^+$·BF$_4$$^-$**, and **1$^•$**, respectively. In addition, the sum of the internal angles in the central seven-membered rings of **1**, **1$^+$·BF$_4$$^-$** and **1$^•$** were 899.9°, 899.5°, and 899.8°, respectively, demonstrating planar heptagon geometries of these rings. In addition, the dihedral angles between the thiophene and outer six-membered rings are also small (12.4(1)° and 6,7(1)° for **1**, 17.0(1)° and 7.9(1)° for **1$^+$·BF$_4$$^-$**, and 14.6(1)° and 14.1(1)° for **1$^•$**).

Table 3-1. Selected Bond Lengths in Crystal Structures of **1**, **1$^+$·BF$_4^-$**, and **1$^•$**

Bond length (Å)[a]	**1**	**1$^+$·BF$_4^-$**	**1$^•$**
C1–C2	1.371(3)	1.379(3)	1.398(2)
C3–C4	1.409(3)	1.373(3)	1.397(2)
C2–C9	1.415(3)	1.407(3)	1.391(2)
C3–C10	1.381(3)	1.414(3)	1.389(2)
C8–C9	1.410(3)	1.430(3)	1.427(2)
C10–C11	1.439(3)	1.427(3)	1.424(2)
C9–C10	1.448(3)	1.439(3)	1.454(2)
C5–C11	1.385(3)	1.400(3)	1.393(2)
C5–C6	1.412(3)	1.380(4)	1.396(2)
C6–C7	1.369(3)	1.395(3)	1.394(2)
C7–C8	1.419(3)	1.389(3)	1.392(2)
C1–12	1.462(3)	1.457(3)	1.415(2)
C4–C18	1.411(3)	1.461(3)	1.417(2)
C12–C13, C12–C17	1.399(3), 1.396(3)	1.399(3), 1.404(3)	1.422(2), 1.429(2)
C13–C14, C16–C17	1.391(3), 1.384(3)	1.388(3), 1.382(3)	1.361(2), 1.356(2)
C14–C15, C15–C16	1.411(3), 1.417(3)	1.414(3), 1.420(3)	1.479(2), 1.478(2)
C15–O1	1.356(3)	1.363(3)	1.245(2)
C18–C19, C18–C23	1.420(3), 1.427(3)	1.393(3), 1.407(3)	1.429(2), 1.425(2)
C19–C20, C22–C23	1.367(3), 1.364(3)	1.379(3), 1.399(3)	1.368(2), 1.356(2)
C20–C21, C21–C22	1.469(3), 1.467(3)	1.423(3), 1.412(3)	1.478(2), 1.477(2)
C21–O2	1.262(3)	1.352(3)	1.246(2)

[a] Atom labelng scheme for these compounds is shown below:
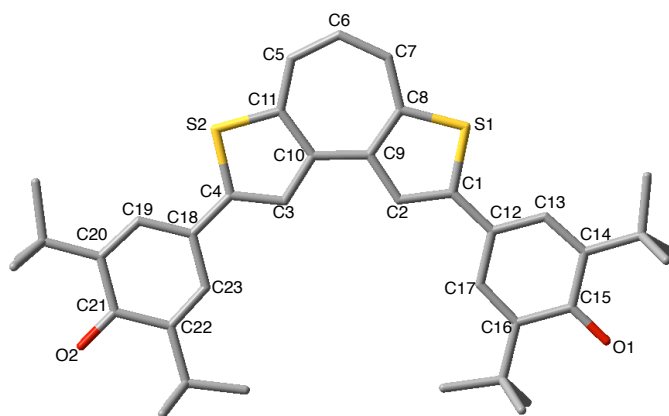
Comparison of the bond lengths in the bis(hydroxyphenyl)-substituted cycloheptadithiophene framework revealed that the predominant resonance structure of each species are totally different from one another (Table 3-1).

First, in charge neutral **1**, the bis(hydroxyphenyl)-substituted cycloheptadithiophene framework has a highly unsymmetrical geometry. Whereas the benzene ring composed of C12–C13–C14–C15–C16–C17 has a relatively small bond alternation with the C–C bond lengths in the range of 1.38 Å–1.42 Å, the other six-membered ring composed of C18–C19–C20–C21–C22–C23 has a large bond alternation, where the four carbon–carbon bonds C18–C19 (1.420(3) Å), C18–C23 (1.427(3) Å), C20–C21 (1.469(3) Å), and C21–C22 (1.467(3) Å) are significantly longer than those of the other two bonds, C19–C20 (1.367(3) Å) and C22–C23 (1.364(3) Å). Furthermore, the C4–C18 (1.411(3) Å) and C15–O1 (1.262(3) Å) bonds are much shorter than the C1–C12 (1.462(3) Å) and C15–O1 (1.356(3) Å) bonds, indicative of the double bond character for the former C–C and C–O bonds. The two thiophene rings in the cycloheptadithiophene also have different geometries. One of the thiophene rings, S2–C4–C3–C10–C11, has a quinoidal geometry, while the other thiophene ring, S1–C1–C2–C9–C8, maintains a thiophene-like geometry. All these structural characteristics demonstrate the unsymmetrical quinoidal structure of charge neutral **1** (Figure 3–1). In light of the NMR spectral data, this compound likely has this quinoidal structure both in a dilute solution and in the crystalline state.

In contrast to the unsymmetrical structure of **1**, the corresponding cation **1^{+}·BF$_4^{-}$** adopts an almost symmetrical geometry. The bond lengths of each six-membered rings composed of C12–C13–C14–C15–C16–C17 and C18–C19–C20–C21–C22–C23 exhibit relatively small bond alternation in the range of 1.38 Å–1.43 Å. The bond lengths of C15–O1 (1.363(3) Å) and C21–O2 (1.352(3) Å) are within the range of C–O single bonds. These results demonstrate that **1^{+}·BF$_4^{-}$** has a dithienotropylium ion character with two phenol moieties in the terminal positions, which is consistent with the ^{1}H NMR spectrum in a dilute solution.

In neutral radical **1$^{•}$**, whereas bis(hydroxylphenyl)-substituted cycloheptadithiophene framework also has an almost symmetrical geometry, the degree of bond alternation is large, different from those of **1** and **1^{+}·BF$_4^{-}$**. In the two six-membered rings in the hydroxyphenyl moieties, C13–C14 (1.361(2) Å), C16–C17 (1.356 (2) Å), C19–C20 (1.368(2) Å), and C22–C23 (1.356(2) Å) are significantly

shorter than those of the adjacent C–C bonds C14–C15 (1.479(2) Å), C15–C16 (1.478(2) Å), C20–C21 (1.478(2) Å) and C21–C22 (1.477(2) Å). The bond lengths of C1–C12 (1.415(2) Å) and C4–C18 (1.417(2) Å) are within the range of C=C double bonds. Moreover, the short distances of the C15–O1 (1.245(2) Å) and C21–O2 (1.246(2) Å) bonds indicate their C=O double bond characters. In light of these results, neutral radical **1**$^\bullet$ can be best described a quinoidal resonance structure, which indicates effective spin delocalization over the entire molecular skeleton (*vide infra*).

Photophysical Properties of 1. Bis(hydroxylphenyl)-substituted cycloheptadithiophene **1** showed characteristic photophysical properties highly dependent on its charge states. Firstly, charge neutral **1** showed broad absorption bands that covers the visible region, and its longest absorption maximum wavelength (λ_{abs}) was 854 nm in CH_2Cl_2 (Figure 3-2). Compound **1** exhibited almost identical absorption spectra irrespective of solvents with different polarity, such as cyclohexane, benzene, CH_3CN, and MeOH, although the molar absorption coefficient (ε) values vary to some extent. Exceptions were the absorption spectra in DMF and DMSO, in which **1** showed a significantly red-shifted and intense absorption band with λ_{abs} at 967 nm and 964 nm, respectively. This specific solvent effect observed in DMF and DMSO is likely due to the deprotonation of **1** induced in the basic media generated in these solvents in the presence of a trace amount of water.[18]

Second, in consistent with the observation in DMF and DMSO, **1** exhibited significantly red-shifted absorption and fluorescence bands under the basic conditions. Thus, upon addition of 0.067 M of 1,8-diazabicyclo[5.4.0]undec-7-ene (DBU) to a CH_2Cl_2 solution of **1** (1.0 x 10^{-5} M), a broad and strong absorption band appeared in the NIR region with the λ_{abs} of 964 nm (ε = 74700 $M^{-1}cm^{-1}$). This intense absorption is obviously ascribed to anion **1**$^-$ generated by deprotonation under the basic conditions. The anion **1**$^-$ also showed a NIR emission with the emission maximum wavelength (λ_{em}) of 1024 nm, although the quantum yield is very low (Φ_F = 0.0004).

Third, upon addition of 0.13 M of trifluoroacetic acid (TFA) to a CH_2Cl_2 solution of **1** (1.0 x 10^{-5} M), a sharp absorption band appeared at λ_{abs} = 600 nm with the ε value of 44700 $M^{-1}cm^{-1}$ and an intense red emission was also observed with the λ_{em} of 654 nm. Its fluorescence quantum yield Φ_F was 0.43. These absorption and fluorescence spectra are ascribed to a protonated species **1**$^+$. Indeed, almost identical spectra were

obtained with the isolated $1^+\cdot\mathbf{BF_4^-}$ in CH_2Cl_2 (Figure 3-4 and Table 3-2). The generation of tropylium ion 1^+ in an acidic solution was also supported by the ^1H NMR spectrum of **1** in CD_2Cl_2 with the addition of a few droplets of TFA-d_1 (Figure 3-5).
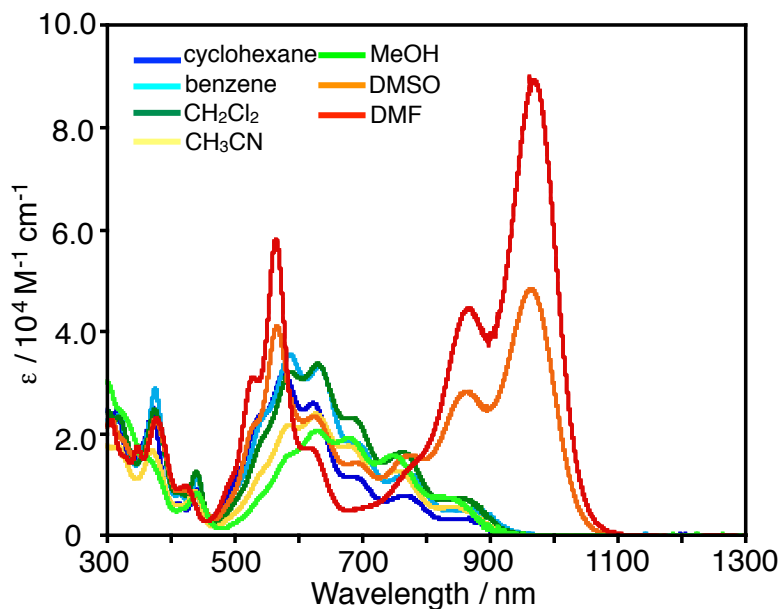

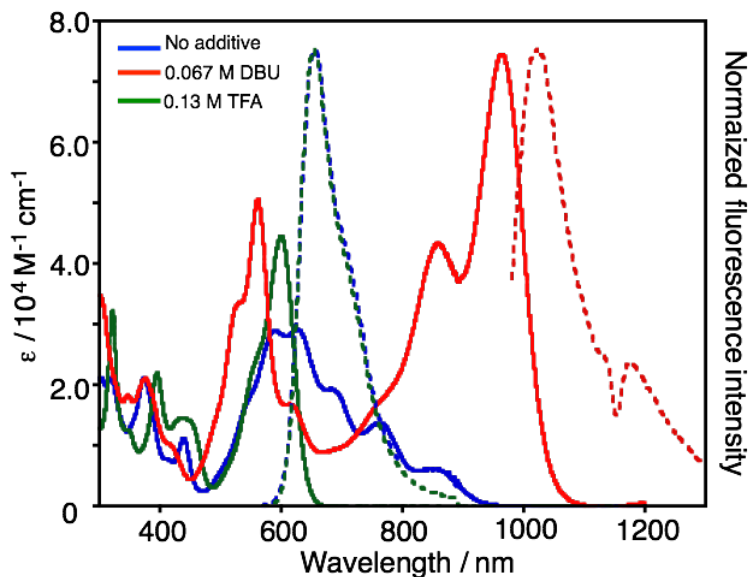**Figure 3-2.** UV-vis-NIR absorption spectra of **1** in various solvents.

Figure 3-3. Absorption (solid line) and fluorescence (broken line) spectra of **1** in CH_2Cl_2 without additive (blue), with 0.067 M of DBU (red), and with 0.13 M of TFA (green).

Table 3-2. Photophysical Data of **1**, **1$^+$·BF$_4^-$**, and **1$^•$** in CH$_2$Cl$_2$

Cmpd	additive	λ_{abs} [nm]	ε [10^4 M^{-1} cm^{-1}]	λ_{em} ^{a} [nm]	Φ_F ^{a}
1	–	590	2.91	654	0.12
		626	2.93		
		683	1.94		
		761	1.39		
		854	0.63		
	TFA	600	4.47	654	0.43
	DBU	562	5.07	1024	0.0004
		854	4.33		
		964	7.47		
1$^+$·BF$_4^-$	–	600	5.19	650	0.34
1$^•$	–	559	3.59	n.d.^{b}	n.d.^{b}
		754	2.91		
		838	7.10		
		1596	0.32		

^{a} Absolute fluorescence quantum yields determined with a calibrated integrating sphere system. ^{b} Not detected.
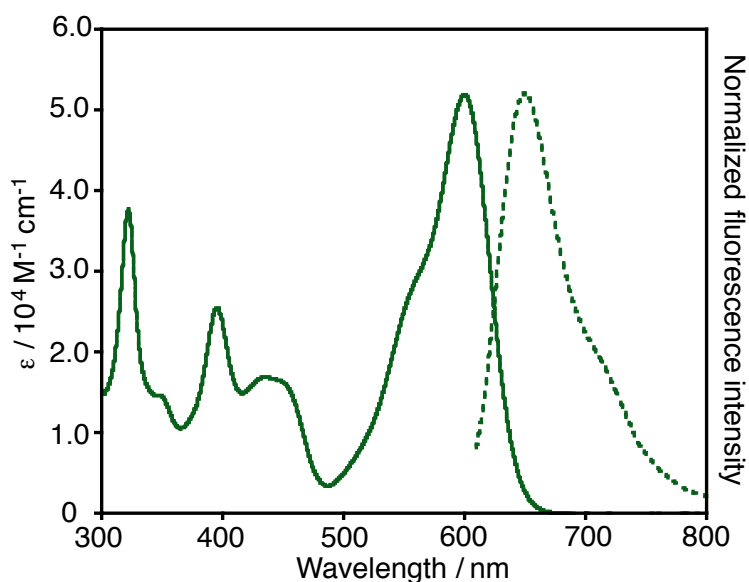
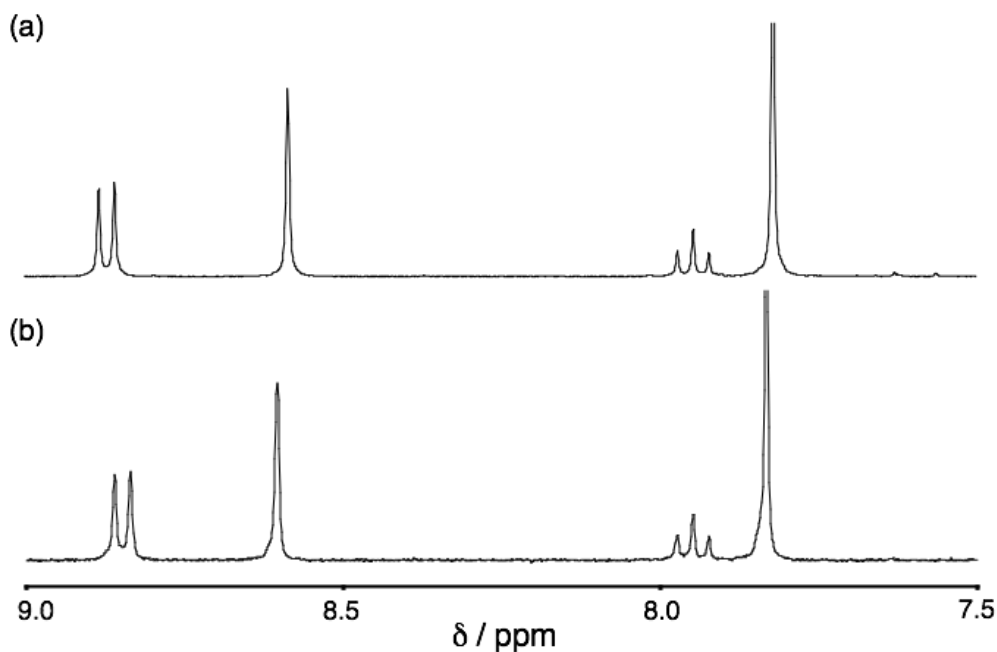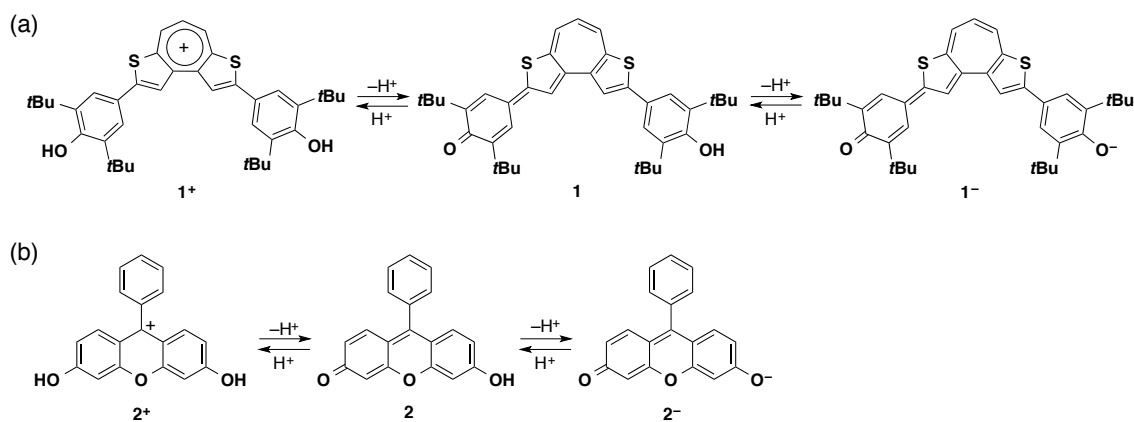**Figure 3-4.** Absorption (solid line) and fluorescence (broken line) spectra of **1$^+$·BF$_4^-$** in CH$_2$Cl$_2$.

Figure 3-5. ^{1}H NMR spectra of (a) **1** in CD$_2$Cl$_2$ with the addition of a few droplets of TFA-d_1 and (b) **1**$^+$·**BF$_4$**$^-$ in CD$_2$Cl$_2$.

Scheme 3-3. Two-step acid-base equilibria in (a) **1** and (b) fluorescein derivative **2**.

The two-step changes in the photophysical properties due to the acid-base equilibria among three species, **1**$^+$, **1**, and **1**$^-$ are similar to those observed for fluoresceins (Scheme 3-3). To evaluate the pK_a values of **1**, the pH-dependent absorption spectra in 50% aqueous CH$_3$CN solutions were next investigated (Figure 3-6 and 3-7). In consistent with the absorption spectra in CH$_2$Cl$_2$, as the pH value of the solution was increased from 1.8 to 6.9, the absorption band of **1**$^+$ at λ_{abs} = 573 nm decreased, while a broad absorption band of charge neutral **1** emerged. Upon further increasing in the pH

value to 13.9, the absorption bands of $\mathbf{1}^-$ with the λ_{abs} of 538 nm and 878 nm emerged. Based on the fitting of the plots of the absorbance at 538 nm as a function of the pH values, the pK_a values of $\mathbf{1}$ were determined to be $pK_{a1} = 6.3$, and $pK_{a2} = 11.0$ (Figure 3-6). These values are higher than the corresponding pK_a values of the fluorescein derivatives $\mathbf{2}$ ($pK_{a1} = 3.1$, and $pK_{a2} = 6.3$).[19] The high pK_{a1} value of $\mathbf{1}$ is particularly worth noting, which is much higher than the pK_{a1} value of $\mathbf{2}$ and comparable even to the pK_{a2} of $\mathbf{2}$. The 6π aromatic stabilization in the tropylium ring should contribute to the significant stabilization of the cation species $\mathbf{1}^+$. It should be also noteworthy that the extent of the pH-dependent change in $\mathbf{1}$ in terms of the absorption wavelength, ranging from 573 nm and 878 nm, is much larger than that of fluorescein derivative $\mathbf{2}$ (from 437 nm to 492 nm).[9a] This difference should be an advantage of the π-extended polymethine dye $\mathbf{1}$ over the conventional fluorescein-based dyes and suggests the potential use of $\mathbf{1}$ as a pH-responsive NIR dye.
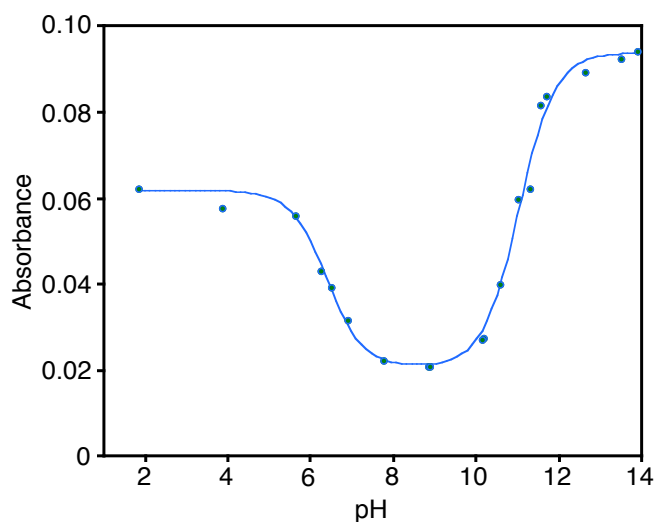

Figure 3-6. Change of the absorbance at 538 nm of $\mathbf{1}$ ($c = 2.5 \times 10^{-6}$ M) as a function of pH values in 50% aqueous CH_3CN between pH 1.9 and 13.9.
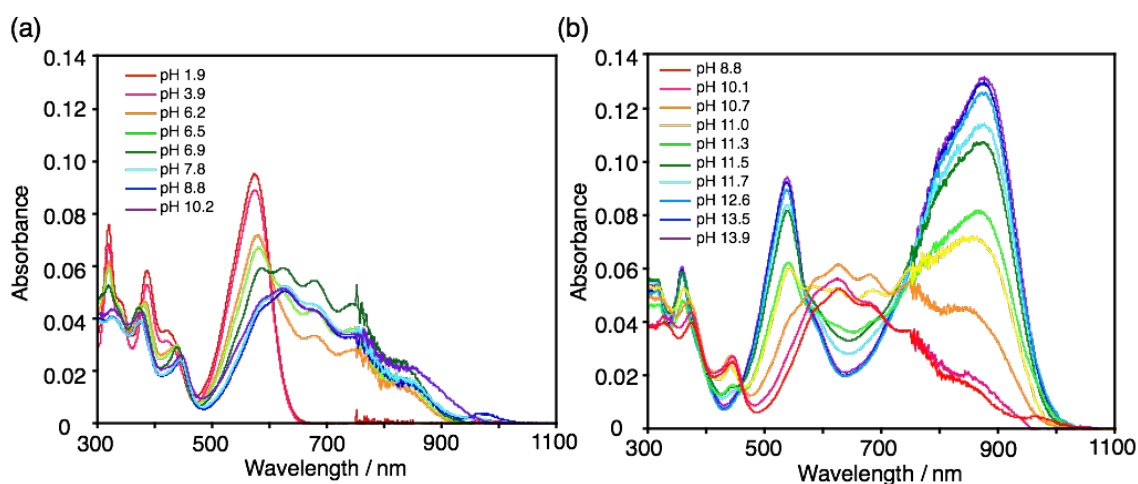
Figure 3-7. UV-vis-NIR absorption spectra of **1** in 50% CH$_3$CN aqueous solution at varied pH values (a) between the pH values of 1.9 and 10.2 and (b) between the pH values of pH 8.8 and 13.9.

DFT Calculations. To gain better understanding of the pH-dependent photophysical properties of **1**, theoretical calculations were conducted. The structural optimization of **1**, **1$^+$**, and **1$^-$**, without including counter ions for simplicity, and their TD-DFT calculations were performed at the B3LYP/6-311+G(d,p) level of theory. The results were summarized in Figure 3-8. In charge neutral **1**, both the HOMO and LUMO are mainly delocalized over the quinoid conjugated moiety consisting of the central cycloheptadithiophene and the terminal *p*-quinone methide moiety. Based on the TD-DFT calculation, the absorption band at λ_{abs} = 854 nm is assignable to the HOMO →LUMO transition (S$_1$) with a moderate oscillator strength of f = 0.2412. The broad absorption bands observed in the shorter wavelength region between 600 nm and 800 nm are assigned to the HOMO−1→LUMO (S$_2$, f = 0.2459) and HOMO→LUMO+1 (S$_3$, f = 0.5484) transitions with vibronic structures. In stark contrast, the HOMOs and LUMOs of **1$^+$** and **1$^-$** are delocalized over the entire skeleton. In **1$^+$** and **1$^-$**, the longest wavelength absorption bands are also attributable to the HOMO→LUMO transitions. The higher oscillator strength in these species (**1$^+$**: f = 0.7245, **1$^-$**: f = 0.7848) compared to that of charge neutral **1** are consistent with the experimental results. The HOMO→ LUMO gaps and predicted transition energies for the lowest energy transition to S$_1$ decrease in the order of **1$^+$**, **1** and **1$^-$**. This trend is in agreement with that observed in the absorption spectra.
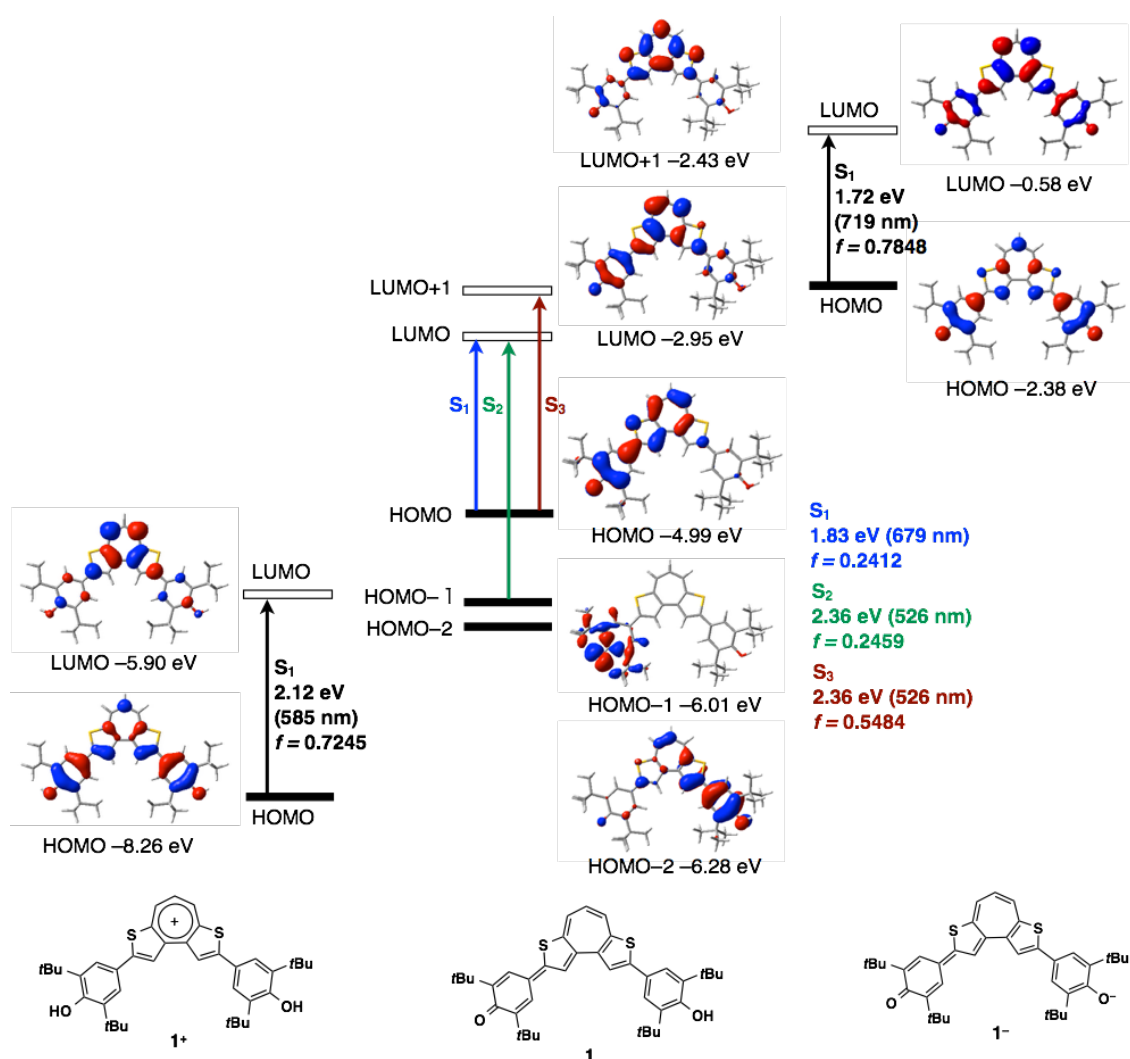
Figure 3-8. Energy diagrams and pictorial representations of Kohn-Sham molecular orbitals of **1**, **1**+, and **1**− calculated at the B3LYP/6-311+G(d,p) level. The transition energies, the corresponding wavelengths, and the oscillator strengths calculated at the same level of theory are also given.

The intense absorption of **1**− with the λ_{abs} of 964 nm, which is significantly longer than those of fluorescein derivatives, is worth noting. In the optimized structure of anion **1**−, bis(hydroxyphenyl)-substituted cycloheptadithiophene framework adopts a symmetrical geometry (Figure 3-9). Both the terminal six-membered rings have quinoidal geometries with large bond alternations. The C13–C14 (1.370 Å) and C16–C17 (1.370 Å) bonds are much shorter than the C12–C13 (1.423 Å), C12–C17 (1.425 Å), C14–C15 (1.475 Å), and C15–C16 (1.475 Å) bonds. In addition, the C15–O1 and C21–O2 bonds are as short as 1.252 Å, indicative of the C=O double bond character.

109

The four non-fused C–C bonds in the seven-membered ring do not have significant bond alternation and are much shorter (1.39 Å) than the other three C–C bonds fused with the bithiophene substructure (1.43 Å–1.46 Å), suggesting a pentadienyl anion character of the C11–C5–C6–C7–C8 moiety. All these structural features indicate that this anion form has the quinoidal structure extended over the entire skeleton and thereby has a narrow HOMO–LUMO gap, giving rise to the long-wavelength absorption in the NIR region.
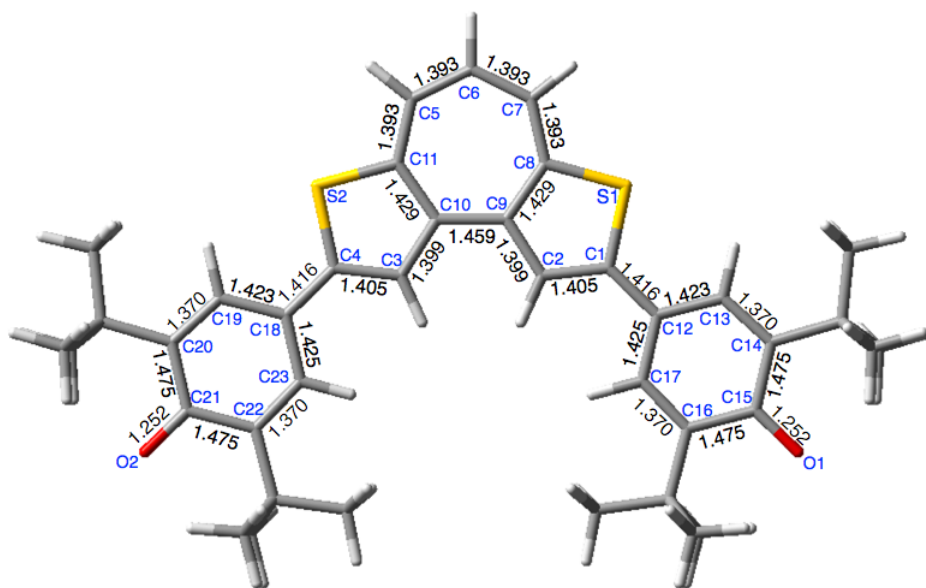

Figure 3-9. Optimized structure of 1^- and its selected bond lengths (Å) calculated at the B3LYP/6-311+G(d,p) level of theory.

To assess the aromaticity of the central seven-membered ring in the protonated form 1^+, the nucleus-independent chemical shift (NICS) values[20] were calculated at the HF/6-31+G(d,p) level of theory for the optimized geometries of **1**, 1^+, and 1^-. The NICS(0) value of the seven-membered ring in 1^+ (−5.8 ppm) is significantly lower than that in **1** (+2.2 ppm) and in 1^- (−1.5 ppm), indicating that the seven-membered ring in 1^+ has pronounced aromaticity. These results are in good accordance with the ^{1}H NMR spectrum of **1** and *in situ* generated 1^+ by the addition of TFA-d_1 in CD_2Cl_2. These studies clearly demonstrated that aromatic stabilization in the tropylium ion substructure is responsible for the relatively high pK_{a1} value for **1** (Scheme 3-3).

Photophysical Properties of Radical 1˙. In the UV-vis-NIR absorption spectrum, radical **1˙** showed a characteristic broad band in the NIR region around 1600 nm in addition to an intense absorption band with λ_{abs} of 838 nm (Figure 3-10). The longest maximum wavelength λ_{abs} of 1596 nm is much longer than that of charge neutral **1** and even longer than that of **1⁻**, which has the longest-wavelength absorption band among the three species in the acid-base equilibria. All attempts to measure the NIR fluorescence of **1˙** at ambient temperature failed, indicating **1˙** is virtually non-fluorescent under the conditions.
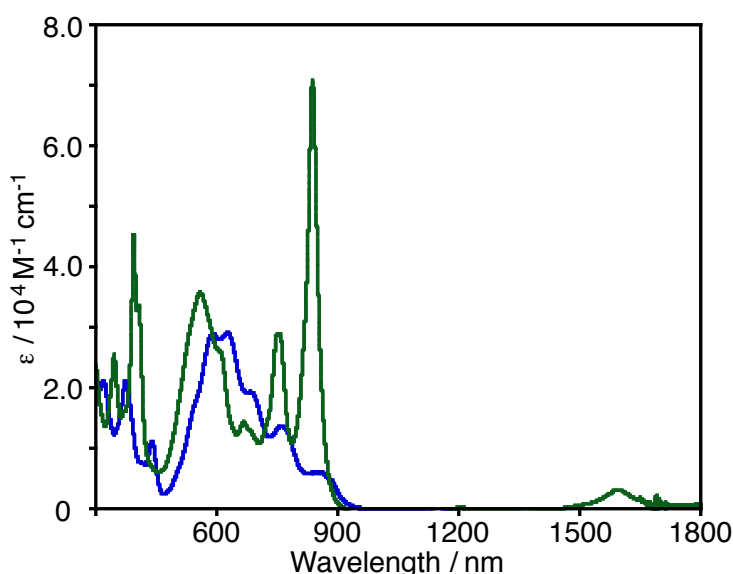
Figure 3-10. UV-vis-NIR absorption spectra of **1** (blue) and **1˙** (green) in CH_2Cl_2.

The NIR absorption of **1˙** was elucidated by the TD-DFT calculations at the UB3LYP/6-311+G(d,p) level of theory (Figure 3-11). The symmetrical structure of **1˙** obtained by the structural optimization is in good agreement with the crystal structure (Figure 3-12). The two outer six-membered rings have quinoidal structures with large bond alternation. The terminal C–O bonds are as short as 1.239 Å, indicative of the C=O double bond character. These structural features indicate the effective spin delocalization over the π framework. In this structure, the HOMO, SOMO, and LUMO of **1˙** are delocalized over the entire π skeleton. The TD-DFT calculation indicated that the longest-wavelength absorption band of **1˙** (1594 nm) is attributable to the β–HOMO →β–SOMO transition with the oscillator strength of f = 0.1590. The narrow energy gap between these orbitals of 1.26 eV results in the long-wavelength absorption in the
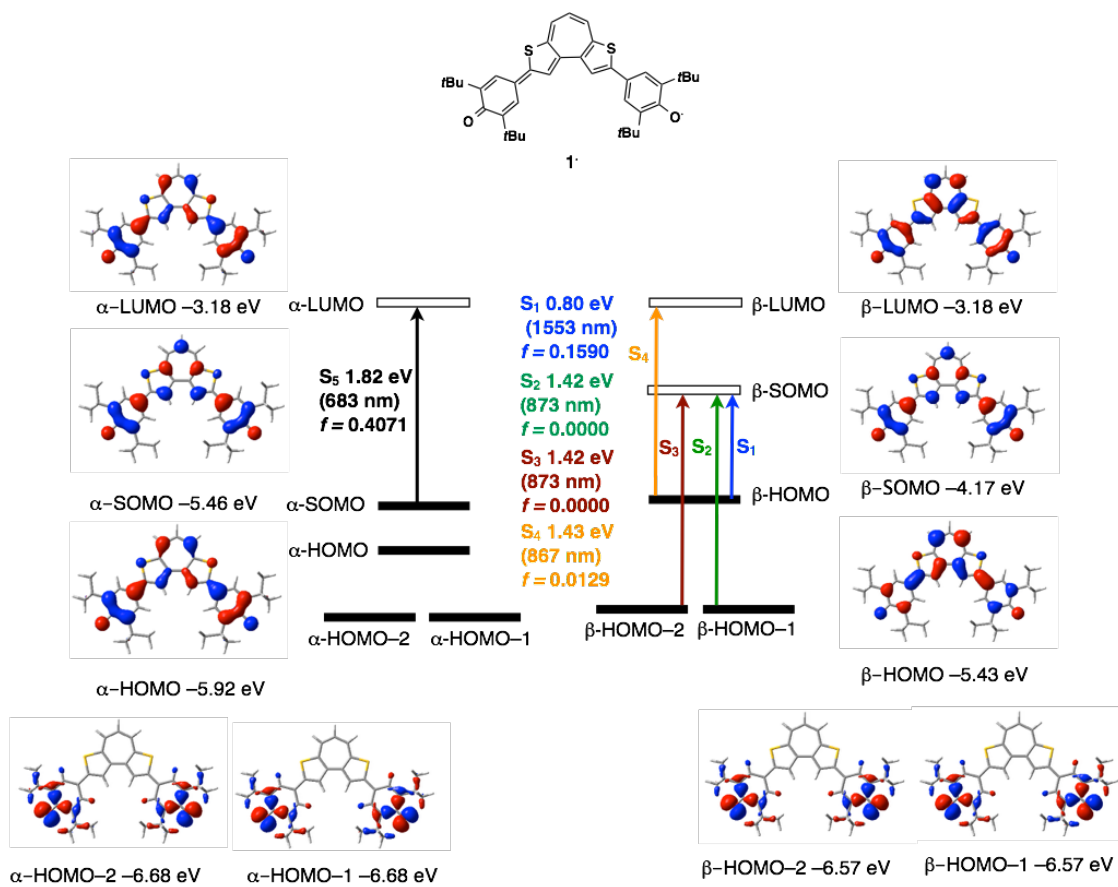
111

NIR region.

Figure 3-11. Pictorial representations of Kohn-Sham molecular orbitals and transition energies for **1·** calculated at the UB3LYP/6-311+G(d,p) level.
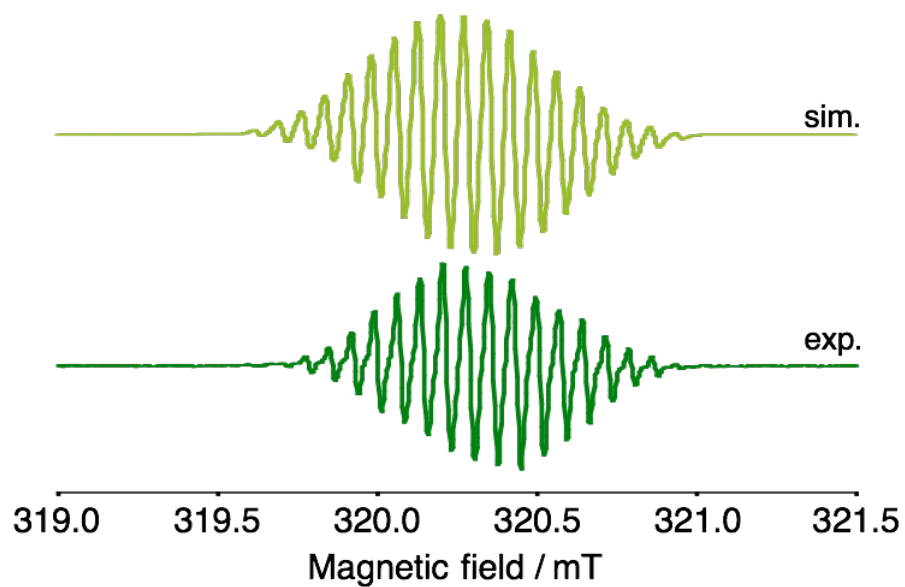
Figure 3-12. Optimized structure of **1**˙ and its selected bond lengths (Å) calculated at the B3LYP/6-311+G(d,p) level of theory.

EPR Study. EPR spectroscopy of radical **1**˙ enabled the elucidation of the distribution of spin density. The measurement was conducted in CH_2Cl_2 at 200 K (Figure 3-13). A well-defined EPR signal with hyperfine coupling was observed (g = 2.0027). The spectrum was reproduced by a simulation analysis based on which the hyperfine coupling constants were estimated. The coupling constants vary in the range from 0.08 mT to 0.28 mT (Figure 3-14). DFT calculation at the UB3LYP/6-311+G(d,p) level of theory suggested that the unpaired electron spin is delocalized over the entire π skeleton involving central seven-membered ring (Figure 3-15). The largest spin densities are located on the C12 and C18 atoms. Interestingly, the spin densities with the same sign are located on the C10 and C11 atoms in the 3,3′-bithiophene substructure. This fact indicates that the electronic interaction through the β,β′-linkage of two thiophenes may be not significant and thereby results in the effective delocalization of the unpaired electron spin over the entire skeleton, giving rise to the high stability and long-wavelength absorption.

113

Figure 3-13. EPR spectra of neutral radical **1˙** in CH$_2$Cl$_2$ measured at 200 K (green line) and simulated pattern (light green line).
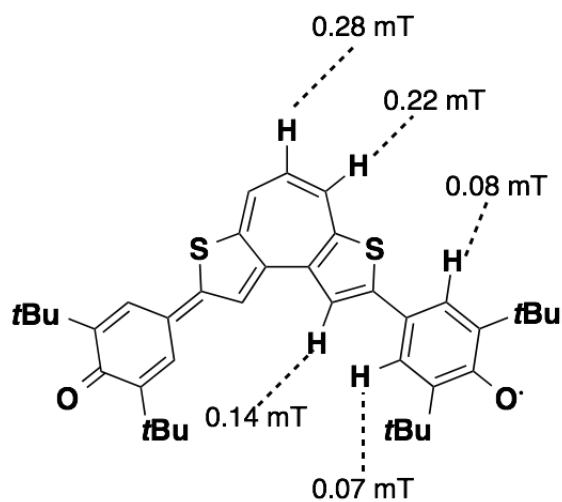

Table 3-14. Hyperfine coupling constants of **1˙** estimated from simulated EPR signal.
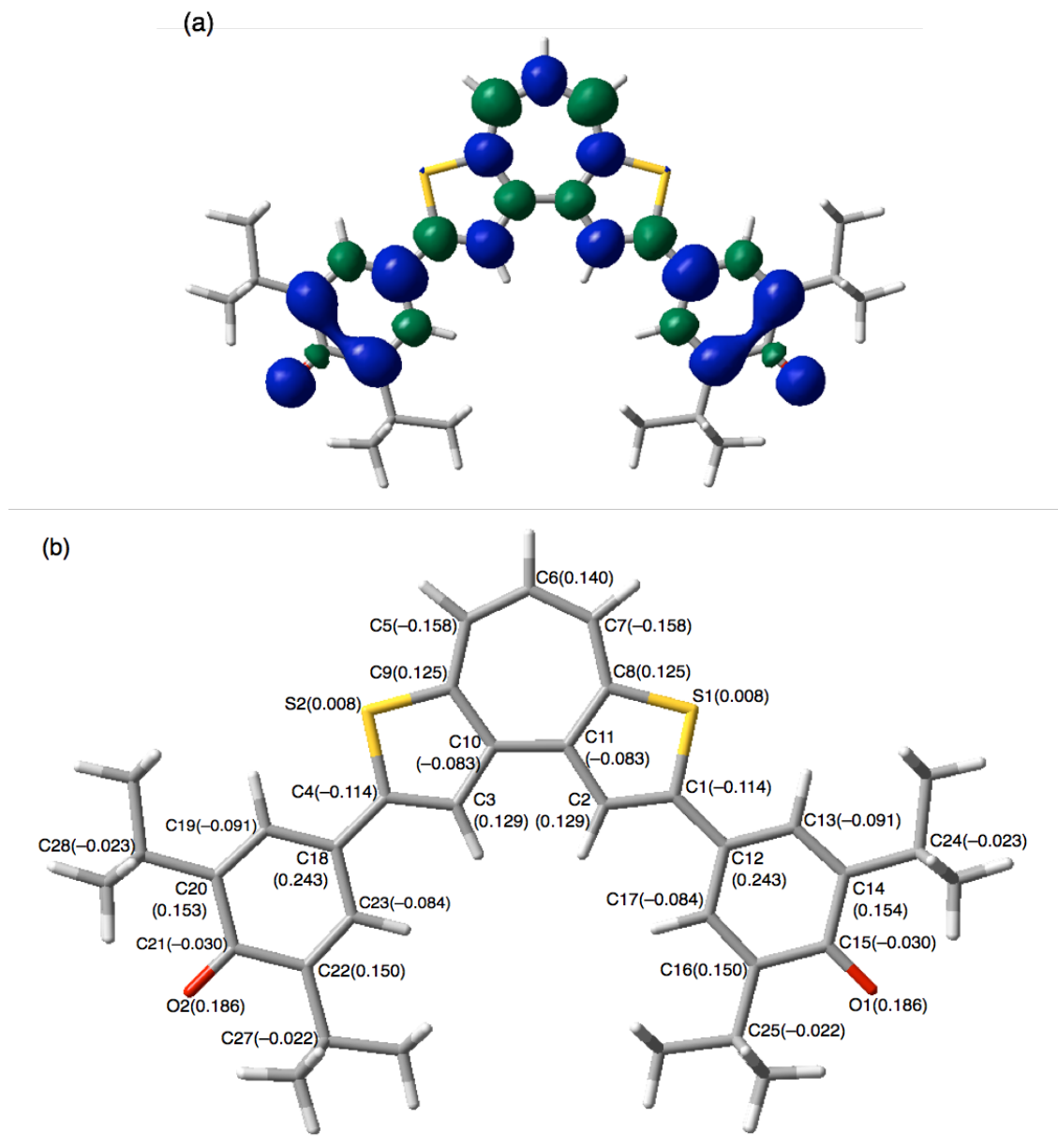
Figure 3-15. (a) Pictorial representation of spin distribution in neutral radical **1**˙ (isovalue = 0.02) and (b) spin densities in parentheses calculated at the UB3LYP/6-311+G(d,p) level.

Electrochemical Properties. Radical $1^\bullet$ showed multi-steps reversible redox properties under the electrochemical conditions. The cyclic voltammograms (CV) of $1^\bullet$ in CH_2Cl_2 showed two reversible redox waves with a half-wave potential ($E_{1/2}$) of –0.56 V and +0.16 V (vs. Fc/Fc$^+$) for the reduction and oxidation, respectively (Figure 3-16). Further oxidation and reduction processes were found to be irreversible with a cathodic peak potential (E_{pc2}) of –1.72 V (in THF) and an anodic peak potential (E_{pa2}) of +1.08 V (in CH_2Cl_2). The reversible redox processes of $1^\bullet$ presumably correspond to one-electron oxidation and reduction, which produce the corresponding anion 1^- and cation 1^{r+} as depicted in Scheme 3-4, where, notably, the structures of 1^+ and 1^{r+} are different from each other.
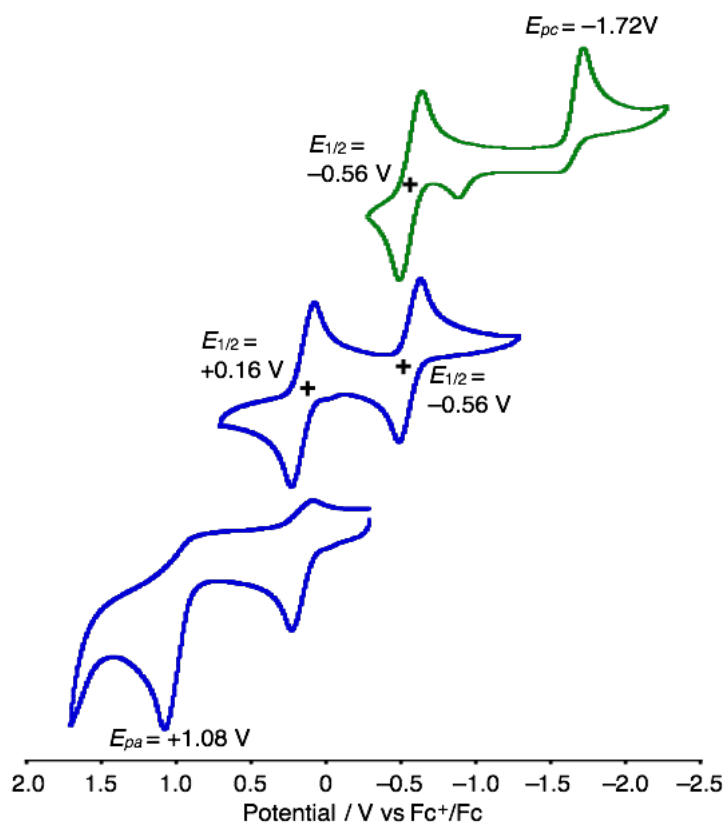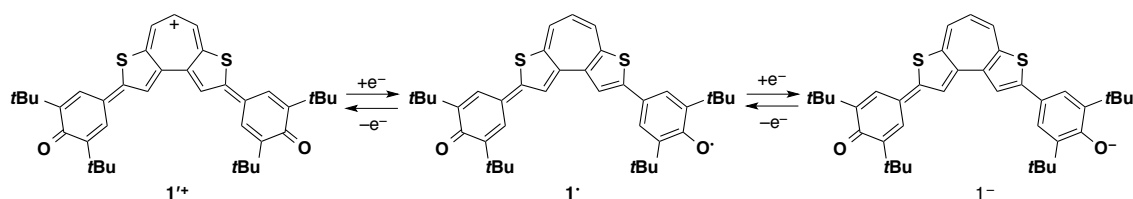

Figure 3-16. Cyclic voltammograms of radical $1^\bullet$ at a scan rate of 0.1 V s^{-1} in CH_2Cl_2 (blue line) and in THF (green line) with Bu_4NPF_6 as a supporting electrolyte. All oxidation and reduction potentials are referenced vs. Fc/Fc$^+$.

116

Scheme 3-4. Electrochemical transformations of **1**˙.

In order to gain deeper insights into the structure and properties of the electrochemically reduced or oxidized species, the redox processes were monitored by *in situ* UV-vis-NIR absorption spectroscopy. The absorption spectrum of **1**˙ was dramatically changed depending on the applied potentials (Figure 3-17). Upon applying the potential of -1.14 V (vs Fc/Fc$^+$), the sharp absorption band of **1**˙ at $\lambda_{abs} = 835$ nm is gradually diminished and, conversely, new absorption bands emerged with the maxima of 567 nm and 993 nm (Figure 3-17(a)). An isosbestic point was observed at 585 nm, 775 nm, and 849 nm, implying that the electrochemical reduction **1**˙ cleanly produced **1**$^-$ as a sole product. Notably, the resulting spectrum after the electrochemical reduction is almost identical with that of **1** in THF containing 0.067 M DBU (Figure 3-18).

On the other hand, when the potential of $+0.44$ V (vs Fc/Fc$^+$) was applied to a CH$_2$Cl$_2$ solution of **1**˙, a new absorption band appeared at $\lambda_{abs} = 1055$ nm with an isosbestic point at 864 nm (Figure 3-17(b)). This absorption band is attributable to the one-electron oxidized species **1**$^{˙+}$. This species can be also produced by chemical oxidation of **1**˙. Thus, the treatment of **1**˙ with 1.2 equivalents of tris(*p*-bromophenyl)aminium hexachloroantimonate ($E^o_1 = +0.70$ V vs. Fc/Fc$^+$) produced a sole product, which exhibited an almost identical absorption spectrum ($\lambda_{abs} = 1065$ nm, Figure 3-19) with that of the electrochemically oxidized species.

The multi-step reversible redox properties of **1**˙ are worth noting, because galvinoxyl showed only one-step reversible redox process at -0.06 V (vs Ag/AgCl) that corresponds to one-electron reduction.[21] This comparison shed light on the characteristic feature of **1**˙ in comparison with the conventional stable galvinoxyl-based radicals. This is definitely due to the delocalization of the positive charge over the more expanded π skeleton containing the seven-membered ring.

117
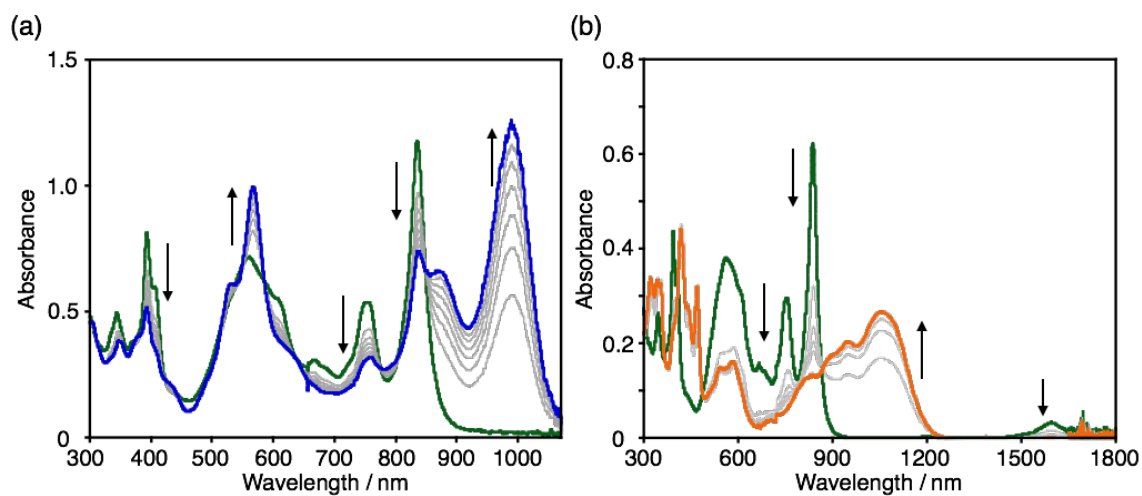
Figure 3-17. UV-vis-NIR absorption spectra of **1**$^{\bullet}$ with Bu$_4$NPF$_6$ as a supporting electrolyte (a) before (green line) and after reduction (blue line) at -1.14 V (blue line) in THF and (b) before (green line) and after oxidation (orange) at $+0.44$ V in CH$_2$Cl$_2$. The applied potentials were referenced vs. Fc/Fc^{+}.

Figure 3-18. Absorption spectra of **1** in THF with 0.067 M DBU (purple line) and **1**$^{\bullet}$ in THF with Bu$_4$NPF$_6$ as a supporting electrolyte after reduction at -1.14 V (green line).

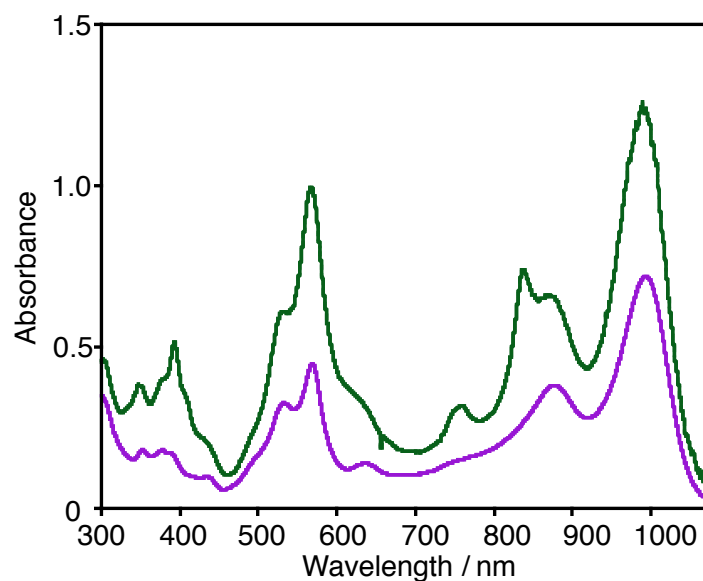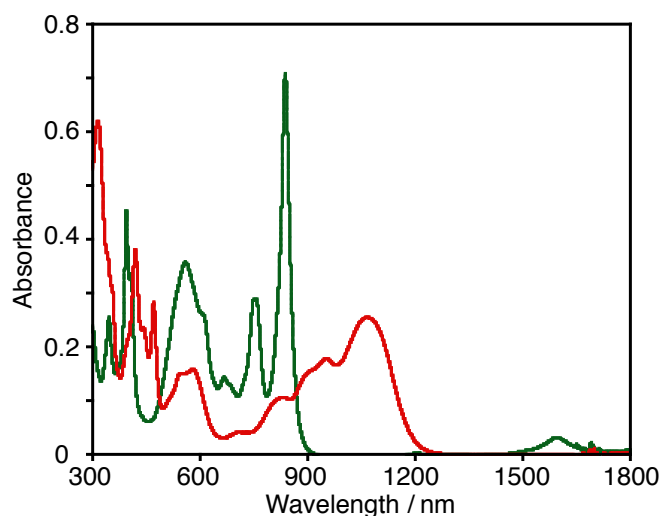**Figure 3-19.** Absorption spectra of **1**$^{\bullet}$ before (green line) and after (red line) the addition of 1.2 equivalents of $(p\text{-}BrC_6H_4)_3N^{\bullet+}SbCl_6^-$ in CH_2Cl_2.

Notably, radical **1**$^{\bullet}$ can be also generated by the electrochemical oxidation of charge neutral **1** *via* the proton-coupled electron transfer (PCET) process. The cyclic voltammograms of **1** in CH_2Cl_2 and in THF are shown in Figure 3-20. In CH_2Cl_2, reversible redox waves were observed in the oxidation process at $E_{1/2}$ = +0.15 V, accompanied by a shoulder-like anodic peak at E_{pa} = +0.03 V (Figure 3-20). The oxidation potential of **1** (+0.15 V) is comparable with that of radical **1**$^{\bullet}$, implying that radical **1**$^{\bullet}$ was *in situ* generated upon one-electron oxidation of **1**. To elucidate this process, the *in situ* absorption spectrum of **1** under the electrochemical conditions by applying the potential of +0.42 V (vs Fc/Fc$^+$) was measured (Figure 3-21). Upon electrochemical oxidation, the broad absorption band of **1** gradually decreased, and a new absorption band with the λ_{abs} of 838 nm, which is identical with that of **1**$^{\bullet}$, emerged with an isosbestic point at 866 nm. This result suggests that charge neutral **1** undergoes the one-electron oxidation followed by fast deprotonation or directly produce a radical **1**$^{\bullet}$. This PCET reaction is also reported for other phenol-containing compounds.[22] Moreover, upon continuous applying the potential of +0.42 V for 140 min, a new absorption band appeared at λ_{abs} = 1057 nm, which is identical with that of **1**$^{r+}$. Overall the phenolic compound **1** was transformed into a cationic species **1**$^{r+}$ *via* the two-electron and one-proton transfer process (Scheme 3-5).

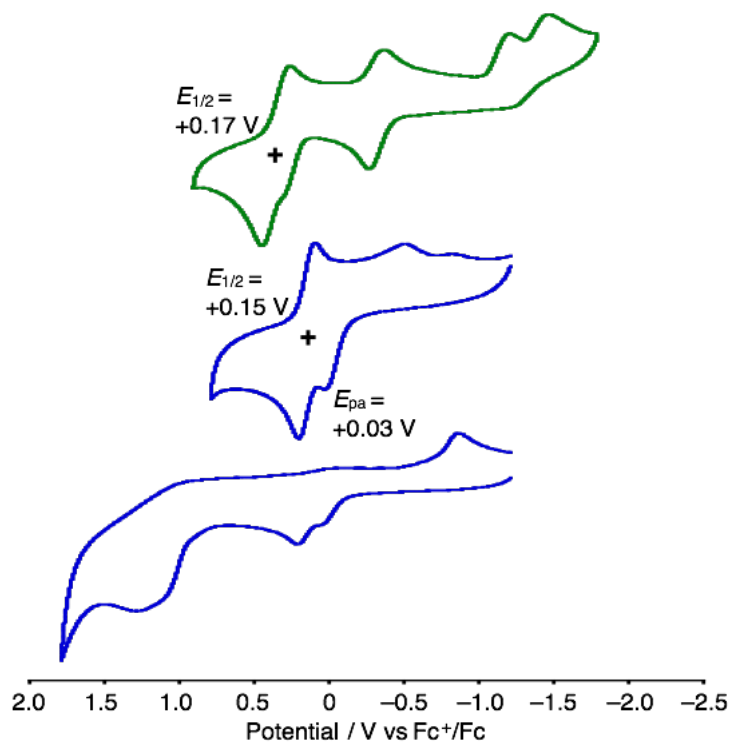**Figure 3-20.** Cyclic voltammogram of **1** at a scan rate of 0.1 V s^{-1} in CH$_2$Cl$_2$ (blue line) and in THF (green line) with Bu$_4$NPF$_6$ as a supporting electrolyte. All oxidation and reduction potentials are referenced vs. Fc/Fc$^+$.
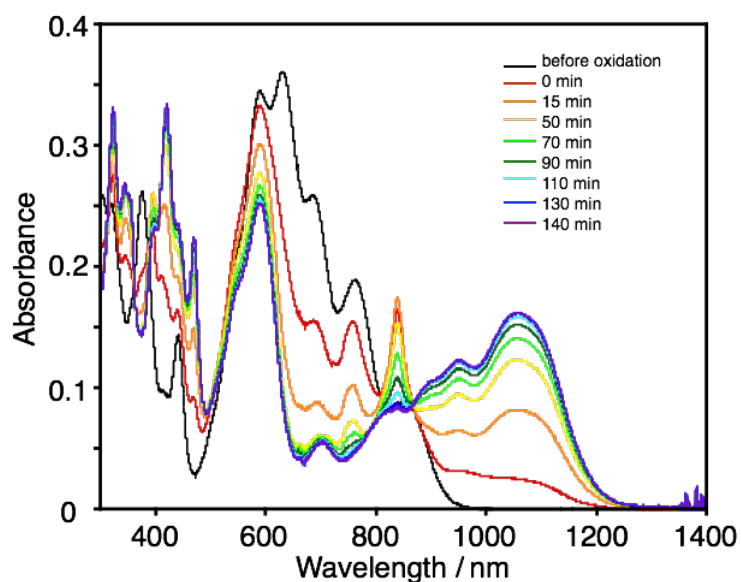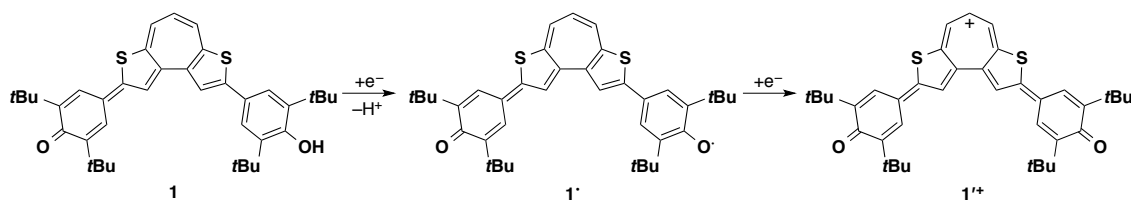

Figure 3-21. *In situ* UV-vis-NIR absorption spectra of **1** at the applied potential of +0.42 V (vs. Fc/Fc$^+$) in CH$_2$Cl$_2$ with Bu$_4$NPF$_6$ as a supporting electrolyte.

Scheme 3-5. Generation of $\mathbf{1}^{r+}$ from **1** via two-electron/one-proton transfer process.

3.3 Conclusion

A new NIR dye **1** consisted of a cyclohepta[1,2-*b*;4,3-*b'*]dithiophene skeleton and phenol moieties has been synthesized in this study. This compound can be regarded as a π-extended analogue of fluorescein and therefore shows pH-responsive photophysical properties due to the acid-base equilibria among the cation, neutral, and anion forms. Under the acidic conditions, **1** was transformed to the corresponding cation $\mathbf{1}^+$, which showed a strong absorption and red fluorescence. The contribution of the tropylium ion character to the resonance structure is responsible for the higher pK_a value of **1** than those of other fluorescein derivatives. On the other hand, under the basic conditions, a strong and broad NIR absorption band between 700 nm and 1100 nm was observed. The significantly red-shifted absorption of the anion $\mathbf{1}^-$ is due to the contribution of the quinoidal resonance structure with the charge delocalization over the entire π-conjugated skeleton. Moreover, compound **1** can be also transformed into neutral radical $\mathbf{1}^{\bullet}$ by the chemical or electrochemical oxidation. This radical can be regarded as a π-extended analogue of galvinoxyl radical and showed outstanding stability. Its longest-wavelength absorption reached the NIR region around 1600 nm due to the effective spin delocalization over the entire π-conjugated skeleton. Radical $\mathbf{1}^{\bullet}$ showed the reversible electrochemical redox process, and produced a cationic species $\mathbf{1}^{r+}$ different from $\mathbf{1}^+$, by one-electron oxidation and the anion $\mathbf{1}^-$ by one-electron reduction. These species also showed characteristic absorption bands in the NIR region. Overall, compound **1** can exhibit significant photophysical properties changes in multi stages based on the acid-base equilibria and the redox properties. Extension of π-conjugation of the polymethine skeleton with the cycloheptatriene skeleton plays crucial role to realize these properties. These results would provide important knowledge for the molecular design of polymethine-based NIR dyes and compound **1** would have potential for the application as the stimuli-responsive NIR-absorbing materials.

3.4 Experimental Section

General. Melting points (mp) or decomposition temperatures were determined with a Yanaco MP-S3 instrument (MP-S3). Thermal gravimetric analyses (TGA) for the determination of the 5% weight loss temperature (T_{d5}) were conducted using a SII TGA6200 instrument. ^{1}H and ^{13}C{^{1}H} spectra were recorded with a JEOL AL-400 spectrometer (400 MHz for ^{1}H and 100 MHz for ^{13}C) in CDCl$_3$, CD$_2$Cl$_2$, C$_6$D$_6$, THF-d_8, and CD$_3$CN. The chemical shifts in ^{1}H spectra are reported in δ ppm using the residual proton of the solvents, CHCl$_3$ (7.26 ppm), CH$_2$Cl$_2$ (5.32 ppm) and C$_6$H$_6$ (7.16 ppm) as an internal standard. The chemical shifts in ^{13}C spectra are reported in δ ppm using the solvent signals of CDCl$_3$ (77.16 ppm), THF-d_8 (67.21 ppm), and CD$_3$CN (118.26 ppm) as an internal standard. Mass spectra were measured with a Bruker micrOTOF Focus spectrometer with the APCI ionization method or electrospray ionization (ESI). Thin layer chromatography (TLC) was performed on plates coated with 0.25 mm thick silica gel 60F$_{254}$ (Merck). Column chromatography was performed using PSQ100B (Fuji Silysia Chemicals) or Wakosil 50NH$_2$(HC) (Wako Pure Chemicals Industries, Ltd). Anhydrous toluene and CH$_2$Cl$_2$ were purchased from Kanto Chemicals and further purified by Glass Contour solvent systems. CH$_3$CN and EtOAc were stored over 3 Å molecular sieves prior to use. All reactions were performed under a nitrogen or an argon atmosphere. 2,8-Dibromo-4*H*-cyclohepta[1,2-*b*;4,3-*b′*]dithiophene **2** was prepared according to Chapter 2. 3,5-di-*tert*-butyl-4-hydroxyphenylboronic acid was prepared according to the literature method.[23]

2,8-Bis(3,5-di-*tert*-butyl-4-hydoroxyphenyl)-4*H*-cyclohepta[1,2-*b*;4,3-*b′*]dithiophene (3). To a solution of **2** (0.804 g, 2.22 mmol), in a mixed solvent of degassed DMF (20 mL) and degassed water (5 mL) was added 3,5-di-*tert*-butyl-4-hydroxylphenylboronic acid (1.22 g, 4.88 mmol), Pd(PPh$_3$)$_4$ (0.129 g, 0.112 mmol) and Na$_2$CO$_3$ (0.706 g, 6.66 mmol). The reaction mixture was stirred at 80 °C for 34 h. After addition of water, the aqueous layer was extracted with Et$_2$O. The combined organic layer was washed with brine, dried over Na$_2$SO$_4$, filtered, and concentrated under reduced pressure. The crude products were purified by column chromatography (Wakosil 50NH$_2$(HC), hexane/toluene = 10/1, R_f = 0.20) to afford **3** as white solids (0.944 g, 1.54 mmol, 69% yield). Mp: 123.0 °C (decomp.). ^{1}H NMR (400 MHz, C$_6$D$_6$): δ 1.35 (s, 18H), 1.36 (s, 18H), 3.16 (d, J = 6.4 Hz, 2H), 4.99 (s, 1H), 5.02 (s, 1H), 5.40 (dt, J = 6.4 Hz, 10.0 Hz,

1H), 6.57 (d, *J* = 10.0 Hz, 1H), 7.55 (s, 1H) 7.62 (s, 2H), 7.64 (s, 1H), 7.67 (s, 2H). $^{13}C\{^{1}H\}$ NMR (100 MHz, THF-d_8): δ 27.6, 30.4, 30.4, 35.1, 35.2, 122.1, 122.7, 123.2, 123.5, 123.6, 124.5 126.6, 127.1, 130.6, 135.7, 136.0, 138.1, 138.5, 138.6, 142.6, 145.1, 154.6, 155.1. HRMS (APCI): *m/z* calcd. for $C_{39}H_{48}O_2S_2$: 612.3090 ($[M]^+$); Obsd. 612.3079.

Compound 1. To a solution of **3** (0.327 g, 0.534 mmol) in CH_2Cl_2 (5 mL) was added DDQ (0.122 g, 0.537 mmol). The reaction mixture was stirred at ambient temperature for 19 h. After addition of a saturated aqueous solution of NH_4Cl, the aqueous layer was extracted with EtOAc. The combined organic layer was washed with brine, dried over Na_2SO_4, filtered, and concentrated under reduced pressure. The crude product was purified by column chromatography (PSQ100B, the eluent was changed from CH_2Cl_2/EtOAc = 10/1 (R_f = 0.20) to EtOAc containing 1% NEt_3 (R_f = 1.0)) and recrystallized from $CHCl_3$/hexane to afford **1** as dark blue solids (0.203 g, 0.332 mmol, 62% yield). TGA: T_{d5} = 328.5 °C (without melting). ^{1}H NMR (400 MHz, $CDCl_3$): δ 1.37 (s, 9H), 1.40 (s, 9H), 1.51 (s, 18H), 5.52 (s, 1H), 6.36 (dd, *J* = 9.6 Hz, 10.8 Hz, 1H), 6.83 (d, *J* = 9.6 Hz, 1H), 6.89 (d, *J* = 10.8 Hz, 1H), 7.15 (d, *J* = 2.4 Hz, 1H), 7.37 (s, 1H) 7.41 (d, *J* = 2.4 Hz, 1H), 7.47 (s, 2H), 7.49 (s, 1H). $^{13}C\{^{1}H\}$ NMR (100 MHz, THF-d_8): δ 29.8, 29.9, 30.2, 35.2, 35.8, 35.9, 118.2, 120.7, 123.5, 124.0, 124.9, 125.5, 125.5, 125.9, 127.6, 128.1, 137.8, 138.8, 138.9, 144.2, 144.5, 145.9, 147.0, 152.4, 152.8, 157.0, 184.6. HRMS (APCI): *m/z* Calcd. for $C_{39}H_{46}O_2S_2$: 610.2934 ($[M]^+$); Obsd. 610.2955.

2,8-Bis(3,5-di-*tert*-butyl-4-hydroxyphenyl)-dithieno[1,2-*b*;4,3-*b′*]tropylium tetrafluoroborate ($1^+ \cdot BF_4^-$). To a solution of **3** (48.2 mg, 0.0786 mmol) in EtOAc (2 mL) was added a solution of triphenylmethylium tetrafluoroborate (32.0 mg 0.0969 mmol) in CH_3CN (1 mL). The reaction mixture was stirred at ambient temperature for 9.5 h, and then concentrated under reduced pressure. The crude product was washed with toluene, and further recrystallized from CH_2Cl_2/hexane to afford $1^+ \cdot BF_4^-$ as brown solids (44.4 mg, 0.0635 mmol, 81% yield). TGA: T_{d5} = 254.0 °C (without melting). ^{1}H NMR (400 MHz, CD_2Cl_2): δ 1.56 (s, 36H), 6.01 (s, 2H), 7.83 (s, 4H), 7.95 (t, *J* = 10.0 Hz, 1H), 8.61 (s, 2H), 8.85 (d, *J* = 10.0 Hz, 2H). $^{13}C\{^{1}H\}$ NMR (CD_3CN, 100Hz): δ 30.2, 35.4, 123.8, 124.5, 126.6, 128.8, 139.6, 143.0, 149.4, 152.1, 159.7, 165.9. HRMS

(APCI): m/z calcd. for $C_{37}H_{47}O_2S_2$: 611.3012 ($[M]^+$); Obsd. 611.3030.

Neutral radical 1•. To a solution of $K_3Fe(CN)_6$ (65.7 mg, 0.200 mmol) in toluene (0.5 mL) was added a 1M aqueous solution of KOH (0.2 mL). The mixture was stirred at ambient temperature for 15 min and then, was added a solution of **1** (48.6 mg, 0.0795 mmol) in toluene (4 mL). The reaction mixture was stirred at ambient temperature for 19 h. After addition of water, the aqueous layer was extracted with toluene. The combined organic layer was washed with brine, dried over Na_2SO_4, filtered, and concentrated under reduced pressure. The crude product was recrystallized from toluene/hexane to afford **1•** as dark purple solids (23.4 mg, 0.0384 mmol, 48% yield). TGA: T_{d5} = 320.6°C (without melting). HRMS (APCI): m/z Calcd. for $C_{39}H_{46}O_2S_2$: 610.2934 ($[M+H]^+$); Obsd. 610.2952. Anal. Calcd. for $C_{39}H_{45}O_2S_2$: C, 76.80; H, 7.44. Obsd.: C, 76.81; H, 7.44.

Chemical oxidation of 1•. To a solution of **1•** (3.0 mg, 4.9 μmol) in degassed and dehydrated CH_2Cl_2 (5 mL) was added tris(*p*-bromophenyl)aminium hexachloroantimonate (4.9 mg, 6.0 μmol) under an argon atmosphere. The mixture was stirred at ambient temperature for 1 h. The solution was diluted for UV-vis-NIR measurement (ca. 1.0×10^{-4} M).

X-ray Crystallographic Analysis

Structural analysis of 1. Single crystals of **1** suitable for X-ray crystallographic analysis were obtained by recrystallization from acetone and CH_3CN using vapor diffusion method. Intensity data were collected at 123 K on a Rigaku X-ray diffractometer equipped with a molybdenum FR-X microfocus generator, VariMax-Mo optics, and a PILATUS 200K detector. Total of 48310 reflections were measured with the maximum 2θ angle of 55.0°, of which 8465 were independent reflections (R_{int} = 0.0537). The structure was solved by direct methods (SHELXS-2013) and refined by the full-matrix least-squares on F^2 (SHELXL-2013). All non-hydrogen atoms were refined anisotropically and all hydrogen atoms were placed using AFIX instructions. The crystal data are as follows: $C_{41}H_{49}NO_2S_2$; FW = 651.93, crystal size 0.16 × 0.07 × 0.06 mm^3, monoclinic, $P2_1/a$, a = 11.430(2) Å, b = 27.524(5) Å, c = 12.095(2) Å, β =

103.777(2)°, $V = 3695.6(11)$ Å^3, $Z = 4$, $D_c = 1.172$ g cm^{-3}, $\mu = 0.179$ mm^{-1}, $R_1 = 0.0628$ ($I > 2\sigma(I)$), $wR_2 = 0.2027$ (all data), GOF = 1.143.
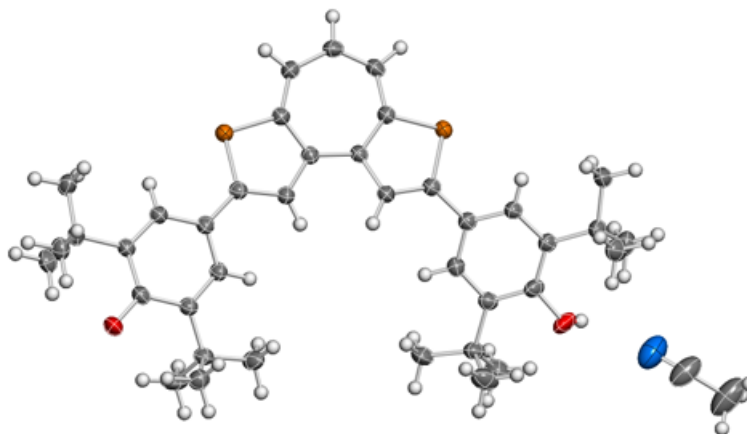

Figure 3-22. X-ray crystal structure of **1** including CH$_3$CN. Thermal ellipsoids are scaled to the 50% probability level.
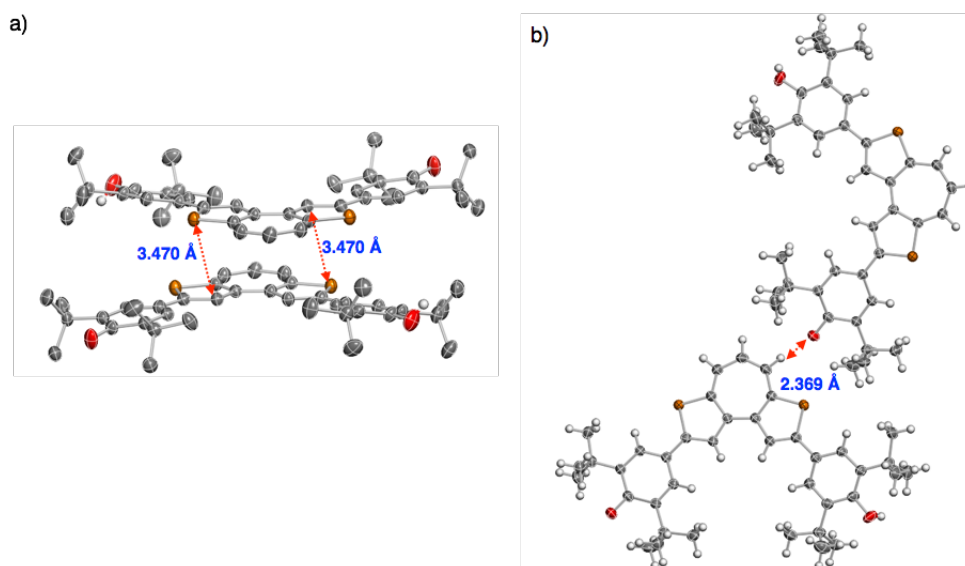

Figure 3-23. Packing structure of **1** where thermal ellipsoids are scaled to the 50% probability level: (a) Side view (Hydrogen atoms except hydroxy groups are omitted) and (b) top view.

Structural analysis of $1^+ \cdot BF_4^-$. Single crystals of $1^+ \cdot BF_4^-$ suitable for X-ray crystallographic analysis were obtained by recrystallization from chlorobenzene and cyclohexane using vapor diffusion method. Intensity data were collected at 123 K on a Rigaku X-ray diffractometer equipped with a molybdenum FR-X microfocus generator, VariMax-Mo optics, and a PILATUS 200K detector. Total of 52776 reflections were measured with the maximum 2θ angle of 55.0°, of which 9710 were independent reflections (R_{int} = 0.0370). The structure was solved by direct methods (SHELXS-2013) and refined by the full-matrix least-squares on F^2 (SHELXL-2013). All non-hydrogen atoms were refined anisotropically and all hydrogen atoms were placed using AFIX instructions. The crystal data are as follows: $C_{45}H_{52}BClF_4O_2S_2$; FW = 811.24, crystal size $0.20 \times 0.12 \times 0.04$ mm^3, monoclinic, $P2_1/n$, a = 9.7186(5) Å, b = 30.7170(15) Å, c = 14.4559(7) Å, β = 97.2055(17)°, V = 4281.4(4) Å^3, Z = 4, D_c =1.259 g cm^{-3}, μ = 0.240 mm^{-1}, R_1 = 0.0686 ($I > 2\sigma(I)$), wR_2 = 0.2418 (all data), GOF = 1.102.
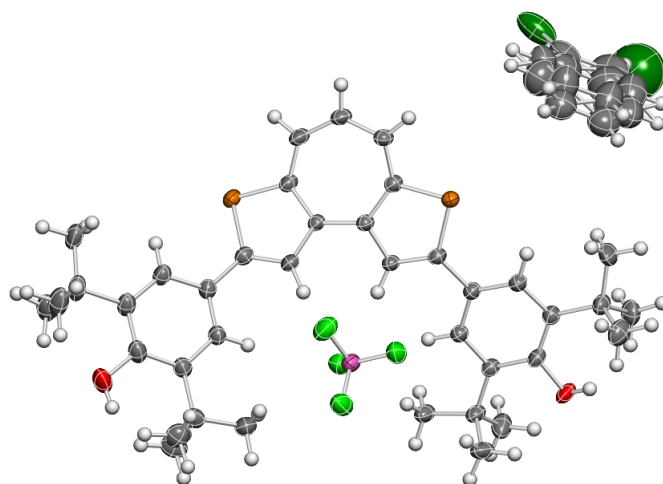
Figure 3-24. X-ray crystal structure of $1^+ \cdot BF_4^-$ including chlorobenzene. Thermal ellipsoids are scaled to the 50% probability level.

Structural analysis of $1^\bullet$. Single crystals of $1^\bullet$ suitable for X-ray crystallographic analysis were obtained by recrystallization from 1,2-dichloroethane and CH$_3$CN using vapor diffusion method. Intensity data were collected at 123 K on a Rigaku X-ray diffractometer equipped with a molybdenum FR-X microfocus generator, VariMax-Mo optics, and a PILATUS 200K detector. Total of 49353 reflections were measured with

the maximum 2θ angle of 55.0°, of which 7734 were independent reflections (R_{int} = 0.0300). The structure was solved by direct methods (SHELXS-2013) and refined by the full-matrix least-squares on F^2 (SHELXL-2013). All non-hydrogen atoms were refined anisotropically and all hydrogen atoms were placed using AFIX instructions. The crystal data are as follows: $C_{39}H_{45}O_2S_2$; FW = 609.87, crystal size 0.16 × 0.10 × 0.06 mm^3, monoclinic, $P2_1/c$, a = 14.2946(14) Å, b = 11.7691(11) Å, c = 20.1810(19) Å, β = 95.450(2)°, V = 3379.8(6) Å^3, Z = 4, D_c =1.199 g cm^{-3}, μ = 0.190 mm^{-1}, R_1 = 0.0437 ($I > 2\sigma(I)$), wR_2 = 0.1424 (all data), GOF = 1.112.
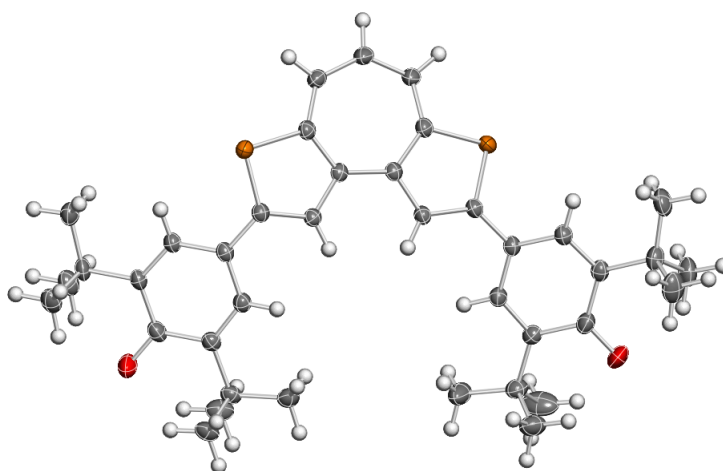
Figure 3-25. X-ray crystal structure of **1**$^\bullet$. Thermal ellipsoids are scaled to the 50% probability level.
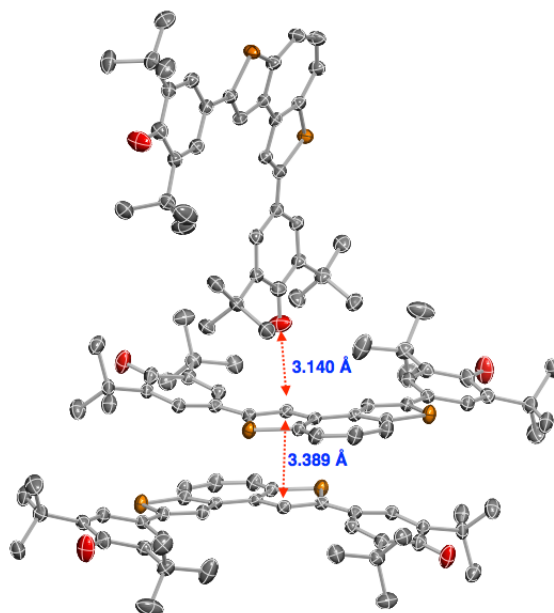
Figure 3-26. Packing structure of **1**$^\bullet$. Thermal ellipsoids are scaled to the 50% probability level.

Photophysical Measurements. UV-vis-NIR absorption spectra were measured with a Shimadzu UV-3650 spectrometer with a resolution of 1.0 nm using dilute sample solutions in spectral grade solvents in a 1 cm or 1 mm square quartz cuvette. Emission spectra were measured with a Hitachi F-4500 spectrometer with a resolution of 1 nm. NIR emission spectra were measured with a Horiba SPEX Fluorolog 3 spectrofluorometer equipped with a Hamamatsu PMA R5509-73 and a cooling system C9940-01. Absolute fluorescence quantum yield were determined with a Hamamatsu photonics C-9920-02 calibrated integrating sphere system, with two photonic multichannel analyzers C10027-02 and C10028-01 for **1** in CH_2Cl_2 with addition of DBU,[24] and with a multichannel spectrometer PMA 12 for the others.
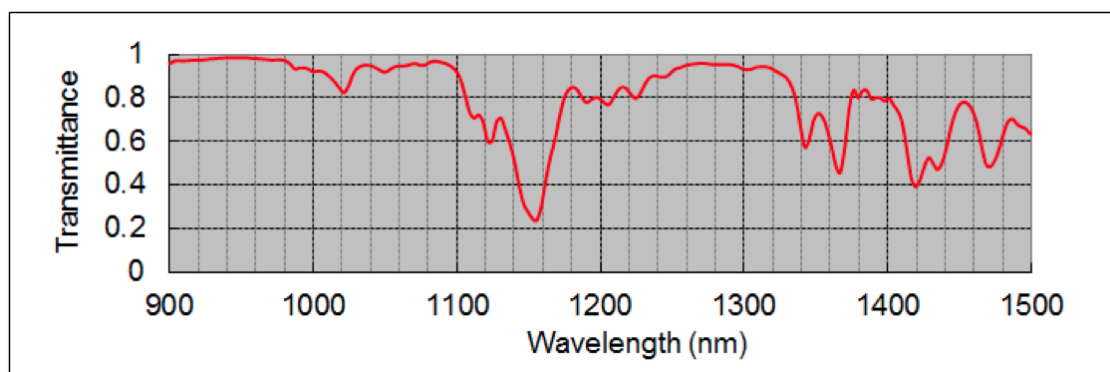
Figure 3-27. Transmittance of CH_2Cl_2. The depression around 1150 nm in the fluorescence spectrum of **1** with 1% DBU should be attributable to the absorption of CH_2Cl_2 used as the solvent.

Electrochemical Properties

Cyclic Voltammetry and Differential Pulse Voltammetry. Cyclic voltammetry (CV) and differential pulse voltammetry (DPV) measurements were performed on an ALS/chi-617A electrochemical analyzer. The CV cell consisted of a glassy carbon electrode, a Pt wire counter electrode, and an $Ag/AgNO_3$ reference electrode. The measurements were carried out under an argon atmosphere using THF solution of sample with a concentration of 1 mM, and 0.1 M tetrabutylammonium hexafluorophosphate as a supporting electrolyte. The oxidation potentials were calibrated with ferrocene/ferrocenium ion couple.

Electrochemical Absorption Spectroscopy for reduction. Electrochemical absorption spectra of **1**˙ for the reduction were measured with an Ocean Optics HR4000CG-UV-NIR high-resolution spectrometer with a DH-2000-BAL UV-vis-NIR light source by cooperating with ALS/chi-617A electrochemical analyzer. Electrochemical absorption spectra of **1**˙ for the oxidation were measured with a Shimadzu UV-3650 spectrometer with a resolution of 1.0 nm by cooperating with ALS/chi-617A electrochemical analyzer. The electrochemical cell consisted of 1 mm of thin layer quartz cell, a Pt mesh working electrode, a Pt wire counter electrode, and a $Ag/AgNO_3$ reference electrode. The measurements were carried out under argon atmosphere using THF with a concentration of ca. 0.1 mM of **1**˙, and 0.1 M tetrabutylammonium hexafluorophosphate as a supporting electrolyte for reduction, and under flow of nitrogen gas using CH_2Cl_2 solution of sample with a concentration of ca. 0.1 mM of **1**˙ and 0.1 M tetrabutylammonium hexafluorophosphate as a supporting

electrolyte for oxidation. The reduction and oxidation potentials were calibrated with ferrocene/ferrocenium ion couple.

EPR Measurements. Electron paramagnetic resonance (EPR) spectrum was measured with a JEOL JES-FA 200 ESR spectrometer in a sealed tube. The 1.0×10^{-3} M solutions of $\mathbf{1}^{\bullet}$ in CH_2Cl_2 was charged into a quartz EPR tube under an argon atmosphere and degassed by freeze-pump-thaw cycles. The tube was sealed off under vacuum. The obtained spectrum was simulated with Lorentz functions.

Computational Method. The geometry optimization of **1, $\mathbf{1}^{+}$** and $\mathbf{1}^{-}$ were performed using the B3LYP[25] theory with the 6-311+G(d,p) basis set, implemented in the Gaussian 09 program.[26] For the geometry optimizations, a stationary point was optimized without any symmetry assumptions and characterized by frequency analysis at the same level of theory (the number of imaginary frequencies, NIMAG, was 0). TD-DFT vertical excitation calculations of **1**, $\mathbf{1}^{+}$, and $\mathbf{1}^{-}$ were performed using the optimized geometry at the B3LYP/6-311+G(d,p) level, implemented in the Gaussian 09 program. The geometry optimization of $\mathbf{1}^{\bullet}$ was performed using the UB3LYP theory with the 6-311+G(d,p) basis set, implemented in the Gaussian 09 program. For the geometry optimizations, a stationary point was optimized without any symmetry assumptions and characterized by frequency analysis at the same level of theory (the number of imaginary frequencies, NIMAG, was 0.) TD-DFT vertical excitation calculations of $\mathbf{1}^{\bullet}$ was performed using the optimized geometry at the UB3LYP/6-311+G(d,p) level, implemented in the Gaussian 09 program. The Cartesian coordinates for **1**, $\mathbf{1}^{+}$, $\mathbf{1}^{-}$, and $\mathbf{1}^{\bullet}$ are given in Tables 3-4–3-7.

Table 3-4. Cartesian Coordinates of the Optimized Structure for **1** at the B3LYP/6-311+G(d,p) Level

atom	x	y	z	atom	x	y	z
S	3.1685962	3.15013388	-0.36368816	H	7.96811622	-1.6095718	2.14314446
C	1.47044439	3.59183154	-0.34420233	C	8.66320636	0.02387668	-0.14284465
C	2.81042316	1.44928905	-0.19300788	H	8.77266085	-1.01074919	-0.47826643
C	1.45099469	1.25995098	-0.14397557	H	9.63880653	0.34286501	0.23451435
H	1.02392298	0.27694551	-0.01333222	H	8.43295652	0.61732987	-1.03106764
C	0.66480973	2.44603447	-0.23049152	C	4.27740649	-3.32178562	-0.88611294
C	1.15974689	4.97364793	-0.44343033	C	4.46215428	-4.29421611	0.30486349
H	2.0090828	5.64479658	-0.52371631	H	4.20343677	-5.31074863	-0.00693639
C	-0.08056442	5.55198561	-0.44572563	H	3.80041242	-4.01986526	1.13173803
H	-0.10507855	6.63348114	-0.52947145	H	5.48670731	-4.3010933	0.6718096
C	-1.34677383	4.92407707	-0.34998433	C	2.81861829	-3.46657493	-1.36536165
H	-2.19867026	5.59716941	-0.36964859	H	2.64395662	-4.50417615	-1.65998219
C	3.87320028	0.44598041	-0.12630516	H	2.60445827	-2.8402278	-2.23572902
C	5.8737828	-1.4937313	0.02786924	H	2.09906863	-3.22685321	-0.57761925
C	3.62440131	-0.87708771	-0.51370079	C	5.18721139	-3.74042465	-2.06711881
C	5.15266167	0.77139704	0.33211096	H	4.92840026	-4.7536538	-2.38945399
C	6.17883025	-0.16884918	0.42173257	H	6.24123453	-3.72918962	-1.79597497
C	4.59430849	-1.87256566	-0.44762307	H	5.04260137	-3.07156949	-2.92076507
H	2.64560754	-1.12068953	-0.89886995	C	-4.05243672	-3.48162663	0.2556181
H	5.33908517	1.78736793	0.64841811	C	-4.65215075	-4.25144298	-0.94697774
O	6.81142683	-2.49015498	0.08579511	H	-4.29799121	-3.82839343	-1.89231978
H	7.64413348	-2.14355056	0.4138744	H	-5.73985994	-4.21423047	-0.93444661
C	-0.79063373	2.41166764	-0.18557896	H	-4.33768896	-5.29978847	-0.90949427
C	-1.63950593	3.58572488	-0.23908299	C	-4.54255618	-4.11737646	1.58011939
C	-1.5228008	1.24372839	-0.0851952	H	-5.62743883	-4.07643868	1.6577944
H	-1.0660541	0.26795632	-0.03674148	H	-4.109534	-3.59820138	2.44099649
C	-2.93340387	1.38222901	-0.04815727	H	-4.2280515	-5.16531068	1.62677293
S	-3.33293059	3.10402763	-0.14642088	C	-2.52182605	-3.65216905	0.19831718
C	-3.91263871	0.38961468	0.04544033	H	-2.0980243	-3.25962308	-0.73128287
C	-6.29295457	-0.22058926	0.16917593	H	-2.27840153	-4.71701325	0.24379881
C	-4.46982184	-2.00155274	0.19562468	H	-2.02126163	-3.16663204	1.04187136
C	-5.91358407	-1.65567475	0.23577316	C	-7.78159024	0.1648525	0.20525539
C	-3.55406028	-0.99760324	0.10722689	C	-8.52343509	-0.47097105	-0.99658107
C	-5.3069548	0.71444437	0.07933653	H	-9.57862013	-0.17912681	-0.97523031
H	-2.50262046	-1.24553782	0.07839258	H	-8.46240868	-1.55726836	-0.96685835
H	-5.57552225	1.76253725	0.0314668	H	-8.09779915	-0.12130308	-1.94239351
O	-6.7786072	-2.53942178	0.32141538	C	-8.42144972	-0.31974422	1.5299731
C	7.57857006	0.24471113	0.94540131	H	-9.47644389	-0.02782178	1.55913469
C	7.6352931	1.74475195	1.30467889	H	-7.92276589	0.13838211	2.38992213
H	6.93239521	2.00337435	2.10021257	H	-8.35749553	-1.40218344	1.62515793
H	7.43169808	2.38144769	0.44036963	C	-7.98422157	1.69025757	0.121839
H	8.63874869	1.98840516	1.66244352	H	-9.05453405	1.91100011	0.1518449
C	7.93113213	-0.5221776	2.24769884	H	-7.59038447	2.10844245	-0.80949053
H	7.19176901	-0.30760131	3.02312498	H	-7.5189991	2.21529498	0.96166507
H	8.91018661	-0.20169224	2.61510141				

Table 3-5. Cartesian Coordinates of the Optimized Structure for **1**$^+$ at the B3LYP/6-311+G(d,p) Level

atom	x	y	z	atom	x	y	z
S	-3.2432803	3.11792495	0.00016072	H	-7.44602127	2.2728924	-0.88895417
C	-1.55058032	3.57716122	0.00018239	H	-7.44591464	2.27290468	0.88863197
C	-2.86302586	1.40991713	0.00005491	C	-8.50059305	-0.20612836	1.27997871
C	-1.48910304	1.22995655	0.00004122	H	-9.53338156	0.15137933	1.276487
H	-1.04882263	0.24566216	-0.00002555	H	-8.00936887	0.18856421	2.17265494
C	-0.72001973	2.41350303	0.00011161	H	-8.54219691	-1.29217213	1.3987191
S	3.24328422	3.11792089	0.00019206	C	-4.15818176	-3.45395494	-0.0000334
C	1.5505848	3.57715922	0.0001991	C	-4.69904573	-4.15307546	-1.2717068
C	2.86302751	1.40991353	0.00006729	H	-4.30289855	-3.6776042	-2.17379306
C	1.48910455	1.22995468	0.00004181	H	-5.7858302	-4.13370414	-1.3210843
H	1.04882303	0.24566075	-0.00004114	H	-4.37902884	-5.1988773	-1.27780793
C	0.72002272	2.41350214	0.00011542	C	-2.62653595	-3.63523251	0.00006261
C	1.24960145	4.93702231	0.00027278	H	-2.15796211	-3.20461988	-0.8899219
H	2.10143697	5.610651	0.00031682	H	-2.39785966	-4.70308819	0.00006868
C	0.0000035	5.54731007	0.0002967	H	-2.15807525	-3.20463371	0.89011336
H	0.00000418	6.63138935	0.00035377	C	-4.69920855	-4.15309941	1.27155713
C	-1.24959527	4.93702387	0.00025637	H	-5.78599938	-4.13372897	1.3207964
H	-2.10142993	5.61065359	0.00028845	H	-4.30317779	-3.67764517	2.17370345
C	3.90805565	0.40592757	0.00001176	H	-4.37919239	-5.19890138	1.27767996
C	5.91056019	-1.53679315	-0.00009418	C	4.15818013	-3.45395967	0.00000053
C	3.58781732	-0.96344988	0.000026	C	4.69908836	-4.15309581	-1.27164514
C	5.26385037	0.767127	-0.00005312	H	4.3790885	-5.19890296	-1.27773564
C	6.29068895	-0.16789102	-0.00010682	H	5.78587418	-4.13370757	-1.32099294
C	4.55284987	-1.95863194	-0.00002399	H	4.30295823	-3.67764725	-2.17375085
H	2.54907959	-1.25452236	0.00008959	C	2.62653514	-3.63524304	0.00005387
H	5.52120856	1.81662705	-0.00006336	H	2.39786255	-4.70309947	0.00007812
C	-3.90805563	0.40593285	0.0000015	H	2.15798686	-3.20465334	-0.88995522
C	-5.91056379	-1.53678315	-0.00009176	H	2.15804577	-3.20462449	0.89008
C	-5.26384937	0.76713543	-0.00004508	C	4.69917347	-4.15308041	1.27161832
C	-3.58782023	-0.96344573	0.00000037	H	4.37916384	-5.19888431	1.27774863
C	-4.55285419	-1.95862676	-0.00004444	H	4.30311287	-3.6776141	2.17374519
C	-6.29068864	-0.16788178	-0.00009471	H	5.78596276	-4.1337021	1.32088933
H	-5.52120496	1.81663596	-0.00004238	C	7.77299179	0.2856462	-0.00015796
H	-2.54908302	-1.25451999	0.00004559	C	8.50056373	-0.20619042	-1.28025404
O	-6.83734805	-2.52528175	-0.00011479	H	8.00931516	0.18845277	-2.17293886
O	6.83733318	-2.52530248	-0.00013891	H	8.54217892	-1.29223951	-1.39895272
H	-7.72643229	-2.15887948	-0.0002021	H	9.53335013	0.15132282	-1.27680647
H	7.72642165	-2.15891166	-0.00025154	C	8.50059564	-0.20603601	1.27997923
C	-7.77299301	0.28564596	-0.00012424	H	8.5422095	-1.29207009	1.3987981
C	-8.50055436	-0.20613161	-1.28024831	H	8.00936532	0.18871369	2.17262678
H	-9.53334584	0.15136636	-1.27678364	H	9.53338013	0.15148353	1.27646583
H	-8.542155	-1.29217574	-1.39900078	C	7.89636524	1.82374483	-0.00025423
H	-8.0093097	0.18856434	-2.172912	H	7.44599724	2.27283592	-0.88910325
C	-7.89638344	1.8237442	-0.00013106	H	8.9539529	2.09599547	-0.00021036
H	-8.95397412	2.09598257	-0.00007098	H	7.44589141	2.27295142	0.88848294

132

Table 3-6. Cartesian Coordinates of the Optimized Structure for **1⁻** at the B3LYP/6-311+G(d,p) Level

atom	x	y	z	atom	x	y	z
S	-3.25293936	3.11692401	0.00007162	H	9.53663108	0.02741425	1.26326005
C	-1.54984286	3.58028841	0.00011786	C	7.93717173	1.80008299	0.00012883
C	-2.88183318	1.39057048	0.00004719	H	7.49230295	2.26163853	-0.88672533
C	-1.48604814	1.23382689	0.00006933	H	9.00310722	2.04784494	0.00015958
H	-1.03853905	0.25241368	0.00006855	H	7.49226929	2.26156145	0.88700626
C	-0.72930473	2.41065572	0.00010249	C	4.15093916	-3.4612048	-0.00017888
C	-1.25067506	4.94059692	0.00016972	C	4.7149594	-4.1536321	-1.26541513
H	-2.10611958	5.61040202	0.00018569	H	4.44346614	-5.21565917	-1.26359077
C	0.00000496	5.55356325	0.00020216	H	5.79974582	-4.06758118	-1.30257873
H	0.00000571	6.63871412	0.00024327	H	4.2951924	-3.7008281	-2.16957434
C	1.25068416	4.94059515	0.00018772	C	4.71492311	-4.15376386	1.26500109
H	2.10612962	5.610399	0.0002162	H	4.44342845	-5.21579062	1.26305928
C	-3.90056326	0.40670603	0.00000596	H	4.29513088	-3.70105334	2.16919542
C	-5.9625074	-1.59779461	-0.00011654	H	5.79970856	-4.06771823	1.30220405
C	-3.58476734	-0.98255195	-0.00006588	C	2.62448649	-3.67188222	-0.00021179
C	-5.27884639	0.75880299	0.00004921	H	2.40862904	-4.74435644	-0.00026725
C	-6.29406637	-0.16077629	0.00001091	H	2.14892583	-3.24277456	-0.88735304
C	-4.53524662	-1.96909918	-0.00011017	H	2.14890014	-3.24286137	0.88695778
H	-2.5395717	-1.25996434	-0.00009014	C	-4.15094949	-3.46119913	-0.00018415
H	-5.52439854	1.81400041	0.00012555	C	-4.71490491	-4.15373666	1.26501997
O	-6.86168327	-2.46953069	-0.00006109	H	-4.44342495	-5.21576718	1.26308159
C	0.72931012	2.41065473	0.00010936	H	-5.79968819	-4.06767512	1.3022545
C	1.54984997	3.58028624	0.00013854	H	-4.29508013	-3.70102192	2.16919699
C	1.48605178	1.23382482	0.00007528	C	-4.71501843	-4.15363531	-1.26539335
H	1.03854111	0.25241236	0.00005672	H	-4.44354381	-5.21566705	-1.26356117
C	2.8818371	1.39056631	0.00006836	H	-4.29527108	-3.70085162	-2.16957177
S	3.25294582	3.11691923	0.00011325	H	-5.79980482	-4.06756562	-1.3025264
C	3.9005655	0.40670016	0.00002633	C	-2.6244984	-3.6718917	-0.00026043
C	6.29406764	-0.16078603	0.00001599	H	-2.40865213	-4.74436816	-0.00030241
C	4.5352449	-1.96910628	-0.00009671	H	-2.1488804	-3.24285887	0.88688633
C	5.96250735	-1.59780253	-0.00008147	H	-2.14896048	-3.24280627	-0.88742454
C	3.5847674	-0.98255756	-0.00004878	C	-7.77349663	0.26760753	0.00007281
C	5.27884896	0.75879505	0.00005891	C	-8.48293329	-0.27530788	-1.26485386
H	2.5395714	-1.25996897	-0.00007306	H	-8.42875803	-1.36218026	-1.30100666
H	5.52440135	1.81399221	0.00012551	H	-8.01740273	0.12973124	-2.16928596
O	6.86168629	-2.4695353	-0.00008599	C	-8.48284979	-0.27536144	1.26502344
C	7.77350017	0.26758857	0.00005909	H	-8.42868643	-1.36223593	1.3011191
C	8.48290794	-0.27531028	-1.26489031	H	-9.53660595	0.02749111	1.26331601
H	8.01736807	0.1297535	-2.16930638	H	-8.01724948	0.12962727	2.16944221
H	8.4287157	-1.36218133	-1.30106566	C	-7.93714972	1.80010292	0.00011135
H	9.53667241	0.02751307	-1.26310354	H	-7.49229798	2.26163211	-0.88676514
C	8.48287	-0.27542078	1.26498242	H	-7.49221722	2.26159574	0.88696635
H	8.42868834	-1.36229565	1.30105489	H	-9.00308198	2.04787888	0.00016406
H	8.01729441	0.12955349	2.16942016				

133

Table 3-7. Cartesian Coordinates of the Optimized Structure for **1·** at the UB3LYP/6-311+G(d,p) Level

atom	x	y	z	atom	x	y	z
S	-3.25357381	3.12078132	-0.00038239	H	-7.99103441	0.10258394	2.17318363
C	-1.55965738	3.57580902	-0.00027466	H	-8.43577783	-1.37523736	1.29873165
C	-2.88085418	1.39930033	-0.00011471	H	-9.51260331	0.03237647	1.27408431
C	-1.48752725	1.23623337	0.00002169	C	-4.1027966	-3.45967838	0.00014567
H	-1.04329679	0.25323811	0.00024599	C	-4.66200885	-4.15306516	-1.26758938
C	-0.73052466	2.41025447	-0.00008468	H	-4.3608481	-5.20536984	-1.27336985
C	-1.25564199	4.93835517	-0.00032316	H	-4.26264525	-3.68562357	-2.17300909
H	-2.10455795	5.61468057	-0.00048374	H	-5.74870614	-4.10357718	-1.29951512
C	-0.00000254	5.53856758	-0.00013221	C	-2.57407775	-3.65451862	0.00012738
H	0.00000006	6.62369025	-0.00015297	H	-2.35027626	-4.72411703	0.00017204
C	1.25564345	4.9383513	0.0000833	H	-2.10268746	-3.22402726	0.88888898
H	2.10455597	5.61468121	0.00021877	H	-2.1027192	-3.2241073	-0.88868975
C	-3.89283833	0.40884673	-0.00005507	C	-4.6619632	-4.1529424	1.2679683
C	-5.9290253	-1.59667975	0.00008713	H	-4.36080125	-5.20524608	1.27384049
C	-3.55546772	-0.97997994	0.00002103	H	-5.74865942	-4.10345196	1.29992778
C	-5.27479419	0.76512145	-0.00007294	H	-4.26256729	-3.68541178	2.17332784
C	-6.28390157	-0.15411789	-0.00000502	C	4.10279337	-3.45968027	-0.00003053
C	-4.49209048	-1.97254426	0.0000824	C	4.66196569	-4.15301572	1.26774945
H	-2.50826944	-1.24509973	0.00000637	H	4.26256362	-3.68554554	2.17313749
H	-5.52126306	1.81912356	-0.0001267	H	5.74866148	-4.1035141	1.29971338
O	-6.81240179	-2.46599426	0.00015964	H	4.36081661	-5.20532363	1.27355681
C	0.73052736	2.41025141	-0.00005355	C	2.57407528	-3.65452951	-0.00006005
C	1.55966164	3.57581322	0.00008918	H	2.10268277	-3.22409595	0.8887283
C	1.48752688	1.23623558	-0.00011013	H	2.35028013	-4.72412931	-0.00008099
H	1.04329821	0.25323949	-0.00029087	H	2.10271422	-3.22406619	-0.88885063
C	2.88085961	1.39929984	0.00002567	C	4.66200975	-4.1529903	-1.26780576
S	3.25357959	3.12078314	0.00022211	H	5.74870704	-4.10349592	-1.29972683
C	3.8928365	0.40884867	0.000017	H	4.26264617	-3.68549603	-2.17319829
C	6.28390008	-0.15412148	0.00004145	H	4.36085318	-5.2052957	-1.27364902
C	4.49208466	-1.97254505	-0.00001055	C	7.76351005	0.260164	0.00005852
C	3.5554646	-0.97998013	-0.00001283	C	8.46594437	-0.28788403	-1.26763568
C	5.27479612	0.76511892	0.00004418	H	9.51263692	0.03227446	-1.27397513
H	2.50826577	-1.24509732	-0.00001741	H	7.9910913	0.10240308	-2.17311976
H	5.52126703	1.81912076	0.00005361	H	8.43581874	-1.37534551	-1.29853697
C	-7.76351037	0.26017031	-0.00001293	C	8.46591363	-0.28787749	1.26777308
C	-7.93112186	1.79213843	-0.00012709	H	9.51260363	0.03228889	1.27414075
H	-7.49176922	2.25618551	0.88798648	H	8.43579365	-1.37533898	1.29867498
H	-8.9967944	2.03441338	-0.00012804	H	7.99103256	0.1024071	2.17324352
H	-7.49179706	2.25604995	-0.88832525	C	7.93112266	1.7921319	0.00005661
C	-8.46594935	-0.28797123	-1.26766472	H	8.99679541	2.03440625	0.00006441
H	-8.4358354	-1.3754354	-1.29847899	H	7.49177732	2.25611324	0.88820815
H	-7.99109061	0.10223737	-2.17317956	H	7.49179071	2.25610938	-0.88810355
H	-9.51263803	0.03219902	-1.27403086	C	5.92902107	-1.59668456	0.00001844
C	-8.46590966	-0.28777848	1.26774363	O	6.81239311	-2.46600161	0.00004002

134

3.5 References

(1)   (a) Fabian, J.; Nakazumi, H.; Matsuoka, M. *Chem. Rev.* **1992**, *92*, 1197. (b) Qian, G.; Wang, Z. Y. *Chem. Asian J.* **2010**, *5*, 1006. (c) Hu, L.; Yan, Z.; Xu, H. *RSC Adv.* **2013**, *3*, 7667. (d) Ni, Y.; Wu, J. *Org. Biomol. Chem.* **2014**, *12*, 3774.

(2)   (a) Singh, S. P.; Sharma, G. D. *Chem. Rec.* **2014**, *14*, 419. (b) Zitzler-Kunkel, A.; Lenze, M. R.; Kronenberg, N. M.; Krause, A.-M.; Stolte, M.; Meerholz, K.; Würthner, F. *Chem. Mater.* **2014**, *26*, 4856. (c) Hendriks, K. H.; Li, W.; Wienk, M. M.; Janssen, R. A. J. *J. Am. Chem. Soc.* **2014**, *136*, 12130. (d) Shimizu, S.; Iino, T.; Saeki, A.; Seki, S.; Kobayashi, N. *Chem. Eur. J.* **2015**, *21*, 2893.

(3)   (a) Yuan, L.; Lin, W.; Zheng, K.; He, L.; Huang, W. *Chem. Soc. Rev.* **2013**, *42*, 622. (b) Guo, Z.; Park, S.; Yoon, J.; Shin, I. *Chem. Soc. Rev.* **2014**, *43*, 16. (c) Chen, H.; Lin, W.; Cui, H.; Jiang, W. *Chem. Eur. J.* **2015**, *21*, 733.

(4)   (a) Lovell, J. F.; Jin, C. S.; Huynh, E.; Jin, H.; Kim, C.; Rubinstein, J. L.; Chan, W. C. W.; Cao, W.; Wang, L. V.; Zheng, G. *Nat. Mater.* **2011**, *10*, 324. (b) Jin, C. S.; Lovell, J. F.; Chen, J.; Zheng, G. *ACS. Nano.* **2013**, *7*, 2541. (c) Spence, G. T.; Hartland, G, V.; Smith, B. D. *Chem. Sci.* **2013**, *4*, 4240. (d) Gao, F.-P.; Lin, Y.-X.; Li, L.-L.; Mayerhöffer, U.; Spenst, P.; Su, J.-G.; Li, J.-Y.; Würthner, F.; Wang, H. *Biomaterials* **2014**, *35*, 1004. (e) Chen, Q.; Wang, C.; Zhan, Z.; He, W.; Cheng, Z.; Li, Y.; Liu, Z. *Biomaterials* **2014**, *35*, 8206. (f) Jiao, Y.; Liu, K.; Wang, G.; Wang, Y.; Zhang, X. *Chem. Sci.* **2015**, *6*, 3975.

(5)   (a) Kim, C.; Song, K. H.; Gao, F.; Wang, L. V. *Radiology.* **2013**, *255*, 442. (b) Zhang, Y.; Jeon, M.; Rich, L. J.; Hong, H.; Geng, J.; Zhang, Y.; Shi, S.; Barnhart, T. E.; Alexandridis, P.; Huizinga, J. D.; Seshadri, M.; Cai, W.; Kim, C.; Lovell, J. F. *Nat. Nanotech.* **2014**, *9*, 631.

(6)   (a) Yang, Y.; Farley, R. T.; Steckler, T. T.; Eom, S.-H.; Reynolds, J. R.; Schanze, K. S.; Xue, J. *J. Appl. Phys.* **2009**, *106*, 044509. (b) Qian, G.; Zhong, Z.; Luo, M.; Yu, D.; Zhang, Z.; Ma, D.; Wang, Z. Y. *J. Phys. Chem. C* **2009**, *113*, 1589. (c) Qian, G.; Zhong, Z.; Luo, M.; Yu, D.; Zhang, Z.; Wang, Z. Y.; Ma, D. *Adv. Mater.* **2009**, *21*, 111. (d) Fenwick, O.; Sprafke, J. K.; Binas, J.; Kondratuk, D. V.; Stasio, F. D.; Anderson, H. L.; Cacialli, F. *Nano. Lett.* **2011**, *11*, 2451. (e) Yao, L.; Zhang, S.; Wang, R.; Li, W.; Shen, F.; Yang, B.; Ma, Y. *Angew. Chem. Int. Ed.* **2014**, *53*, 2119.

(7)   Ptaszek, M. *Prog. Mol. Biol. Transl. Sci.* **2013**, *113*, 59.

(8)   (a) Lavis, L. D.; Raines, R. T. *ACS. Chem. Biol.* **2008**, *3*, 142. (b) Razgulin, A.; Ma, N.; Rao, J. H. *Chem. Soc. Rev.* **2011**, *40*, 4186. (c) Chan, J.; Dodani, S. C.; Chang, C. J. *Nature Chem.* **2012**, *4*, 973. (d) Lavis, L. D.; Raines, R. T. *ACS. Chem. Biol.* **2014**, *9*, 855. (e) Dean, K. M.; Palmer, A. E. *Nat. Chem. Biol.* **2014**, *10*, 512. (f) Yu, F. B.; Han, X.; Chen, L. *Chem. Commun.* **2014**, *50*, 12234. (g) Li, X. H.; Gao, X.; Shi, W.; Ma, H. *Chem. Rev.* **2014**, *114*, 590.

(9)   Margulies, D.; Melman, G.; Shanzer, A. *Nat. Mater.* **2005**, *4*, 768.

(10)   Lee, L. G.; Berry, G. M.; Chen, C.-H. *Cytometry* **1989**, *10*, 151.

(11)   Whitaker, J. E.; Haugland, R. P.; Prendergast, F. G. *Anal. Biochem.* **1991**, *194*, 330.

(12)   (a) Yang, Y. J.; Lowry, M.; Xu, X.; Escobedo, J. O.; Sibrian-Vazquez, M.; Wong, L.; Schowalter, C. M.; Jensen, T. J.; Fronczek, F. R.; Warner I. M.; Strongin, R. M. *Proc. Natl. Acad. Sci. U. S. A.* **2008**, *105*, 8829. (b) Sibrian-Vazquez, M.; Escobedo, J. O.; Lowry, M.; Fronczek, F. R.; Strongin, R. M. *J. Am. Chem. Soc.* **2012**, *134*, 10502.

(13)   Azuma, E.; Nakamura, N.; Kuramochi, K.; Sasamori, T.; Tokitoh, N.; Sagami, I.; Tsubaki, K. *J. Org. Chem.* **2012**, *77*, 3492.

(14)   (a) Gierke, W.; Harrer, W.; Kirste, B.; Kurreck, H.; Reusch, J. *Naturforsch., B: Anorg. Chem. Org. Chem.* **1976**, *31*, 965. (b) Khudyakov, I. V.; Levin, P. P.; Kuz'min, V. A.; De Ionge, K. *Bull. Acad. Sci. USSR. Div. Chem. Sci.* **1977**, *27*, 1200. (c) Khudyakov, I. V.; Levin, P. P.; De Ionge, K.; Bekman, K.-M. *Bull. Acad. Sci. USSR. Div. Chem. Sci.* **1977**, *27*, 1525. (d) Grilj, J.; Zonca, C.; Daku, L. M. L.; Vauthey, E. *Phys. Chem. Chem. Phys.* **2012**, *14*, 6352.

(15)   Morita, Y.; Ueda, A.; Nishida, S.; Fukui, K.; Ise, T.; Shiomi, D.; Sato, K.; Takui, T.; Nakasuji, K. *Angew. Chem. Int. Ed.* **2008**, *47*, 2035.

(16)   Nishida, S.; Kawai, J.; Moriguchi, M.; Ohba, T.; Haneda, N.; Fukui, K.; Fuyuhiro, A.; Shiomi, D.; Sato, K.; Takui, T.; Nakasuji, K.; Morita, Y. *Chem. Eur. J.* **2013**, *19*, 11904.

(17)   Schmidt, D.; Son, M.; Lim, J. M.; Lin, M.-J.; Krummenacher, I.; Braunschweig, H.; Kim, D.; Würthner, F. *Angew. Chem. Int. Ed.* **2015**, *54*, 13980.

(18)   Mchedlov-Petrossyan, N. O.; Kukhtik, V. I.; Bezugliy, V. D. *J. Phys. Org. Chem.*

2003, *16*, 380.

(19)   Martin, M. M.; Lindqvist, L. *J. Lumin.* **1975**, *10*, 381.

(20)   (a) Schleyer, P. v. R.; Maerker, C.; Dransfeld, A.; Jiao, H.; van Eikema Hommes, N. J. R. *J. Am. Chem. Soc.* **1996**, *118*, 6317. (b) Corminboeuf, C.; Heine, T.; Seifert, G.; Schleyer, P. v. R.; Weber, J. *Phys. Chem. Chem. Phys.* **2004**, *6*, 273. (c) Fallah-Bagher-Shaidaei, H.; Wannere, C. S.; Corminboeuf, C.; Puchta, R.; Schleyer, P. v. R. *Org. Lett.* **2006**, *8*, 863.

(21)   Jähnert, T.; Hager, M. D.; Shubert, U. S. *J. Mater. Chem. A.* **2014**, *2*, 15234.

(22)   (a) Williams, L. L.; Webster, R. D. *J. Am. Chem. Soc.* **2004**, *126*, 12441. (b) Lee, S. B.; Willis, A. C.; Webster, R. D. *J. Am. Chem. Soc.* **2006**, *128*, 9332. (c) Huynh, M. H. V.; Meyer, T. J. *Chem. Rev.* **2007**, *107*, 5004. (d) Costentin, C. *Chem. Rev.* **2008**, *108*, 2145. (e) Koo, B. J.; Huynh, M.; Halbach, R. L.; Stubbe, J.; Nocera, D. G. *J. Am. Chem. Soc.* **2015**, *137*, 11860.

(23)   Kuss-Petermann, M.; Wenger, O. S. *J. Phys. Chem. A.* **2013**, *117*, 5726.

(24)   Hasebe, N.; Suzuki, K.; Horiuchi, H.; Suzuki, H.; Yoshihara, T.; Okutsu, T.; Tobita, S. *Anal. Chem.* **2015**, *87*, 2360.

(25)   Adamo, C.; V. Barone, *J. Chem. Phys.,* 1999, **110**, 6158.

(26)   Gaussian 09, (Revision C.01), Frisch, M. J.; Trucks, G. W.; Schlegel, H. B.; Scuseria, G. E.; Robb, M. A.; Cheeseman, J. R.; Scalmani, G.; Barone, V.; Mennucci, B.; Petersson, G. A.; Nakatsuji, H.; Caricato, M.; Li, X.; Hratchian, H. P.; Izmaylov, A. F.; Bloino, J.; Zheng, G.; Sonnenberg, J. L.; Hada, M.; Ehara, M.; Toyota, K.; Fukuda, R.; Hasegawa, J.; Ishida, M.; Nakajima, T.; Honda, Y.; Kitao, O.; Nakai, H.; Vreven, T.; Montgomery, J. A., Jr.; Peralta, J. E.; Ogliaro, F.; Bearpark, M.; Heyd, J. J.; Brothers, E.; Kudin, K. N.; Staroverov, V. N.; Kobayashi, R.; Normand, J.; Raghavachari, K.; Rendell, A.; Burant, J. C.; Iyengar, S. S.; Tomasi, J.; Cossi, M.; Rega, N.; Millam, J. M.; Klene, M.; Knox, J. E.; Cross, J. B.; Bakken, V.; Adamo, C.; Jaramillo, J.; Gomperts, R.; Stratmann, R. E.; Yazyev, O.; Austin, A. J.; Cammi, R.; Pomelli, C.; Ochterski, J. W.; Martin, R. L.; Morokuma, K.; Zakrzewski, V. G.; Voth, G. A.; Salvador, P.; Dannenberg, J. J.; Dapprich, S.; Daniels, A. D.; Farkas, O.; Foresman, J. B.; Ortiz, J. V.; Cioslowski, J.; Fox, D. J. Gaussian, Inc., Wallingford CT, 2010.

Conclusion

In this thesis, the author has achieved the synthesis of a new cyclic oligothiophene and π-extended polymethine dyes containing 3,3′-bithiophene substructures. These compounds have characteristic molecular structures and exhibit outstanding properties, reflecting 3,3′-bithiophene character. Throughout the study on the fundamental properties of these compounds, several important findings can be extracted which are summarized as follows:

1. A cyclic octithiophene containing 3,3′-bithiophene moieties, which is regarded as the α-quaterthiophene dimer connected *via* β,β′-linkages, was synthesized. It has an elliptical structure due to highly twisted 3,3′-bithiophene moieties.

2. Highly twisted 3,3′-bithiophene moieties induce a large structural change in the excited state, resulting in the red-shifted fluorescence. In addition, spin delocalization through the β,β′-linkages is suggested in the oxidized forms. While the electronic interaction is negligible in the ground state, π-conjugation through the β,β′-linkages is extended both in the excited state and in the oxidized state.

3. 3,3′-Bithiophene-fused tropylium ions with electron-donating amino groups show the pronounced quinoidal resonance character. Reflecting the contribution of rhodamine-like quinoidal structures, these compounds show high stability, intense absorption bands in the visible region, and red emissions.

4. 3,3′-Bithiophene-fused cycloheptatriene bearing two phenol moieties at the termini exhibited the pH-responsive photophysical properties, which are reminiscent of that observed for fluorescein derivatives. In particular, its anionic form shows an intense absorption in the NIR region due to the effective charge delocalization. Moreover, this compound can be also converted to the galvinoxyl-like neutral radical by chemical oxidation. Spin delocalization over the entire molecular skeleton gives rise to high stability as well as a NIR-absorption.

5. For the molecular design of charge- or spin-delocalized π-conjugated systems, 3,3′-bithiophene-fused skeleton is crucial. The ineffective π-conjugation through the β,β′-linkage should be responsible for the charge or spin delocalization through the four non-fused C-C bonds in seven-membered ring.

These findings should not only demonstrate the potential of the 3,3′-bithiophene as building blocks, but also provide important implications into the molecular design of oligothiophene-based π-conjugated systems. The author believes that these results/findings would contribute to further advance in the chemistry of functional π-conjugated materials.